

Geavanceerde microkinetiek
van reversibele additiefragmentatie-ketentransferpolymerisatie

Advanced Microkinetics
of Reversible Addition-Fragmentation Chain Transfer Polymerization

Pieter Derboven

Promotoren: prof. dr. M.-F. Reyniers, prof. dr. ir. G. B. Marin
Proefschrift ingediend tot het behalen van de graad van
Doctor in de Ingenieurswetenschappen: Chemische Technologie

Vakgroep Chemische Proceskunde en Technische Chemie
Voorzitter: prof. dr. ir. G. B. Marin
Faculteit Ingenieurswetenschappen en Architectuur
Academiejaar 2015 - 2016



ISBN 978-90-8578-868-3
NUR 952
Wettelijk depot: D/2016/10.500/1

Publication list

Published manuscripts:

- Derboven, P.; D'hooge, D. R.; Stamenovic, M. M.; Espeel, P.; Marin, G. B.; Du Prez, F. E.; Reyniers, M.-F. *Kinetic modeling of radical thiol-ene chemistry for macromolecular design: importance of side reactions and diffusional limitations*, *Macromolecules* **2013**, *46*, 1732-1742
- Derboven, P.; D'hooge, D. R.; Reyniers, M.-F.; Marin, G. B.; Barner-Kowollik, C. *The long and the short of radical polymerization*, *Macromolecules* **2015**, *48*, 492-501
- D'hooge, D. R.; Van Steenberge, P. H. M.; Derboven, P.; Reyniers, M.-F.; Marin, G. B. *Model-based design of the polymer microstructure: bridging the gap between polymer chemistry and engineering*, *Polymer Chemistry* **2015**, *6*, 7081-7096 (front cover)

Accepted manuscripts:

- Derboven, P.; Van Steenberge, P. H. M.; Vandenberghe, J.; Reyniers, M.-F.; Junkers, T.; D'hooge, D. R.; Marin, G. B. *Improved livingness and control over branching in RAFT polymerization of acrylates: could microflow synthesis make the difference?*, *Macromolecular Rapid Communications* **2015**, DOI: 10.1002/marc.201500357 (front cover)
- Derboven, P.; Van Steenberge, P. H. M.; Reyniers, M.-F.; Barner-Kowollik, C.; D'hooge, D. R.; Marin, G. B. *Chain transfer in degenerative RAFT polymerization revisited: a comparative study of literature methods*, *Macromolecular Theory and Simulations* **2015**, accepted (awaiting proofs)

Submitted manuscripts:

- Derboven, P.; Van Steenberge, P. H. M.; Reyniers, M.-F.; Barner-Kowollik, C.; D'hooge, D. R.; Marin, G. B. *A novel method for accurate degenerative chain transfer coefficients: proof of concept and experimental validation*, *Polymer Chemistry* **2015**, submitted

Contents

Preface.....	vii
Nederlandstalige samenvatting.....	ix
English summary.....	xv
List of symbols.....	xxi
Chapter 1: Introduction.....	1
1.1 General scope of the PhD thesis.....	1
1.2 Main methods to determine rate coefficients in RAFT polymerization.....	3
1.2.1 Intrinsic rate coefficients.....	7
1.2.2 Apparent rate coefficients.....	8
1.2.3 Initiation.....	12
1.2.4 Propagation.....	17
1.2.5 Termination.....	20
1.2.6 Chain Transfer to CTA.....	29
1.2.7 RAFT specific transfer reactions.....	34
1.3 Outline.....	43
1.4 References.....	45
Chapter 2: The long and the short of radical polymerization.....	53
2.1 Introduction.....	54
2.2 Experimental Section	57
2.2.1 Materials.....	57
2.2.2 Methods and Analysis.....	57

2.3	Results and Discussion.....	62
2.3.1	Extension of state-of-the-art theories for the short-long-termination reactivity.....	62
2.3.2	Improved determination of accurate homotermination rate coefficients.....	66
2.3.3	First-time experimental quantification of possible matrix effects on homotermination reactivity.....	77
2.3.4	First-time experimental determination of short-long termination rate coefficients.....	80
2.4	Conclusions.....	88
2.5	References.....	88
Chapter 3: Chain transfer in degenerative RAFT polymerization revisited: a comparative study.....		95
3.1	Introduction.....	96
3.2	Methods to determine RAFT transfer coefficients.....	102
3.2.1	Methods to determine $C_{(-)tr,0}$	102
3.2.2	Methods to determine C_{tr}	103
3.3	<i>In silico</i> evaluation of literature models to determine $C_{tr(0)}$	106
3.3.1	Simulation of a ‘perfect experiment’.....	109
3.3.2	Methods to determine $C_{tr,0}$	111
3.3.3	Models to determine C_{tr}	118
3.4	Conclusions.....	120
3.5	References.....	121
Chapter 4: A novel method to measure degenerative RAFT exchange reactivities: proof of concept and experimental validation.....		125

4.1	Introduction.....	126
4.2	Method section.....	128
4.3	Results and discussion.....	139
4.3.1	Proof of concept by the simulation of perfect experiments.....	139
4.3.2	RAFT polymerization of MMA with CPDB as RAFT CTA at 353 K.....	154
4.4	Conclusions.....	160
4.5	References.....	161
Chapter 5: Improved livingness and control over branching in RAFT polymerization of acrylates: could microflow synthesis make the difference?.....		165
5.1	Introduction.....	166
5.2	Experimental section.....	168
5.2.1	Materials.....	168
5.2.2	Experimental procedure of the batch reaction (TCL 80).....	168
5.2.3	Experimental procedure of the microreactor reaction (TCL 80).....	169
5.2.4	Characterization.....	170
5.3	Model details.....	171
5.4	Kinetic parameters.....	174
5.5	Results and discussion.....	175
5.6	Conclusions.....	193
5.7	References.....	194
Chapter 6: General conclusions and future outlook.....		199
6.1	General conclusions.....	199
6.2	Future outlook.....	202

Appendix A: Modification of the RAFT-CLD-T equation for homotermination.....	205
A.1 Reaction rates for a general elementary reaction.....	205
A.2 Reaction rates for isolated termination by recombination reactions	206
A.3 Termination by recombination reaction rates for simple case of chain length distribution involving only two chain lengths.....	207
A.4 Termination by recombination reaction rates for general case of chain length distribution involving N chain lengths.....	209
A.5 References.....	211
Appendix B: Detailed discussion on the determination of the RAFT-CLD-T homotermination surface (Figure 2.4).....	213
B.1 Limited impact of volume contraction during RAFT-CLD-T measurement of homotermination rate coefficients.....	213
B.2 Reliability of RAFT-CLD-T homotermination experimental data.....	215
B.3 Propagation of uncertainty analysis (Figure 2.4b in Chapter 2).....	219
B.4 Regression of the improved homotermination surface (Figure 2.4c in Chapter 2).....	219
B.5 References.....	221
Appendix C: Details on the quantification of matrix effects for the homotermination rate coefficients.....	223
C.1 Consistency of the modified RAFT-CLD-T homo-termination experiments to quantify the influence of matrix effects.....	223
C.2 Regression of the surface function to evaluate the effect of the polymer matrix (Figure 2.11c in Chapter 2).....	225
Appendix D: Detailed discussion on the RAFT-CLD-T short-long termination experiments.....	229

D.1	Derivation of CTA conversion from SEC traces in RAFT-CLD-T short-long termination experiments.....	229
D.2	Propagated error on the measured short-long-termination rate coefficients...	230
D.3	Verification of the reliability of the short-long termination data.....	231
D.4	Overview of all short-long termination results.....	236
D.5	Simulation details.....	241
D.6	References.....	242
Appendix E: Full RAFT polymerization scheme and approximation via degenerative transfer mechanism.....		243
E.1	Full RAFT polymerization scheme.....	243
E.2	Degenerative transfer mechanism.....	245
E.1.1	Reaction scheme.....	245
E.2.1	Derivation of the expressions for $k_{tr,0}$, $k_{tr,0}$ and k_{tr}	249
E.3	References.....	250
Appendix F: The Newton-Raphson method to solve non-linear equations and its modification used in Chapter 4.....		253
F.1	Original Newton-Raphson method.....	253
F.2	Application to methodology presented in Chapter 4 to determine the RAFT transfer reactivity assuming a degenerative RAFT reaction scheme.....	254
F.3	References.....	258
Appendix G: Experimental protocol for reliable measurement of the transfer reactivity in reversible addition-fragmentation chain transfer (RAFT) polymerization.....		261
G.1	Propagation reactivity.....	261
G.2	Termination reactivity.....	262

G.3	RAFT CTA conversion.....	262
G.4	Total radical concentration.....	263
G.5	Experimental protocol.....	264
G.1.1	Determination of $\langle C_{tr} \rangle$ for the complete conversion region.....	264
G.2.1	Determination of $\langle C_{tr} \rangle$ at the start of the RAFT polymerization, i.e. $C_{tr,0}$	265
G.6	References.....	266
Appendix H: Additional experimental data for the RAFT polymerization of nBuA.....		269
H.1	Batch measurements for different reactor volumes.....	269
H.2	ESI-MS spectra.....	269
Appendix I: Kinetic parameters for the RAFT polymerization of nBuA and reaction scheme for the MCRs.....		273
I.1	References.....	275
Appendix J: Influence of the targeted chain length on the poly(butyl acrylate) microstructure in a microreactor at 343 K.....		277
Appendix K: Alternative representation of the branching content.....		279
Appendix L: Glossary.....		281
List of figures.....		287
List of schemes.....		319
List of tables.....		323

Preface

The four years of my PhD have led to both a strong professional and personal development. Many persons/institutes have contributed to achieve both and deserve a special thanks.

First of all I would like to thank the Institute for the promotion of Innovation through Science and Technology in Flanders (IWT Vlaanderen) for financial support. Next, a special thanks goes to my supervisors professor G. B. Marin and professor M.-F. Reyniers for triggering a more critical view on the performed work and raising my research to a higher level. Although not my official supervisor, professor D. R. D'hooge is especially thanked for his excellent guidance, motivation and interesting discussions. Also the collaborative partners professor C. Barner-Kowollik and professor T. Junkers are thanked for their very efficient collaboration and professor C. Barner-Kowollik in particular for hosting and guiding me for five months in his group in Karlsruhe. Proper technical support is indispensable for a successful PhD and therefore I would like to thank Michaël Lottin, George Verenghen, Erwin Turtelboom, Hans Heene, Marcel Vervust, Brecht Vervust, Jaimy Strobbe, Bert Depuydt and the technical personnel at the KIT in Karlsruhe: Helena Hörig, Maria Schneider and Vincent Schüler.

Second, I can honestly say that I have always liked to 'go to the lab', due to the great atmosphere that was created by the people working there. Many colleagues have become true friends from whom I have been learning a lot. A special thanks goes to Martin Purino, Evgeniy Redekop and Carolina de los Angeles Toloza Porras for being my coach in life, Gonzalo Canduela Rodriguez for being my sporting partner and the second half of the Halloween costume, Gilles Desmet for being a good friend and the great dinners, José Guillermo Rivera de la Cruz for the laughs and the proper Mexican food, Jelena Kovacevic for her everlasting enthusiasm, Tapas Rajkhowa and Chetan Shreedhar Raghuveer for the great food and chats, Pieter Verhees for the sports and evenings out at Blaarmeersen, Daria

Otyuskaya and Maria del Mar Torregrosa Galindo for the better dancing; Marko Djokic, Luis Alberto Lozano Guerra, Carl Schietekat, David Van Cauwenberge, Natalia Lilka, Vaios Alexiadis, Nenad Ristic, Stavros Theofanidis, Maria Pantzali, Andres Muñoz, Arturo Gonzales Quiroga, Aditya Dharanipragada Naga Venkata Ranga, Kevin Payne, William Scott, Gaoping Xue and Israel Chavez for the great moments in and around Gent.

Furthermore I would like to thank Nils De Rybel, Stijn Fierens, Dries Devlaminck and Paul Van Steenberge for being a great team of nearest colleagues with a great sense of humor. The final two persons of the lab who deserve a special thanks from me for their great administrative work and smile throughout every single day are Petra Vereecken and Sarah Verschooren. I would also like to thank my friends at the KIT for the good time over there: Anja Goldmann, Kim Oehlenschlaeger, Bernhard Schmidt, Eva Blascop, Kai Hildebrandt, Andrew Vogt, Elena Fick and Guillaume Delaittre, with a special thanks to Anja for travelling with me through Australia. Finally, there is also a life besides work and both my family and dearest friends outside work deserve a special word of thanks. I would like to thank, my parents Luc and Lieve and my two brothers Jeroen and Michiel for their great support and the nice time together; my (upcoming) sisters in law Stefania and Jolien and my little nephew Massimo for taking so good care of my brothers; Lies for the great years; our KG crew including the non-official insiders Tim and Sanne for the great evenings/weekends/traveling and true friendship; Dries, Jacob, Michael and Philip for being such good friends; our band Pieter, Ruben, Heleen and Lukas for the perfect relaxing and great music; Famke, Stijn and Helen for the nice dance classes; Daniela and Camila for the great time in Gent; Jokin, Lucio, Emma and Yumi for nice sports/evenings in Gent.

Pieter 23/09/2015, Brisbane

Nederlandstalige samenvatting

Oorspronkelijk gedreven door het streven naar het namaken van natuurlijke vezels en rubbers via een synthetische equivalent, zijn synthetische polymeerproducten tegenwoordig niet meer weg te denken uit het dagelijks leven. Het initiële doel om ‘natuurlijke’ eigenschappen te verkrijgen op een kunstmatige manier heeft geleidelijk aan plaats gemaakt voor de algemene consensus dat synthetische polymeren de inherente mogelijkheid hebben om op maat te worden gemaakt voor een beoogde toepassing. Verschillende monomeertypes kunnen gecombineerd worden om gewenste eigenschappen te incorporeren in het resulterende (co)polymeer, bv. taaigheid, ketenflexibiliteit, *etc.* Anderzijds kunnen via de additie van specifieke componenten, die interfereren met het polymerisatiemechanisme gedurende de polymeersynthese, voordien onbereikbare fysische eigenschappen verkregen worden, of kan door menging van het resulterende polymeer met additieven de verdere verwerking verbeterd worden, twee voorbeelden van ontwikkelingen om te voldoen aan de specifieke eisen van de consument. Dit heeft geleid tot verschillende nieuwe toepassingsvelden met voornamelijk verdiensten in de (voedsel) verpakkingindustrie en de productie van constructiematerialen.

In het bijzonder heeft reversibele deactivering radicalaire polymerisatie (RDRP), ook gekend als ‘gecontroleerde radicalaire polymerisatie (CRP)’ nieuwe wegen geopend voor de synthese van polymeerproducten met een zeer specifieke structuur. Via de additie van een deactiverend agens wordt een functionaliteit geïntroduceerd in de polymeerketen zodat geavanceerde macromoleculaire architecturen zoals (multi-)blokcopolymeren, sterpolymeren en moleculaire borstels onmiddellijk toegankelijk zijn, uiteindelijk resulterend in niche toepassingen in elektronica, de deklagenindustrie en biomedische technologie. Onder ideale condities worden via deze RDRP-methoden polymeereigenschappen verkregen die aanleunen tegen diegene

verkregen door levende ionaire polymerisatie, maar dan onder aanzienlijk mildere reactiecondities.

In deze doctoraatsthesis wordt reversibele additiefragmentatie-ketentransferpolymerisatie (RAFT-polymerisatie) behandeld, de meest veelzijdige RDRP-methode wat monomeercompatibiliteit betreft en daarom veelvuldig toegepast voor precisiepolymeersynthese. In tegenstelling tot de andere RDRP-technieken wordt in RAFT-polymerisatie de controle over de polymeereigenschappen verwezenlijkt door een uitwisselingsmechanisme tussen macroradicalen en slapende macrospecies via een opeenvolgende additie- en fragmentatiereactie. Een groot aantal kinetische parameters moeten precies gekend zijn voor een volledig fundamenteel begrip van RAFT-polymerisatie, zoals wordt aangetoond in hoofdstuk 1. Bovendien kunnen reactiesnelheden diffusiegecontroleerd worden op de microschaal door de sterke toename in viscositeit van het polymerisatiemengsel, wat de beschouwing van ‘schijnbare’ kinetiek vereist. In het bijzonder worden terminatiereacties gekenmerkt door een sterk schijnbare reactiviteit. Directe experimentele meting van deze (schijnbare) snelheidscoëfficiënten is aangewezen en heeft belangrijke verdiensten in de bepaling van betrouwbare propagatiesnelheidscoëfficiënten via gepulseerde lazer polymerisatie- (PLP-) technieken en schijnbare homoterminatiesnelheidscoëfficiënten via PLP en de RAFT – ketenlengte afhankelijke – terminatie- (RAFT-CLD-T-) techniek. In vele radicalaire polymerisatieprocessen wordt terminatie echter gedomineerd door kort-lang-terminatiereacties, voor dewelke noch een experimenteel protocol noch data beschikbaar waren tot nu toe en enkel vereenvoudigde theoretische modellen toegepast konden worden voor modelgebaseerd ontwerp. Bovendien is voor RAFT-polymerisatie de accurate kwantificering van de verscheidene additiefragmentatie-

snelheidscoëfficiënten een fundamenteel knelpunt dat verdere industriële exploitatie belemmert.

Daarom worden in dit proefschrift nieuwe methoden (hoofdstuk 2-4) ontwikkeld om (i) op een betrouwbare manier alle terminatiesnelheidscoëfficiënten te bepalen met RAFT-polymerisatie als kinetische methode en (ii) om voor een degeneratief RAFT-polymerisatiemechanisme de transferreactiviteit van het initiële RAFT-ketentransferagens (KTA) en macro-RAFT-agens, gebaseerd op analytische uitdrukkingen voor de gemiddelde polymeereigenschappen. Via gedetailleerde deterministische RAFT-polymerisatiesimulaties worden de huidige literatuurmodellen geëvalueerd en wordt conceptuele validatie verkregen voor de methoden ontwikkeld in dit doctoraatsproefschrift. Nadien worden deze toegepast op eigen experimentele data voor de RAFT-polymerisatie van methylmethacrylaat (MMA) met cyanoisopropyl-dithiobenzoaat (CPDB) als RAFT-KTA en geïnitieerd door azo(bisisobutyronitrile) bij 353 K.

In hoofdstuk 2 wordt een algemeen en flexibel experimenteel protocol uiteengezet dat, gebaseerd op de eenvoudige RAFT-CLD-T-techniek, naast de bepaling van betrouwbare schijnbare *homo*-terminatiesnelheidscoëfficiënten ook de eerste meting toelaat van schijnbare kort-lang-terminatie-snelheidscoëfficiënten onder goed gecontroleerde RAFT-polymerisatiecondities. De algemene toepasbaarheid van de ontwikkelde procedure wordt bevestigd door de mogelijkheid om de invloed van de polymeermatrix, een belangrijke dynamische variabele in elk polymerisatieproces, te kwantificeren. De experimentele resultaten tonen aan dat de diffusie van korte macroradicalen de kort-lang-terminatie domineert conform eerdere theoretische bevindingen. Bovendien wordt bewijs geleverd voor het falen van de huidige vereenvoudigde theoretische modellen gebaseerd op gemiddelden. Voor de verkregen experimentele data voor MMA wordt echter aangetoond dat in het

bestudeerde monomeerconversiebereik met weinig effect van de polymeermatrix, de geobserveerde gemiddelde polymeereigenschappen (bv. eindgroepfunctionaliteit) nog steeds benaderd kunnen worden door gebruik van deze vereenvoudigde modellen.

In hoofdstuk 3 worden de momenteel in de literatuur beschikbare analytische methoden om RAFT-transfercoëfficiënten voor degeneratieve RAFT-polymerisatie te bepalen, gerevalueerd door middel van de simulatie van perfecte experimenten. De accuraatheid van elke methode wordt vervolgens in kaart gebracht voor een brede waaier reactiecondities om nuttige richtlijnen te formuleren voor de experimentele chemici. Er wordt aangetoond dat geen algemene methode beschikbaar is. Elke methode is slechts bruikbaar voor welbepaalde reactiecondities die afhangen van de gemaakte modelveronderstellingen. Meer bepaald wordt er aangetoond voor de bepaling van de RAFT-transferreactiviteit met macro-RAFT-KTA, C_{tr} , dat de huidige analytische literatuurmethoden beperkt zijn tot RAFT-polymerisaties gekarakteriseerd door een zeer hoge transferreactiviteit met klein RAFT-KTA, $C_{tr,0}$. Bijgevolg is een belangrijke openstaande onderzoekstaak de ontwikkeling van meer gedetailleerde analytische modellen die toelaten om een breder bereik aan RAFT-transferreactiviteiten te bepalen.

Aan deze tekortkoming wordt tegemoet gekomen in hoofdstuk 4 waarin een verbeterde methode wordt ontwikkeld om RAFT-transfercoëfficiënten te bepalen. In deze methode worden de transferreactiviteiten verkregen door de numerieke oplossing van een analytische uitdrukking voor de polymeerdispersiteit als functie van de monomeerconversie, rekening houdend met schijnbare terminatiekinetiek en een mogelijke intrinsieke/schijnbare ketenlengteafhankelijkheid van de RAFT-additievoëfficiënt. De voorgestelde methode wordt *in silico* gevalideerd als een meer nauwkeurige manier om $C_{tr,0}$ te bepalen, dewelke in principe verkregen kan worden van één enkele meting van de polymeerdispersiteit bij lage

monomeerconversie. Bovendien kan ook een waarde voor C_{tr} en de mogelijke ketenlengteafhankelijkheid ervan bepaald worden uit hetzelfde experiment bij hogere monomeerconversies. Daarnaast kan de betrouwbaarheid van de metingen afgeleid worden uit de beschouwing van additionele convergentiecriteria voor de numerieke oplossingsprocedure. Toepassing van de voorgestelde methode op experimentele data voor RAFT polymerisatie van MMA bij 353 K met CPDB als RAFT-KTA leidt tot een waarde voor $C_{tr,0}$ van 20, terwijl andere literatuurmethoden minder betrouwbaar blijken. Voor C_{tr} wordt een benaderde waarde van 76 verkregen en geen ketenlengteafhankelijkheid wordt gedetecteerd voor de huidige experimentele dataset.

Uiteindelijk wordt in hoofdstuk 5 de sterkte van een gedetailleerde kinetische modelleringsaanpak geïllustreerd door de simulatie van een complexere oplossings-RAFT polymerisatie van *n*-butylacrylaat in batch en in een microreactor bij een insteltemperatuur van 373 K. Er wordt aangetoond dat de isothermiciteit in de microreactor de reden is voor de superieure controle over de polymeereigenschappen in vergelijking met de batch reactor, waarin een geobserveerde piek in het temperatuurprofiel leidt tot een verhoogde bijdrage van zijproducten. Verder kunnen in een microreactor voor een gegeven RAFT-KTA ook de vertakkingsgraad en het verlies aan eindgroepfunctionaliteit aanzienlijk verminderd worden door de beoogde ketenlengte, de temperatuur en de verdunningsgraad te verlagen. De simulaties bevestigen dus dat microreactoren ideaal zijn voor geavanceerd macromoleculair ontwerp van polyacrylaten waaronder de synthese van goed gedefinieerde blokcopolymeren. Bovendien laat de gedetailleerde kinetische analyse toe om ondubbelzinnig de fundamentele oorzaken te bepalen voor de invloed van de microreactorcondities op de cumulatieve vertakkingsgraad en het levend karakter van het resulterende polyacrylaatpolymeer.

Tenslotte worden in hoofdstuk 6 de belangrijkste conclusies van dit doctoraat en mogelijk toekomstig werk weergegeven.

English summary

Originally driven by the endeavor to mimic natural fibers and rubbers by a synthetic equivalent, nowadays, synthetic polymer products have taken an indispensable position in everyday life. The initial incentive to access ‘natural’ characteristics via other resources has long since been gradually overruled by the general acknowledgement that synthetic polymers retain the inherent ability to be tailor-made for the aspired use. Particularly, different monomer types can be combined to incorporate the desired properties in the resulting synthetic (co)polymer, *e.g.* toughness, chain flexibility, *etc.* Moreover, the addition of compounds that interfere with the polymerization mechanism during the polymer synthesis to obtain previously unattainable physical properties or the mixing of the resulting polymer with additives to enhance the further processability, are two other examples of developments that have been established to match the specific consumer demands. Numerous new application fields have arisen quickly with main merits in the (food) packaging and the consumer goods industry, and the production of new construction materials.

Particularly, reversible deactivation radical polymerization (RDRP), also known as ‘controlled radical polymerization (CRP)’, has paved new avenues towards the synthesis of polymer products with a very high degree of structural specificity. Via addition of a reversible deactivating agent, which also introduces functionality into the polymer chain, tailor-made macromolecular architectures such as (multi-)block copolymers, star polymers and molecular brushes are readily obtained via well-established experimental procedures, leading to niche applications in electronics, the coating industry and biomedical technology. Under ideal conditions, the polymer properties obtained via these RDRP methods tend towards the characteristics obtained by living ionic polymerization but under far less stringent reaction conditions.

In this PhD thesis, reversible addition-fragmentation chain transfer (RAFT) polymerization is studied, which is the most versatile RDRP method regarding monomer compatibility and consequently widely applied for precision polymer synthesis. In contrast to the other RDRP techniques, the control over the polymer properties in RAFT polymerization is established by an exchange mechanism between macroradicals and dormant macrospecies via a consecutive addition and fragmentation reaction. This process involves a large number of kinetic parameters that need to be accurately known for a proper fundamental understanding of RAFT polymerization, as demonstrated in Chapter 1. Furthermore, reaction rates can become diffusion-controlled at the micro-scale due to the strong increase in viscosity of the polymerization mixture which necessitates the consideration of ‘apparent’ kinetics. In particular, termination reactions are characterized by a strong apparent reactivity. Direct experimental measurement of (apparent) rate coefficients is recommended and has important merits in the determination of reliable propagation rate coefficients via pulsed laser polymerization (PLP) techniques and of reliable apparent *homo*-termination rate coefficients via PLP and the RAFT – chain length dependent – termination (RAFT-CLD-T) technique. Yet, in many radical polymerization processes termination is dominated by *short-long* termination reactions, for which neither an experimental protocol nor data were available and only simplified theoretical models could be applied for model-based design. Furthermore, for RAFT polymerization, reliable quantification of the different addition-fragmentation rate coefficients remains a fundamental bottleneck, hampering its industrial application.

Therefore, in the present work, novel methodologies (Chapter 2-4) have been developed to (i) reliably quantify all apparent termination rate coefficients, using RAFT polymerization as a kinetic tool and (ii) to determine for a degenerative RAFT polymerization mechanism the transfer reactivity of the initial RAFT chain transfer agent (CTA) and macro-RAFT agent,

based on analytical expressions for the average polymer properties. Detailed deterministic simulations of RAFT polymerization have been employed to evaluate current literature models and provide proof of concept for the methods proposed in this PhD thesis after which they have been successfully applied to own experimental data for RAFT polymerization of methyl methacrylate (MMA) with cyano isopropyl dithiobenzoate (CPDB) as RAFT CTA and initiated by azobis(isobutyronitrile) (AIBN) at 353 K.

In Chapter 2, a generic and flexible experimental framework, based on the straightforward RAFT-CLD-T technique, is presented that not only allows to obtain reliable absolute apparent *homo*-termination coefficients but also the very first measurement of apparent *short-long*-termination rate coefficients under well-defined RAFT polymerization conditions. The generic nature of the framework is evidenced by its capability to quantify the influence of the polymer matrix, an important dynamic variable in any polymerization process. In line with previous theoretical postulations, the experimental results show that the diffusivity of the *short-chain* macroradicals dominates the *short-long* termination reactivity. Furthermore, data analysis unveils compelling evidence for the deficiency of the currently used simplified mean models. It is, however, shown that in the studied intermediate MMA conversion range with limited matrix effects, the observed average polymer properties (*e.g.* end-group functionality) can still be approximated by these models.

In Chapter 3, the analytical methods currently available in literature to determine the RAFT transfer coefficients for degenerative RAFT polymerization are re-evaluated based on the simulation of perfect experiments and their accuracy is mapped for a broad range of reaction conditions in order to provide useful guidelines for the experimentalist. It is found that no general method is available, instead, each method is only effective for a well-defined limited

range of conditions which depends on the corresponding model assumptions. Moreover, it is shown that for the determination of the RAFT exchange reactivity with macro-RAFT CTA, C_{tr} , the analytical methods currently available in literature are limited to RAFT polymerizations characterized by a very high exchange reactivity with small RAFT CTA, $C_{tr,0}$. Hence, an important outstanding research task is the development of more detailed analytical models capable of covering a wider range of RAFT exchange reactivities.

This deficiency is redressed in Chapter 4, in which an improved method to determine RAFT transfer coefficients has been developed. In this method, the transfer reactivities are obtained by numeric solution of an analytical expression for the polymer dispersity as a function of monomer conversion, including apparent termination kinetics and a possible intrinsic/apparent chain length dependency of the RAFT addition rate coefficient. The presented method is validated *in silico* as a more accurate way to determine $C_{tr,0}$ compared to current literature models, which value can in principle be obtained from one single reliable measurement of the polymer dispersity at low monomer conversion. Importantly, also a value for C_{tr} and its possible chain length dependency can be accessed from the same experiment at higher monomer conversions. Furthermore, the reliability of the measurements can be directly deduced via the consideration of additional convergence criteria for the numeric solution procedure. Application of the presented methodology to experimental data for RAFT polymerization of MMA at 353 K with CPDB as RAFT CTA has led to a value for $C_{tr,0}$ of 20, whereas other literature methods are shown to be less reliable. For C_{tr} an approximate value of 76 is obtained and no chain length dependency is detected for the current experimental dataset.

Finally, in Chapter 5 the strength of a detailed kinetic modeling approach is illustrated by the simulation of the more complex solution RAFT polymerization of *n*-butyl acrylate in a batch and microreactor at a set-temperature of 373 K, demonstrating the cause for the better control of the polymer microstructure obtained in the latter reactor. It is found that the isothermicity of the microreactor is the reason for the superior control over polymer properties compared to the batch reactor, in which the recorded temperature spike results in an increased contribution of side products. Moreover, in a microreactor for a given RAFT CTA, the branching level and loss of functionality can be significantly reduced by lowering the targeted chain length, temperature and dilution degree. The simulations thus confirm that microreactors are ideally suited for advanced macromolecular design involving acrylate monomers, including the synthesis of well-defined block copolymers. Importantly, detailed kinetic analysis also allows to determine unambiguously the fundamental underlying causes for the effect of the microreactor conditions on the cumulative branching content and the degree of livingness. For the first time, a complete understanding of the reduced short chain branching in acrylate polymerization under RDRP conditions is thus obtained.

Finally, in Chapter 6 the main conclusions of this PhD thesis are summarized and an outlook is provided towards possible future work.

List of symbols

Roman symbols

a	root-mean-square end-to-end distance of a linear polymer chain averaged over all conformations of the chain (m)
A	reactant molecule, conventional chain transfer agent in FRP (-)
$[A]$	concentration of A (mol m^{-3})
A_a	pre-exponential factor ($\text{m}^3 \text{mol}^{-1} \text{s}^{-1}$)
AB	encounter pair of molecules A en B (-)
$[AB]$	concentration of AB (mol m^{-3})
$[AIBN]$	concentration of AIBN (mol m^{-3})
B	reactant molecule (-)
b	parameter (-)
$[B]$	concentration of B (mol m^{-3})
C	product molecule (-)
$[C]$	concentration of C (-)
$[CTA_{\text{tot}}]$	total CTA concentration: small RAFT CTA and macro-RAFT CTA
$C_{tr,0}$	transfer coefficient for RAFT exchange of macroradicals with R_0X (-)
$C_{-tr,0}$	transfer coefficient for RAFT exchange of R_0 with dormant polymeric species (-)

C_{tr}	transfer coefficient for conventional chain transfer in FRP, for RAFT exchange between macroradicals and dormant polymeric species in RAFT polymerization (-)
$\langle C_{tr} \rangle$	average transfer coefficient based on $\langle k_{tr} \rangle$ (-)
D	polymer dispersity (-)
D_A	self-diffusion coefficient of A ($\text{m}^2 \text{s}^{-1}$)
$D_{A,0}$	pre-exponential factor for self-diffusion coefficient of A ($\text{m}^2 \text{s}^{-1}$)
D_I	self-diffusion coefficient of the conventional initiator-derived radicals ($\text{m}^2 \text{s}^{-1}$)
D_m	self-diffusion coefficient of monomer ($\text{m}^2 \text{s}^{-1}$)
$[DoPAT]$	concentration of DoPAT (mol m^{-3})
$D_{p,n}$	self-diffusion coefficient of polymer with chain length n ($\text{m}^2 \text{s}^{-1}$)
D_{rd}	diffusion coefficient for reaction diffusion of a macroradical ($\text{m}^2 \text{s}^{-1}$)
E_A	activation energy (J mol^{-1})
f	initiator efficiency (-)
$f(x)$	function of x
f_l	molar fraction of long chain macroradicals
f_{branch}	cumulative branching fraction (-)
F_{MM}	molar fraction of macromonomers (-)
F_X	RAFT CTA functionality (-)

i	chain length (-)
i^*	number average chain length of macroradicals, polymer matrix is assumed to be approximately represented by single chain length (-)
i_s	chain length corresponding to the s^{th} inflection point of the CLD (-)
i_{SL}	cross-over chain length between the short and long chain length range (-)
I^*	conventional initiator-derived radical (-)
I_2	conventional radical initiator (-)
$[I_2]$	concentration of I_2 (mol m^{-3})
IX	species formed upon RAFT exchange of I^* with (macro-) RAFT CTA
J_m^*	mass average chain length of the total polymer matrix (-)
K_{diff}	equilibrium coefficient for the diffusion process ($\text{m}^3 \text{mol}^{-1}$)
K_{eq}	RAFT equilibrium coefficient of the addition-fragmentation process between macroradicals and dormant polymeric species ($\text{m}^3 \text{mol}^{-1}$)
k	rate coefficient ($\text{m}^3 \text{mol}^{-1} \text{s}^{-1}$ or s^{-1})
k_l	rate coefficient of reaction step l ($\text{m}^3 \text{mol}^{-1} \text{s}^{-1}$ or s^{-1})
$\langle k \rangle$	distribution averaged rate coefficient ($\text{m}^3 \text{mol}^{-1} \text{s}^{-1}$ or s^{-1})
$\langle k_{tr} \rangle$	average RAFT exchange rate coefficient based on different order moments of the CLD ($\text{m}^3 \text{mol}^{-1} \text{s}^{-1}$)

$k_{p,chem,0}$	intrinsic rate coefficient for propagation of macroradical of chain length one ($\text{m}^3 \text{mol}^{-1} \text{s}^{-1}$)
$k_{p,chem,\infty}$	intrinsic rate coefficient for propagation of macroradical of longer chain length, <i>i.e.</i> the long chain limit for $k_{p,chem}$ ($\text{m}^3 \text{mol}^{-1} \text{s}^{-1}$)
$k_{t,0}$	termination rate coefficient between two macroradicals of chain length one ($\text{m}^3 \text{mol}^{-1} \text{s}^{-1}$)
L^*	number average chain length of the long chain macroradicals (-)
m	chain length (-)
M	monomer molecule (-), molar mass in SEC trace (g mol^{-1})
M_n	number average molar mass (g mol^{-1})
$[M]$	concentration of monomer M (mol m^{-3})
[macro-RAFT CTA]	concentration of macro-RAFT CTA (mol m^{-3})
[MMA]	concentration of MMA (mol m^{-3})
n	chain length (-)
N	maximum chain length considered in the microkinetic model
N_A	Avogadro constant (mol^{-1})
[$n\text{BuA}$]	concentration of $n\text{BuA}$ (mol m^{-3})
N_L	upper limit of the chain length range for the long chain macroradicals (-)

N_S	upper limit of the chain length range for the short chain macroradicals (-)
p	probability for propagation (-)
P_n	dead polymer molecule with chain length n (-)
$[P_n]$	concentration of P_n (mol m^{-3})
Q_1	initial condition for τ_1 at x_0 (start conversion of integration interval)
Q_2	initial condition for τ_2 at x_0 (start conversion of integration interval)
R	universal gas constant ($\text{J mol}^{-1} \text{K}^{-1}$)
r	reaction rate ($\text{mol m}^{-3} \text{s}^{-1}$)
R_0	RAFT CTA derived radicals (-)
$[R_0]$	concentration of R_0 (mol m^{-3})
R_0X	small RAFT CTA (-)
$[R_0X]$	concentration of R_0X (mol m^{-3})
R_n	macroradical with chain length n (-)
$[R_n]$	concentration of R_n (mol m^{-3})
$[R_{tot}]$	total radical concentration (mol m^{-3})
R_nX	macro-RAFT CTA with chain length n (dormant polymeric species) (-)
$[R_nX]$	concentration of R_nX (mol m^{-3})
r_l	volumetric rate of the reaction l ($\text{mol m}^{-3} \text{s}^{-1}$)

S^*	number average chain length of the short chain macroradicals (-)
s	variable (-)
t	time (s)
t_0	dead time between two laser pulses (s)
T	temperature (K)
\bar{v}	average fluid velocity (m s^{-1})
V	volume of reaction mixture (-)
\tilde{V}_A^*	critical molar hole free volume for a jumping unit of the molecule A ($\text{m}^3 \text{mol}^{-1}$)
\tilde{V}_{FH}	total hole free volume per mole of jumping units ($\text{m}^3 \text{mol}^{-1}$)
$w(M)$	mass based polymer CLD: mass fraction of polymer with molar mass M (-)
w_m	mass fraction of monomer (-)
w_p	mass fraction of polymer (-)
w_{ST}	mass fraction of polymer standard (-)
x	monomer conversion (-)
x_0	start conversion of integration interval (-)
x_{R_0X}	conversion of R_0X (-)
X	functionality (-)

x_m	mass average chain length (-)
x_n	number average chain length (-)
x_n^0	initial number average chain length (-)
$x_{n,R}$	number average chain length of the macroradicals (-)
y_n	number fraction of dead polymer chains with chain length n (-)
z	spatial coordinate of the reactor (m)

Greek symbols

α	exponent in power law model for chain length dependency of $k_{t,app}$ (-)
β	parameter that takes into account the totally flexible and rigid chain limits for reaction diffusion (-)
γ	overlap factor (-)
Δ	width (-)
ΔH	reaction enthalpy (kJ mol^{-1})
λ_s	s^{th} order moment of the macroradical distribution, $s = 0,1,2,3$ (mol m^{-3})
τ_s	s^{th} order moment of the dormant polymer distribution, $s = 0,1,2,3$ (mol m^{-3})
σ'	collision radius approximated by the Lennard Jones diameter (m)
κ	ratio of the initial monomer concentration to the initial conventional radical initiator concentration (-)

θ ratio of the total radical concentration to the initial conventional radical initiator concentration (-)

φ fragmentation probability (-)

Subscripts

0 initial

add addition

app apparent

bb backbiting

β β -scission

$chem$ intrinsic chemical contribution

d decomposition of the conventional radical initiator

$+diff$ diffusional contribution of reactants towards each other

$-diff$ diffusional contribution of reactants away from each other

$diff,I$ diffusional contribution for the initiator-derived radicals for movement out of the solvent cage

DMM diffusion mean model

$dormant$ dormant polymeric species

eq at equilibrium

$escape$ exit out of the solvent cage

<i>exch</i>	RAFT exchange
<i>exp</i>	experimental
<i>frag</i>	fragmentation
<i>GMM</i>	geometric mean model
<i>HMM</i>	harmonic mean model
<i>i*</i>	number average chain length of the involved macroradicals
<i>IN</i>	input for the microkinetic simulations
<i>ini</i>	initiation
<i>L</i>	corresponding to long chain length range
<i>NU</i>	in non-uniform polymer matrix
<i>OUT</i>	output of the microkinetic simulations
<i>p</i>	propagation
<i>p,0</i>	propagation of R_0 with monomer
<i>p,I</i>	propagation of I^* with monomer
<i>p,macro</i>	propagation of macroradical with macromonomer
<i>pol</i>	polymerization
<i>prop</i>	propagation
<i>re-in</i>	re-initiation
<i>S</i>	corresponding to short chain length range

t	termination
tc	termination by recombination
td	termination by disproportionation
$term$	termination
$t=0$	at time $t = 0$ s
tot	total
tr	transfer to conventional CTA in FRP, degenerative RAFT exchange between macroradical and dormant polymeric species in RAFT polymerization
$tr,0$	degenerative RAFT exchange between macroradical (R_n) and R_0X
$-tr,0$	degenerative RAFT exchange between macro-RAFT CTA (R_nX) and R_0
trM	transfer to monomer
U	in uniform polymer matrix
$x=0$	at zero monomer conversion

Superscripts

*	radical center
i,j	chain length of involved macromolecules
i^*	number average chain length of the involved macroradicals
L^*	number average chain length of the involved long chain macroradicals

<i>L</i>	long chain population
<i>n,m</i>	chain length of involved macromolecules
<i>S*</i>	number average chain length of the involved short chain macroradicals
<i>S</i>	short chain population
<i>SS</i>	only secondary radical(-derived) species involved
<i>ST</i>	secondary and tertiary radical(-derived) species involved, first species in chemical reaction equation secondary, second is tertiary
<i>TS</i>	secondary and tertiary radical(-derived) species involved, first species in chemical reaction equation tertiary, second is secondary
<i>TT</i>	only tertiary radical(-derived) species involved
<i>T</i>	tertiary radical(-derived) species involved

Abbreviations

AIBN	azobis(isobutyronitrile)
ATR	attenuated total reflection
ATRP	atom transfer radical polymerization
backb	backbiting
β -sc	β -scission
CTA	chain transfer agent

CL	chain length
CLD	chain length distribution
CPDB	2-cyano-2-propyl dithiobenzoate
CRP	controlled radical polymerization
DMPA	2,2-dimethoxy-2-phenyl acetophenone
DoPAT	2-(dodecylthiocarbonothioylthio) propionic acid
DSC	differential scanning calorimetry
DMM	diffusion mean model
EPR	electron paramagnetic resonance
ESI-MS	electron spray ionization – mass spectrometry
ESR	electron spray resonance
exch	RAFT exchange
exchT	RAFT exchange involving tertiary radical(-derived) species
FRP	free radical polymerization
FTIR	fourier transform infrared
FVT	free volume theory
GMM	geometric mean model
HMM	harmonic mean model
¹ H-NMR	proton nuclear magnetic resonance

INT	RAFT intermediate radical species formed by addition of a (macro)radical onto a dormant polymeric species or initial small RAFT CTA
INT-(n,m)	RAFT intermediate radical species formed by addition of R_n onto R_mX (if $n, m = 0$: R_0 or R_0X)
LCB	long chain branch
LSODA	Livermore solver for ordinary differential equations
macro-RAFT CTA	macro-reversible addition-fragmentation chain transfer agent (dormant polymeric species)
macroprop	macropropagation: propagation of macroradical with macromonomer
MeOH	methanol
MM	macromonomer
MMA	methyl methacrylate
MCR	mid-chain radical
<i>n</i> BuA	<i>n</i> -butyl acrylate
(N)IR	(near) infrared
NMP	nitroxide mediated polymerization
PLP	pulsed laser polymerization
PMMA	poly(methyl methacrylate)
P <i>n</i> BuA	poly(<i>n</i> -butyl acrylate)

prop	propagation
propT	tertiary propagation
PS	polystyrene
RAFT	reversible addition-fragmentation chain transfer
RAFT-CLD-T	RAFT – chain length dependent – termination
RAFT CTA	reversible addition-fragmentation chain transfer agent
RDRP	reversible deactivation radical polymerization
SCB	short chain branch
SEC	size exclusion chromatography
SG1	N-(2-methyl-2-propyl)-N-(1-diethylphosphono-2,2-dimethylpropyl)-N-oxyl
side	side reactions
SP-PLP	single pulse pulsed laser polymerization
STDEV	standard deviation
TCL	targeted chain length
term	termination
termT	tertiary termination
THF	tetrahydrofuran
UV-VIS	ultraviolet – visible

Chapter 1: Introduction

1.1 General scope of the PhD thesis

Originally driven by the endeavor to mimic natural fibers and rubbers by a synthetic equivalent, nowadays, synthetic polymer products have taken an indispensable position in everyday life.¹ The initial incentive to access ‘natural’ characteristics via other resources has long since been gradually overruled by the general acknowledgement that synthetic polymers retain the inherent ability to be tailor-made for the aspired use.^{2,3} Particularly, different monomer types can be combined to incorporate the desired properties in the resulting synthetic (co)polymer, *e.g.* toughness, chain flexibility, *etc.* Moreover, the addition of compounds that interfere with the polymerization mechanism during the polymer synthesis to obtain previously unattainable physical properties or the mixing of the resulting polymer with additives to enhance the further processability, are two other examples of developments that have been established to match the specific consumer demands.²⁻⁴ Numerous new application fields have arisen quickly with main merits in the (food) packaging and the consumer goods industry, and the production of new construction materials.

One of the most important polymerization mechanisms is free radical polymerization (FRP). The vast industrial exploitation of FRP, covering both commodity and high-tech polymer production, is ascribed to its high monomer versatility, broad operating window (-80 up to 250 °C) and compatibility with benign solvents such as water, both in homogeneous and heterogeneous fashion (*e.g.* emulsion and suspension polymerization).²⁻⁴ However, in FRP, a broad chain length distribution (CLD) is typically obtained and thus a highly inhomogeneous polymer product. Additionally, no precise control over the topology and composition of the individual polymer chains is accessible, which can be detrimental in for instance biomedical applications, *e.g.* drug encapsulants.

Alternatively, reversible deactivation radical polymerization (RDRP), also known as ‘controlled radical polymerization (CRP)’, has paved new avenues towards the synthesis of polymer products with a very high degree of structural specificity.^{4,5} Via addition of a reversible deactivating agent, which also introduces functionality (X) into the polymer chain, tailor-made macromolecular architectures such as (multi-)block copolymers, star polymers and molecular brushes are readily obtained via well-established experimental procedures, leading to niche applications in electronics,⁶ the coating industry⁷⁻⁹ and biomedical technology.^{4,5} Due to the temporal deactivation of the macroradicals into dormant polymer species by the mediating agent at each moment during the polymerization a well-defined polymer matrix is obtained which is characterized by a single predefined chain length under ideal well-controlled conditions. Three main classes of RDRP techniques can be discerned, for which a differentiation is made based on the nature of the reversible deactivation mechanism of the macroradicals, *i.e.* nitroxide mediated polymerization (NMP), transition metal-based RDRP, *e.g.* atom transfer radical polymerization (ATRP), and reversible addition-fragmentation chain transfer (RAFT) polymerization.^{4,5} In ideal conditions, the polymer properties obtained via these RDRP methods tend towards the characteristics obtained by living ionic polymerization but under far less stringent reaction conditions. Accordingly, the associated market value of these RDRP products is anticipated to be over 20 billion dollar per year,¹⁰ invoking a huge scientific interest, as evidenced by the large number of papers published.

In this PhD thesis, RAFT polymerization is studied, which is the most versatile RDRP method regarding monomer compatibility. In addition, due to its strong resemblance to FRP it contains the highest potential for large scale industrial realization.^{5,11} In contrast to NMP and ATRP, the control over the polymer properties in RAFT polymerization is established by an *exchange* mechanism, involving a large number of kinetic parameters that need to be

accurately known for a proper fundamental understanding of the RAFT polymerization process (requirement (i)). Furthermore, reaction rates can become diffusion-controlled at the micro-scale due to the strong increase in viscosity of the polymerization mixture.^{12,13} Hence, it is imperative for an efficient optimization of RAFT polymerization and radical polymerization in general, that the influence of diffusional limitations on the chemical reaction rates is mapped for all occurring reactions (requirement (ii)). Only in case these requirements (i)-(ii) are met, model-guided design of polymer materials can be applied to unlock the full potential of radical polymerization techniques.^{14,15}

In the following chapters, on the one hand fundamental methods are developed and validated to retrieve lacking fundamental knowledge for the requirements (i)-(ii) (Chapter 2-4) and on the other hand model-guided design is applied to design RAFT polymerization processes (Chapter 5). In the current chapter, the developed methodologies are situated with respect to previous kinetic studies on radical polymerization kinetics, followed by a more detailed outline of the remaining chapters.

1.2 Main methods to determine rate coefficients in RAFT polymerization

As highlighted above, RAFT polymerization exhibits many similarities to FRP.^{5,11,16} Since radicals (I^*) are generated by decomposition of a conventional radical initiator I_2 in a polymerization mixture that contains besides monomer (M) also a (small) RAFT chain transfer agent (RAFT CTA; R_0X), RAFT specific *exchange* events with R_0X are superimposed on a conventional FRP scheme, mainly consisting of initiation, propagation and termination, as shown in Figure 1.1. One of the key features of RAFT polymerization is that a dormant polymer molecule, *i.e.* a polymer chain with X -moiety in Figure 1.1 as initially formed upon exchange with R_0X , also acts as a macro-RAFT CTA later on (Scheme 1.1). All dormant macrospecies thus induce exchange events with other radicals in the polymerization mixture.

Hence, under ideal conditions uniform characteristics of all polymer chains can be obtained due to an equal “growth probability” for every macrospecies. Ideally, all polymer chains possess end-group functionality X and a narrow chain length distribution (CLD) is obtained. A proper choice of the RAFT CTA R_0X is crucial for an efficient RAFT polymerization, which is determined by the chemical nature of the R_0 - and the Z -group (Scheme 1.1). The Z -group (de)activates the carbon-sulphur double bond and (de)stabilizes the RAFT intermediate radical (INT in Figure 1.1 and Scheme 1.1) thus determining the addition/fragmentation rates. On the other hand, R_0 must exhibit a reactivity for addition to the monomer of at least the same magnitude as the macroradicals in order not to induce an inhibition period before the start of the polymerization. However, besides the RAFT exchange mechanism, interference of side reactions, such as termination between macroradicals, classical chain transfer, and the RAFT specific cross-termination between macroradicals and the RAFT intermediate radicals (INT), typically also take place, leading to a loss of control. The fate of these intermediate radicals (INT) has been the subject of an intense scientific debate in an attempt to explain the significant retardation induced by some RAFT CTAs compared to the corresponding FRP reaction.^{13,14} Many theories have been proposed among which termination reactions of the intermediate radical with itself or any other radical in the polymerization mixture, *i.e.* so-called ‘cross-termination’, and slow fragmentation of the initial RAFT CTA towards the side of the dormant polymer species were the main conflicting hypotheses. However, for many RAFT CTA monomer combinations, such retardation compared to FRP is not observed and they will be designated further as ‘efficient’ RAFT polymerizations. In case of such efficient RAFT exchange, side reactions with the intermediate RAFT radical can be ignored and a degenerative RAFT polymerization mechanism can be assumed in which the exchange event can be formally described by an exchange rate coefficient.^{5,11,16}

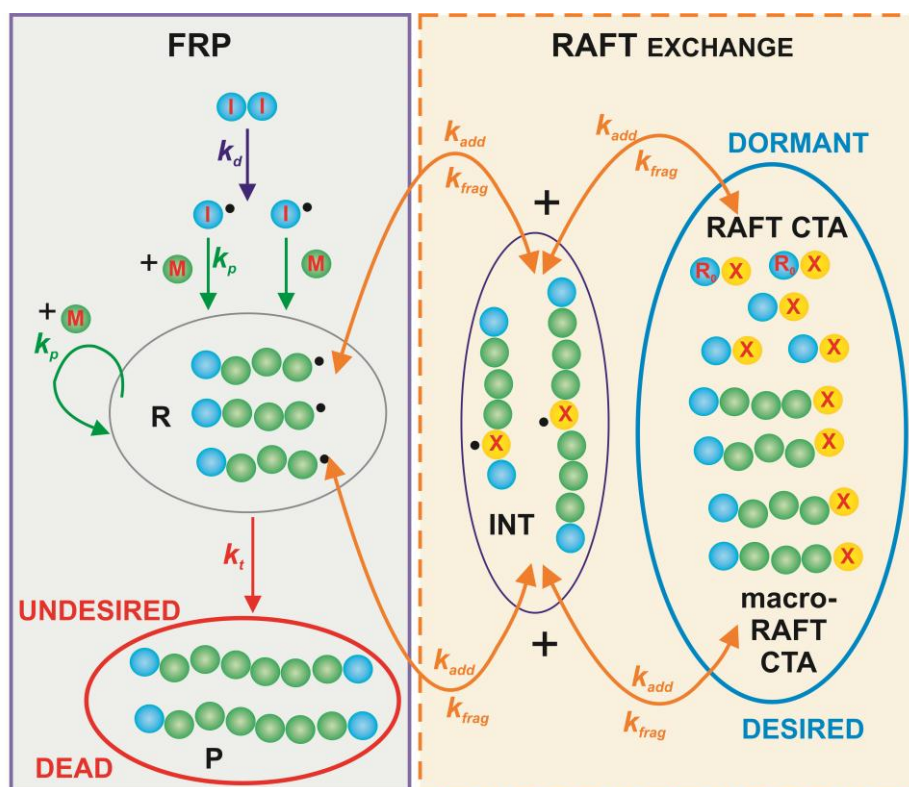
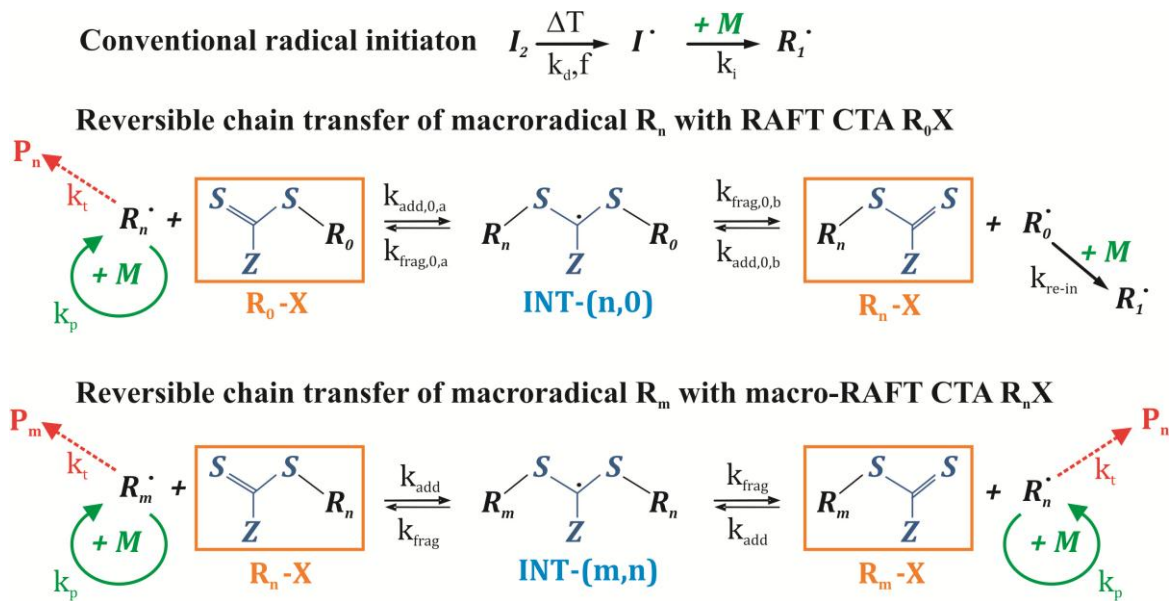


Figure 1.1: Schematic representation of the RAFT polymerization mechanism as a RAFT exchange process superimposed on a conventional FRP scheme. For simplicity, both the conventional initiator-derived radicals (I^*) and the RAFT CTA derived radicals (R_0) are depicted in blue. R stands for macroradical, P for dead polymer, INT for intermediate radical species, M for monomer and X denotes the RAFT CTA functionality (yellow). Radical center indicated by black dot.

Since in a RAFT polymerization in principle three different types of radical species (I^* , R_0 and R_n ; Scheme 1.1) and consequently also three types of RAFT CTA-derived non-radical species (IX , R_0X and R_nX) can be present, a large number of individual addition and fragmentation rate coefficients need to be known for a full description of the RAFT exchange process (Scheme 1.1). Furthermore, a proper understanding of RAFT polymerization kinetics cannot be decoupled from a profound knowledge of FRP kinetics (Figure 1.1). In general, an accurate kinetic description of radical polymerization is a tedious task as a large number of different radical species has to be tracked for which additionally the reactivity can depend on the chain length. The latter prompts for an inclusion of the complete CLD for each macrospecies for which such chain length dependency is observed, highly complicating the kinetic model.^{14,15,17} Furthermore, diffusional limitations at the micro-scale can influence the

observed reaction rates if the viscosity of the polymerization mixture becomes sufficiently high.^{13,17,18} This often leads to the consideration of so-called ‘apparent’ kinetics. It can be concluded that multiple hurdles need to be overcome to enable model-guided design of RAFT polymerization in which, ultimately, a relation between the reaction conditions and the final macroscopic material properties is aimed at via an accurate description of the corresponding polymer microstructure.¹⁴



Scheme 1.1: RAFT polymerization scheme with as RAFT CTA R_0X . R_n : macroradical of chain length n ; P_n : dead polymer chain of chain length n ; R_nX : dormant species with chain length n ; $INT-(m,n)$: intermediate radical species with chain lengths m and n for the two arms; I^\cdot : conventional initiator radical fragment; M : monomer; for I^\cdot different from R_0 : no exchange considered with I^\cdot and IX .

Several methodologies have been currently developed based on both experimental and theoretical results to determine the intrinsic/apparent rate coefficients common with FRP and those for the RAFT specific exchange reactions. The fundamental concepts of intrinsic and apparent rate coefficients are first explained, followed by a concise overview of the main methods to determine these rate coefficients for the most important reactions in FRP and RAFT polymerization. This overview is included to clarify the relevance of the developed techniques in the following chapters in this PhD thesis.

1.2.1 Intrinsic rate coefficients

The intrinsic reactivity for a reaction (k_{chem}) reflects the chemical reactivity of the corresponding reactants if they are at reaction distance from each other. Up to this point of technological development, it is impossible to experimentally probe a single elementary reaction step. Instead, k_{chem} must ideally be derived by the measurement of overall kinetics via advanced spectroscopic techniques for conditions that correspond to the ‘reaction-controlled regime’, *i.e.* the time-scale for reaction needs to be significantly larger than the one for diffusion of the reactant molecules, so that the observed reaction rate will only be determined by the intrinsic or chemical reactivity.^{17,18}

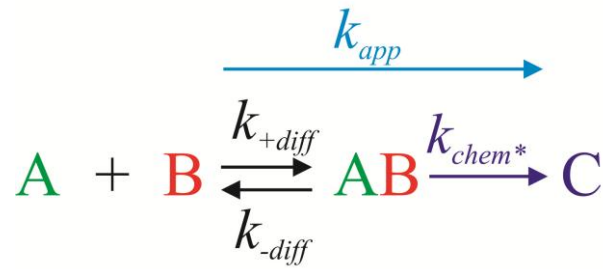
In particular, the advent of pulsed laser polymerization (PLP) techniques has revolutionized the study of radical polymerization kinetics^{13,19-21} as it enables the accurate determination of the intrinsic propagation rate coefficient $k_{p,chem}$ as function of temperature in a straightforward way (*cf.* Section 1.2.4). Since $k_{p,chem}$ is used as input variable for a multitude of other experimental methods to obtain (intrinsic) rate coefficients in radical polymerization (see further), the development of PLP can be considered as a milestone in the understanding and modeling of radical polymerization kinetics.^{13,15} Alternatively, parameter fitting by regression to experimental polymerization data, again with $k_{p,chem}$ often as input, can in many cases be a valuable tool to quantify the intrinsic reactivity of certain reactions.²² However, inappropriate choice of the kinetic model can induce large systematic errors and thus unreliable rate coefficients can result, which is particularly relevant for complex polymerization systems.^{23,24} On the other hand, significant research effort has been devoted to the identification of model compounds that mimic individual reactions occurring during the radical polymerization, thus markedly lowering the complexity of the parameter fitting procedure.^{5,25} Although valuable qualitative data can be retrieved, corresponding reported rate coefficients should be treated with care as changes in the chemical environment can have a pronounced effect on the

intrinsic reactivity.^{26,27} Finally, it should be stressed that the scope of the outlined experimental methods above is additionally constrained by the possible intrinsic chain length dependency of the rate coefficients in radical polymerization,²⁸ as discussed in the following sections (Section 1.2.4-2.7).

Complementary to the aforementioned experimental-based techniques, theoretical or *ab initio* calculations can be performed which in principle allow to deduce the intrinsic reactivity of the considered reaction, as reactants are assumed to be at reaction distance, and, importantly, to assess the influence of chain length dependencies and penultimate effects.²⁹⁻³³ However, as the accuracy of the calculations is inversely proportional to its corresponding computational cost, a compromise needs to be made between both, particularly for macromolecular systems in the condensed phase.^{5,15} Nevertheless, structure reactivity trends have been successfully determined via theoretical calculations for reversible mediating agents in ATRP, NMP and RAFT polymerization, enabling an efficient screening of virtual candidate molecules for a given monomer system prior to experiment.^{30,34,35}

1.2.2 Apparent rate coefficients

The strong increase of the viscosity of the polymerization mixture in radical polymerization induces a competition at the micro-scale between transport of the reacting molecules (A , B) towards (k_{+diff}) and away from each other (k_{-diff}) and the subsequent chemical reaction (k_{chem*}) as shown in Scheme 1.2, necessitating the consideration of ‘apparent’ kinetics.¹⁵



Scheme 1.2: Fundamental basis of the parallel encounter pair model for the description of apparent kinetics (k_{app}). Reactants can diffuse towards (k_{+diff}) or away from each other (k_{-diff}) and need to be at reaction distance (forming the encounter pair AB) for chemical reaction (k_{chem*}) to occur.

The most fundamental implementation of Scheme 1.2 is the so-called ‘parallel encounter pair model’,^{15,17,18,36-38} which calculates the apparent rate coefficient for the irreversible reaction between reactants A and B producing C (k_{app}) based on the pseudo-steady-state assumption for the calculation of the concentration of the ‘encounter pair’ AB:

$$\frac{d[C]}{dt} = k_{app}[A][B] = k_{chem*}[AB] \quad (1)$$

$$\frac{d[AB]}{dt} = 0 = k_{+diff}[A][B] - k_{-diff}[AB] - k_{chem*}[AB] \quad (2)$$

and thus:

$$[AB] = \frac{k_{+diff}[A][B]}{k_{-diff} + k_{chem*}} \quad (3)$$

In which [] denotes the concentration (mol L⁻¹). By substitution of Equation (3) in Equation (1) an expression for k_{app} is obtained:¹⁷

$$\frac{1}{k_{app}} = \frac{1}{k_{+diff}} + \frac{1}{K_{diff}k_{chem*}} \quad (4)$$

in which K_{diff} is the equilibrium coefficient for the diffusion process:

$$K_{diff} = \frac{k_{+diff}}{k_{-diff}} \quad (5)$$

Via Equation (4) the relevance of physical transport phenomena on the observed (apparent) reaction rate can be assessed. For $k_{chem*} \ll k_{diff}$ and thus $K_{diff}k_{chem*} \ll k_{+diff}$ the first term on

the right-hand-side of Equation (4) is negligible compared to the first one, which corresponds to the reaction-controlled limit:¹⁷

$$k_{app} = K_{diff} k_{chem*} \quad (6)$$

On the other hand, if $k_{chem*} \gg k_{diff}$, the diffusion-controlled limit is obtained:

$$k_{app} = k_{+diff} \quad (7)$$

In practice, it is assumed that K_{diff} is conversion independent and, hence, $K_{diff} k_{chem*}$ can be replaced by an intrinsic rate coefficient k_{chem} ($\text{L mol}^{-1} \text{s}^{-1}$) at each moment during the polymerization:^{13,17,36,37}

$$\frac{1}{k_{app}} = \frac{1}{k_{+diff}} + \frac{1}{k_{chem}} \quad (8)$$

When apparent kinetics hold and the limiting conditions in Equation (6) and (7) are not met, both k_{chem} and k_{+diff} have to be accurately known for a proper understanding of the considered polymerization process. General methods to determine k_{chem} have been discussed in the previous section, whereas for k_{+diff} the pioneering Smoluchowski theory can be applied:³⁸

$$k_{+diff} = 4\pi\sigma'N_A(D_A + D_B) \quad (9)$$

In this expression, σ' is the reaction distance (m) which can be approximated by the Lennard Jones diameter,³⁹ N_A the Avogadro constant and $D_{A,B}$ the translational diffusion coefficient of component A and B ($\text{m}^2 \text{s}^{-1}$). Note that in general, for macromolecules, besides translational diffusion of the polymer coil as a whole, also a contribution of segmental rearrangement of the polymer coil for the active centers to diffuse towards each other, and the spatial displacement of the chain end due to propagation, *i.e.* reaction diffusion, have to be included for the calculation of $D_{A,B}$.¹⁸ However, reaction diffusion can often be neglected and for simplicity the translational and segmental diffusion coefficients are mostly assumed equal as this only leads to minor deviations.¹³ In contrast, for termination reactions, which involve two

macroradicals, both segmental diffusion and reaction diffusion need to be additionally considered particularly at higher monomer conversions^{13,40} as discussed further.

Several theories exist to calculate the diffusion coefficients in Equation (9), but the most important one in radical polymerization is the Vrentas and Duda free volume theory (FVT).⁴¹⁻

⁴⁴ This theory relies on the basic idea that a molecule (or part of it) is only able to move in a polymerization mixture if hole free volume is available for a jump of the molecule (or part of it).¹⁵

For a binary polymerization mixture with polymer fraction w_p and monomer mass fraction w_m , the corresponding diffusion coefficient for a non-polymeric component A is given by:

$$D_A = D_{A,0} \exp\left(-\frac{E_a}{RT}\right) \exp\left(-\frac{\tilde{V}_A^*}{\frac{\tilde{V}_{FH}}{\gamma}}\right) \quad (10)$$

with $D_{A,0}$ an average pre-exponential factor, E_a the activation energy for a diffusional jump, \tilde{V}_A^* the critical molar hole free volume for a jumping unit of the molecule A , γ an overlap factor to account for the competition of multiple (jumping units of) species in the polymerization mixture for the same hole free volume, and \tilde{V}_{FH} the total hole free volume per mole of jumping units.^{15,36,37,41} The pre-exponential factor $D_{A,0}$ in Equation (10) accounts for interactions with neighboring molecules during a diffusional jump and can be determined based on the Flory-Huggins theory,⁴⁵ however often an average value derived from experiment or model compounds is used.^{15,36} The critical molar hole free volume \tilde{V}_A^* can be calculated based on group contribution methods and the total hole free volume is typically assumed as an additive property with the individual contributions calculated based on dynamic viscosity measurements.³⁶

On the other hand, for the calculation of the diffusion coefficient of a polymeric species, an extra scaling factor for the pre-exponential factor is added to Equation (10), which depends on the chain length n and reflects the diffusion behavior of the polymer chains in the polymerization mixture. Scaling laws are often used which depend besides the chain length also on the polymer mass fraction in the reaction mixture and tend to the Stokes-Einstein ($D \sim n^{-0.5}$) and reptation diffusion limit ($D \sim n^{-2}$) for w_p respectively close to zero and one.^{15,46} An example of a commonly applied universal scaling law was proposed by Griffiths *et al.*:⁴⁷

$$D_{p,n} = \frac{D_m}{n^{0.664+2.02w_p}} \quad (11)$$

in which $D_{p,n}$ is the translational diffusion coefficient of the polymer with chain length n and D_m is the translational diffusion coefficient of the monomer.

It is clear from Equation (8)-(11) that a large amount of parameter values need to be accurately known in order to calculate reliable diffusion coefficients (Equation (9)-(11)) and subsequently predict their contribution to the observed apparent kinetics (Equation (8)). Therefore, the development of experimental techniques that *directly* determine k_{app} at different stages of the polymerization reaction has received considerable research interest (*cf.* Section 1.2.3-2.7).^{13,19,20} The derived semi-empirical correlations for k_{app} should however be regarded with caution as the application scope can be limited and often parameters are used with no physical relevance. In what follows, the main methods for the calculation of intrinsic/apparent rate coefficients are highlighted for each key reaction in FRP/RAFT polymerization.

1.2.3 Initiation

In radical polymerization, radicals are typically generated by decomposition of an initiator molecule under influence of an external heat or radiation source, as shown in Figure 1.1 with

a conventional radical initiator I_2 . If the initiator molecule is not involved in any other side reaction, *e.g.* transfer reactions with macroradicals, its concentration decay is independent from other reactions occurring in the polymerization process and can be described in an ideal batch reactor by the following continuity equation:³

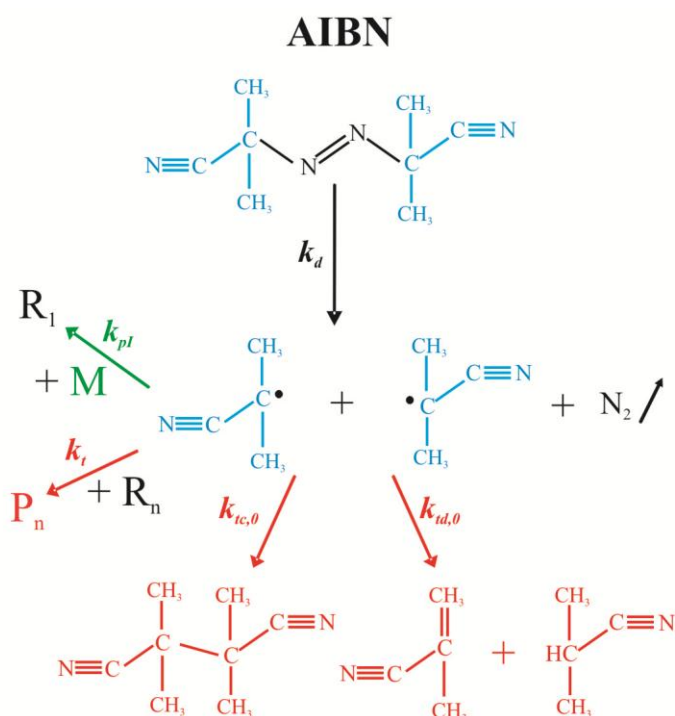
$$\frac{d[I_2]}{dt} = -k_d[I_2] \quad (12)$$

In this expression, k_d is the decomposition rate coefficient (s^{-1}) and $[I_2]$ the concentration of initiator I_2 (mol L^{-1}) and assuming a constant reaction volume. Integration of Equation (12) enables the direct determination of k_d if the concentration decay of I_2 is monitored as function of the reaction time t :

$$[I_2] = [I_2]_0 \exp(-k_d t) \quad (13)$$

In RAFT polymerization, the conventional radical initiator azobis(isobutyronitrile) (AIBN) is the most important thermally induced radical source and is widely applied for a large range of monomers both in homogeneous and heterogeneous systems.⁵ The thermal decomposition mechanism of AIBN and the main consecutive reactions of the formed cyano-isopropyl radicals are presented in Scheme 1.3.⁴⁸ As nitrogen is eliminated, the initiator-derived radicals (cyano-isopropyl) do not form AIBN again upon recombination, instead a dinitrile is formed (Scheme 1.3). The cyano-isopropyl radicals can also react with each other via disproportionation and can undergo termination reactions with other radical species present in the polymerization mixture in spite of the desired propagation reaction with monomer molecules (Scheme 1.3). This is quantified by the (apparent) initiator efficiency f , which denotes the fraction of conventional initiator-derived radicals that can escape or diffuse out of a theoretical solvent cage around I_2 to react with monomer and thus to effectively initiate chain growth, implicitly assuming that the concentration of I_2 species is very low so that the initiator radicals from different solvent cages cannot encounter each other.^{3,4,49,50} Hence, in

kinetic modeling studies, this apparent initiator efficiency replaces the explicit modeling of the side reactions indicated with red in Scheme 1.3. Since in RAFT polymerization more radical species types are present in the polymerization mixture than in the corresponding FRP, in principle, the initiator efficiency as defined above corrects for the corresponding additional side reactions not leading to chain initiation.^{5,51} However, it is recommended to use the definition for f in the corresponding FRP and add the additional side reactions in the RAFT polymerization explicitly, *i.e.* implicitly assuming that they take place outside the solvent cage.



Scheme 1.3: Decomposition scheme of AIBN in which nitrogen is released and subsequent main reaction possibilities of the cyano-isopropyl radicals. Undesired side reactions which are covered by the initiator efficiency f are marked in red. R_n : macroradical of chain length n ; P_n dead polymer species of chain length n .

It should be stressed that for AIBN, k_d in Equation (12)-(13) is an intrinsic rate coefficient which is not influenced by the increasing viscosity throughout the polymerization. Different on-line analysis techniques have been used in literature to determine the AIBN conversion and subsequently k_d via Equation (13). UV-VIS spectrophotometry has been demonstrated to yield the most accurate results by following the decay of the absorbance at 347 nm.^{48,52,53}

However, as the nature of the solvent and monomer significantly influence the intrinsic decomposition reactivity of AIBN, separate studies for each polymerization system need to be performed in principle.⁵⁴

On the other hand, the initiator efficiency f is much more difficult to quantify and is affected by diffusional limitations at higher monomer conversions,^{17,18,50,55,56} hence an apparent f needs to be considered. During the transition of the initiator-derived radicals, side reactions with other molecules inside the solvent cage can take place with an increasing probability for slower diffusion rates, *i.e.* the so-called cage effect.^{50,55} For a slower diffusion out of the cage a lower apparent initiator efficiency is thus obtained. Hence, for AIBN, at high viscosities the formation of the dinitrile by recombination of the initiator-derived radicals will be promoted (*cf.* Scheme 1.3). It should be mentioned for completeness that in the case of a radical initiator which undergoes homolytic cleavage of a single bond upon decomposition, the recombination of the initiator-derived radicals yields the original initiator molecule, implying that the initiator decomposition rate coefficient in Equation (14)-(15) becomes in principle an apparent rate coefficient for very high viscosities as it will include an additional efficiency factor to correct the intrinsic rate coefficient for the regenerated fraction of initiator.^{56,57}

The initiator efficiency f of AIBN can be experimentally accessed via (i) the addition of a radical scavenger and the subsequent simultaneous monitoring of the concentration decay of both AIBN and the added compound, (ii) the quantification of the product spectrum in a FRP initiated by AIBN, or (iii) via the regression of expressions based on overall reaction kinetics to experimental conversion or radical concentration data.^{49-51,55} In method (i), f is determined from the difference between the rate of depletion of AIBN and the radical scavenger. On the other hand, in method (ii), the increase of nitrile end-groups in FRP initiated by AIBN is compared with the decrease of the AIBN concentration. In the third method (iii), the determination of f relies on the availability of accurate rate coefficients for propagation and

termination throughout the polymerization reaction, and either the pseudo-steady-state assumption for the calculation of the total radical concentration or the accurate measurement of the latter, *e.g.* via electron paramagnetic resonance (EPR) spectroscopy.

To describe the influence of diffusional limitations on the initiator efficiency f , two important models have been put forward in literature to determine the apparent initiator efficiency f_{app} . In the first method, a parallel encounter based model is assumed to hold for f_{app} similar to the description of apparent rate coefficients (*cf.* Section 1.2.2):^{17,18,56}

$$\frac{1}{f_{app}} = \frac{1}{f_{chem}} + \frac{1}{k_{diff,I}} \quad (14)$$

In this expression, on the one hand, f_{chem} is the intrinsic initiator efficiency which accounts for all the side reactions of the initiator-derived radicals preventing the desired propagation with monomer in FRP, including the termination reactions with other initiator-derived radicals within the solvent cage. On the other hand, $k_{diff,I}$ is the rate coefficient for diffusion of the initiator-derived radicals out of the solvent cage and can be determined based on the Smoluchowski equation (Equation (9)). If $k_{diff,I}$ becomes small, *i.e.* at high monomer conversions, f_{app} will be significantly affected by diffusional limitations. The second method was originally developed by Shen *et al.*⁵⁵ and is based on the rationale that f_{app} will mainly be determined by the diffusion and termination reactions of the initiator-derived radicals inside the solvent cage. Once exited from the solvent cage, the initiator-derived radicals are assumed to undergo solely propagation reactions with monomer. Hence, f_{app} can be expressed as a probability to exit the solvent cage:

$$f_{app} = \frac{r_{escape}}{r_{escape} + r_{term}} \quad (15)$$

in which r_{escape} and r_{term} are respectively the rates for initiator-derived radicals to exit the solvent cage or terminate with each other inside the solvent cage. Based on Equation (15) and

on the idea that $r_{escape} \sim D_I$, the diffusion coefficient of the initiator-derived radicals in the solvent cage, Shen *et al.* derived a simple expression for f_{app} .⁵⁵

$$\frac{1}{f_{app}} = 1 - \frac{D_{I,x=0}}{D_I} \left(1 - \frac{1}{f_{x=0}} \right) \quad (16)$$

in which $D_{I,x=0}$ and $f_{x=0}$ are, respectively, the diffusion coefficient and initiator efficiency of the initiator-derived radicals at zero conversion. The diffusion coefficients $D_{I(x=0)}$ are calculated via the free volume theory, in which lacking parameters are determined based on a fit to experimental data.^{50,55}

Although diffusional limitations on initiation only become important at higher monomer conversion, they can be of high relevance for RAFT polymerization in which the presence of conventional radical initiator throughout the entire polymerization reaction is a prerequisite to reach high monomer conversions, as dictated by many applications and also desired in an industrial context.¹⁷

1.2.4 Propagation

The propagation reaction is one of the most important steps in a radical polymerization process as it embodies on the one hand the actual growth of the polymer chains, and, on the other hand, determines the rate at which a certain extent of reaction is reached and its concomitant heat production. While the former feature directly relates to the resulting polymer properties and thus the end-use of the polymer product, the latter is crucial to assess the economic feasibility of the polymerization process at industrial scale and the necessary reactor control equipment. Moreover, as propagation is the key reaction of a radical polymerization process, many techniques to quantify the (apparent) reactivity of other reactions occurring in radical polymerization, *e.g.* termination, chain transfer, ..., are contingent upon accurate knowledge of the propagation rate coefficient k_p (see further).¹⁹

Also, the contribution of reaction diffusion to the observed polymerization rate in the gel regime directly depends on k_p (see further).¹⁸ Hence, for a proper understanding of radical polymerization kinetics, the accurate determination of k_p is indispensable.

As highlighted before, the development of pulsed laser polymerization (PLP) has enabled the reliable quantification of the intrinsic propagation reactivity $k_{p,chem}$ as a function of temperature.²⁰ In particular, the combination of an evenly spaced sequence of laser pulses to initiate the polymerization, with straightforward size exclusion chromatography (SEC) measurements to characterize the CLD, *i.e.* the so-called PLP-SEC method, has emerged as the standard technique to determine $k_{p,chem}$ for a broad range of monomers.²¹ Mostly a laser in the UV-range is used and via a photoinitiator, typically benzoin or acetophenones such as 2,2-dimethoxy-2-phenyl acetophenone (DMPA), during each laser pulse, a nearly instantaneous production of primary photoinitiator-derived radicals results after which propagation and termination reactions can occur in the ‘dark’ period.²⁰ The instantaneous burst of primary radicals at each pulse increases the probability of the macroradicals formed during a previous pulse and still residing in the polymerization mixture to terminate with these photoinitiator-derived radicals. This leads to a characteristic CLD at steady state, as shown in Figure 1.2 which was taken from the recent review by D’hooge *et al.*¹⁵ The chain lengths determined by the inflection points of the CLD, i_s , correspond to the macroradicals for which chain growth occurred during s pulses before terminating with primary photoinitiator-derived radicals:^{15,20,21}

$$i_s = s k_{p,chem} t_0 [M]_0 \quad (17)$$

In this expression, t_0 is the dead time between two pulses (s), *i.e.* the ‘dark’ period, and $[M]_0$ the initial monomer concentration (mol L^{-1}). The exact position of the inflection points, i_s , is relatively easily derived as they correspond to a maximum in the first derivative of the CLD. Hence, Equation (17) provides a straightforward way to determine $k_{p,chem}$ from the CLD at

steady state after pulsed laser initiation, independent of the knowledge of any other kinetic parameter.

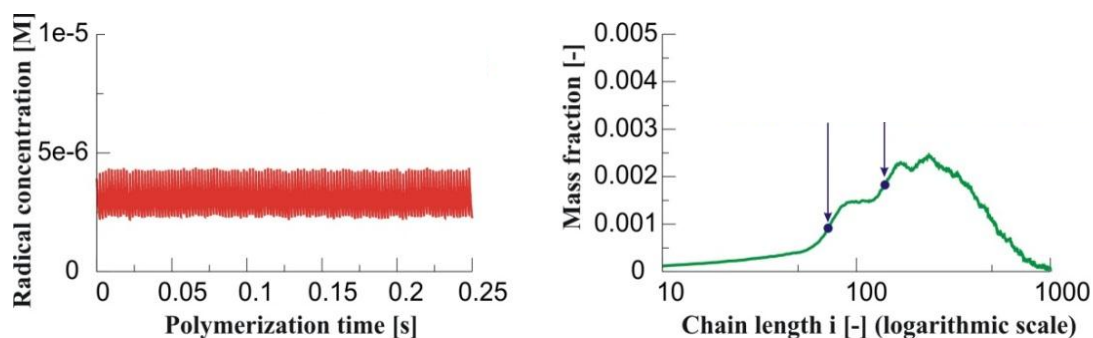


Figure 1.2: Principle of the pulsed laser polymerization – size exclusion chromatography (PLP-SEC) method. Left: Radical concentration for a pulse frequency of 500 Hz. Right: Characteristic chain length distribution. From the position of the inflection points (Equation (17)) the intrinsic propagation rate coefficient can be determined. Figure taken from D’hooge et al.¹⁵

However, for more complex radical polymerizations in which macroradical species with different propagation reactivity are present due to intra- and/or intermolecular chain transfer (e.g. the radical polymerization of acrylates), a featureless CLD can be obtained for which Equation (17) cannot be applied. A careful choice of the PLP conditions via adapting the laser frequency and polymerization temperature, allows to suppress the latter reactions and often to resolve this issue.⁵⁸ Furthermore, the intrinsic propagation rate coefficient is shown to vary significantly with the chain length of the macroradicals and the polarity of the solvent used, which can both be explained by transition state theory.^{27,28,59} Particularly, due to an increased hindrance of the translational and rotational modes in the transition state, the intrinsic propagation reactivity decreases from an initial value $k_{p,chem,0}$ at a chain length of one towards its ‘long chain value’ $k_{p,chem,\infty} \cong 0.1 k_{p,chem,0}$ at a macroradical chain length around 10, as indicated both theoretically and experimentally by Heuts and coworkers^{28,59} and Smith et al.⁶⁰ More recently, Haven et al. highlighted the use of single unit monomer insertion under RAFT conditions to identify more accurately the chain length dependent propagation reactivity.⁶¹ Although of significant fundamental importance, this chain length dependency of $k_{p,chem}$ will

only affect the radical polymerization kinetics to a significant extent if low chain lengths of the final polymer product are aimed at, *i.e.* by addition of large amounts of conventional CTA in FRP or RAFT CTA (R_0X) in RAFT polymerization, and is therefore often neglected in kinetic modeling studies.¹³

Finally, since the propagation reaction involves a small monomer molecule, and intrinsic reactivities as quantified by $k_{p,chem}$ for most monomers are not too high ($\leq 10^5 \text{ L mol}^{-1} \text{ s}^{-1}$), the propagation reaction is chemically controlled until high monomer conversions (80-90%) due to the much larger values of the corresponding translational diffusion coefficients of the monomer.^{17,18} Only in the so-called ‘glass regime’ in which the glass-transition temperature of the polymerization mixture becomes lower than the reaction temperature, the diffusion of the monomer becomes significantly hindered and the apparent propagation rate coefficient drops rapidly towards zero, leading to a cessation of the polymerization reaction. For this reason, diffusional limitations on propagation reactions are often omitted in kinetic studies of RAFT polymerization.

1.2.5 Termination

Of equal importance as the previously discussed propagation reaction are termination reactions between macroradicals. Such reactions stop the chain growth process and consequently directly determine the obtained polymer properties and the time needed to obtain a given polymer product yield. Additionally, in RAFT polymerization (and RDRP in general), termination reactions lead to the undesired formation of dead polymer molecules that contain no RAFT CTA functionality, and are thus unavailable for post-modification reactions or subsequent RAFT polymerization with a different monomer, hampering precision macromolecular design. In contrast to propagation, however, termination reactions in radical polymerization involve two macroradicals and are strongly influenced by diffusional

limitations from low monomer conversions onwards (< 20%) so that always an apparent termination reactivity needs to be considered.^{13,17,18,40} In particular, at intermediate conversions, the apparent termination reactivity drops drastically leading to a rapid autoacceleration of the polymerization rate, *i.e.* the so-called ‘gel-effect’, as first described by Norrish and coworkers.^{62,63} Hence, quantitative insight into the influence of the viscosity of the reaction mixture and the composition and topology of the polymer matrix on the apparent termination reactivity is of utmost importance for an accurate description of radical polymerization processes. For example, the broad CLD obtained in FRP for both the macroradicals and the dead polymer matrix leads to a termination behavior dominated by short-long termination, which denotes the termination between macroradicals with significantly different chain length. The latter differs markedly from the termination between macroradicals of approximately equal chain length in an equivalent as good as uniform dormant polymer matrix as encountered in a well-controlled RAFT polymerization.¹³

For a termination reaction between two macroradicals to occur, three consecutive steps need to take place as put forward by Benson and North:^{64,65} *(i)* the macroradical polymer coils need to diffuse towards each other by translational diffusion, *(ii)* upon encounter, the chain ends carrying the radical centers must undergo segmental diffusion to be eventually at reaction distance from each other so that *(iii)* the chemical termination reaction can occur. Depending on the chain length of the macroradicals and the composition of the polymerization matrix, *i.e.* polymer mass fraction, chain lengths of the polymer matrix, solvent, ..., the diffusion steps *(i)-(ii)* can be significantly retarded and their relative contribution different.^{13,18,40} For example, a transition from a low to a high chain length at low monomer conversion will cause a shift from translational diffusion to segmental rearrangement of the polymer coils to be controlling the total rate of the diffusive steps as shown in Figure 1.3 taken from Johnston-Hall *et al.*⁴⁰ At higher monomer conversion, a more complex situation is obtained.

Entanglements between the polymer coils will reduce the mobility of the polymer chains and reaction diffusion will start to compete with the diffusion steps (i)-(ii).^{13,18,40} If reaction diffusion becomes rate-determining, the spatial displacement of the radical chain end is predominantly caused by propagation reactions which consecutively increase the macroradical chain length with one monomer unit. The diffusion coefficient for reaction diffusion of the macroradical, D_{rd} , is proportional to the propagation rate coefficient $k_{p,chem}$ as put forward by Russell and coworkers,^{66,67} implying that for highly active monomer molecules the termination rate is more likely to be controlled by reaction diffusion from a lower conversion onwards:

$$D_{rd} = \beta k_{p,chem} [M] \frac{a^2}{6} \quad (18)$$

with $[M]$ the monomer concentration (mol L^{-1}), a the root-mean-square end-to-end distance per square root of the number of monomer units (m) and β a parameter to take into account the totally flexible and rigid chain limits (-). Importantly, it should be stressed that also the topology of the polymer matrix has a significant influence on the diffusion behavior as the presence of additional entanglement points, induced by *e.g.* cross-links in polymer networks, will impede translational and segmental diffusion and favor reaction diffusion.^{15,18,40}

The previous discussion demonstrates that a proper understanding of the apparent termination reactivity is not straightforward as it is governed by a multitude of different factors that continuously change during the radical polymerization process. As highlighted before, the most complete theoretical description of the apparent termination rate coefficient is obtained by application of the encounter pair model (Equation (8)-(9)) in which the diffusion coefficients of the macroradicals are calculated based on the free volume theory (Equation (10)-(11)).^{13,15,17,18} In principle, contributions of a translational (step (i)), a segmental (step (ii)) and reaction diffusion (competing for (i)-(ii)) are needed. In many cases it suffices to

consider only one average mode of diffusivity. However, the use of the simplified encounter pair model still requires many physical parameters which are often not available and for which the experimental determination is not straightforward.

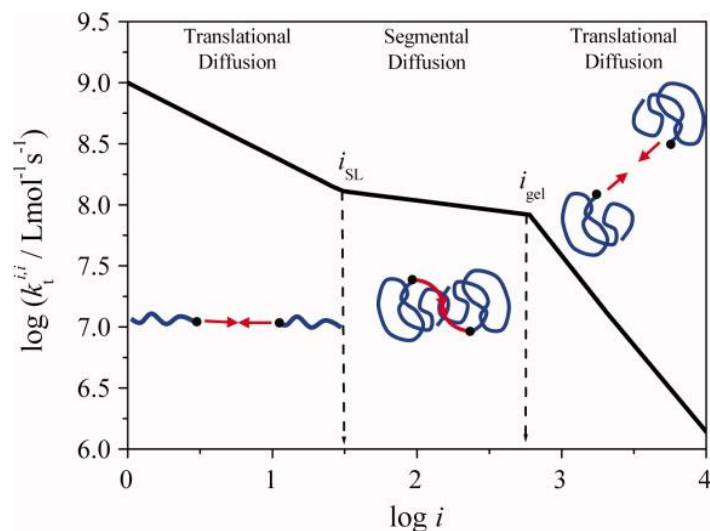


Figure 1.3: Homotermination rate coefficient as function of the chain length at low monomer conversion. Different diffusion mechanisms control the rate of diffusion depending on the chain length of the involved macroradicals. Figure taken from Johnston-Hall and Monteiro.⁴⁰

Alternatively, a large number of experimental techniques have been developed to directly determine the apparent termination reactivity throughout the polymerization reaction.^{13,19}

Although initially a scatter of more than 300% was observed between the outcome of the different methods to determine $k_{t,app}$, significant progress has been made in the last decade and a large set of consistent results are obtained. Earlier deviations are ascribed to the use of non-accurate input parameters for the different methods and substantial differences between the polymer matrices in which the respective values for $k_{t,app}$ were determined.^{13,19} Two main techniques can be discerned that have revolutionized the study of apparent termination and hence radical polymerization kinetics, *i.e.* time-resolved pulsed laser polymerization methods and the RAFT – chain length dependent – termination (RAFT-CLD-T) technique. The kinetic basis of both methods is the continuity equation for the total macroradical concentration (λ_0) in FRP if the contribution of transfer reactions can be neglected:^{13,19,68}

$$\frac{d\lambda_0}{dt} = r_{ini} - r_{term} \quad (19)$$

in which r_{ini} and r_{term} are respectively the rate of initiation and termination.

On the one hand, in PLP a nearly instantaneous initiation of a photoinitiator takes place during the laser pulse (*cf.* Section 1.2.4) so that in the time between two pulses the decay of the radical concentration can be attributed to termination reactions only, at least in a first approximation:

$$\frac{d\lambda_0}{dt} = -r_{term} = -2 \langle k_{t,app} \rangle \lambda_0^2 \quad (20)$$

in which $\langle k_{t,app} \rangle$ is the distribution averaged apparent termination rate coefficient ($\text{L mol}^{-1} \text{s}^{-1}$). The factor 2 is added according to the IUPAC convention although the latter is demonstrated to be wrong in Chapter 2 of this PhD thesis in agreement with earlier literature reports.⁶⁹ However, as in the present chapter an overview of literature methods is aimed at, the kinetic equations as stated in literature will be adopted, which include the (erroneous) factor 2. If the total radical concentration is monitored in time after a single laser pulse, by integration of Equation (20) the corresponding $\langle k_{t,app} \rangle$ can be determined by a regression to the recorded radical concentration profile. The latter can be established in a direct way via coupling of the PLP equipment with time-resolved electron spray resonance (ESR) or EPR measurements in the so-called single pulse (SP) – PLP – ESR/EPR technique,^{70,71} or, in an indirect way by recording the concomitant decay of the monomer concentration $[M]$ after the laser pulse via time-resolved near infrared (NIR) measurements, *i.e.* the SP – PLP – NIR method.⁷²

$$\frac{d[M]}{dt} = -k_p[M]\lambda_0 \quad (21)$$

For both SP-PLP methods, originally, $\langle k_{t,app} \rangle$ in Equation (20) is assumed constant, *i.e.* k_t , and thus apparent termination kinetics are neglected. Note that $\langle k_{t,app} \rangle$ and thus also k_t

accounts for both recombination and disproportionation reactions.⁷⁰⁻⁷² Integration of consecutively Equation (20) and Equation (21) from time $t = 0$ s (end of the laser pulse) to time t after the pulse yields an expression for the decay of the monomer concentration in the time after the pulse:

$$\frac{[M]}{[M]_0} = (2k_t\lambda_{0,t=0} t + 1)^{-\frac{k_p}{2k_t}} \quad (22)$$

In this expression $\lambda_{0,t=0}$ is the amount of radicals generated instantaneously during the laser pulse. In order to determine k_t via SP-PLP-NIR based on Equation (22), accurate values for k_p need to be known, which is not the case in the SP-PLP-ESR/EPR method (Equation (20)).

However, as the macroradical chain length i increases with the time t after a laser pulse according to:⁷⁰⁻⁷²

$$i = k_p[M] t \quad (23)$$

termination is shown to depend on the chain length of the macroradical from the start of the polymerization onwards. Hence, a model for the chain length dependency of $\langle k_{t,app} \rangle$ at constant monomer conversion x (only 0.1% after a laser pulse) is needed for a proper integration of Equation (20). Gilbert *et al.* put forward that for a given conversion, the apparent termination rate coefficients obey to a power law dependency on the chain length i in agreement with Equation (11) for the diffusion coefficient of the polymer molecules:³⁹

$$k_{t,app}^{ii} = k_{t,0} i^{-\alpha} \quad (24)$$

In this expression, $k_{t,app}^{ii}$ is the apparent termination rate coefficient for macroradicals of equal size i ($\text{L mol}^{-1} \text{s}^{-1}$), $k_{t,0}$ is the termination rate coefficient for macroradicals of chain length one ($\text{L mol}^{-1} \text{s}^{-1}$) and α is an exponent which depends on the monomer type. Equation (24) can be directly included in the integration of Equation (20), since in a SP-PLP experiment a Poisson distribution is obtained for the macroradical population due to the

instantaneous initiation and equal propagation probability for each radical, so that $\langle k_{t,app} \rangle \approx k_{t,app}^{ii} = k_{t,0} i^{-\alpha}$. It should be stressed that now two parameters ($k_{t,0}$ and α) instead of one ($\langle k_{t,app} \rangle$) need to be estimated from the regression to the experimental monomer/radical concentration profile. Smith *et al.* extended this power-law model for $k_{t,app}^{ii}$ based on the rationale that depending on the macroradical chain length i translational or segmental diffusion will become rate-determining, as explained previously, leading to different values of the exponent α , *i.e.* the so-called composite model:⁷³

$$\begin{aligned} k_{t,app}^{ii} &= k_{t,0} i^{-\alpha_S} & i < i_{SL} \\ k_{t,app}^{ii} &= k_{t,0} i_{SL}^{-\alpha_S + \alpha_L} i^{-\alpha_L} & i \geq i_{SL} \end{aligned} \quad (25)$$

in which α_S and α_L are the exponents for respectively the short chain and long chain regime, and i_{SL} the so-called cross-over chain length. Via SP-PLP-NIR and SP-PLP-EPR or -ESR, α_S and α_L have been successfully determined for a large number of monomers.¹³ However, the main drawback of these methods is that $k_{t,app}^{ii}$ is always determined in a FRP polymer matrix of dead terminated chains with a broad CLD which differs depending on the experimental conditions, making an unambiguous assessment of the conversion dependency of $k_{t,app}^{ii}$ impossible. Also, $k_{t,app}^{ii}$ for very short chains cannot be accessed via these methods.^{13,19}

Based on the controlled growth of the chain length along the course of a RAFT polymerization, the more elegant SP-PLP-RAFT technique has been developed which enables a pointwise probing of $k_{t,app}^{ii}$ as a function of i and x , independent of any model assumption for $k_{t,app}^{ii}$.⁷⁴ Via addition of an efficient RAFT CTA to a SP-PLP-NIR mixture, that does not degrade upon application of UV-laser pulses and does not cause retardation, only a very small increase of the chain length occurs after each pulse and, importantly, the polymer matrix consists of dormant polymer chains of approximately the same chain length i as the macroradicals, resolving both limitations of conventional SP-PLP-NIR and SP-PLP-EPR/ESR

highlighted above. Since in each pulse only very small changes in i and x are induced, Equation (22) can be safely applied to determine the corresponding $\langle k_{t,app} \rangle \approx k_{t,app}^{ii}$, even for small chain lengths.⁷⁴ On the other hand, as a well-controlled CLD is a key requirement of the SP-PLP-RAFT method, very high chain lengths (> 10000) are not accessible as they are characterized by a loss of control over the polymer properties.¹³

Despite important merits in the study of apparent termination kinetics, PLP equipment is expensive and experimental calibration and data analysis are not always straightforward. Therefore, Barner-Kowollik and coworkers developed the RAFT-CLD-T technique which takes profit of the same features of an efficient RAFT polymerization as SP-PLP-RAFT, *i.e.* at each monomer conversion x termination occurs between macroradicals of approximately equal length i in a polymer matrix of dormant polymer chains also of size i , whereas in principle only a simple differential scanning calorimetric measurement is required.⁶⁸ Furthermore, laser-induced degradation of the RAFT CTA is not an issue anymore as the RAFT-CLD-T technique is based on a conventional thermally initiated RAFT polymerization. Therefore, Equation (19) holds during a RAFT-CLD-T experiment, provided that the RAFT CTA does not induce inhibition or retardation:

$$\frac{d\lambda_0}{dt} = r_{ini} - r_{term} = 2fk_d[I_2] - 2 \langle k_{t,app} \rangle \lambda_0^2 \quad (26)$$

From Equation (21) it is derived that:

$$\lambda_0 = \frac{-\frac{d[M]}{dt}}{k_p[M]} = \frac{r_{pol}}{k_p[M]} \quad (27)$$

in which $r_{pol} = -\frac{d[M]}{dt}$ is the polymerization rate ($\text{mol L}^{-1} \text{s}^{-1}$) if the contribution of transfer to monomer reactions is negligible. Combination of Equation (26)-(27) yields an expression for $\langle k_{t,app} \rangle$ (again including at this stage the erroneous factor 2):^{68,75,76}

$$k_{t,app}^{ii} \approx \langle k_{t,app} \rangle = \frac{2fk_d[I_2] - \frac{d\lambda_0}{dt}}{2\lambda_0^2} = \frac{2fk_d[I_2] - \frac{d\left(\frac{r_{pol}}{k_p[M]}\right)}{dt}}{2\left(\frac{r_{pol}}{k_p[M]}\right)^2} \quad (28)$$

Measurement of the polymerization rate r_{pol} via isothermal DSC measurements thus enables to map $\langle k_{t,app} \rangle$ as a function of i and x throughout the RAFT polymerization reaction by application of Equation (28). However, from this equation it is clear that only reliable values for $\langle k_{t,app} \rangle$ can be obtained if f , k_d and k_p are accurately known. For standard monomer systems (styrene, methyl methacrylate, ...) these kinetic parameters are well-documented in literature. If not, separate measurements need to be performed first (*cf.* Section 1.2.3-2.4). In order to avoid the interference of diffusional limitations on f and k_p , Equation (28) is usually only applied up to 70% conversion.^{68,75,76} Since for each RAFT-CLD-T experiment, a different range of i and x can be accessed by variation of the monomer to RAFT CTA molar ratio, the subsequent combination of the total experimental data set into a surface function $k_{t,app}(i,x)$ as was first done by Johnston-Hall *et al.* can provide useful physical insights into *e.g.* the onset of the gel-effect and can be used as a plug-in for kinetic modeling studies of the corresponding monomer.⁷⁷

While all the previously discussed experimental techniques focus on the determination of the apparent homotermination rate coefficient $k_{t,app}^{ii}$ leading to accurate values for a broad range of monomers, no experimental data was available yet before the start of this PhD research for termination between macroradicals of different length, *i.e.* short-long termination. Instead, simplified models based on different types of averages of the corresponding homotermination rate coefficients are currently used:¹³

$$\text{geometric mean model: } k_{t,app}^{ij} = \sqrt{k_{t,app}^{ii} k_{t,app}^{jj}} \quad (29)$$

$$\text{diffusion mean model: } k_{t,app}^{ij} = 0.5 (k_{t,app}^{ii} + k_{t,app}^{jj}) \quad (30)$$

$$\text{harmonic mean model: } \frac{1}{k_{t,app}^{ij}} = 0.5 \left(\frac{1}{k_{t,app}^{ii}} + \frac{1}{k_{t,app}^{jj}} \right) \quad (31)$$

It should be stressed that only the diffusion mean model (Equation (30)) has a physical basis as it agrees with the Smoluchowski equation for k_{+diff} (Equation (9)). In FRP and a less controlled RDRP, however, a broad CLD for the macroradicals results and short-long termination is the dominant termination process. In order to obtain a full understanding of radical polymerization, it is thus of paramount importance to gain fundamental knowledge on the apparent short-long termination reactivity by experimental determination of $k_{t,app}^{ij}$. Yet, only a theoretical thought experiment of Lovestead *et al.* has been reported in which the RAFT-CLD-T technique is applied to a RAFT polymerization mixture that contains besides RAFT CTA also a certain amount of the corresponding macro-RAFT CTA.^{78,79} Under such conditions a parallel growth of two macroradical distributions with a different average chain length is established and the short-long termination can be accessed, as will be illustrated in this work.

1.2.6 Chain Transfer to CTA

In FRP, chain transfer to a so-called chain transfer agent (CTA) is widely applied to regulate the resulting number average chain length x_n . Particularly, the addition of a large amount of CTA will significantly lower x_n which enhances the processability. In such chain transfer reactions, a radical center is ‘transferred’ from a polymer chain (R_n) towards a CTA by means of a hydrogen abstraction forming a dead polymer molecule P_n :



in which A^* is the resulting radical after transfer to CTA and k_{tr} the rate coefficient for radical chain transfer ($\text{L mol}^{-1} \text{s}^{-1}$). Similar to propagation, chain transfer involves a macroradical and

a small molecule (CTA vs. monomer), so that a pronounced intrinsic chain length dependency of $k_{tr,chem}$ can be expected, however, this still awaits experimental validation. On the other hand, diffusional limitations can be neglected up to very high monomer conversions (> 80%). Classification of the chain transfer reactivity of a CTA for a given monomer is usually done based on the chain transfer coefficient C_{tr} , which is defined as the ratio of k_{tr} to k_p . Several methods have been developed to determine C_{tr} ; the Mayo method and the CLD method being the two most important ones. In the following the main concepts and underlying assumptions of both methods are presented.

In FRP, the number chain length distribution of dead polymer can be approximated at a given conversion by a Flory-Shulz distribution, which was originally derived for linear polycondensation processes.² For a basic FRP scheme in which chain growth is only ended via termination by disproportionation, Equation (33) is an exact equality:

$$y_n = (1 - p)p^{n-1} \quad (33)$$

with y_n the number fraction of dead polymer chains with chain length n and p the propagation probability. At low conversion this probability can be approximated by:

$$p = \frac{k_p[M]_0\lambda_0}{k_p[M]_0\lambda_0 + \langle k_{td} \rangle \lambda_0^2} \quad (34)$$

in which $\langle k_{td} \rangle$ is the distribution averaged termination rate coefficient by disproportionation ($L \text{ mol}^{-1} \text{ s}^{-1}$). The concentration of dead polymer chains with a chain length n , $[P_n]$, is thus given by:

$$[P_n] = y_n[P_{tot}] \quad (35)$$

in which $[]$ refers to concentration (mol L^{-1}) and tot to the total population of dead polymer molecules. In case a conventional chain transfer agent (CTA) A is added to the FRP mixture and chain transfer to monomer can be still neglected, the propagation probability p at low conversion can be expressed as:^{2,4}

$$p = \frac{k_p[M]_0\lambda_0}{k_p[M]_0\lambda_0 + k_{tr}\lambda_0[A]_0 + \langle k_{td} \rangle \lambda_0^2} \quad (36)$$

in which $[A]_0$ is the initial concentration of CTA and k_{tr} the rate coefficient ($\text{L mol}^{-1} \text{s}^{-1}$) for chain transfer of a macroradical R_n (chain length n) with A via Equation (32). The number average chain length x_n of the number dead polymer distribution in Equation (33), (35) can be calculated as:

$$x_n = \frac{1}{1-p} \quad (37)$$

Based on this expression for x_n and Equation (36) for the propagation probability of the macroradicals, Mayo *et al.*⁸⁰ put forward a simple experimental method to determine the transfer coefficient C_{tr} ($= \frac{k_{tr}}{k_p}$) at low monomer conversion via regression analysis based on experiments with different initial CTA to monomer molar ratios (*i.e.* different $\frac{[A]_0}{[M]_0}$) via:

$$\frac{1}{x_n} = \frac{k_{tr}\lambda_0[A]_0 + \langle k_t \rangle \lambda_0^2}{k_p\lambda_0[M]_0} = C_{tr} \frac{[A]_0}{[M]_0} + \frac{\langle k_t \rangle \lambda_0}{k_p[M]_0} \quad (38)$$

Despite its ease and wide application, the accuracy of the *Mayo method* is however limited by the precision of size exclusion chromatography (SEC) measurements to determine x_n , which are often relative and highly sensitive to baseline fluctuations, especially at the low chain length region of the CLD.^{39,81,82}

Gilbert and Clay put forward that the chain transfer reactivity can also be derived from the CLD obtained by SEC, and not just its average properties.³⁹ Their method, *i.e.* the so-called *CLD method*, is based on the analytical integration of the continuity equations for the macroradicals R_n , assuming again a basic FRP scheme:

$$\frac{d[R_n]}{dt} = k_p[M][R_{n-1}] - k_p[M][R_n] - k_{tr}[A][R_n] - \sum_{m=1}^{\infty} k_t^{n,m}[R_n][R_m] \quad (39)$$

in which $k_t^{n,m}$ is the total (apparent) termination rate coefficient (= disproportionation + recombination) between macroradicals of chain length n and m (mol L^{-1}). Note that transfer to monomer is again neglected. By application of the pseudo-steady state assumption (PSSA) for the calculation of the concentration of R_n and via transition towards continuous chain length variables based on:

$$k_p[M][R_{n-1}] - k_p[M][R_n] = -k_p[M]([R_n] - [R_{n-1}]) =$$

$$-k_p[M] \frac{[R_n] - [R_{n-1}]}{n - (n-1)} = -k_p[M] \frac{\Delta[R_n]}{\Delta n} = -k_p[M] \frac{\partial[R_n]}{\partial n} \quad (40)$$

it can be written down that:³⁹

$$\lim_{n \rightarrow \infty} [R_n] \sim \exp \left(- \frac{k_{tr}[A] + \langle k_t \rangle \int_{m=1}^{\infty} [R_m] dm}{k_p[M]} n \right) \quad (41)$$

In case termination by recombination is not important, Equation (41) also holds for the dead polymer molecules P_n .³⁹ Hence, via the slope of the natural logarithm of the number CLD derived from the SEC trace, *i.e.* the number CLD of the dead polymer molecules, C_{tr} can be obtained via regression analysis at low monomer conversion based on experiments with different initial CTA to monomer molar ratios (*i.e.* different $\frac{[A]_0}{[M]_0}$) via:

$$\frac{d \ln([P_n])}{dn} = - \frac{k_{tr}[A]_0 + \langle k_t \rangle \int_{m=1}^{\infty} [R_m] dm}{k_p[M]_0} = -C_{tr} \frac{[A]_0}{[M]_0} + a \quad (42)$$

In this expression, a is the contribution originating from termination reactions and is assumed to be equal for different $\frac{[A]_0}{[M]_0}$ if the initiator concentration is kept the same.³⁹ Moreover, the contribution of termination in Equation (42) is often neglected compared to the transfer reactions. Note that the use of Equation (42) is similar to the application of the Mayo method⁸⁰ (Equation (38)). However, it is more robust since only the part of the CLD at high chain lengths is considered for application of Equation (42), *cf.* Equation (41), whereas in the

Mayo method⁸⁰ the complete CLD is used in order to determine its average properties which are thus more sensitive to baseline fluctuations of the SEC trace typically in the low chain length region. It should be stressed that in theory both the Mayo method⁸⁰ and the CLD method of Gilbert and Clay³⁹ can also be applied at higher monomer conversions if in Equations (38) and (42) the initial concentrations of monomer ($[M]_0$) and CTA ($[A]_0$) are replaced by the instantaneous concentrations at the considered conversion. However, in practice small monomer conversions are usually considered.

The analogy between the CLD and the Mayo method⁸⁰ was highlighted by Moad and coworkers who showed that in case of a Flory-Schulz distribution, the following expression holds:⁸²

$$\frac{d \ln([P_n])}{dn} = 1 - \frac{1}{p} = -\frac{1}{x_n - 1} \quad (43)$$

Since for a Flory-Schulz distribution $[P_n]$ is given by Equation (33)-(36) if termination only occurs by disproportionation, it also holds that:

$$\frac{d \ln([P_n])}{dn} = \ln(p) \quad (44)$$

This expression states that at each monomer conversion, a plot of the natural logarithm of the number CLD of the dead polymer versus the chain length yields a straight line with slope $\ln(p)$.⁸² Note that Equations (43) and (44) converge for higher values of x_n (< 1% mismatch if $x_n > 50$).⁸² On the other hand, if termination only occurs by recombination, the fraction of dead polymer molecules with chain length n (y_n) is given by:^{2,3}

$$y_n = (n - 1)(1 - p)^2 p^{n-2} \quad (45)$$

The slope of $\ln(P_n)$ versus n then becomes:

$$\frac{d \ln([P_n])}{dn} = \ln(p) + \frac{1}{n-1} \quad (46)$$

For large values of n , the second term in Equation (46) can be neglected and Equation (44) is again obtained. Moad and coworkers thus showed that in the high chain length region of the number CLD, irrespective of the mode of termination, accurate values for C_{tr} can be obtained via Equation (44) which is equivalent to Equation (42) for $x_n > 50$.^{81,82} In addition, they evaluated via simulations the importance of chain length dependent termination kinetics and fluctuations in the baseline of the SEC trace on the determined transfer coefficients. They found that if the region of the CLD with the highest signal to noise ratio was considered for application of Equation (42)-(44), *i.e.* the top 80% of the CLD as shown in Figure 1.4, and not only the high chain length region, the most accurate results for C_{tr} were obtained.^{81,82}

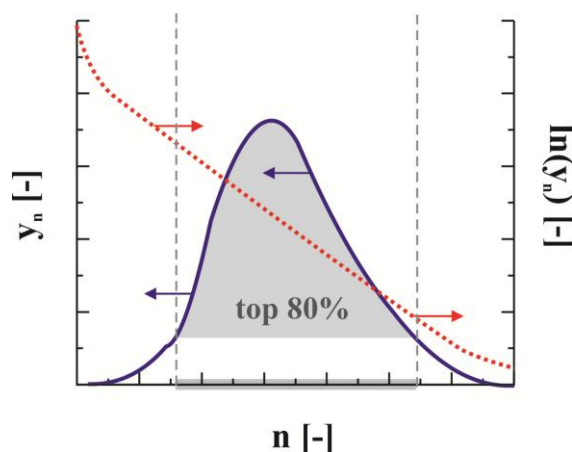


Figure 1.4: Conceptual representation of the CLD method of Moad and coworkers.^{81,82} Full blue line is number CLD of dead polymer (y_n , Equation (1) if disproportionation is only termination mechanism); dotted red line is natural logarithm of the number CLD. Top 80% (highest signal to noise ratio) of CLD is marked by a shading as in that region the most accurate C_{tr} values are obtained.

1.2.7 RAFT specific transfer reactions

As highlighted previously (Figure 1.1), the reaction scheme for reversible addition-fragmentation chain transfer (RAFT) polymerization is much more complex than a conventional FRP (*cf.* Figure 1.1 and Scheme 1.1).¹¹ For an efficient RAFT ‘exchange’

between a (macro)radical and a (macro-) RAFT CTA to take place, a sequence of a bimolecular addition reaction and a monomolecular fragmentation reaction have to take place without interference of possible side reactions of the intermediate radical (INT in Figure 1.1 and Scheme 1.1).

The situation is even further complicated by the theoretical observation of Coote and coworkers that the addition reaction is characterized by a strong intrinsic chain length dependency based on high level *ab initio* calculations up to tetramers for styrene.³² This, however, still needs to be verified experimentally. Moreover, from full conversion of the initial RAFT CTA onwards (typically below 40% monomer conversion), the RAFT exchange process will be exclusively governed by addition reactions that involve two polymeric species, similar to the case of termination which is strongly influenced by viscosity effects (*cf.* Section 1.2.5). Hence, it can be expected that the addition reaction at high monomer conversion is also susceptible to pronounced diffusional limitations and apparent addition kinetics need to be considered, which will become more pronounced for higher values of the corresponding intrinsic addition rate coefficient. This is confirmed by simulations by Wang and Zhu,⁸³ Peklak and Butté,⁸⁴ and D'hooge *et al.*¹⁷ Yet, experimental verification is not possible as long as no experimental method is available that allows to monitor the apparent addition rate coefficient throughout the polymerization reaction and/or reliable RAFT specific intrinsic parameters are still an issue. In the following, the different literature methods that were developed to quantify the RAFT exchange reactivity are briefly discussed.

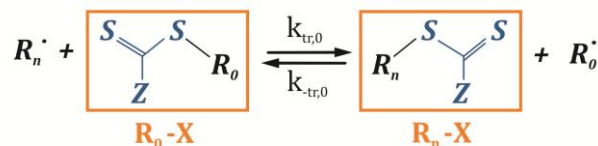
Most experimental methods to determine the chain transfer reactivity in RAFT polymerization are based on the degenerative transfer mechanism. This degenerative mechanism assumes an efficient RAFT exchange for which no rate retardation compared to the corresponding FRP is observed (Scheme 1.4) and is formally derived by application of the pseudo-steady state assumption to the concentration of the intermediate radical species (INT

in Figure 1.1 and Scheme 1.1).^{5,16} In case the degenerative transfer mechanism holds, the continuity equation for the macroradical R_n becomes (in case I^* different from R_0 : no exchange considered with I^* and IX):

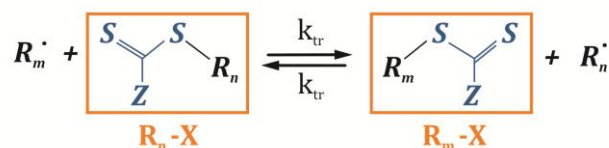
$$\frac{dR_n}{dt} = k_p[M][R_{n-1}] - k_p[M][R_n] - k_{tr,0}[R_0X][R_n] + k_{-tr,0}[R_0][R_nX] - k_{tr}[R_n] \sum_m [R_mX] + k_{tr}[R_nX] \sum_m [R_m] - \sum_{m=1}^{\infty} k_t^{n,m}[R_n][R_m] \quad (47)$$

in which R_0X is the initial RAFT CTA, R_nX the dormant polymer species of chain length n and $k_{tr,0}$, $k_{-tr,0}$ and k_{tr} the RAFT exchange rate coefficients according to Scheme 1.4 ($\text{L mol}^{-1} \text{s}^{-1}$). Similar to conventional chain transfer in FRP (*cf.* Section 1.2.6) a classification of the RAFT exchange reactivity is usually made based on the corresponding RAFT transfer coefficients $C_{tr,0} = \frac{k_{tr,0}}{k_p}$, $C_{-tr,0} = \frac{k_{-tr,0}}{k_p}$ and $C_{tr} = \frac{k_{tr}}{k_p}$.

Degenerative transfer of macroradical R_n with RAFT CTA R_0X



Degenerative transfer of macroradical R_m with macro-RAFT CTA R_nX



Scheme 1.4: Simplified RAFT degenerative transfer mechanism based on the pseudo-steady state assumption for the calculation of the concentration of the intermediate radical species in Scheme 1.3 (INT). Only RAFT exchange reactions are shown.

For very low values of the RAFT transfer rate coefficient for the reaction between R_n and R_0X ($k_{tr,0}$; $C_{tr,0} < 1$), Equation (47) will simplify to an expression similar to Equation (39) as the contribution of the R_0 and R_nX species will be negligible. In that case the resulting CLD will tend towards the Flory-Schulz distribution since only minor control over the polymer

properties is established, implying a safe use of the CLD method (Equation (39)-(46))^{39,81,82} and the Mayo method⁸⁰ to determine the corresponding RAFT transfer reactivity $C_{tr,0}$.

For RAFT polymerizations characterized by a higher transfer reactivity with R_0X , $C_{tr,0}$ can often be directly determined from the concentration decay of the latter. In particular, Moad and coworkers developed an experimental method to determine $C_{tr,0}$ ($= k_{tr,0}/k_p$) from the measurement of both the monomer and R_0X concentration as a function of batch time (for I^* different from R_0 : no exchange considered with I^* and IX):^{85,86}

$$\frac{d[M]}{dt} = -k_{p,0}[M][R_0] - k_p[M]\lambda_0 \quad (48)$$

$$\frac{d[R_0X]}{dt} = -k_{tr,0}[R_0X]\lambda_0 + k_{-tr,0}[R_0]\tau_0 \quad (49)$$

in which τ_0 is the total concentration of dormant polymer molecules and $k_{p,0}$ the propagation rate coefficient of a R_0 radical with monomer M . Combination of Equation (48)-(49) yields:

$$\frac{d[R_0X]}{d[M]} = \frac{-k_{tr,0}[R_0X]\lambda_0 + k_{-tr,0}[R_0]\tau_0}{-k_{p,0}[M][R_0] - k_p[M]\lambda_0} \quad (50)$$

Subsequent elimination of the concentrations of R_0 and λ_0 by application of the PSSA leads to:^{85,86}

$$\frac{d[R_0X]}{d[M]} \approx \frac{k_{tr,0}[R_0X]}{k_p[M] + k_{tr,0}[R_0X] + k_{-tr,0}\tau_0} = C_{tr,0} \frac{[R_0X]}{[M] + C_{tr,0}[R_0X] + C_{-tr,0}\tau_0} \quad (51)$$

Note that τ_0 can be directly related to $[R_0X]$ as the total number of RAFT CTA moieties in the reaction mixture stays constant if no degradation occurs for the considered conditions. Equation (50) could be used to estimate both $C_{tr,0}$ and $C_{-tr,0}$. However, if reverse degenerative transfer ($C_{-tr,0}$) becomes negligible compared to transfer with R_0X ($C_{tr,0}$), it enables the direct evaluation of $C_{tr,0}$ from the slope of a plot of $\ln([R_0X])$ versus $\ln([M])$:^{85,86}

$$\frac{d[R_0X]}{d[M]} \approx \frac{k_{tr,0}[R_0X]}{k_p[M]} = C_{tr,0} \frac{[R_0X]}{[M]} \quad (52)$$

and thus:

$$\frac{d[R_0X]}{[R_0X]} \approx C_{tr,0} \frac{d[M]}{[M]} \quad (53)$$

which yields after integration:

$$\ln\left(\frac{[R_0X]}{[R_0X]_0}\right) \approx C_{tr,0} \ln\left(\frac{[M]}{[M]_0}\right) \quad (54)$$

Hence:

$$C_{tr,0} \approx \frac{d\ln([R_0X])}{d\ln([M])} \quad (55)$$

It is clear that Equation (51) and (55) can only be successfully applied if the RAFT CTA concentration can be accurately monitored, which is only possible for low to intermediate $C_{tr,0}$ values. For a high $C_{tr,0}$ (> 100), the RAFT CTA will be completely consumed after a few percent of monomer conversion and unreliable results can be expected.⁸⁷

An alternative method for the determination of $C_{tr,0}$, was reported by Theis *et al.*⁷⁶ for monomer – R_0X combinations that display “hybrid RAFT polymerization behavior”. As illustrated in Figure 1.5, this term refers to the observed initial very steep increase of x_n before the linear incline with conversion is established (x_n^0) due to an imbalance of the propagation rate (with monomer) and the RAFT exchange rate with R_0X , the former being substantially larger than the latter. Theis *et al.* derived an approximate expression to determine $C_{tr,0}$ from SEC measurements of the initial chain length (x_n^0). Based on the propagation rate r_{prop} and RAFT exchange rate r_{exch} at the start of the polymerization ($x = 0^+$) given by:⁷⁶

$$r_{prop}|_{x=0^+} = -\left.\frac{d[M]}{dt}\right|_{x=0^+} = k_p[M]\lambda_0 \quad (56)$$

$$r_{exch}|_{x=0^+} = -\left.\frac{d[R_0X]}{dt}\right|_{x=0^+} = k_{tr,0}[R_0X]\lambda_0 \quad (57)$$

the number average initial chain length can be approximated by:

$$x_n^0 \approx \frac{r_{prop}|_{x=0^+}}{r_{exch}|_{x=0^+}} + 1 = \frac{k_p[M]_0}{k_{tr,0}[R_0X]_0} + 1 = \frac{[M]_0}{C_{tr,0}[R_0X]_0} + 1 \quad (58)$$

This equation assumes that at the start of the RAFT polymerization, chain growth is only interrupted by exchange with R_0X , thus neglecting the contribution of termination. Furthermore, in Equation (58) one is added on the right-hand-side in order to account for the fact that the first propagation step already leads to a chain length of 2. Theis *et al.* claimed that via Equation (58) the rate coefficient for addition of a macroradical on R_0X ($k_{add,0}$) could be calculated from:⁷⁶

$$x_n^0 \approx \frac{k_p[M]_0}{k_{add,0}\varphi[R_0X]_0} + 1 \quad (59)$$

However, in order to derive $k_{add,0}$ from this expression, a value for the fragmentation probability φ (fragmentation of the RAFT intermediate radical towards products vs. fragmentation towards reactants) needs to be assumed. Theis *et al.* used a value of 0.5 for this parameter φ ,⁷⁶ which is only valid in case the R_0 species and the propagating radicals (R_n) have a similar reactivity.

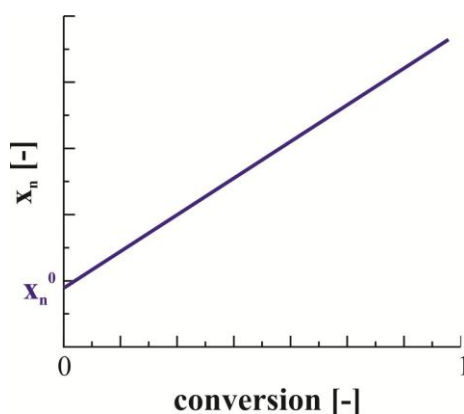


Figure 1.5: Evolution of the number averaged chain length (x_n) with conversion for monomer– R_0X combinations that exhibit hybrid behavior. An initial increase of the chain length (x_n^0) is obtained at the start of the polymerization.

Recently, Barth *et al.* developed an efficient direct experimental method to assess the addition- fragmentation equilibrium coefficient (K_{eq}) for the reversible chain transfer with macro-RAFT CTA.⁸⁸ This was done based on time-resolved electron paramagnetic resonance (EPR) measurements of the concentration ratio of the macroradical (R_n in Scheme 1.1; total concentration λ_0) and intermediate radical species (INT-(m,n) in Scheme 1.1; total concentration $[INT]$) after pulsed laser initiation. If cross-termination of the intermediate radicals (INT) is neglected and a quasi-equilibrium is assumed for the addition-fragmentation reactions with macro-RAFT CTA, it holds that:⁸⁸

$$K_{eq} = \frac{k_{add}}{k_{frag}} = \frac{[INT]_{eq}}{\lambda_{0,eq}\tau_{0,eq}} \approx \frac{[INT]}{\lambda_0\tau_0} \quad (60)$$

in which $[]_{eq}$ denotes the corresponding equilibrium concentration. As only the ratio of concentrations of INT and the propagating radicals is required for application of Equation (60), no calibration of the EPR equipment for absolute concentration measurements is required, which significantly enhances the reliability of the method as a proper calibration can be a tedious task.⁸⁸ By plotting the ratio of $[INT]$ and λ_0 for different initial concentrations of R_0X , K_{eq} is obtained by regression as the slope of the resulting straight line:

$$K_{eq}\tau_0 \approx K_{eq}[R_0X]_0 \approx \frac{[INT]}{\lambda_0} \quad (61)$$

It should be stressed that in their method, Barth *et al.* assumed that the RAFT addition-fragmentation reactions with R_0X do not influence the measured concentration of the intermediate radical species (INT) after the laser pulse, and, additionally, that at the moment the EPR spectra are recorded, full conversion of R_0X into dormant polymer species has occurred.⁸⁸

Buback and coworkers⁸⁹⁻⁹¹ showed that after calibration of the EPR equipment for the simultaneous measurement of the absolute concentrations of the RAFT intermediate radical

(INT) and the propagating macroradicals, reliable estimates for the individual k_{add} and k_{frag} could be obtained by regression analysis of a simple kinetic model to the recorded experimental concentration profiles. Higher accuracy for the resulting values of the addition-fragmentation rate coefficients is expected than similar parameter estimation procedures based on (indirect) experimental data for the average polymer properties. However, it should be noted that the obtained values for k_{add} and k_{frag} via these PLP-EPR methods are in disagreement with theoretical calculations⁹² and experimental EPR studies based on model compounds.⁹³ Furthermore, PLP equipment is expensive and limited to RAFT CTAs that do not degrade under the imposed ultraviolet laser pulses, and, as highlighted before, proper calibration of the EPR can be difficult.

RAFT chain transfer reactivities for the macro-RAFT CTA, C_{tr} , have been also determined based on approximate analytical correlations for the polymer dispersity (\mathfrak{D}) profile as a function of the monomer conversion (x). Müller *et al.* derived for a degenerative polymerization scheme (Scheme 1.4) under the assumption of instantaneous initiation and the absence of termination (and hence a constant total radical concentration) a set of analytical expressions for the average polymer properties as function of monomer conversion, based on the moments of the CLD.^{94,95} The resulting expression for \mathfrak{D} is given by:

$$\mathfrak{D} = \frac{1 + \kappa \left[2 + \frac{(2-x)(1-C_{tr})}{C_{tr} - \theta} \right] - \frac{2\theta\kappa(1-\theta)}{(C_{tr}^2 - \theta^2)x} [1 - (1-x)^{1+\frac{C_{tr}}{\theta}}]}{\kappa x} \quad (62)$$

in which θ and κ are respectively the ratio of the total radical concentration and the initial monomer concentration to the initial conventional radical initiator concentration. Based on similar assumptions, Goto and Fukuda proposed an equivalent expression, which relates \mathfrak{D} to the monomer conversion x and the number averaged chain length x_n :⁹⁶

$$\mathfrak{D} = 1 + \frac{1}{x_n} + \frac{2-x}{x C_{tr}} \quad (63)$$

Using Equation (62) or Equation (63), the C_{tr} can be calculated from the measured average polymer properties at a given monomer conversion x . Note that these analytical methods assume that C_{tr} remains constant during the complete polymerization reaction (Equation (62)-(63)).

An important extension of Equation (62)-(63) was reported by Gao and Zhu, who included continuous initiation and the occurrence of termination reactions in their analytical derivations, neglecting the influence of diffusional limitations on the latter.⁸⁷ However, still simplifying assumptions were made that limit the validity of their model over a broad range of conditions as demonstrated in Chapter 3. Only the resulting analytical expression for \mathfrak{D} as a function of monomer conversion is given below:⁸⁷

$$\mathfrak{D} = \frac{\frac{2B}{A-2} \frac{C_{tr}[R_0X]_0 + B}{C_{tr}[R_0X]_0^2} [(1-x)^2 - (1-x)^A]}{[1-x - (1-x)^A]^2} + \frac{\frac{B^2}{(A-1)[R_0X]_0[M]_0} [1-x - (1-x)^A] - \frac{2B}{[R_0X]_0} x(1-x)^A}{[1-x - (1-x)^A]^2} \quad (64)$$

in which $A = \frac{k_t \lambda_0}{k_p [R_0X]_0}$ with k_t the total termination rate coefficient ($\text{L mol}^{-1} \text{s}^{-1}$) and $B =$

$\frac{\langle k_t \rangle \lambda_0}{k_p} - [R_0X]_0$. It is clear that Equation (64) is significantly more complex than Equation

(62)-(63) as a direct consequence of the consideration of a more extended RAFT model including continuous initiation and termination. Furthermore, besides the monomer conversion, also the total radical concentration (λ_0 , for calculation of A) and the total termination rate coefficient are required as input.

Although a wide range of methods is available to determine the RAFT transfer reactivity, it is not always clear when the underlying assumptions limit the accuracy, and systematic errors

will inevitably be made upon blind use of these methods. Also, none of the discussed methods allows to determine both the transfer reactivity of the initial RAFT CTA (R_{0X} ; $C_{tr,0}$) and the macro-RAFT CTA (C_{tr}).

1.3 Outline

As indicated above, the quantification of (apparent) rate coefficients is a prerequisite for the proper understanding and optimization of radical polymerization processes. Therefore, in this PhD thesis, novel methodologies (Chapter 2-4) have been developed to (i) reliably quantify all apparent termination rate coefficients, using RAFT polymerization as a kinetic tool and (ii) to determine for a degenerative RAFT polymerization mechanism the transfer reactivity of the initial RAFT chain transfer agent (CTA) and macro-RAFT agent, based on analytical expressions for the average polymer properties.

In Chapter 2, a generic framework is developed to determine for the first time experimental values for the apparent short-long termination rate coefficients, an outstanding fundamental challenge in radical polymerization kinetics. The proposed methodology is based on an extension of the RAFT-CLD-T technique and is applied to methyl methacrylate (MMA) as monomer at 353 K, supported by model validation. As accurate apparent homotermination rate coefficients are indispensable to obtain reliable apparent short-long termination data, the conventional RAFT-CLD-T technique to determine apparent homotermination rate coefficients is re-evaluated and improved values are reported for MMA at 353 K, including a complete error propagation analysis on the method input parameters. Moreover, the generic nature of the proposed experimental framework is evidenced by its capability to quantify the influence of the polymer matrix on the observed apparent termination reactivity, which is relevant for any radical polymerization process.

In Chapter 3, the wide range of literature methods to determine the exchange reactivity in degenerative RAFT polymerization is re-evaluated based on *in silico* experiments to retrieve useful guidelines for the synthetic chemist to select the most accurate method for a given set of conditions. Next, in Chapter 4, an improved method to determine RAFT transfer coefficients is developed based on an analytical expression for the polymer dispersity in degenerative RAFT polymerization, which takes into account apparent termination kinetics and is more accurate than previous literature methods for all considered conditions, as assessed based on an *in silico* proof of concept. Furthermore, besides a higher inherent accuracy, the proposed method allows for the first time to determine in a single experiment both the RAFT exchange reactivity of the initial RAFT CTA and the macro-RAFT CTA, and, importantly, to capture a possible variation of the RAFT exchange reactivity along the course of the polymerization due to an intrinsic/apparent chain length dependency. After *in silico* validation, the method is applied to available experimental data for RAFT polymerization of MMA at 353 K.

In Chapter 5, it is illustrated how kinetic modeling, provided accurate rate coefficients are available, can be a valuable partner to polymerization experiments to obtain fundamental kinetic knowledge and formulate subsequent guidelines for the optimization of certain polymer properties. In this chapter, the complex RAFT polymerization of *n*-butyl acrylate (*n*BuA) is modeled in a microreactor and a batch reactor to elucidate the superior control over the polymer microstructure in the former. Particularly, based on literature values for the corresponding intrinsic and apparent rate coefficients, it is shown that the non-isothermicity of the batch reactor causes a strong increase of the contribution of β -scission reactions of the tertiary radicals, and hence a significant additional loss of RAFT CTA functionality. Furthermore, a detailed kinetic analysis is performed to determine unambiguously the fundamental underlying causes of the effect of the microreactor conditions on the cumulative

branching content and the degree of livingness, *i.e.* the polyacrylate microstructure. It is particularly explained in detail which are the underlying triggers for reduced branch formation in RAFT polymerization and RDRP in general as compared to FRP.

Finally, in Chapter 6 the main conclusions of this PhD thesis are summarized and an outlook is provided towards possible future work.

1.4 References

- (1) Whitby, G. S. *Synthetic Rubber*; Wiley: New York, 1954.
- (2) Flory, P. J. *Principles of Polymer Chemistry*; Cornell University Press: Ithaca, 1953.
- (3) Odian, G. *Principles of Polymerization*; John Wiley and Sons: New Jersey, 2004.
- (4) Matyjaszewski, K. D., T. P. *Handbook of Radical Polymerization*; John Wiley and Sons: New Jersey, 2002.
- (5) Barner-Kowollik, C. *Handbook of RAFT Polymerization*; Wiley: Weinheim, 2008.
- (6) Destarac, M. *Macromolecular Reaction Engineering* **2010**, *4*, 165-179
- (7) BYK. Additive guide: DISPERBYK. 2009.
- (8) Termaten, A. T. *Abstracts of Papers of the American Chemical Society* **2008**, *236*,
- (9) Destarac, M.; Deroo, S.; Lannibois-Drean, H.; Senechal, A.; Bzducha, W. Title. In *Controlled/Living Radical Polymerization: Progress in Raft, Dt, Nmp & Omp*; Matyjaszewski, K., Ed. 2009; 1024, p. 347-359.
- (10) Matheson, R. R. J. *The commercialization of controlled polymer synthesis*. MA, USA: The Knowledge Foundation; 2000.

- (11) Chiefari, J.; Chong, Y. K.; Ercole, F.; Krstina, J.; Jeffery, J.; Le, T. P. T.; Mayadunne, R. T. A.; Meijs, G. F.; Moad, C. L.; Moad, G.; Rizzardo, E.; Thang, S. H. *Macromolecules* **1998**, *31*, 5559-5562
- (12) Russell, G. T.; Gilbert, R. G.; Napper, D. H. *Macromolecules* **1992**, *25*, 2459-2469
- (13) Barner-Kowollik, C.; Russell, G. T. *Progress in Polymer Science* **2009**, *34*, 1211-1259
- (14) D'hooge, D. R. V. S., Paul H.M.; Derboven, Pieter; Reyniers, Marie-Françoise; Marin, Guy B. *Polymer Chemistry* **2015**, accepted
- (15) D'hooge, D. R. V. S., Paul H.M.; Reyniers, Marie-Françoise; Marin, Guy B. *Progress in Polymer Science* **2015**, submitted
- (16) Moad, G.; Chiefari, J.; Chong, Y. K.; Krstina, J.; Mayadunne, R. T. A.; Postma, A.; Rizzardo, E.; Thang, S. H. *Polymer International* **2000**, *49*, 993-1001
- (17) D'hooge, D. R.; Reyniers, M.-F.; Marin, G. B. *Macromolecular Reaction Engineering* **2013**, *7*, 362-379
- (18) Achilias, D. S. *Macromolecular Theory and Simulations* **2007**, *16*, 319-347
- (19) Barner-Kowollik, C.; Buback, M.; Egorov, M.; Fukuda, T.; Goto, A.; Olaj, O. F.; Russell, G. T.; Vana, P.; Yamada, B.; Zetterlund, P. B. *Progress in Polymer Science* **2005**, *30*, 605-643
- (20) Beuermann, S.; Buback, M. *Progress in Polymer Science* **2002**, *27*, 191-254
- (21) Beuermann, S.; Buback, M.; Davis, T. P.; Gilbert, R. G.; Hutchinson, R. A.; Olaj, O. F.; Russell, G. T.; Schweer, J.; van Herk, A. M. *Macromolecular Chemistry and Physics* **1997**, *198*, 1545-1560

- (22) Fierens, S. K.; D'hooge, D. R.; Van Steenberge, P. H. M.; Reyniers, M.-F.; Marin, G. B. *Chemical Engineering Journal* **2015**, *278*, 407-420
- (23) Ohno, K.; Tsujii, Y.; Fukuda, T. *Macromolecules* **1997**, *30*, 2503-2506
- (24) Woloszyn, J. D.; Hesse, P.; Hungenberg, K.-D.; McAuley, K. B. *Macromolecular Reaction Engineering* **2013**, *7*, 293-310
- (25) Heatley, F.; Lovell, P. A.; Yamashita, T. *Macromolecules* **2001**, *34*, 7636-7641
- (26) Horn, M.; Matyjaszewski, K. *Macromolecules* **2013**, *46*, 3350-3357
- (27) Woecht, I.; Schmidt-Naake, G.; Beuermann, S.; Buback, M.; Garcia, N. *Journal of Polymer Science Part a-Polymer Chemistry* **2008**, *46*, 1460-1469
- (28) Heuts, J. P. A.; Russell, G. T.; Smith, G. B. *Australian Journal of Chemistry* **2007**, *60*, 754-764
- (29) Coote, M. L. *Journal of Physical Chemistry A* **2005**, *109*, 1230-1239
- (30) Coote, M. L.; Henry, D. J. *Macromolecules* **2005**, *38*, 1415-1433
- (31) Coote, M. L.; Krenske, E. H.; Izgorodina, E. I. *Macromolecular Rapid Communications* **2006**, *27*, 473-497
- (32) Izgorodina, E. I.; Coote, M. L. *Macromolecular Theory and Simulations* **2006**, *15*, 394-403
- (33) Izgorodina, E. I.; Coote, M. L. *Chemical Physics* **2006**, *324*, 96-110
- (34) Bagryanskaya, E. G.; Marque, S. R. A.; Tsentlovich, Y. P. *Journal of Organic Chemistry* **2012**, *77*, 4996-5005

- (35) Bertin, D.; Gigmes, D.; Marque, S. R. A.; Tordo, P. *Chemical Society Reviews* **2011**, *40*, 2189-2198
- (36) D'hooge, D. R.; Reyniers, M.-F.; Stadler, F. J.; Dervaux, B.; Bailly, C.; Du Prez, F. E.; Marin, G. B. *Macromolecules* **2010**, *43*, 8766-8781
- (37) Wieme, J.; De Roo, T.; Marin, G. B.; Heynderickx, G. J. *Industrial & Engineering Chemistry Research* **2007**, *46*, 1179-1196
- (38) Smoluchowski, M. *Z Phys Chem* **1917**, *92*, 129
- (39) Clay, P. A.; Gilbert, R. G. *Macromolecules* **1995**, *28*, 552-569
- (40) Johnston-Hall, G.; Monteiro, M. J. *Journal of Polymer Science Part a-Polymer Chemistry* **2008**, *46*, 3155-3173
- (41) Vrentas, J. S.; Duda, J. L. *Journal of Polymer Science Part B-Polymer Physics* **1977**, *15*, 403-416
- (42) Vrentas, J. S.; Duda, J. L. *Journal of Polymer Science Part B-Polymer Physics* **1977**, *15*, 417-439
- (43) Vrentas, J. S.; Duda, J. L.; Ling, H. C. *Journal of Polymer Science Part B-Polymer Physics* **1984**, *22*, 459-469
- (44) Vrentas, J. S.; Duda, J. L.; Ling, H. C. *Journal of Polymer Science Part B-Polymer Physics* **1985**, *23*, 275-288
- (45) Kobuchi, S.; Arai, Y. *Progress in Polymer Science* **2002**, *27*, 811-814
- (46) Graessley, W. W. *Journal of Polymer Science Part B-Polymer Physics* **1980**, *18*, 27-34

- (47) Griffiths, M. C.; Strauch, J.; Monteiro, M. J.; Gilbert, R. G. *Macromolecules* **1998**, *31*, 7835-7844
- (48) Talaterben, M.; Bywater, S. *Journal of the American Chemical Society* **1955**, *77*, 3712-3714
- (49) Hammond, G. S.; Sen, J. N.; Boozer, C. E. *Journal of the American Chemical Society* **1955**, *77*, 3244-3248
- (50) Buback, M.; Huckestein, B.; Kuchta, F. D.; Russell, G. T.; Schmid, E. *Macromolecular Chemistry and Physics* **1994**, *195*, 2117-2140
- (51) Charton, N.; Feldermann, A.; Theis, A.; Stenzel, M. H.; Davis, T. P.; Barner-Kowollik, C. *Journal of Polymer Science Part a-Polymer Chemistry* **2004**, *42*, 5170-5179
- (52) Braun, D.; Quella, F. *Makromolekulare Chemie-Macromolecular Chemistry and Physics* **1978**, *179*, 387-394
- (53) Korbar, A.; Malavasic, T. *Journal of Thermal Analysis* **1995**, *44*, 1357-1365
- (54) Szafko, J.; Feist, W. *Journal of Polymer Science Part a-Polymer Chemistry* **1995**, *33*, 1637-1642
- (55) Shen, J. C.; Yuan, T.; Wang, G. B.; Yang, M. L. *Makromolekulare Chemie-Macromolecular Chemistry and Physics* **1991**, *192*, 2669-2685
- (56) Wieme, J.; Reyniers, M.-F.; Marin, G. B. *Chemical Engineering Journal* **2009**, *154*, 203-210
- (57) Derboven, P.; D'hooge, D. R.; Stamenovic, M. M.; Espeel, P.; Marin, G. B.; Du Prez, F. E.; Reyniers, M.-F. *Macromolecules* **2013**, *46*, 1732-1742

- (58) Arzamendi, G.; Plessis, C.; Leiza, J. R.; Asua, J. M. *Macromolecular Theory and Simulations* **2003**, *12*, 315-324
- (59) Heuts, J. P. A.; Russell, G. T. *European Polymer Journal* **2006**, *42*, 3-20
- (60) Smith, G. B.; Russell, G. T.; Yin, M.; Heuts, J. P. A. *European Polymer Journal* **2005**, *41*, 225-230
- (61) Haven, J. J.; Vandenberg, J.; Junkers, T. *Chemical Communications* **2015**, *51*, 4611-4614
- (62) Norrish, R. G. W. S., R. R. *Nature* **1942**, *150*, 336-337
- (63) Norrish, R. G. W. B., E. F. *Proc R Soc London A* **1939**, *171*, 147-171
- (64) Benson, S. W., North, A. M. *Journal of the American Chemical Society* **1959**, *81*, 1339-1345
- (65) Benson, S. W., North, A. M. *Journal of the American Chemical Society* **1962**, *84*, 935-940
- (66) Russell, G. T.; Napper, D. H.; Gilbert, R. G. *Macromolecules* **1988**, *21*, 2133-2140
- (67) Beuermann, S.; Buback, M.; Russell, G. T. *Macromolecular Chemistry and Physics* **1995**, *196*, 2493-2516
- (68) Vana, P.; Davis, T. P.; Barner-Kowollik, C. *Macromolecular Rapid Communications* **2002**, *23*, 952-956
- (69) Szymanski, R. *Macromolecular Theory and Simulations* **2011**, *20*, 8-12
- (70) Buback, M.; Egorov, M.; Junkers, T.; Panchenko, E. *Macromolecular Rapid Communications* **2004**, *25*, 1004-1009

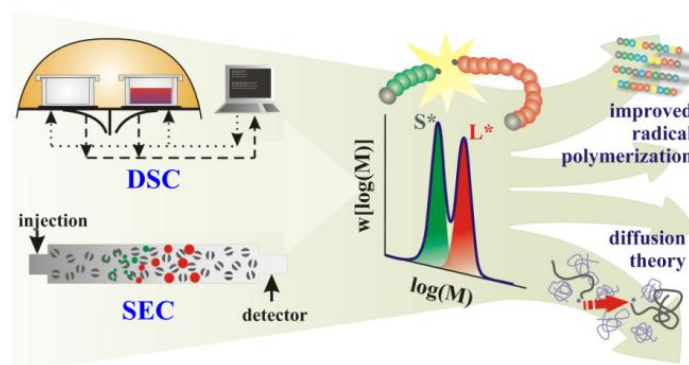
- (71) Kattner, H.; Buback, M. *Macromolecules* **2015**, *48*, 309-315
- (72) Buback, M.; Egorov, M.; Feldermann, A. *Macromolecules* **2004**, *37*, 1768-1776
- (73) Smith, G. B.; Russell, G. T.; Heuts, J. P. A. *Macromolecular Theory and Simulations* **2003**, *12*, 299-314
- (74) Buback, M.; Junkers, T.; Vana, P. *Macromolecular Rapid Communications* **2005**, *26*, 796-802
- (75) Theis, A.; Davis, T. P.; Stenzel, M. H.; Barner-Kowollik, C. *Macromolecules* **2005**, *38*, 10323-10327
- (76) Theis, A.; Feldermann, A.; Charton, N.; Stenzel, M. H.; Davis, T. P.; Barner-Kowollik, C. *Macromolecules* **2005**, *38*, 2595-2605
- (77) Johnston-Hall, G.; Stenzel, M. H.; Davis, T. P.; Barner-Kowollik, C.; Monteiro, M. J. *Macromolecules* **2007**, *40*, 2730-2736
- (78) Lovestead, T. M.; Davis, T. P.; Stenzel, M. H.; Barner-Kowollik, C. *Macromolecular Symposia* **2007**, *248*, 82-93
- (79) Lovestead, T. M.; Theis, A.; Davis, T. P.; Stenzel, M. H.; Barner-Kowollik, C. *Macromolecules* **2006**, *39*, 4975-4982
- (80) Mayo, F. R. *Journal of the American Chemical Society* **1943**, *65*, 2324-2329
- (81) Moad, C. L.; Moad, G.; Rizzardo, E.; Thang, S. H. *Macromolecules* **1996**, *29*, 7717-7726
- (82) Moad, G.; Moad, C. L. *Macromolecules* **1996**, *29*, 7727-7733
- (83) Wang, A. R.; Zhu, S. P. *Macromolecular Theory and Simulations* **2003**, *12*, 196-208
- (84) Peklak, A. D.; Butte, A. *Macromolecular Theory and Simulations* **2006**, *15*, 546-562

- (85) Chiefari, J.; Mayadunne, R. T. A.; Moad, C. L.; Moad, G.; Rizzardo, E.; Postma, A.; Skidmore, M. A.; Thang, S. H. *Macromolecules* **2003**, *36*, 2273-2283
- (86) Chong, Y. K.; Krstina, J.; Le, T. P. T.; Moad, G.; Postma, A.; Rizzardo, E.; Thang, S. H. *Macromolecules* **2003**, *36*, 2256-2272
- (87) Gao, X.; Zhu, S. *Journal of Applied Polymer Science* **2011**, *122*, 497-508
- (88) Barth, J.; Buback, M.; Meiser, W.; Vana, P. *Macromolecules* **2010**, *43*, 51-54
- (89) Buback, M.; Hesse, P.; Junkers, T.; Vana, P. *Macromolecular Rapid Communications* **2006**, *27*, 182-187
- (90) Meiser, W.; Barth, J.; Buback, M.; Kattner, H.; Vana, P. *Macromolecules* **2011**, *44*, 2474-2480
- (91) Meiser, W.; Buback, M.; Barth, J.; Vana, P. *Polymer* **2010**, *51*, 5977-5982
- (92) Lin, C. Y.; Coote, M. L. *Australian Journal of Chemistry* **2009**, *62*, 1479-1483
- (93) Chernikova, E.; Golubev, V.; Filippov, A.; Lin, C. Y.; Coote, M. L. *Polymer Chemistry* **2010**, *1*, 1437-1440
- (94) Muller, A. H. E.; Yan, D. Y.; Litvinenko, G.; Zhuang, R. G.; Dong, H. *Macromolecules* **1995**, *28*, 7335-7338
- (95) Muller, A. H. E.; Zhuang, R. G.; Yan, D. Y.; Litvinenko, G. *Macromolecules* **1995**, *28*, 4326-4333
- (96) Goto, A.; Fukuda, T. *Progress in Polymer Science* **2004**, *29*, 329-385

Chapter 2: The Long and the Short of Radical Polymerization

Summary

Precision functionality is the key feature of next-generation radical polymerization enabling the implementation of applications such as controlled drug delivery, self-healing material design and opto-electronic materials. The incorporation of functionality is however diametrically opposed to diffusion-controlled growth-inhibiting termination reactions. The fundamental bottleneck remains the identification of a generic and flexible protocol to accurately map the *short-*



long termination reactivity. Herein, we introduce a unique framework based on the reversible addition-fragmentation chain transfer – chain length dependent – termination (RAFT-CLD-T) method that encompasses an extension of state-of-the-art fundamental theories and a correction for possible polymer matrix effects. Applied to methyl methacrylate (MMA) polymerization, the *short-long*-termination reactivity is accurately quantified for the first time. Data analysis reveals the deficiency of currently used simplified models to describe the true *short-long*-termination reactivity and the dominance of short-chain diffusivity. The proposed framework and insights are a turnkey prerequisite for the fundamental understanding of radical polymerization processes and to complete current macromolecular diffusion theories.

This work has been published in *Macromolecules* 2015,48,492-501.

2.1 Introduction

Diffusivity lies at the core of virtually all biological and chemical processes, such as the diffusion of drugs according to a predetermined path from polymeric capsules to the human body¹ or crude oil constituents diffusing to the active sites in zeolites for the production of fuels. A pioneering law explaining the net diffusive flux was developed by Fick² in the 19th century, yet only 50 years later Einstein and Smoluchowski were able to calculate fundamentally the corresponding diffusion coefficient, assuming rigid sphere solutes.^{3,4}

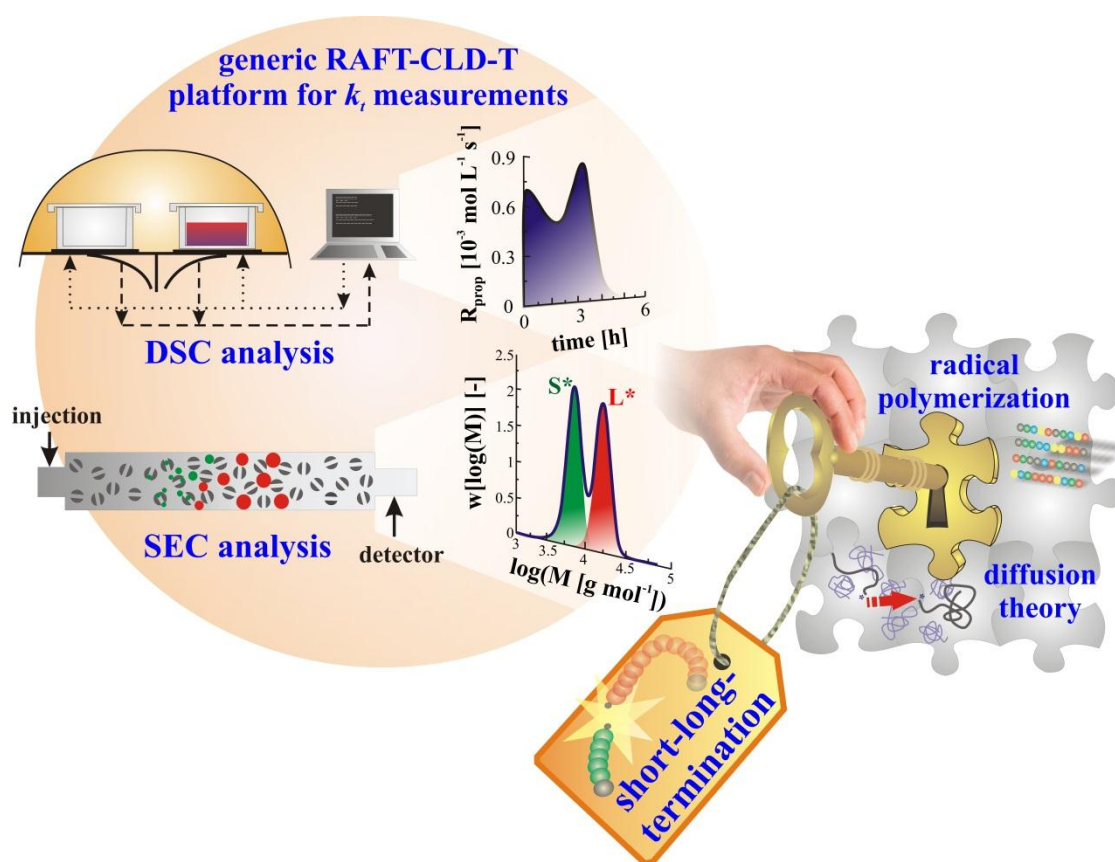


Figure 2.1: The need to quantify short-long-termination reactivities in radical polymerization: a generic and flexible experimental platform is presented to measure such reactivities allowing to exploit the full potential of existing and next-generation polymerization processes and to fill the knowledge gap in current macromolecular diffusion theories.

However, in polymerization chemistry, which provides a plethora of applications in everyday life, the picture is far more complex as the diffusivity is governed by the coil structure of the polymer molecules, as well as the composition and solvating quality of the surrounding matrix, similar to the behavior of proteins in a biological environment.⁵ Although significant research effort has been devoted to this scientifically challenging topic, a tremendous pitfall remains the reliable *quantification* of diffusion-controlled reactivities between *short* and *long* polymer molecules for which currently simplified models without a firm physical nor experimental basis are taken for granted, prohibiting the realization of high-tech polymer applications.⁶

For instance, in radical polymerization, the product quality is determined by a wide spectrum of diffusion-controlled *short-long*-termination reactions, even for relatively narrow chain length distributions (CLDs). Importantly, termination interferes with the synthesis of highly functional polymers via a multitude of promising reversible deactivation radical polymerization (RDRP) techniques,⁷⁻¹⁴ enabling compatibility with the latest developments in organic chemistry (*e.g.* “click” reactions¹⁵⁻¹⁸). Although somewhat suppressed in RDRP under well-selected conditions, termination reactions cause a direct depletion of end-group functionality. This is in particular narrows the reaction condition window for the formation of multi-block copolymers and other molecularly encoded synthetic polymers mimicking nature’s structural specificity.¹⁹⁻²² A quantification of the effect of diffusional limitations on the (apparent) *short-long*-termination reactivity ($k_t^{S^*L^*}$; $L^* > S^*$) in different polymer environments is, hence, the critical prerequisite for unlocking the full potential of existing and next-generation radical polymerization processes (Figure 2.1 right).

Unfortunately, currently available experimental techniques allow only for an assessment of the termination reactivity of macroradicals with equal chain length ($k_t^{i^*i^*}$; $i^*=S^*$ or L^*), *i.e.* *homo*-termination. Originally, due to technological improvements enabling microsecond

concentration measurements, single pulse pulsed laser polymerization (SP-PLP) emerged as the main method to measure $k_t^{i^*i^*}$.^{23,24} In particular, in combination with electron paramagnetic resonance spectroscopy a high accuracy is accessed^{25,26} while a synergetic coupling with reversible addition-fragmentation chain transfer (RAFT) polymerization, an important RDRP technique, enables a pointwise probing of the chain length dependency of $k_t^{i^*i^*}$, in a model-independent way under well-known but uniform polymer matrix conditions,²⁷ *i.e.* a very narrow CLD with predetermined number average chain length i^* . Alternatively, it has been demonstrated that the chain length and conversion dependency of $k_t^{i^*i^*}$ can be obtained via the experimentally much simpler yet almost equally effective RAFT – chain length dependent – termination (RAFT-CLD-T) technique,²⁸⁻³⁶ by combining rate measurements via differential scanning calorimetric (DSC) analysis with size exclusion chromatography (SEC) analysis. Interestingly, using the RAFT-CLD-T concept, Lovestead, Barner-Kowollik *et al.* formulated a pioneering thought experiment to determine $k_t^{S^*L^*}$ in case solubility limits could be neglected, which is in practice not the case.^{37,38}

In the current contribution, a generic and flexible experimental framework to measure not only $k_t^{i^*i^*}$ but also $k_t^{S^*L^*}$ (Figure 2.1 left) is proposed accounting directly for the polymer matrix composition. Accordingly, the theoretical model of Lovestead *et al.* is first refined and extended to all physically relevant experimental conditions. The developed protocol is subsequently applied to measure, for the first time, *short-long*-termination rate coefficients for the illustrative case of methyl methacrylate (MMA) radical polymerization at 353 K using the same RAFT chain transfer agent (CTA), 2-cyano-2-propyl dithiobenzoate (CPDB) as previous work of Johnston-Hall *et al.* on homotermination.^{28,29} It should be stressed that the proposed generic methodology opens new perspectives to unravel the complexity of radical polymerization kinetics and finally close the hiatus of diffusion theories to describe the diffusion of long and short macrospecies.

The RAFT-CLD-T measurements provide compelling evidence that the hitherto used simplified models for the calculation of $k_t^{S^*L^*}$ from $k_t^{S^*S^*}$ and $k_t^{L^*L^*}$ are inadequate to describe the true *short-long*-termination reactivity. It is, however, shown that in the studied intermediate MMA conversion range with limited matrix effects, the observed average polymer properties (*e.g.* end-group functionality) can still be approximated by these models.

2.2 Experimental Section

2.2.1 Materials

Azobis(2-methylpropionitrile) (AIBN, 98%) and methyl methacrylate (MMA, 99%, stabilized) were purchased from Acros organics. AIBN was re-crystallized twice in ethanol prior to use and MMA was passed through a column of basic alumina (VWR) to remove the inhibitor. Both were stored afterwards at -18°C . 2-Cyano-2-propyl dithiobenzoate was purchased from Sigma Aldrich (> 97%) and was used as received.

2.2.2 Methods and Analysis

The generic experimental platform to measure *short-long*-termination rate coefficients consists of three main steps and can be applied to a broad range of vinyl monomers in a straightforward manner. In what follows, these steps are discussed focusing on the experimental methods applied while providing general experimental guidelines. In the present work, the conditions listed in Table 2.1 are selected.

Table 2.1: Overview of the experimental conditions applied for the RAFT-CLD-T homo-termination experiments (entry 1-14), modified homo-termination experiments to quantify matrix effects (entry 15-19) and short-long-termination experiments (entry 20-23) of methyl methacrylate (MMA) at 353 K in bulk. CPDB: 2-cyano-2-propyl dithiobenzoate; AIBN: azobis(isobutyronitrile); Subscript zero: initial concentration; CL: chain length. For entry 1-19, $[CTA_{tot}]_0 = [CPDB]_0$. For entry 15-19, $[macro-RAFT CTA]_0$ refers to initial concentration of dead PMMA standard ($M_n = 9800 \text{ g mol}^{-1}$; $\bar{D} = 1.05$). $[M]_0 \approx 9.3 \text{ mol L}^{-1}$ for entry 1-14; $[M]_0 \approx 8.3 \text{ mol L}^{-1}$ for entry 15-23.

Entry	$[MMA]_0/[CTA_{tot}]_0$	$[CTA_{tot}]_0/[AIBN]_0$	$[macro-RAFT CTA]_0 / ([CPDB]_0 + [macro-RAFT CTA]_0)$	initial CL macro-RAFT CTA
1	179	11.4	–	–
2	94	16.3	–	–
3	398	9.5	–	–
4	298	13.2	–	–
5	59	30.3	–	–
6	713	8.2	–	–
7	175	11.5	–	–
8	35	53.1	–	–
9	158	18.3	–	–
10	349	10.2	–	–
11	61	29.9	–	–
12	741	9.8	–	–
13	1423	7.3	–	–
14	997	8.0	–	–
15	60	30	0.20 ^a	–
16	741	10	0.31 ^a	–
17	741	10	0.65 ^a	–
18	1423	7	0.60 ^a	–
19	1423	7	0.76 ^a	–
20	135	13.0	0.183	140
21	166	11.7	0.284	140
22	126	16.6	0.297	100
23	292	9.7	0.224	260

^a $[macro-RAFT CTA]_0$ should be replaced by $[PMMA \text{ standard}]_0$

Step 1: Measurement of *homo*-termination rate coefficients in a uniform polymer matrix

An accurate surface describing the chain length and polymer mass fraction dependency of the *homo*-termination rate coefficients in a uniform polymer matrix is constructed by regression to an extensive dataset of conventional RAFT-CLD-T measurements which involve on-line differential scanning calorimetric (DSC) measurements and size exclusion chromatography (SEC) analysis for parallel sampling experiments (*cf.* Figure 2.1). For a detailed technical description of these measurements, the reader is referred to the open literature.^{29,30} The reliability of the surface can be improved by adding the propagated uncertainty from the input parameters as a random scatter to the measured termination data before the regression is performed.

On-line differential scanning calorimetric (DSC) analysis

After the sample mixture was degassed by four freeze-evacuate-thaw cycles, it was sealed and transferred to a glove box, which operates under argon. In this glove box, a small amount of sample was withdrawn from the flask to fill the aluminium Tzero DSC pans (TA instruments). Each pan with corresponding Tzero hermetic lid was weighed before introduction in the glove box, inside which it was filled with two droplets of sample mixture (~10 mg) and hermitically closed with a press. After withdrawal from the glove box, the closed pans were weighed again to exactly determine the amount of sample inside, necessary for processing the DSC results. The measurements were performed with a Waters GmbH TA Instruments DSC Q200 with RCS 90 cooling system using an isothermal temperature program at 353 K for the complete duration of the polymerization reaction. The standby temperature of the instrument was set to 353 K in order to reduce the necessary equilibration time after sample insertion to a minimum (< 1 minute). Every day the calibration of the DSC instrument was checked with an Indium standard of known mass, melting point temperature

and associated enthalpy change, before any RAFT polymerization mixtures were analyzed. The DSC measurement of the sample was only stopped when a stable baseline signal was obtained, which was then extrapolated to the whole timespan of the reaction.

RAFT-CLD-T homo-termination sampling experiment

In parallel with the on-line DSC analysis, the same sample flask was transferred from the glove box to an oil bath at 353 K and samples were taken at definite times during the polymerization reaction with a 5 time nitrogen flushed syringe and a back-pressure of nitrogen. Each sample was analysed by both SEC to determine the CLD and off-line $^1\text{H-NMR}$ to measure the monomer conversion independently from the DSC data, the latter as an additional reliability check (*cf.* Supplementary section 3.3).

Size exclusion chromatography (SEC) analysis

SEC measurements were performed on a PL-SEC 50 Plus Integrated System, comprising an autosampler, a PLgel 5 μm bead-size guard column (50×7.5 mm) followed by one PLgel 5 μm Mixed E column (300×7.5 mm), three PLgel 5 μm Mixed C columns (300×7.5 mm) and a differential refractive index (RI) detector using THF as the eluent at 308 K with a flow rate of $1 \text{ mL}\cdot\text{min}^{-1}$. The SEC system is calibrated using linear poly(methyl methacrylate) standards ranging from 700 to $2 \times 10^6 \text{ g}\cdot\text{mol}^{-1}$.

Proton nuclear magnetic resonance spectroscopy ($^1\text{H-NMR}$)

$^1\text{H-NMR}$ measurements were conducted on a Bruker AM400 spectrometer at 400 Mhz with a relaxation time of 10s.

Surface regression

Surface regression was performed using the SYSTAT TableCurve 3D 4.0 software package for which only functions linear with respect to the parameters were considered.

Step 2: Measurement of *short-long* termination rate coefficients

RAFT-CLD-T *short-long* experiments starting from both a pre-synthesized macro-RAFT CTA and the corresponding small CTA were performed. In these experiments, the average *overall* termination rate coefficient was again derived from the DSC data, whereas the SEC measurements required an extra peak deconvolution procedure to yield the individual average chain lengths.

SEC peak deconvolution

SEC peak deconvolution was performed using the PeakFit 4.12 software package. Always R²-values higher than 0.99 were obtained.

Step 3: Correction for a possible matrix effect on the *homo*-termination rate coefficients

For the selected conditions of the *short-long* experiments, the influence of the polymer matrix on the generated *homo*-termination rate coefficients from the surface needs to be quantified in order to be able to calculate the *short-long*-termination rate coefficients (*cf.* Results and Discussion). This is achieved via RAFT-CLD-T *homo*-termination measurements starting from a mixture of conventional RAFT CTA and a certain amount of non-functional polymer standard and a comparison of these data to data obtained in step 1. Ideally, conditions of the *short-long* experiments should be mimicked and one should aim at conditions that yield different mass fractions of standard for the same terminating radical chain length and *overall* polymer mass fraction.

2.3 Results and Discussion

2.3.1 Extension of state-of-the-art theories for the short-long-termination reactivity

Currently, the *short-long-termination* rate coefficient for macroradicals with a chain length S^* and L^* ($k_t^{S^*L^*}$; $S^* < L^*$) is derived from the corresponding *homo-termination* rate coefficients ($k_t^{S^*S^*}$ and $k_t^{L^*L^*}$) using a simplified mean model without a clear physical explanation nor benchmark with experimental data. The most frequently applied models are the diffusion mean model (DMM), the geometric mean model (GMM) and the harmonic mean model (HMM):⁶

$$k_{t,DMM}^{S^*L^*} = 0.5 [k_t^{S^*S^*} + k_t^{L^*L^*}] \quad (1)$$

$$k_{t,GMM}^{S^*L^*} = \sqrt{k_t^{S^*S^*} \times k_t^{L^*L^*}} \quad (2)$$

$$k_{t,HMM}^{S^*L^*} = 2 \frac{k_t^{S^*S^*} k_t^{L^*L^*}}{k_t^{S^*S^*} + k_t^{L^*L^*}} \quad (3)$$

It should be remembered that the termination rate coefficients in these equations are all apparent rate coefficients, but to avoid overloading this is not explicitly specified here and throughout the remainder of the text.

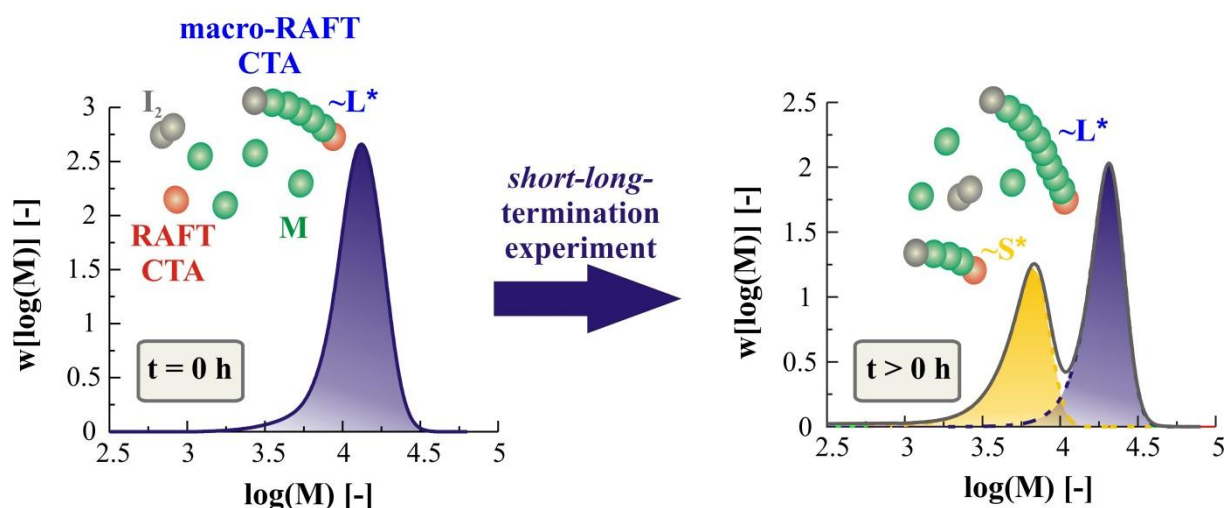


Figure 2.2: Composition of the polymerization mixture at the start (top left) and at a certain time (top right) of a RAFT-CLD-T short-long-termination experiment; ● = monomer molecule M , ● = RAFT CTA molecule, ● = conventional radical initiator fragment I originating from conventional radical initiator I_2 and S/L^* = number average chain length of short/long chain length distribution; also given are SEC traces of dormant species with w the mass fraction and the full grey line in right subfigure the total SEC trace, with in turn the dashed yellow and dashed blue lines the individual peaks after deconvolution.

On the other hand, based on the RAFT-CLD-T concept, Lovestead *et al.* showed via an *in silico* thought experiment starting with both pre-synthesized macro-RAFT agent and conventional RAFT CTA, that for *ideal* chain length distributions, *i.e.* assuming the presence of only two significantly separate macroradical chain lengths (S^* and L^* ; ideal case for Figure 2.2), $k_t^{S^*L^*}$ can be calculated as a function of the polymerization time t by following simple equation:^{37,38}

$$k_t^{S^*L^*}(t) = 2 \langle k_t \rangle (t) - \frac{1}{2} k_t^{S^*S^*}(t) - \frac{1}{2} k_t^{L^*L^*}(t) \quad (4)$$

when $\langle k_t \rangle$, the observed overall termination rate coefficient, is tracked and the same molar amounts for both the short and long macroradicals can be established along the polymerization. However, this assumption requires equimolar initial RAFT CTA amounts, which is in practice impossible due to the limited solubility of the macro-RAFT CTA. Hence, in the current work, the RAFT-CLD-T *short-long-termination* model of Lovestead *et al.*^{37,38} is extended so that it is also applicable if the assumption of equal concentration for both macroradical populations is invalid and non-monodisperse distributions are obtained, even

with possible overlap (*cf.* Figure 2.2 right). This generalization is based on the modification of the expression for the average termination rate coefficient for a single macroradical distribution to the case of two macroradical distributions:

$$\begin{aligned}
 r_{term,tot} = \langle k_t \rangle &= \left(\sum_{i=1}^{N_L} [R_i^L] + \sum_{i=1}^{N_S} [R_i^S] \right)^2 \quad (5) \\
 &= \sum_{i=1}^{N_S} \sum_{j=1}^{N_S} k_t^{ij,*} [R_i^S] [R_j^S] + \sum_{i=1}^{N_L} \sum_{j=1}^{N_L} k_t^{ij,*} [R_i^L] [R_j^L] \\
 &+ 2 \sum_{i=1}^{N_L} \sum_{j=1}^{N_S} k_t^{ij,*} [R_i^L] [R_j^S]
 \end{aligned}$$

in which $k_t^{i,j,*} = k_t^{ij}$ if $i \neq j$ and $k_t^{i,j,*} = 2 k_t^{ij}$ if $i = j$, and $[R_i^L]$ and $[R_i^S]$ are the concentrations of a macroradical with chain length i respectively belonging to the long chain (L) and short chain (S) macroradical population. The corresponding chain length ranges go from one to respectively N_L and N_S .

By subsequently introducing the molar fraction of the long chain radicals as:

$$f_1 = \frac{\sum_{i=1}^{N_L} [R_i^L]}{\sum_{i=1}^{N_L} [R_i^L] + \sum_{i=1}^{N_S} [R_i^S]} \quad (6)$$

and:

$$\langle k_t^{S*L*} \rangle = \frac{\sum_{i=1}^{N_L} \sum_{j=1}^{N_S} k_t^{ij,*} [R_i^L] [R_j^S]}{\sum_{i=1}^{N_L} [R_i^L] \sum_{i=1}^{N_S} [R_i^S]} \quad (7)$$

it can be derived from Equation (5) that:

$$\langle k_t^{S*L*} \rangle (t) = \frac{\langle k_t \rangle (t) - \langle k_t^{L*L*} \rangle (t) f_1^2(t) - \langle k_t^{S*S*} \rangle (t) (1 - f_1(t))^2}{2 f_1(t) (1 - f_1(t))} \quad (8)$$

Note that for f_1 equal to 0.5 Equation (4) is again obtained, which validates the original constrained model of Lovestead *et al.*^{37,38} Contrary to Equation (4), this extended expression for k_t^{S*L*} (Equation (8)) thus holds for *every* initial ratio of conventional RAFT agent to

macro-RAFT CTA, and is in practice only limited by the solubility of the macro-RAFT CTA in the polymerization mixture.

Importantly, Equation (8) uncovers the main hurdle that needs to be overcome to obtain reliable *short-long*-termination data, *i.e.* accurate values for $k_t^{S^*S^*}$ and $k_t^{L^*L^*}$ have to be known at each instant during the RAFT-CLD-T *short-long*-termination experiment, which is clearly characterized by a dynamically changing non-uniform polymer matrix (bimodal CLD in Figure 2.2 right) that might influence the diffusion behavior of the short and long radicals. Therefore, in the present work, besides the development of an improved RAFT-CLD-T protocol for the determination of accurate *homo*-termination rate coefficients, additionally the influence of the polymer matrix on the *homo*-termination reactivity is experimentally quantified to allow for a correct use of Equation (8) for the quantification of *short-long*-termination reactivities.

2.3.2 Improved determination of accurate *homo*-termination rate coefficients

For ideal conventional RAFT polymerizations³⁹ in which at any conversion a *perfectly uniform* polymer matrix is formed (Figure 2.3a; one chain length i^*) and retardation/inhibition phenomena can be neglected, Barner-Kowollik and coworkers previously reported that $k_t^{i^*i^*}$ can be obtained via following RAFT-CLD-T equation:²⁸⁻³⁶

$$k_t^{i^*i^*}(t) \approx \langle k_t \rangle (t) = \frac{r_{ini} - \frac{d}{dt} \left[\frac{r_{prop}(t)}{k_p([M]_0 - \int_0^t r_{prop}(t) dt)} \right]}{b \left[\frac{r_{prop}(t)}{k_p([M]_0 - \int_0^t R_{prop}(t) dt)} \right]^2} \quad (9)$$

in which r_{ini} is the initiation rate, r_{prop} the propagation rate, $[M]_0$ the initial monomer concentration, k_p the propagation rate coefficient, and b a parameter possessing a value of 2 to

account for the presence of a single chain length i^* . Note that Equation (9) is based on the change of the total radical concentration ($[R_{tot}]$), which in this specific case reduces to:

$$\frac{d[R_{tot}]}{dt} = \frac{d[R_{i^*}]}{dt} = r_{ini} - r_{term,tot} = 2fk_d[I_2] - 2k_t^{i^*i^*}[R_{i^*}]^2 \quad (10)$$

in which f is the initiator efficiency, k_d the dissociation rate coefficient, $[I_2]$ the concentration of conventional radical initiator and $r_{term,tot}$ the total termination rate, including a factor 2 in agreement with IUPAC recommendations.⁴⁰

However, in practice, in a RAFT-CLD-T *homo*-termination experiment the requirement for homogeneity of the polymer matrix is not completely fulfilled, since even under well-controlled RAFT polymerization conditions a macroradical CLD with a dispersity somewhat higher than one is established (Figure 2.3b). Under such conditions, termination mainly occurs between chains possessing *approximately* a chain length of i^* and hence, to guarantee the measurement of correct *absolute* $k_t^{i^*i^*}$ values, the factor 2 for $r_{term,tot}$ in Equation (10) has to be removed (*cf.* Appendix A):

$$r_{term,tot} = \langle k_t(t) \rangle [R_{tot}]^2 \approx k_t^{i^*i^*}(t) \left(\sum_{i=1}^N [R_i] \right)^2 \quad (11)$$

Consequently, in practice, the parameter b in Equation (9) has to be given a value of 1 instead of 2. The necessity of this update has been confirmed with deterministic simulations explicitly integrating all chain length dependent populations balances (Figure 2.3c) showing that the observed termination rate coefficient as based on Equation (9) with b equal to 1 is approximately equal to the real *homo*-termination rate coefficient $k_t^{i^*i^*}$ (dashed blue line). Average relative errors range from 5-15 % and are around 0.5-1 % on a log-basis. Clearly, the original equation assuming a dispersity of one (b equal to 2 in Equation (9); full red line), leads to a significant underestimation of the true $k_t^{i^*i^*}$. The parameters used in the simulations are taken from the previous work of Monteiro and coworkers⁴¹ and are listed for completeness

in Table 2.2. It is important to note that this modification applies to every $k_t^{i^*i^*}$ determination technique (including also PLP-based techniques coupled with ESR and IR detection) that is based on Equation (10). Despite this mismatch in absolute values, the chain length and conversion dependency of $k_t^{i^*i^*}$ do not change, as evident from the equal slopes, implying that all previously reported α -values remain valid.^{6,31,42}

At first sight, one could argue about the relevance of the aforementioned factor 2 for the absolute values of $k_t^{i^*i^*}$, since their scatter in literature spans one order of magnitude (MMA case), even after correction for the correct IUPAC recommended k_p values.^{43,44} However, it is generally accepted that this scatter in absolute values can be mostly ascribed to a significant difference in the polymerization matrices in which the $k_t^{i^*i^*}$ values were determined.^{31,42} Moreover, based on literature data for single experimental techniques, it follows that the error on absolute $k_t^{i^*i^*}$ values typically amounts to a factor 1.35, which is well below a factor of 2.³¹ In particular, Junkers *et al.*³¹ compared absolute $k_t^{i^*i^*}$ values for *n*-butyl acrylate (*n*BA) obtained both via the RAFT-CLD-T and the SP-PLP-RAFT technique. The relative discrepancy between the absolute $k_t^{i^*i^*}$ values was below a factor 1.6, even in the presence of smaller but significant matrix differences; data of a RAFT polymerization with a dithio-RAFT agent were compared with those with a symmetrical trithio-RAFT agent, implying a chain length of the dormant polymer molecules which is twice as high. The factor 2 is therefore significant with regards to the error of the respective experimental method, requiring a correct application of Equation (11). In addition, it should be remembered that this correction for the absolute values of the *homo*-termination rate coefficients is of paramount importance for a fundamental understanding and an accurate optimization of radical polymerization processes, which is illustrated in Figure 2.3d for the exemplary case of nitroxide mediated polymerization (NMP), an important RDRP technique.

Table 2.2: Parameters used in the simulations performed in order to support the modification of the RAFT-CLD-T formula with a factor 2 (Equation (9) with $b=1$ in the main text). Parameters are taken from the work of Monteiro and coworkers.⁴¹ C_{tr} is the transfer coefficient corresponding with the macro-addition-fragmentation. $C_{tr,0}$ corresponds with the addition-fragmentation reactions involving initiator species or conventional CTA.

parameter	value
k_d [s^{-1}]	1.1×10^{-4}
f [-]	0.7
k_p [$L \text{ mol}^{-1} \text{ s}^{-1}$]	1332
k_{tc}/k_{td}	0.01
k_t [$L \text{ mol}^{-1} \text{ s}^{-1}$]	composite k_t model
C_{tr} [-]	140
$C_{tr,0}$ [-]	15.2

It is clear that the incorrect absolute values of k_t (red lines in Figure 2.3c) induce a significant underestimation of the reaction time, while the end-group functionality is slightly overestimated (red line in Figure 2.3d). The mismatch in reaction time has a pronounced effect on the optimization of the considered NMP process. Simulations were performed for the NMP of styrene mediated by N-(2-methyl-2-propyl)-N-(1-diethylphosphono-2,2-dimethylpropyl)-N-oxyl (SG1) at 120 °C and a targeted chain length of 500. Rate coefficients were taken from literature.⁴⁵

For completeness it is mentioned here that, under viscous conditions, Equation (9) can be further improved by accounting for the volume contraction throughout the polymerization as illustrated in the Appendix B.1.

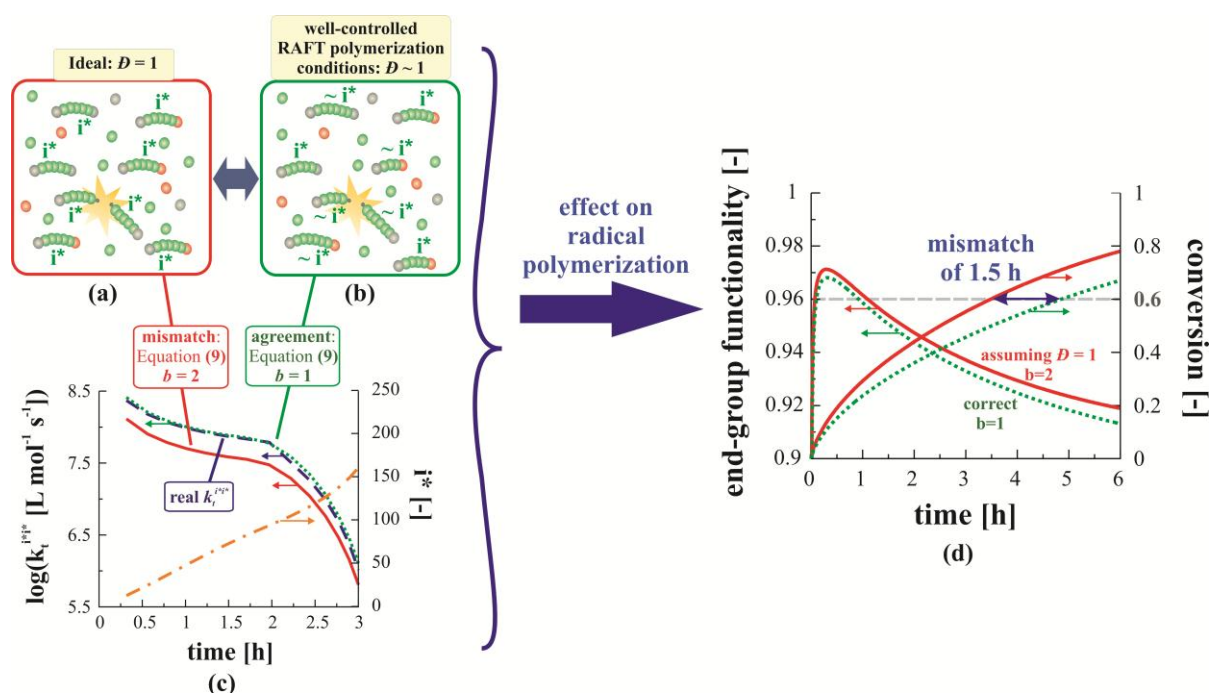


Figure 2.3: Importance of the use of the improved RAFT-CLD-T formula for homo-termination experiments ($b=1$ instead of 2 in Equation (6)): Schematic representation of (a) ideal and theoretical conditions in which all macrospecies possess a chain length i^* (dispersity (\mathcal{D}) = 1; only case in which Equation (9) ($b=2$) is valid); (b) “well-Controlled” RAFT polymerization conditions with macrospecies possessing a chain length close or equal to i^* (\mathcal{D} slightly different from one; Equation (9) ($b=1$) is valid); ● = monomer molecule, ● = RAFT CTA molecule and ● = conventional radical initiator fragment originating from conventional radical initiator I_2 . (c) Correctness of the improved Equation (9) ($b=1$; dotted green line; logarithmic scale) to measure $k_t^{i^*i^*}$ during a RAFT-CLD-T experiment, as good agreement with the implemented $k_t^{i^*i^*}$ (dashed blue line); i^* = number average chain length (dashed-dotted orange line). The original RAFT-CLD-T equation (full red line; Equation (9) ($b=2$)) leads however to a mismatch. (d) Illustration of necessity of correct absolute values for $k_t^{i^*i^*}$ for optimization of radical polymerization processes (factor 2 difference between green and red lines for a representative RDRP case); Intrinsic kinetic parameters for (c): Table 2.2 and for (d): reference⁽⁴⁵⁾.

For MMA radical polymerization at 353 K, Monteiro and coworkers^{28,29} previously highlighted the different *homo*-termination regimes with respect to a dominance in diffusion mode based on a measured $k_t^{i^*i^*}$ surface as function of the chain length and the polymer mass fraction, and provided a detailed understanding of the gel-effect and its physical interpretation.²⁸ However, this $k_t^{i^*i^*}$ surface was derived from a fit to a limited RAFT-CLD-T experimental data set aiming mostly at higher chain lengths, ignoring density differences, and using Equation (9) with b equal to 2 instead of 1, *i.e.* neglecting the effect of the macroradical

CLD and thus inducing a significant error on the *absolute* termination rate coefficients. In the present contribution, not only a broader range of (w_p, i^*) combinations is considered (entry 1-14 in Table 2.1) but the surface interpolation (Figure 2.4) is also performed via the improved RAFT-CLD-T equation (Equation (6); $b = 1$), including an additional correction for the propagated error on its input parameters (Table 2.3 and Appendix B.3) and for the volume contraction throughout the polymerization (Appendix B.1). Note that the calculated propagated error for each RAFT-CLD-T *homo*-termination experiment has been added as a random scatter to the corresponding $k_t^{i^*j^*}$ before the surface interpolation is performed (Figure 2.4).

Table 2.3: Input parameters of the RAFT-CLD-T equation (Equation (9)) and their standard deviation (STDEV). Specified values are based on literature data.

Parameter	units	Mean value	STDEV ^a	reference
ΔH	kJ mol^{-1}	-54	2	46-50
k_d	10^{-4} s^{-1}	1.30	0.25	48,49,51-53
f	–	0.6	0.1	48,52,53
k_p	$\text{L mol}^{-1} \text{ s}^{-1}$	1318	264	43,44
<i>volumetric sampling</i> ^c	mL	5 ^b	0.1	–
<i>weighing</i> ^c	g	0.01 ^b	0.0001	–

^asince the error is assumed to be distributed normally, STDEV corresponds with the 66% confidence interval

^btypical values

^cdetermined by the precision of the employed syringes and balance.

An *average* relative error of 50% on $k_t^{i^*j^*}$ and correspondingly 3% on log scale are obtained (*cf.* Appendix B.3), which are only slightly higher compared to those for the PLP based techniques.^{24,42,43} As shown in Figure 2.4b, the propagated error increases for higher polymer mass fractions and chain lengths, which is related to the cumulative nature of the DSC data.

The equation of the improved surface function and its regression characteristics can be found in Appendix B.4. As highlighted before, access to accurate *homo*-termination rate coefficients is crucial for the reliable determination of the corresponding *short-long*-termination rate coefficients via Equation (8). Therefore, in the present work, the high accuracy of the obtained *homo*-termination surface is confirmed in two ways as explained below.

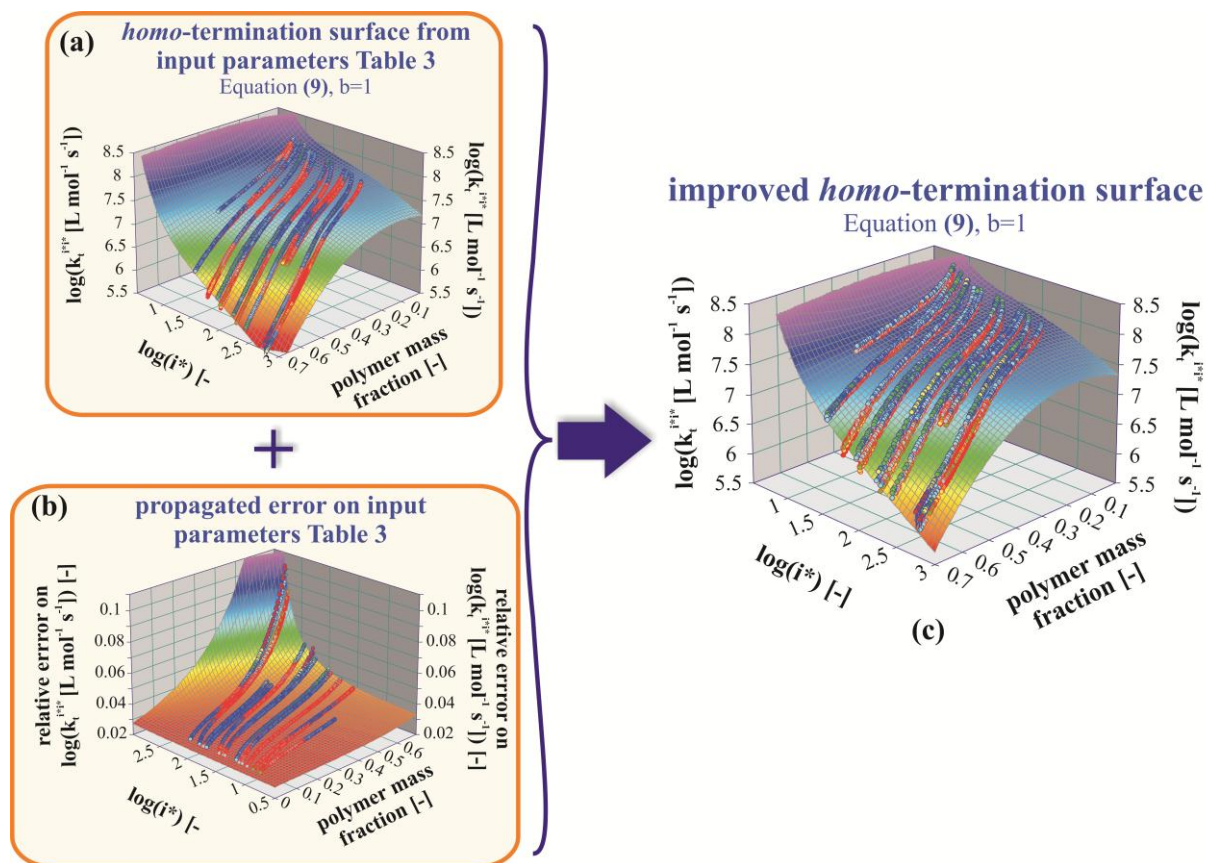


Figure 2.4: Generic framework for the improved homo-termination ($k_t^{i*i^*}$) surface for MMA polymerization at 353 K: (a) Improved RAFT-CLD-T $k_t^{i*i^*}$ surface (Equation (6); $b = 1$) for regression analysis (a) prior and (c) after a correction for the uncertainty on its input parameters (Table 2.3). This correction is obtained by adding the relative maximal error data in (b) as obtained via a propagation of uncertainty analysis as scatter; blue points are located above the surface function, whereas the red points are located below the surface; only conversions between 0.05 and 0.7 are included (cf. Appendix B.2). Drop lines indicate minor deviation from the surface; experimental conditions: entry 1-14 in Table 2.1; surface equations and regression characteristics are provided in Appendix B.4.

On the one hand, since in the RAFT-CLD-T method k_t is calculated based on on-line DSC measurements combined with off-line SEC measurements in a parallel sampling experiment, it is highly recommended to verify this coupling of two different datasets by the measurement

of a common response. The conversion is deduced from the recorded DSC heat flux signal and it is also measured by $^1\text{H-NMR}$ for each sample (in parallel with the SEC measurement). In the current work, only conversion regions for which there is a good agreement between the on-line DSC analysis and the off-line $^1\text{H-NMR}$ analysis (parallel experiment) are included in the surface fitting procedure to avoid possible systematic errors when coupling the off-line $^1\text{H-NMR}$ and SEC (w_p , i^*) data with the on-line DSC based $k_i(t)$ data. This requirement implies that some of the experimental lines for which the conditions are specified in Table 2.1 have to be already truncated at 50% conversion. Conversions lower than 5% and higher than 70% are also excluded from the surface fitting procedure to allow for a sufficient equilibration time of the DSC instrument and a sufficiently narrow macroradical chain length distribution (conversions $> 5\%$), and to prevent any interference of diffusional limitations on the conventional radical initiation process and propagation (conversions $< 70\%$). These additional constraints are indicated in Figure 2.5 by a grey zone.

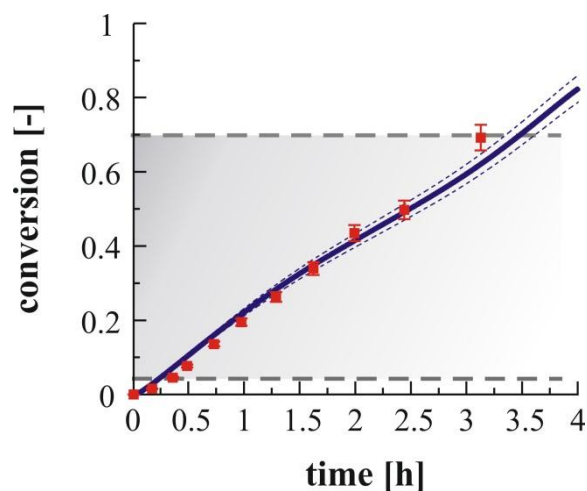


Figure 2.5: Comparison of conversion measurements via on-line DSC (full blue line) and off-line $^1\text{H-NMR}$ analysis (red squares); red error bars indicate 5% relative error; dashed blue lines represent error on the conversion via DSC (4.5%); the grey zone marks the 5% to 70% conversion region outside of which no data are considered to allow for a sufficient equilibration time of the DSC instrument and a sufficiently narrow macroradical chain length distribution and to prevent any significant interference of diffusional limitations on the conventional radical initiation process and propagation; Conditions: entry 4 in Table 2.1.

Figure 2.5 shows for entry 4 in Table 2.1 the good agreement between the conversion measured by on-line DSC (full blue line) and off-line $^1\text{H-NMR}$ analysis (red squares). Conversion data from off-line $^1\text{H-NMR}$ and on-line DSC measurements are also subject to error. On the one hand, repeat experiments revealed a relative error lower than 5% on the conversion measurements in the off-line sampling experiments, as is clear from Figure 2.6. On the other hand, the scatter on the ΔH values in Table 2.3 yields a deviation of 4.5% on the conversion calculated from the DSC heat profiles. Hence, possible systematic errors when coupling the off-line $^1\text{H-NMR}$ and SEC (w_p, i^*) data with the on-line DSC k_t data value up to 5% on conversion (see Figure 2.5), yielding a maximum systematic error of 15% on $k_t(w_p, i^*)$ via the propagation of error formulas. The repeat experiments (Figure 2.6) also clearly indicate the high reproducibility of the chain length data measured via SEC, with average deviations on (i^*) lower than 5% (translates to an error $< 5\%$ on $\log(i^*)$).

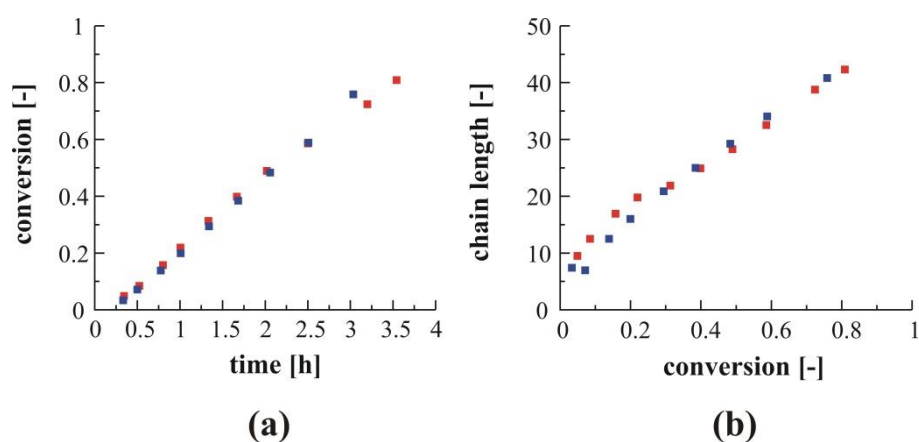


Figure 2.6: Very good agreement between conversion (a) and chain length (b) profiles for two duplicate experiments to check the reproducibility of the applied experimental procedure. Duplicate experiments were performed on different days. Conditions: entry 5 (blue dots) and 11 (red dots) in Table 2.1.

Note that in general the errors on the conversion and chain length data result in a beamlike error for each $k_t(w_p, i^*)$ data point as demonstrated by Figure 2.7. However, since these deviations are small, only one-dimensional vertical error bars can be considered for the reported $k_t^{i^*}$ values in this contribution.

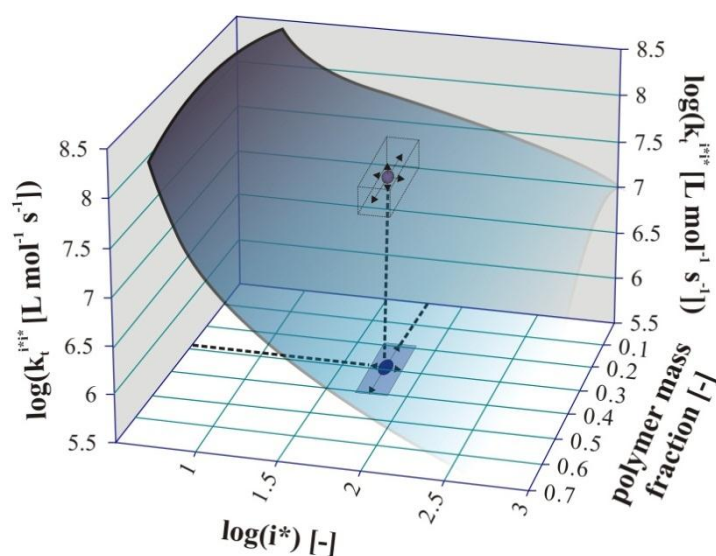


Figure 2.7: Schematic representation of the beamlike error on the $\log[k_t(w_p, i^*)]$ values. In this work only the vertical error bar is considered as the deviations on $\log(i^*)$ and the polymer mass fraction are small.

It should be stressed that each DSC analysis has been performed at least in duplicate and a good agreement is obtained between the calculated *homo*-termination rate coefficients corresponding to the reproducibility check experiments in entry 5 (full blue line) and 11 (dotted red line) in Table 2.1, which were thus performed on different days (Figure 2.8).

In accordance with the IUPAC guideline^{31,42} that for each k_t measurement the corresponding polymer matrix should be specified, and to prove the reliability of the performed k_t -measurements and consequently the fitted $k_t^{i^*i^*}$ surface function, in Appendix B.2 for all RAFT-CLD-T *homo*-termination experiments the chain length, dispersity and conversion data are plotted. For the latter, both the on-line DSC results (full blue line) and off-line $^1\text{H-NMR}$ data (red squares) are shown together with their respective scatter.

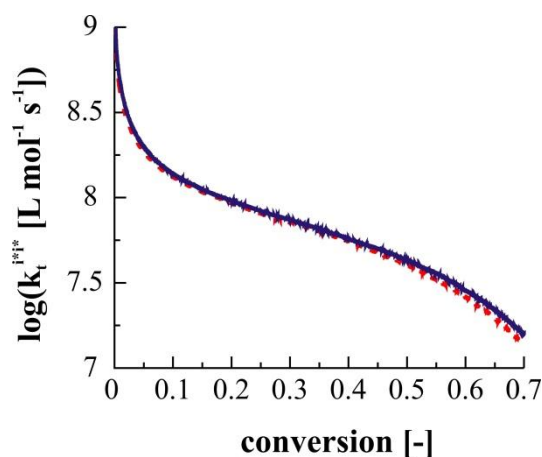


Figure 2.8: Good reproducibility of the calculated termination rate coefficient in the RAFT-CLD-T *homo*-termination experiments on different days. Conditions: entry 5 (full blue line) and entry 11 (dotted red line) in Table 2.1.

On the other hand, an important aspect of the successfulness of the proposed technique to measure *short-long*-termination coefficients (Equation (8)), is the accuracy of the *homo*-termination surface in case macro-RAFT CTA is present. Therefore, a modified RAFT-CLD-T *homo*-termination experiment starting with macro-RAFT CTA instead of conventional small RAFT CTA is first analyzed. For this experiment, it is tested whether the obtained *homo*-termination rate coefficients (Equation (9) $b = 1$; full green line in Figure 2.9) agree with the corresponding values derived from the previously determined *homo*-termination surface function (Figure 2.4c) at the average chain length and polymer mass fraction reached.

As shown in Figure 2.9, a good overall agreement is obtained for the test experiment and consequently it could be concluded at first sight that the values for the *homo*-termination rate coefficients during a cross-termination experiment can always be safely obtained from the *homo*-termination surface function (Figure 2.4c).

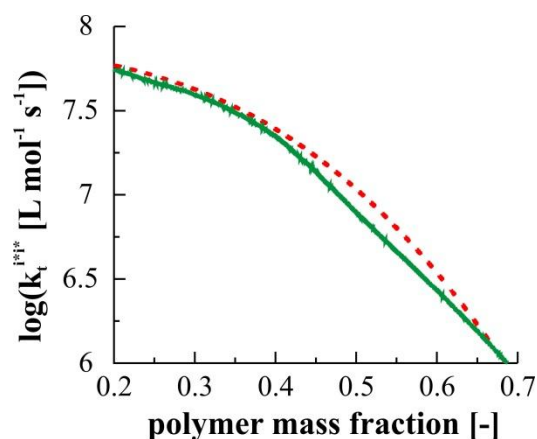


Figure 2.9: A good agreement between the homo-termination rate coefficient obtained via the RAFT-CLD-T technique when started from a polymerization mixture containing macro-RAFT CTA instead of conventional RAFT agent (full green line) and the homo-termination rate coefficient derived from the homo-termination surface function in Figure 2.4c at the corresponding average chain lengths and polymer mass fractions (dashed red line).

For completeness, also the number average chain length, dispersity and polymer mass fraction data are given in Figure 2.10a-c. The conditions of the performed modified RAFT-CLD-T experiment starting from macro-RAFT CTA instead of conventional RAFT CTA are:

$$[MMA]_0/[macro-RAFT\ CTA]_0 = 880 \text{ and } [macro-RAFT\ CTA]_0/[AIBN]_0 = 6.$$

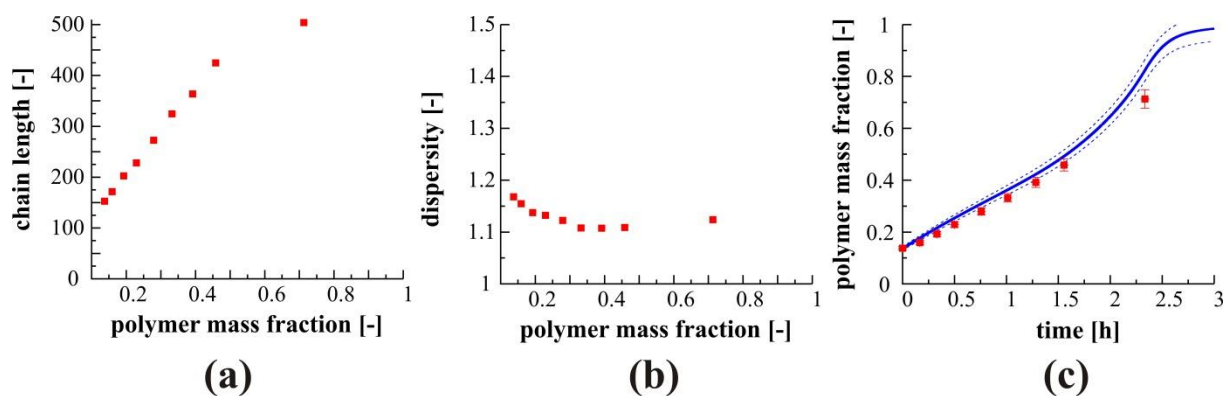


Figure 2.10: Number average chain length (left), dispersity (middle) and polymer mass fraction data (right) for the modified RAFT-CLD-T homo-termination experiment starting from macro-RAFT CTA instead of conventional (small) RAFT CTA. For the conversion results, both the on-line DSC (full blue line) and the off-line 1H -NMR data (red squares) are shown together with their respective error, similar to Figure 2.5.

2.3.3 First-time experimental quantification of possible matrix effects on homo-termination reactivity

As explained above, due to the *non-uniform* polymer matrix in a RAFT-CLD-T *short-long*-termination experiment (Equation (8)), it cannot be taken for granted that the corresponding *homo*-termination rate coefficients $k_t^{S^*S^*}$ and $k_t^{L^*L^*}$ are well represented by the *homo*-termination surface determined in a uniform polymer matrix (*cf.* Figure 2.4c), *i.e.* a correction for a so-called ‘matrix effect’ could be required. This non-uniform character is schematically presented in Figure 2.11a considering chains with a length i of 20 and 200. For *homo*-termination between radicals with $i = 20$ (grey macromolecules), the corresponding uniform matrix is presented in Figure 2.11b. Note that only in case the diffusion behavior of the macroradicals in both polymer matrices is similar, matrix effects can be neglected and thus matrix (b) can serve as a valid approximation for matrix (a).

To quantify the extent to which matrix effects influence the values of $k_t^{S^*S^*}$ and $k_t^{L^*L^*}$, an additional set of five modified RAFT-CLD-T *homo*-termination experiments was performed in which a given amount of dead narrow PMMA standard was initially added ($M_n = 9800$ g mol⁻¹; $\mathcal{D} = 1.05$; conditions entry 15-19 in Table 2.1; conversion, chain length and dispersity data in Appendix C.1). As the mass fraction of the PMMA standard does not change during the RAFT polymerization, the relative importance of its presence decreases and therefore a range of different types of polymer matrices is accessed per RAFT-CLD-T experiment. In Figure 2.11c, the measured *homo*-termination rate coefficients in these non-uniform polymer matrices (denoted $k_{t,NU}^{ii}$) are compared with those in the corresponding uniform polymer matrix (*cf.* Figure 2.11b; denoted $k_{t,U}^{ii}$) by plotting their ratio (full blue lines) as a function of the polymer mass fraction and the logarithm of the *mass* average chain length of the polymer matrix (J_m^*), two key properties to represent the average polymer matrix composition. The color map in Figure 2.11c is the corresponding fitted surface function and its regression

characteristics can be found in the Appendix C.2. It is clear that for a higher j_m^* , thus a higher chain length i , the ratio of $k_{t,NU}^{ii}$ to $k_{t,U}^{ii}$ fluctuates around one, evidencing a negligible interference of matrix effects under such conditions. In contrast, for lower j_m^* values (blue zone in Figure 2.11c) a significant influence is observed, indicative of an increased free volume and, hence, a higher mobility for the terminating short chain radicals (*cf.* Figure 2.11a versus 2.11b).

Importantly, for the performed *short-long*-termination experiments (entry 20-23 Table 2.1) of which the corresponding (w_p, j_m^*) combinations are depicted as fuchsia lines in Figure 2.11c, *no correction* for the required $k_t^{S^*S^*}$ and $k_t^{L^*L^*}$ values is needed (orange zone in Figure 2.11c; ratio of *ca.* 1). The absence of matrix effects for these higher chain lengths can also be deduced from Figure 2.11d, which focuses on specific (w_p, j_m^*) combinations in the higher chain length region of Figure 2.11c (entry 16-19 in Table 2.1). It shows four sets of interconnected points of similar i and same w_p as illustrated in Figure 2.12. However, since for each corresponding experiment (entry 16-19 in Table 2.1) a different initial amount of PMMA standard was added, each intersection point in Figure 2.12 yields two points on Figure 2.11d, as the total polymer mass fraction is the same but the mass fraction of PMMA standard (w_{ST}) is different. The third point for each series in Figure 2.11d is obtained from the *homo*-termination surface in Figure 2.4c at that particular termination chain length i and polymer mass fraction w_p , as this surface function was obtained in the absence of any PMMA standard. The error bars in Figure 2.11d are the propagated errors from the RAFT-CLD-T input parameters (Table 2.3). It is clear that no influence of the polymer matrix is observed for the considered (w_p, i) combinations.

For completeness it should be mentioned that a reliable quantification of matrix effects in a broad range of polymer environments requires a much more extended data set than the one used to determine the interpolated surface function presented in Figure 2.11c (color map) for

the studied *short-long*-termination conditions. Such extension is straightforward using the described generic experimental procedure.

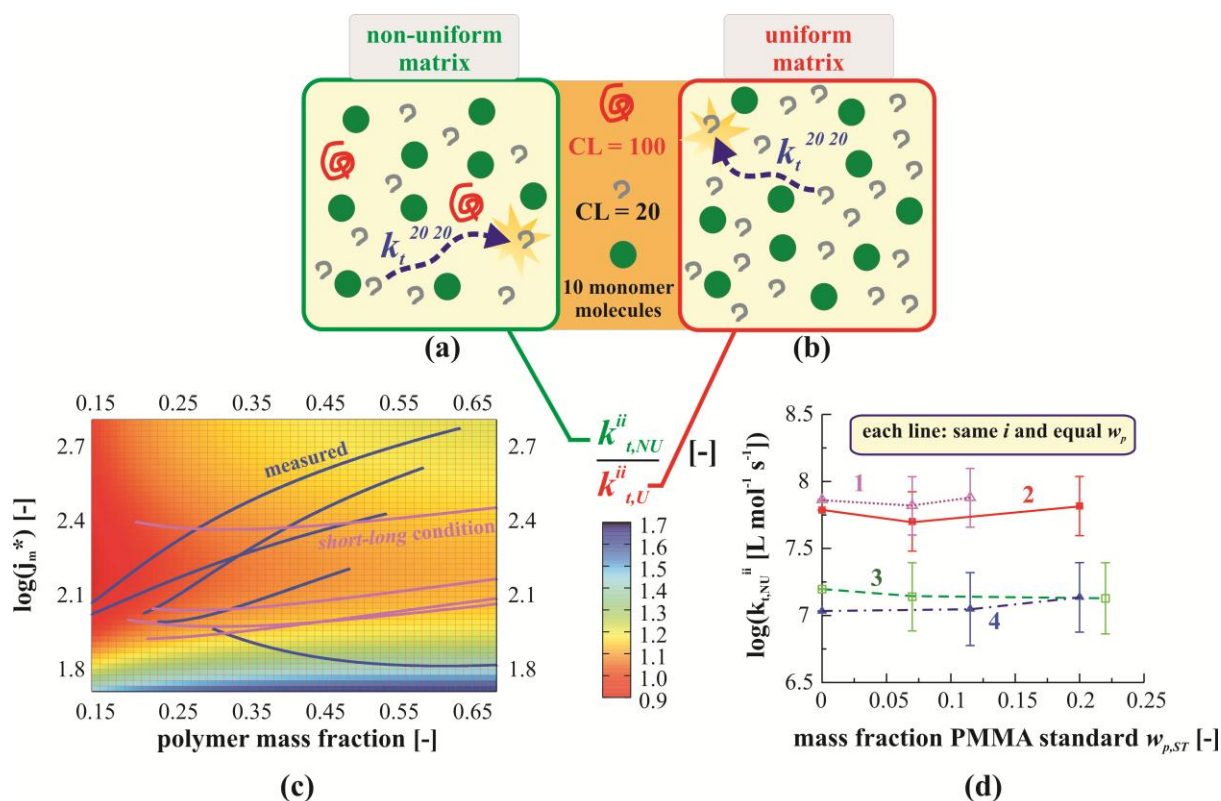


Figure 2.11: Conceptual representation of a possible matrix effect with (a) non-uniform matrix with 100 monomer molecules, 10 chains of chain length CL 20 and 2 chains of CL 100 and with (b) the corresponding uniform matrix (CL=20) (c) Quantification of a possible matrix effect for k_t^{ii} by the ratio of the homo-termination coefficient obtained via the RAFT-CLD-T technique (Equation (9); $b=1$; blue lines) in the presence of dead PMMA standard (non-uniform matrix; $k_{t,NU}^{ii}$), to the homo-termination rate coefficient assuming a uniform matrix as determined from the surface function in Figure 2.4c ($k_{t,U}^{ii}$); j_m^* : the mass average chain length of the polymer matrix; fuchsia lines: RAFT-CLD-T short-long-termination experiments (entry 20-23 in Table 2.1). (d) $k_{t,NU}^{ii}$ for increasing amounts of dead PMMA standard based on entry 16-19 in Table 2.1 but with a fixed (total) polymer mass fraction w_p and chain length i of the terminating radicals. Points for $w_{p,ST} = 0$ are derived from Figure 2.4c; the error bars are calculated via the propagation of error analysis; negligible matrix effect for the considered conditions as almost flat lines result; points of similar i and w_p are indicated in Figure 2.12.

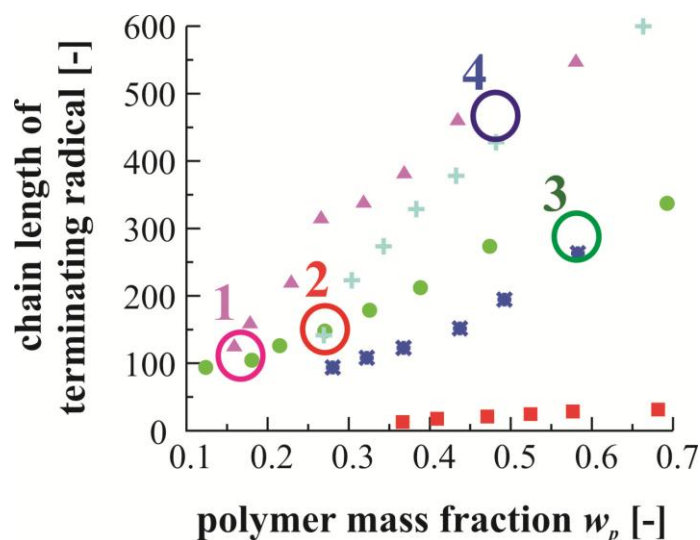


Figure 2.12: Chain length of the terminating macroradicals versus the total polymer mass fraction for entry 15-19 in Table 2.1. Points of similar i and equal w_p are marked by a colored circle and yield two corresponding points with different mass fraction of PMMA standard ($w_{p,ST}$) in Figure 2.11d (same number).

2.3.4 First-time experimental determination of short-long termination rate coefficients

Various conditions have been screened in which the ratio of monomer to total RAFT agent, the average chain length of the macro-RAFT agent and its initial concentration were varied as listed in Table 2.1 (entry 20-23). The macro-RAFT agents of three different chain lengths were synthesized and isolated via a conventional RAFT polymerization procedure and high end-group functionality was ensured by $^1\text{H-NMR}$ measurements and elemental analysis. Similarly to the RAFT-CLD-T *homo*-termination experiments, the reliability of the obtained experimental data has been verified by the agreement between the off-line $^1\text{H-NMR}$ and on-line DSC conversion data and by additional repeat experiments (*cf.* Appendix D.3).

For a representative *short-long*-RAFT-CLD-T experiment (entry 20 in Table 2.1) with the observed average termination rate coefficient $\langle k_t \rangle$ as direct output (Figure 2.13a), Figure 2.13c shows the evolution of $k_t^{S^*L^*}$ at intermediate polymer mass fractions ($0.2 < w_p < 0.5$; dotted fuchsia line), as calculated via Equation (8). In agreement with diffusion studies,^{54,55} the measured $k_t^{S^*L^*}$ data are located between the $k_t^{S^*S^*}$ (full yellow line) and $k_t^{L^*L^*}$ (full blue

line) data. It should be remembered that for these *homo*-termination data, no correction for a polymer matrix effect is needed (*cf.* Figure 2.11c-d). Moreover, based on Figure 2.13b, it follows that they are obtained from the ‘safe’ non-extrapolated region of the *homo*-termination surface (*cf.* also Appendix D.3). Furthermore, a propagation of error analysis revealed that the relative error on $k_t^{S^*L^*}$ amounts to 50%, which is comparable to the error on $k_t^{S^*S^*}$ and $k_t^{L^*L^*}$, highlighting the physical relevance of the reported *short-long*-termination data (*cf.* Appendix D.2). The maximum value of 0.5 for w_p is selected to avoid the interference of diffusional limitations on initiation and propagation.⁵⁶⁻⁵⁸ As such limitations are ignored for the calculation of the termination rate coefficients in the present work (Equation (8) with intrinsic rate coefficients), the “measured” *short-long*-termination rate coefficients become too low at polymer mass fractions above 0.5. As expected, the onset of the diffusional limitations moves towards lower polymer mass fractions for polymer matrices consisting of higher chain lengths, which is illustrated in Figure 2.14.

The proposed generic framework, which requires in principle only a sensitive DSC instrument and dedicated SEC analysis (*cf.* Methods and Analysis sub section for summary), yields thus reliable *short-long*-termination data and allows to address for the first time the important scientific question to the relation between these model-free data and the currently widespread average-based diffusion theories.

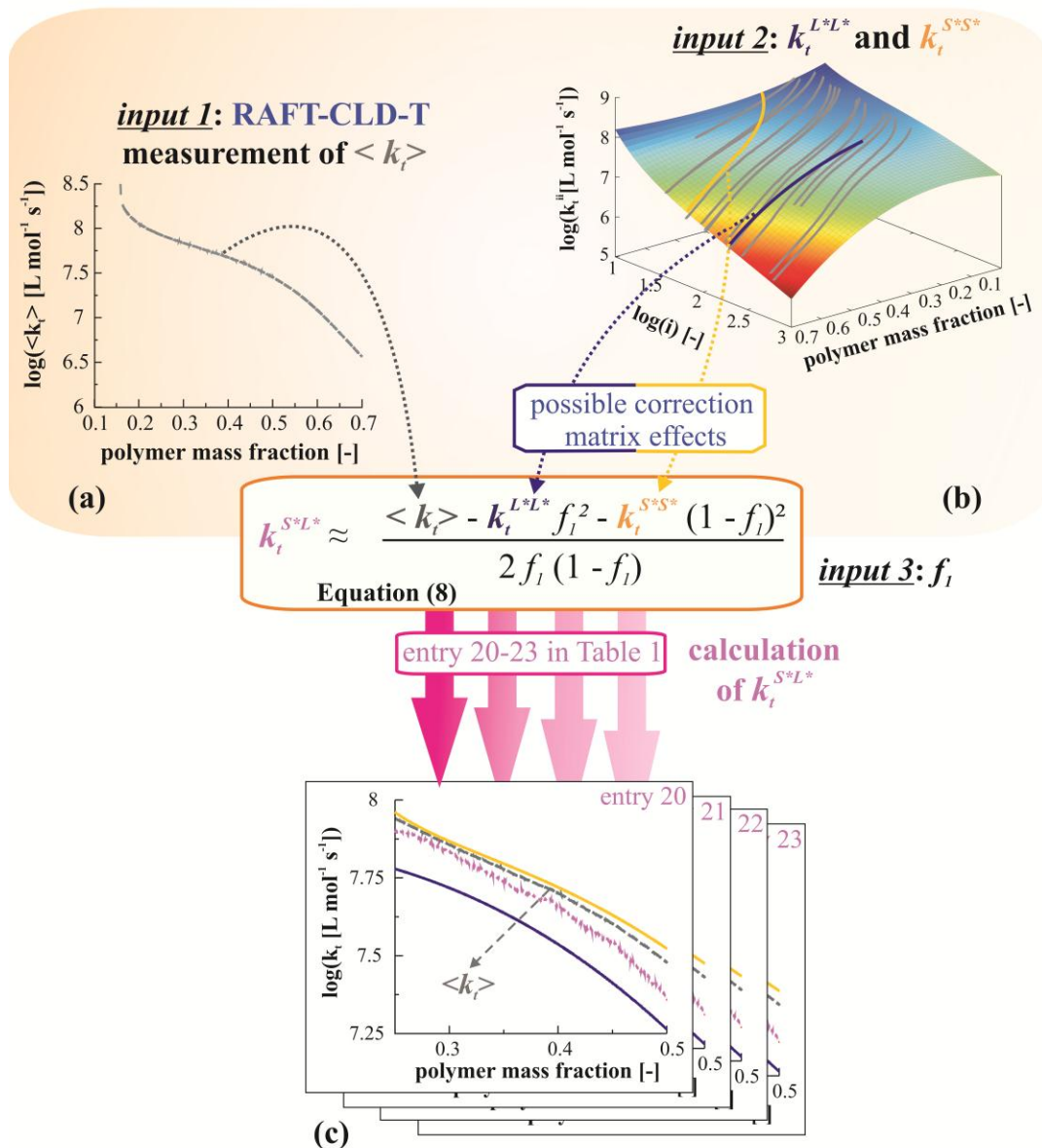


Figure 2.13: Generic framework for the reliable quantification of short-long-termination reactivities and the validation of diffusion theories, applied to MMA polymerization at 353 K: (a) $\langle k_t \rangle$ (Equation (9), $b=1$) derived from DSC measurements (dashed grey line) (b) Illustration that $k_t^{L^*L^*}$ and $k_t^{S^*S^*}$ can be directly and reliably determined from the non-extrapolated region of the homo-termination surface (Figure 2.4c), taking into account that no correction for a matrix effect is needed (fuchsia lines in Figure 2.11c) (c) $k_t^{S^*L^*}$ for entry 20 in Table 2.1 assuming a constant f_i given by the initial molar fraction of macro-RAFT CTA (dotted fuchsia line); $k_t^{L^*L^*}$ (full yellow line), $k_t^{S^*S^*}$ (full blue line) and $\langle k_t \rangle$ (dashed black line)

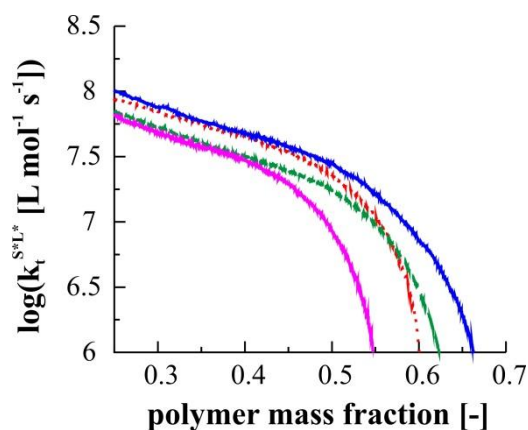


Figure 2.14: Short-long-termination rate coefficient as function of the polymer mass fraction for entry 20-23 in Table 2.1. The onset of the diffusional limitations on initiation shifts to lower polymer mass fractions for higher chain lengths. Entry 20, TCL 135, CL macroCTA 140: red; entry 21, TCL 166 CL macroCTA 140: green; entry 22, TCL 126 CL macroCTA 100: blue; entry 23 TCL 292 CL macroCTA: fuchsia.

For simplicity, when applying Equation (8) in Figure 2.13, the molar fraction of macro-RAFT CTA-derived radicals (f_l) is taken equal to the initial molar fraction of macro-RAFT CTA along the *short-long*-RAFT-CLD-T experiment. In general, f_l is however time dependent. Its variation in time is governed by the probability of a radical to add to either dormant macrospecies or conventional RAFT CTA and, hence, depends on the difference in value of the transfer coefficient for addition/fragmentation of small and macroradical species. Simulations elucidated that equal values for both transfer coefficients yield a constant f_l -value, which can be safely approximated by the initial molar fraction of macro-RAFT CTA with regard to the total amount of CTA in the mixture (macro-RAFT CTA and conventional RAFT CTA together). For a higher macro-transfer coefficient, as expected for the considered RAFT polymerization of MMA,⁴¹ f_l approaches the previous boundary only at higher times; a value close to one results initially which then decreases according to the conventional RAFT CTA conversion, which can be derived from the SEC traces (*cf.* Appendix D.1).

Figure 2.15 depicts the simulation results for both possible situations for f_l depending on the relative values of the transfer coefficients. In case f_l is time dependent (dashed green line; higher macro-addition/fragmentation transfer coefficient), it clearly reaches its final value at

the same rate as the consumption of conventional RAFT CTA (full red line corresponds to conventional RAFT CTA conversion). Hence, in the limit two calculation methods can be identified for f_I and concomitantly for the *short-long*-termination rate coefficient k_t^{S*L*} (Equation (8)). Since the conventional RAFT CTA is typically fully consumed before the monomer reaches 20% conversion, only at low polymer mass fractions a discrimination can be made between both f_I values and thus the impact of the uncertainty on f_I is limited. Hence, in first approximation f_I can be taken constant, as was done for the construction of Figure 2.13 and 2.15.

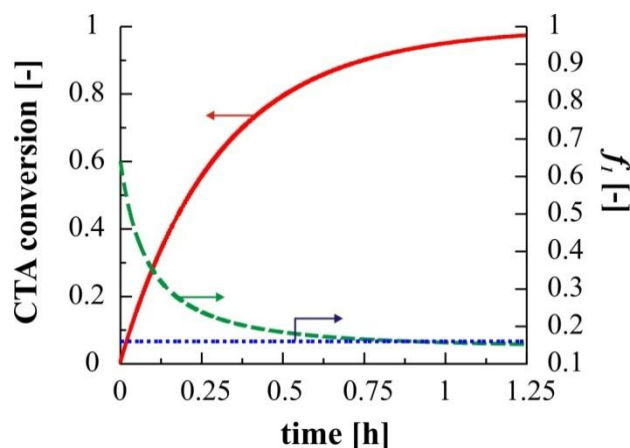


Figure 2.15: Variation of f_I as a function of time. In the case of equal transfer coefficients for the macro-addition/fragmentation and the one involving small molecules, f_I is constant and can be approximated by the initial molar fraction of macro-RAFT CTA (dotted blue line). On the other hand, unequal values of the transfer coefficients induce a time dependency of f_I which then reaches its final value according to (dashed green line) the conventional RAFT CTA conversion (full red line). Rate coefficients used in the simulation: Table 2.2; conditions: $[MMA]_0/[CTA_{tot}]_0 = 150$; $[CTA_{tot}]_0/[AIBN]_0 = 15$; $[macro-RAFT\ CTA]_0/[CTA_{tot}]_0 = 0.2$; initial CL macro-RAFT CTA = 100.

Besides its possible time dependence, also the absolute value of f_I should be taken into consideration. A lower f_I value decreases the contribution of *short-long*-termination to the observed overall termination rate coefficient, which leads to less accurate values for k_t^{S*L*} as the influence of experimental error becomes larger. Ideally, in every *short-long*-termination

experiment the macro-RAFT CTA and the conventional RAFT CTA should be added in equimolar amounts ($f_I = 0.5$), however the finite solubility of the macro-RAFT CTA in MMA limits this to an f_I -value of about 0.3 depending on the chain length of the macro-RAFT CTA. Higher f_I -values could be obtained when targeting higher chain lengths, however, this strongly complicates the deconvolution procedure as the overlap significantly increases. Figure 2.16 depicts an illustrative example how a too low f_I value affects the obtained *short-long*-termination rate coefficient yielding non reliable values for the whole polymer mass fraction range (conditions: $[MMA]_0/[CTA_{tot}]_0 = 97$; $[CTA_{tot}]_0/[AIBN]_0 = 21.8$; $[macro-RAFT\ CTA]_0/[CTA_{tot}]_0 = 0.127$; initial CL macro-RAFT CTA = 260).

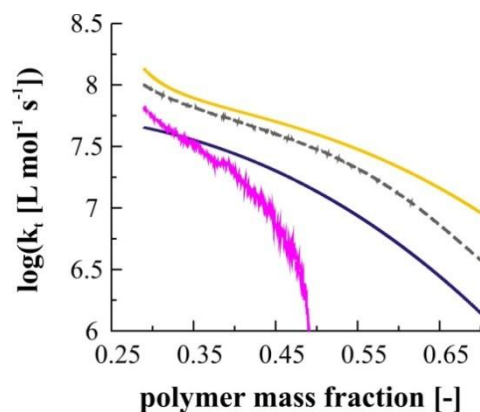


Figure 2.16: Only RAFT-CLD-T *short-long-termination* experiments with a sufficiently high initial molar fraction of macro-RAFT CTA (f_I) compared to conventional small RAFT CTA yield reliable *short-long-termination* data. Here the fuchsia line is the *short-long-termination* rate coefficient for the conditions: $[MMA]_0/[CTA_{tot}]_0 = 97$; $[CTA_{tot}]_0/[AIBN]_0 = 21.8$; $[macro-RAFT\ CTA]_0/[CTA_{tot}]_0 = 0.127$; initial CL macro-RAFT CTA = 260 (too low f_I). $\langle k_t \rangle$ (dashed grey line), $k_t^{L*L^*}$ (full blue line) and $k_t^{S*S^*}$ (full yellow line) are also shown.

As clearly shown in Figure 2.17b for the selected condition (entry 20 in Table 2.1), the simplified average-based models (dashed lines; Equation (1)-(3)) do not suffice for an accurate description of the *short-long-termination* reactivity (dotted fuchsia line). The most pronounced mismatch is obtained at low polymer mass fractions ($w_p < 0.3$) and concomitant low chain lengths S^* , for which the experimental $k_t^{S*L^*}$ data systematically tend towards $k_t^{S*S^*}$ (cf. Figure 2.17b and also Appendix D.4 for entry 21-23 in Table 2.1) indicating that at low

polymer mass fractions, the *short-long*-termination behavior is dominated by the faster diffusion of the shorter chains. Importantly, the $k_t^{S^*L^*}$ data presented in Figure 2.17 are based on a constant value for f_l , which can be safely assumed from a relatively low polymer mass fraction onwards. As a variable f_l induces an even bigger deviation from the simplified mean models, both with regards to the slope and the absolute values of $k_t^{S^*L^*}$ (cf. Appendix D), the conclusions drawn from Figure 2.13 and 2.17 are even enhanced in case f_l is time dependent.

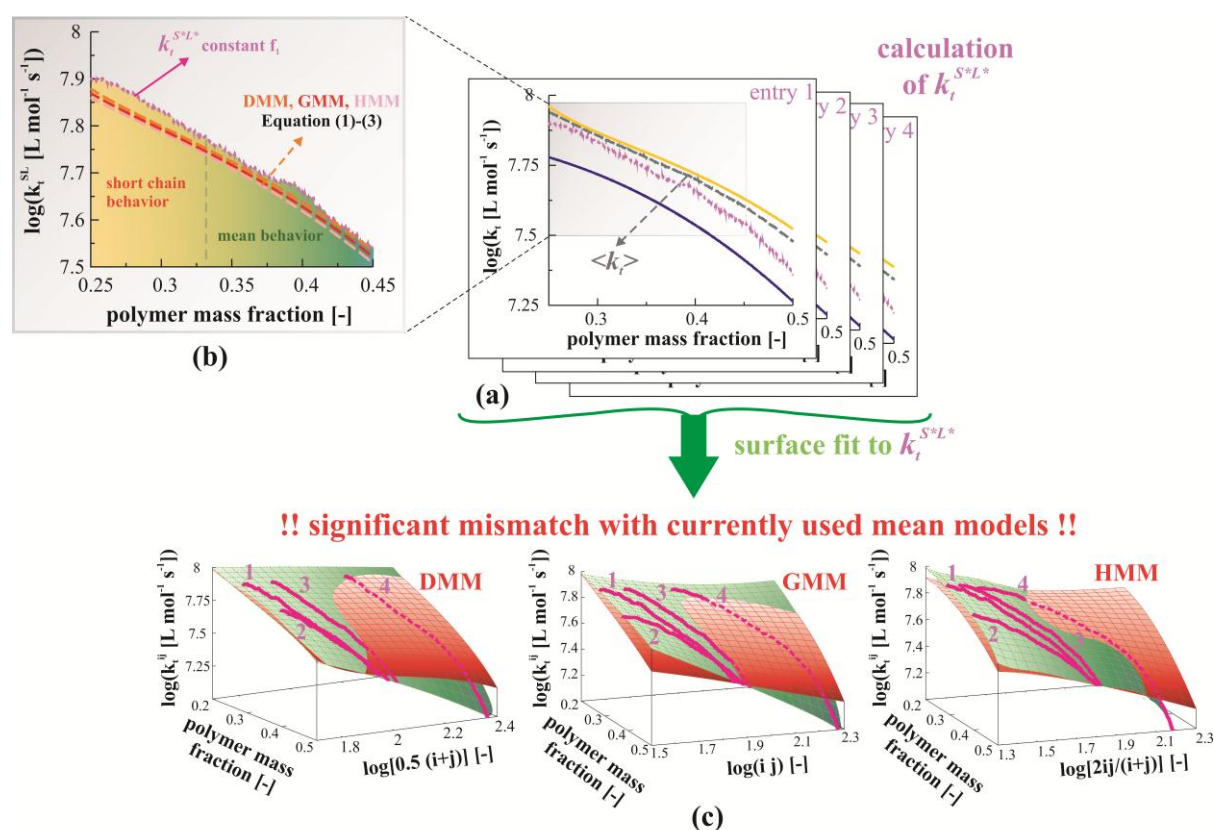


Figure 2.17: (a) $k_t^{S^*L^*}$ for entry 20 in Table 2.1 assuming a constant f_l given by the initial molar fraction of macro-RAFT CTA (dotted fuchsia line); $k_t^{L^*L^*}$ (full yellow line), $k_t^{S^*S^*}$ (full blue line) and $\langle k_t \rangle$ (dashed black line) (b) inset of (a) including a comparison with currently used simplified mean models (DMM, GMM, HMM; Equation (1)-(3)) (c) Comparison between surface function (green surface) fitted to experimental $k_t^{S^*L^*}$ data for specific chain length combinations and polymer mass fractions (full fuchsia lines; entry 20-23 in Table 2.1; constant f_l) and the surface (red) as obtained considering a simplified mean model. Clearly, a significant mismatch is obtained.

Further compelling evidence of the deficiency of the widely applied mean models in describing the *short-long*-termination reactivity is provided in Figure 2.17c (cf. Appendix D.4 for more detail and the corresponding regression characteristics), in which all *short-long*-

termination data (entry 20-23 in Table 2.1) are considered. In particular, the red surfaces as constructed via the aforementioned simplified mean models (Equation (1)-(3)) significantly differ from the green surfaces representing the actually measured *short-long*-termination data, assuming a constant f_t (fuchsia lines; numbers refer to entry 20-23 in Table 2.1). The largest discrepancies are observed for the GMM (Equation (2)) and the HMM (Equation (3)). On the other hand, for lower chain lengths, the DMM still provides a reasonable description of the true *short-long*-termination reactivity, which agrees with the previous theoretical postulation^{54,59,60} that for low S^* , the *short-long*-termination reactivity is predominantly controlled by the translational diffusion of the short-chain macroradicals.

It should however be pointed out that the aforementioned mismatches for the termination reactivity do not automatically imply that these simplified models cannot be used to describe average polymer properties such as the end-group functionality and control over chain length. The latter statement is supported by deterministic simulations including the calculation of the full chain length distribution for the currently investigated range of polymerization conditions. For the studied MMA conversion range, which relates only to 4 conditions with limited matrix effects, the simulation results revealed namely that these average properties remain nearly unaltered when using the measured $k_t^{S^*L^*}$ data (green surface in Figure 2.17c) instead of the theoretical mean models.

On the other hand, it can be expected that the average properties will be wrongly calculated for radical polymerizations which are characterized by a higher degree of matrix effects and/or run to higher conversions. In any case, it should be clear that the developed RAFT-CLD-T methodology will allow to validate the relevance of the reported mismatch for the termination reactivity for the calculation of the average polymer properties.

2.4 Conclusions

A generic and flexible experimental framework, based on the straightforward RAFT-CLD-T technique, is presented that not only allows to obtain reliable absolute *homo*-termination coefficients but also the very first and crucial measurement of *short-long*-termination rate coefficients. The generic nature of the framework is evidenced by its capability to quantify the influence of the polymer matrix (*cf.* Figure 2.11), an important dynamic variable in any polymerization process.

Careful data analysis revealed that the diffusivity of the *short-chain* macroradicals dominates the *short-long*-termination reactivity and that currently used simplified mean models clearly fail for the latter purpose and should be replaced by a measured RAFT-CLD-T surface following the procedure described in Figure 2.13-17. For the studied MMA intermediate conversions with limited matrix effects, however, these primary *short-long*-termination results indicate that the simplified mean models suffice to yield the correct average polymer properties. Importantly, for other reactions conditions, the developed methodology allows to determine whether this statement can be generalized.

In summary, we have unlocked a methodology that enables the model-free investigation of *short-long*-termination processes, which lie at the very heart of *all* radical polymerizations (*cf.* Figure 2.1).

2.5 References

- (1) Bajpai, A. K.; Shukla, S. K.; Bhanu, S.; Kankane, S. *Prog Polym Sci* **2008**, *33*, 1088-1118
- (2) Fick, A. *Poggendorff's Annalen der Physik und Chemie* **1855**, *94*, 59-86
- (3) Einstein, A. *Annalen der Physik* **1905**, *322*, 549-560
- (4) von Smoluchowski, M. *Annalen der Physik* **1906**, *326*, 756-780

- (5) Hawker, C. J.; Wooley, K. L. *Science* **2005**, *309*, 1200-1205
- (6) Barner-Kowollik, C.; Russell, G. T. *Prog Polym Sci* **2009**, *34*, 1211-1259
- (7) Barner-Kowollik, C. *Handbook of RAFT polymerization*; Wiley-VCH, 2008.
- (8) Braunecker, W. A.; Matyjaszewski, K. *Prog Polym Sci* **2007**, *32*, 93-146
- (9) Chiefari, J.; Chong, Y. K.; Ercole, F.; Krstina, J.; Jeffery, J.; Le, T. P. T.; Mayadunne, R. T. A.; Meijs, G. F.; Moad, C. L.; Moad, G.; Rizzardo, E.; Thang, S. H. *Macromolecules* **1998**, *31*, 5559-5562
- (10) Hawker, C. J.; Bosman, A. W.; Harth, E. *Chemical Reviews* **2001**, *101*, 3661-3688
- (11) Kruse, T. M.; Souleimonova, R.; Cho, A.; Gray, M. K.; Torkelson, J. M.; Broadbelt, L. J. *Macromolecules* **2003**, *36*, 7812-7823
- (12) Matyjaszewski, K. *Controlled/Living Radical Polymerization: Progress in RAFT, DT, NMP & OMRP*; American Chemical Society: Washington, DC, 2009.
- (13) Matyjaszewski, K.; Tsarevsky, N. V. *J Am Chem Soc* **2014**, *136*, 6513-6533
- (14) Patten, T. E.; Xia, J. H.; Abernathy, T.; Matyjaszewski, K. *Science* **1996**, *272*, 866-868
- (15) Barner-Kowollik, C.; Du Prez, F. E.; Espeel, P.; Hawker, C. J.; Junkers, T.; Schlaad, H.; Van Camp, W. *Angewandte Chemie-International Edition* **2011**, *50*, 60-62
- (16) Gregory, A.; Stenzel, M. H. *Prog Polym Sci* **2012**, *37*, 38-105
- (17) Kolb, H. C.; Finn, M. G.; Sharpless, K. B. *Angewandte Chemie-International Edition* **2001**, *40*, 2004-+
- (18) Hansell, C. F.; Espeel, P.; Stamenovic, M. M.; Barker, I. A.; Dove, A. P.; Du Prez, F. E.; O'Reilly, R. K. *J Am Chem Soc* **2011**, *133*, 13828-13831

- (19) Gody, G.; Maschmeyer, T.; Zetterlund, P. B.; Perrier, S. *Nature Communications* **2013**, *4*,
- (20) Lutz, J. F.; Ouchi, M.; Liu, D. R.; Sawamoto, M. *Science* **2013**, *341*, 628-+
- (21) Pfeifer, S.; Zarafshani, Z.; Badi, N.; Lutz, J.-F. *J Am Chem Soc* **2009**, *131*, 9195-9197
- (22) Soeriyadi, A. H.; Boyer, C.; Nyström, F.; Zetterlund, P. B.; Whittaker, M. R. *J Am Chem Soc* **2011**, *133*, 11128-11131
- (23) Buback, M.; Kowollik, C. *Macromolecules* **1998**, *31*, 3211-3215
- (24) Beuermann, S.; Buback, M. *Prog Polym Sci* **2002**, *27*, 191-254
- (25) Barth, J.; Buback, M.; Barner-Kowollik, C.; Junkers, T.; Russell, G. T. *Journal of Polymer Science Part a-Polymer Chemistry* **2012**, *50*, 4740-4748
- (26) Barth, J.; Buback, M.; Russell, G. T.; Smolne, S. *Macromol Chem Phys* **2011**, *212*, 1366-1378
- (27) Buback, M.; Junkers, T.; Vana, P. *Macromol Rapid Commun* **2005**, *26*, 796-802
- (28) Johnston-Hall, G.; Stenzel, M. H.; Davis, T. P.; Barner-Kowollik, C.; Monteiro, M. J. *Macromolecules* **2007**, *40*, 2730-2736
- (29) Johnston-Hall, G.; Theis, A.; Monteiro, M. J.; Davis, T. P.; Stenzel, M. H.; Barner-Kowollik, C. *Macromol Chem Phys* **2005**, *206*, 2047-2053
- (30) Vana, P.; Davis, T. P.; Barner-Kowollik, C. *Macromol Rapid Commun* **2002**, *23*, 952-956
- (31) Junkers, T.; Theis, A.; Buback, M.; Davis, T. P.; Stenzel, M. H.; Vana, P.; Barner-Kowollik, C. *Macromolecules* **2005**, *38*, 9497-9508

- (32) Theis, A.; Davis, T. P.; Stenzel, M. H.; Barner-Kowollik, C. *Macromolecules* **2005**, *38*, 10323-10327
- (33) Theis, A.; Davis, T. P.; Stenzel, M. H.; Barner-Kowollik, C. *Polymer* **2006**, *47*, 999-1010
- (34) Theis, A.; Feldermann, A.; Charton, N.; Davis, T. P.; Stenzel, M. H.; Barner-Kowollik, C. *Polymer* **2005**, *46*, 6797-6809
- (35) Theis, A.; Feldermann, A.; Charton, N.; Stenzel, M. H.; Davis, T. P.; Barner-Kowollik, C. *Macromolecules* **2005**, *38*, 2595-2605
- (36) Feldermann, A.; Stenzel, M. H.; Davis, T. P.; Vana, P.; Barner-Kowollik, C. *Macromolecules* **2004**, *37*, 2404-2410
- (37) Lovestead, T. M.; Davis, T. P.; Stenzel, M. H.; Barner-Kowollik, C. *Macromol Symp* **2007**, *248*, 82-93
- (38) Lovestead, T. M.; Theis, A.; Davis, T. P.; Stenzel, M. H.; Barner-Kowollik, C. *Macromolecules* **2006**, *39*, 4975-4982
- (39) Vana, P.; Davis, T. P.; Barner-Kowollik, C. *Macromol Theory Simul* **2002**, *11*, 823-835
- (40) Mills I., C. T., Homann K., Kallay N., Kuchitsu K. *Quantities, Units and Symbols in Physical Chemistry*; Blackwell Scientific Publications: Oxford, 1988.
- (41) Johnston-Hall, G.; Monteiro, M. J. *Macromolecules* **2007**, *40*, 7171-7179
- (42) Buback, M.; Egorov, M.; Gilbert, R. G.; Kaminsky, V.; Olaj, O. F.; Russell, G. T.; Vana, P.; Zifferer, G. *Macromol Chem Phys* **2002**, *203*, 2570-2582
- (43) Beuermann, S.; Buback, M.; Davis, T. P.; Gilbert, R. G.; Hutchinson, R. A.; Olaj, O. F.; Russell, G. T.; Schweer, J.; vanHerck, A. M. *Macromol Chem Phys* **1997**, *198*, 1545-1560

- (44) Gilbert, R. G. *Pure Appl Chem* **1996**, 68, 1491-1494
- (45) Bentein, L.; D'Hooge, D. R.; Reyniers, M. F.; Marin, G. B. *Macromol Theory Simul* **2011**, 20, 238-265
- (46) Armitage, P. D.; Hill, S.; Johnson, A. F.; Mykytiuk, J.; Turner, J. M. C. *Polymer* **1988**, 29, 2221-2228
- (47) Bauduin, G.; Pietrasanta, Y.; Rousseau, A.; Granierazema, D.; Bosc, D.; Guilbert, M. *Eur Polym J* **1992**, 28, 923-927
- (48) J. Brandrup, E. H. I., E. A. Grulke *Polymer Handbook*; John Wiley & Sons: New York, 1998.
- (49) Korbar, A.; Malavasic, T. *J Therm Anal* **1995**, 44, 1357-1365
- (50) Malavašič, T.; Vizovišek, I.; Lapanje, S.; Može, A. *Die Makromolekulare Chemie* **1974**, 175, 873-880
- (51) Szafko, J.; Feist, W. *Journal of Polymer Science Part a-Polymer Chemistry* **1995**, 33, 1643-1655
- (52) Braun, D.; Quella, F. *Die Makromolekulare Chemie* **1978**, 179, 387-394
- (53) Stickler, M. *Makromolekulare Chemie-Macromolecular Chemistry and Physics* **1986**, 187, 1765-1775
- (54) Achilias, D. S. *Macromol Theory Simul* **2007**, 16, 319-347
- (55) D'Hooge, D. R.; Reyniers, M. F.; Marin, G. B. *Macromol React Eng* **2013**, 7, 362-379
- (56) Russell, G. T.; Napper, D. H.; Gilbert, R. G. *Macromolecules* **1988**, 21, 2141-2148

(57) Faldi, A.; Tirrell, M.; Lodge, T. P.; Vonmeerwall, E. *Macromolecules* **1994**, *27*, 4184-4192

(58) Zetterlund, P. B.; Yamazoe, H.; Yamada, B. *Polymer* **2002**, *43*, 7027-7035

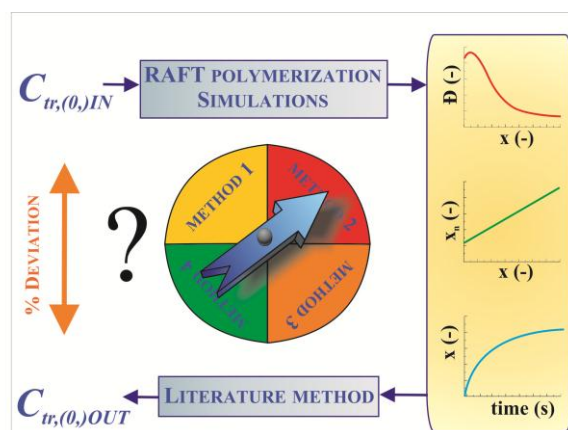
(59) Faldi, A.; Tirrell, M.; Lodge, T. P. *Macromolecules* **1994**, *27*, 4176-4183

(60) O'Neil, G. A.; Torkelson, J. M. *Macromolecules* **1999**, *32*, 411-422

Chapter 3: Chain transfer in degenerative RAFT polymerization revisited: a comparative study

Summary

Under the validity of the degenerative transfer mechanism, the activation/deactivation process in reversible addition-fragmentation chain transfer (RAFT) polymerization can be formally quantified by transfer coefficients, depending on the chemical structure of the participating radicals and dormant species. In the present chapter, the different literature methods to experimentally determine these RAFT transfer coefficients are re-evaluated based on the simulation of perfect experiments, using a complete kinetic model. The accuracy of each method is mapped for a broad range of reaction conditions in order to provide useful guidelines for the experimentalist. This work has been accepted for publication in *Macromolecular Theory and Simulations* 2015.



3.1 Introduction

Transfer of the radical center of a macroradical to a different position on the same chain, *i.e.* *intra*-molecular transfer, or to another species, *i.e.* *inter*-molecular transfer, is ubiquitous in radical polymerization.¹⁻⁴ In particular, the presence of thiols and halocarbons under conventional free radical polymerization (FRP) conditions, leading to intermolecular transfer, has been shown effective in regulating the polymer number average chain length (x_n), as they act as irreversible conventional chain transfer agent (CTA) species.¹⁻⁴ This discovery has revolutionized especially the synthetic rubber industry, since the lower average chain length polymers obtained by FRP with addition of a CTA exhibit a much higher processability.⁵ The intermolecular transfer reaction with CTA can be formally written down as:¹⁻⁴



in which R_n is a macroradical of length n , A the CTA, P_n a dead polymer molecule of length n , A^* the resulting radical after transfer to CTA, and k_{tr} the corresponding intrinsic rate coefficient ($\text{L mol}^{-1} \text{s}^{-1}$).

In order to classify the different types of CTA according to their transfer reactivity for a given monomer, various methods to quantify the so-called transfer coefficient C_{tr} , *i.e.* the ratio of k_{tr} to the corresponding intrinsic propagation rate coefficient k_p , have been developed. For a Flory-Schulz chain length distribution (CLD), as typically encountered in FRP,¹ Mayo and co-workers put forward a simple experimental method to determine C_{tr} at low monomer conversion via regression analysis based on experiments with different initial CTA to monomer molar ratios via (*cf.* Chapter 1):⁶

$$\frac{1}{x_n} = \frac{k_{tr}\lambda_0[A]_0 + \langle k_t \rangle \lambda_0^2}{k_p\lambda_0[M]_0} = C_{tr} \frac{[A]_0}{[M]_0} + \frac{\langle k_t \rangle \lambda_0}{k_p[M]_0} \quad (2)$$

in which $[A]_0$ is the initial CTA concentration, λ_0 the total macroradical concentration (mol L^{-1}), $[M]_0$ the initial monomer concentration (mol L^{-1}), and $\langle k_t \rangle$ the average or population

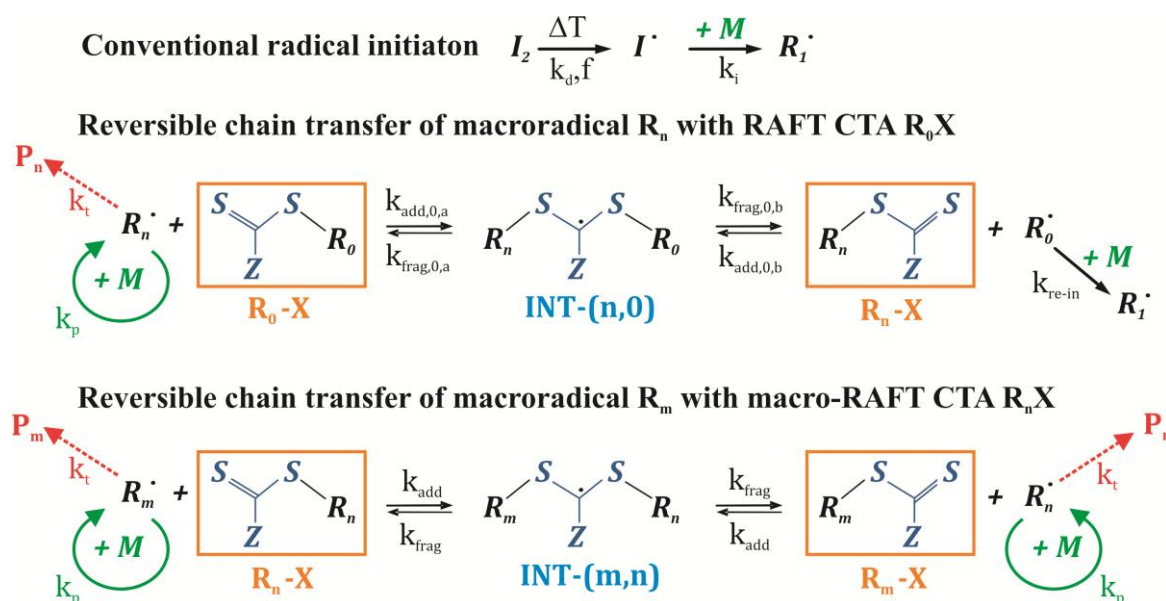
weighted apparent termination rate coefficient ($\text{L mol}^{-1} \text{s}^{-1}$). It should be stressed that the CLD is influenced by diffusional limitations on termination, due to the high chain lengths and typical strong viscosity increase in radical polymerization, which requires the consideration of ‘apparent’ termination kinetics during theoretical derivations (*cf.* Chapter 2).⁷ Despite its ease and wide application, the accuracy of the Mayo method is however limited by the precision of size exclusion chromatography (SEC) measurements which are often relative and highly sensitive to small baseline fluctuations, especially at the low chain length region of the CLD.^{8,9} This could be partially resolved by Gilbert and Clay who introduced a more robust method to determine C_{tr} from the slope of the natural logarithm of the FRP number CLD in the high chain length region for different CTA to monomer molar ratios (*cf.* Chapter 1):⁸

$$\frac{d\ln(y_n)}{dn} \approx -C_{tr} \frac{[A]}{[M]} + \frac{\langle k_t \rangle \lambda_0}{k_p[M]} \quad (3)$$

In Equation (3), y_n is the number fraction of dead polymer molecules with a chain length n and $[A]$ and $[M]$ are the CTA and monomer concentration at the selected monomer conversion. Moad and coworkers demonstrated that Equation (3) applied to the chain length range corresponding to the highest signal to noise ratio of the number CLD, *i.e.* the top 80% of the number CLD (*cf.* Chapter 1), results in C_{tr} values with a very high accuracy, that are not significantly affected by diffusional limitations on termination.^{9,10} Moreover, due to the availability of accurate values for the propagation rate coefficients via pulsed laser polymerization (PLP) based techniques, reliable k_{tr} values can be readily accessed for conventional CTAs.¹¹

On the other hand, for the more recently developed reversible addition-fragmentation chain transfer (RAFT) CTAs the situation is more complex. Almost two decades ago, the CSIRO group discovered that a superior control over the CLD in radical polymerization can be

obtained in case a CTA is used containing a thiocarbonyl moiety.^{12,13} Such agent invokes a RAFT polymerization mechanism, as shown in Scheme 1 for a dithioester as RAFT CTA.¹⁴

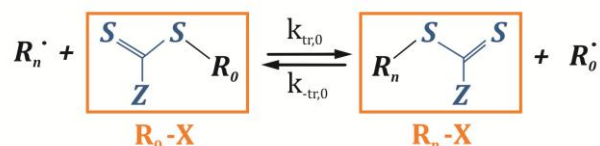


Scheme 3.1: RAFT polymerization scheme with a dithioester as RAFT CTA (R_0X). R_n : macroradical of chain length n ; P_n : dead polymer chain of chain length n ; R_nX : dormant species with chain length n ; $INT-(m,n)$: intermediate radical species with chain lengths m and n for the two arms; I^* : conventional initiator radical fragment; M : monomer; for I^* different from R_0 no RAFT exchange involving I/IX species included; f : efficiency factor

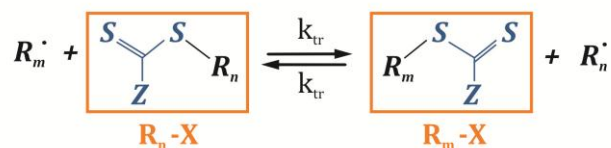
During RAFT polymerization, a propagating radical (R_n), formed upon chain initiation with a conventional radical initiator fragment I^* , can add to the initial RAFT CTA (R_0X) whereby an intermediate radical ($INT-(n,0)$) is formed. Due to the instability of the formed adduct-radical, β -C-S-scission occurs, resulting in either the starting compounds ($k_{frag,0,a}$) or a dormant RAFT polymer species of chain length n (R_nX) and a RAFT CTA derived radical species (R_0) ($k_{frag,0,b}$) that can re-initiate the polymerization (k_{re-in}). Note that besides macroradicals (R_n , $n > 1$), in principle R_0 and I^* species can additionally react with R_0X . However, the latter reaction path can usually be ignored, as assumed in Scheme 3.1 for the case of a chemically different R_0 and I^* . The latter assumption is justified as the conventional radical initiator (I_2) concentration is mostly low when aiming at a proper control of the polymer properties (cf. Appendix E).¹³ On the other hand, in the special case of chemically identical R_0 and I^* species, Scheme 3.1 is complete for $m, n = 0, \dots, +\infty$. In both cases, the formed dormant

polymer species R_nX in Scheme 3.1 can take part in additional exchange reactions with macroradicals (R_m) by an analogous addition-fragmentation mechanism in which R_nX acts as a macro-RAFT CTA (k_{add} , k_{frag}). Note that from its discovery onwards, an intense debate has been going on about the fate of the intermediate radical species (INT), which depending on the time scales can terminate with itself or any other radical, *i.e.* so-called ‘cross-termination’, or can undergo slow fragmentation, possibly leading to a significant retardation compared to FRP.^{13,15}

Degenerative transfer of macroradical R_n with RAFT CTA R_0X



Degenerative transfer of macroradical R_m with macro-RAFT CTA R_nX



Scheme 3.2: Simplified RAFT degenerative transfer mechanism based on the pseudo-steady state assumption allowing the removal of the intermediate radical species in Scheme 1 (INT) (cf. Appendix E). Only RAFT exchange reactions are shown for simplicity.

For an efficient exchange between the macroradicals and the (macro-) RAFT CTA, however, no such retardation is observed and the complex RAFT polymerization scheme (Scheme 3.1) can be approximated by a degenerative transfer mechanism as shown in Scheme 3.2,^{13,16} in which the intermediate radical species (INT , Scheme 3.1) are formally eliminated by application of the pseudo-steady state assumption (PSSA), as explained in Appendix E.¹³ This implies the introduction of three ‘apparent’ transfer rate coefficients given by Equation (4)-(6):^{12,13,17}

$$k_{tr,0} = k_{add,0,a} \frac{k_{frag,0,b}}{k_{frag,0,a} + k_{frag,0,b}} = k_{add,0,a} \phi_{0,a} \quad (4)$$

$$k_{-tr,0} = k_{add,0,b} \frac{k_{frag,0,a}}{k_{frag,0,a} + k_{frag,0,b}} = k_{add,0,b} \varphi_{0,b} \quad (5)$$

$$k_{tr} = k_{add} \frac{k_{frag}}{k_{frag} + k_{frag}} = k_{add} 0.5 \quad (6)$$

Note that in this context ‘apparent’ refers in a first instance to the complex shape of the right hand sizes, which involve combinations of intrinsic rate coefficients often expressed via the fragmentation probability φ towards the products of the considered RAFT exchange reaction (equivalent for “from left to right” or “from right to left” in Scheme 3.1). In addition, it should be noted that Equation (6) is simplified based on the assumption that the addition and fragmentation rate coefficients for the reactions involving macroradicals and dormant polymer species of chain length m and n are equal. The latter assumption holds for chain length independent addition and fragmentation kinetics and for a well-controlled RAFT polymerization which leads to a narrow CLD so that at a given conversion x approximately only one chain length is present in the RAFT polymerization mixture ($m(x) \approx n(x)$).^{12,13}

Similar to conventional CTAs used in FRP, the classification of R_0X species is achieved based on a RAFT transfer coefficient $C_{tr,0}$, defined as the ratio of $k_{tr,0}$ to k_p , with the general rule of thumb that low polymer dispersities are obtained for $C_{tr,0} > 10$.^{13,17,18} Furthermore, for the reverse transfer and for the macro-RAFT CTA a similar ratio can be defined, *i.e.* respectively $C_{-tr,0}$ and C_{tr} . Hence, three transfer coefficients are required for a proper description of the degenerative RAFT polymerization process, as summarized in Table 3.1. Note that under the assumption of Equation (6) C_{tr} relates to the ratio of k_{add} to k_p .

Table 3.1: Summary of the degenerative RAFT transfer coefficients used throughout this chapter (cf. Scheme 3.2); $k_{p,0}$ is the propagation rate coefficient of R_0 with monomer. A more detailed description of the reaction scheme and the assumptions made in Appendix E.

transfer coefficient	expression	reactants	products	transfer reactivity
$C_{tr,0}$	$\frac{k_{tr,0}}{k_p}$	$R_n + R_0X$	$R_nX + R_0$	Eq. (4)
$C_{-tr,0}$	$\frac{k_{-tr,0}}{k_{p,0}}$	$R_0 + R_nX$	$R_0X + R_n$	Eq. (5)
C_{tr}	$\frac{k_{tr}}{k_p}$	$R_m + R_nX$	$R_mX + R_n$	Eq. (6)

Several experimental methods were developed to determine $C_{tr,0}$ (cf. Table 3.1). Yet, in contrast to FRP, no efficient experimental method is currently available to unambiguously determine $C_{tr,0}$ for a wide range of conditions and RAFT CTAs, due to the possible strong interference of $C_{-tr,0}$ (cf. Table 3.1). Furthermore, it is unclear what accuracy can be expected for each individual method and whether the underlying model assumptions limit the reliability of the obtained values for $C_{tr,0}$. A similar conclusion holds for the methods to obtain C_{tr} , the RAFT exchange reactivity with the macro-RAFT CTA (cf. Table 3.1), including those from approximate analytical correlations for the polymer dispersity (\mathcal{D}) profile.^{4,19-21}

In the present work, the different methods to determine the RAFT exchange reactivities ($C_{tr,0}$, $C_{-tr,0}$ and C_{tr}) are concisely discussed, focusing on their model assumptions. Next, the accuracy of the most important analytical methods is assessed for a wide range of representative conditions via the simulation of so-called ‘perfect experiments’, *i.e.* the experimental input values necessary for application of these methods are error-free as they are obtained *in silico* using a completely accurate degenerative RAFT kinetic model.

3.2 Methods to determine RAFT transfer coefficients

In this section, the experimental methods to determine degenerative RAFT transfer coefficients are outlined together with their model assumptions. A more detailed discussion of each method can be found in Chapter 1.

3.2.1 Methods to determine $C_{(-)tr,0}$

The Mayo method and the CLD method in the current form of respectively Equation (2) and (3) for FRP with a conventional CTA, can also be applied to RAFT polymerizations with R_0X species characterized by a low $C_{tr,0}$, as in that case near FRP behavior is obtained and the assumptions underlying the method thus hold.^{6,8-10}

Specifically for the RAFT polymerization process, Moad and coworkers developed an experimental method to directly determine $C_{tr,0}$ based on the measured decay of the R_0X concentration.²²⁻²⁴ Assuming the PSSA for the concentration of the macroradicals and R_0 species they reported that:

$$\frac{d[R_0X]}{d[M]} \approx C_{tr,0} \frac{[R_0X]}{[M] + C_{tr,0}[R_0X] + C_{-tr,0}\tau_0} \quad (7)$$

In this equation, $[R_0X]$ is the RAFT CTA concentration (mol L^{-1}) and τ_0 the concentration of dormant polymer chains (mol L^{-1} ; $R_{n,m}X$ in Scheme 3.1-2), which can be directly related to $[R_0X]$ as the total number of RAFT CTA moieties in the reaction mixture stays constant, at least if no degradation occurs under the studied polymerization conditions. Equation (7) can be used to estimate both $C_{tr,0}$ and $C_{-tr,0}$. Moreover, if reverse degenerative transfer ($C_{-tr,0}$) becomes negligible compared to transfer with R_0X ($C_{tr,0}$), it enables the direct evaluation of $C_{tr,0}$ from the slope of a plot of $\ln([R_0X])$ versus $\ln([M])$:²²⁻²⁴

$$C_{tr,0} \approx \frac{d\ln([R_0X])}{d\ln([M])} \quad (8)$$

It is clear that Equation (7)-(8) are only reliable if the R_0X concentration can be accurately monitored, which is only possible for low to intermediate $C_{tr,0}$ values. For a high $C_{tr,0}$ (> 100), R_0X will be completely consumed after a few percent of monomer conversion and unreliable results can be expected.

An alternative method for the direct determination of $C_{tr,0}$, was developed by Theis *et al.*²⁵ and holds for monomer/ R_0X combinations that display “hybrid RAFT polymerization behavior”, *i.e.* an initial increase of x_n before the start of its linear incline with conversion. Theis *et al.* reported an approximated expression to determine $C_{tr,0}$ from SEC measurements of the initial number average chain length (x_n at conversion $x = 0^+$; x_n^0):²⁵

$$x_n^0 \approx \frac{[M]_0}{C_{tr,0}[R_0X]_0} + 1 \quad (9)$$

3.2.2 Methods to determine C_{tr}

For the reversible chain transfer with the macro-RAFT CTA (k_{add} , k_{frag} in Scheme 3.1; k_{tr} in Scheme 3.2), similar principles hold as discussed for the RAFT exchange reactions with R_0X . The methods of Moad and coworkers and Theis *et al.* (Equation (7)-(9)) can in principle be applied to an initial RAFT polymerization mixture containing macro-RAFT CTA ($R_{n,m}X$ in Scheme 3.1-2) instead of R_0X , to directly determine C_{tr} .¹³ However, the accuracy and application scope of these methods can in certain situations be limited, due to practical reasons. The concentration decay of the macro-RAFT CTA can be difficult to quantify and significant overlap can occur in the SEC trace between the CLDs of the latter species and the macroradicals formed upon further propagation.

Alternatively, values for C_{tr} have also been determined based on approximate analytical correlations for the polymer dispersity (\mathbb{D}) profile. For example, under the stringent model assumptions that conventional radical initiation occurs instantaneously and termination is

irrelevant, Müller *et al.* derived a set of analytical expressions for the average polymer properties as function of the monomer conversion x ,^{19,20} based on which a simplified closed expression to determine C_{tr} from dispersity and x_n data for a batch RAFT polymerization was proposed by Goto and Fukuda:²¹

$$\mathfrak{D} \approx 1 + \frac{1}{x_n} + \frac{2-x}{x C_{tr}} \quad (10)$$

An important extension of Equation (10) was reported by Gao and Zhu,⁴ who included conventional radical initiation and termination reactions in their analytical derivations to eventually obtain a more complex expression for \mathfrak{D} as a function of x :

$$\mathfrak{D} \approx \frac{\frac{2B}{A-2} \frac{C_{tr}[R_0X]_0 + B}{C_{tr}[R_0X]_0^2} [(1-x)^2 - (1-x)^A]}{[1-x - (1-x)^A]^2} + \frac{\frac{B^2}{(A-1)[R_0X]_0[M]_0} [1-x - (1-x)^A] - \frac{2B}{[R_0X]_0} x(1-x)^A}{[1-x - (1-x)^A]^2} \quad (11)$$

in which $A = \frac{k_t \lambda_0}{k_p [R_0X]_0}$ with k_t a constant termination rate coefficient and $B = \frac{\langle k_t \rangle \lambda_0}{k_p} - [R_0X]_0$. However, still simplifying assumptions were made that limit the validity of their method under a broad range of conditions, as will be demonstrated further. Importantly, both Equation (10) and (11) do not take into account the RAFT exchange reactions with R_0X , which is only justified for high values of $C_{tr,0}$ (> 100) as those guarantee a complete R_0X consumption after a few percentages of monomer conversion.

Although the degenerative transfer mechanism which serves as the basis for Equation (4)-(6) (Table 3.1; Scheme 3.2) has been shown to be a valid approximation for many RAFT polymerizations (*cf.* Appendix E),^{13,16} it should be highlighted that it is desirable to obtain values for the individual addition and fragmentation rate coefficients (Scheme 3.1) in order to obtain full insight into the RAFT polymerization process. Transfer coefficients can then be

calculated *a posteriori* and explicitly. Hitherto, more recently high-level *ab initio* calculations^{15,26-29} and parameter estimation procedures based on more extensive kinetic modeling results³⁰⁻³² have been performed. Despite being based on first principles, the former calculations often rely on small model entities to represent the considered system as a compromise between accuracy and computational cost,^{13,29} whereas the parameter estimation methods highly depend on the model reactions included in the kinetic model and the size of the polymerization data set. Care should thus be taken when adapting values for the addition and fragmentation rate and corresponding transfer coefficients from literature. In addition, the model assumptions should always be clearly stated when reporting new parameter values.

Recently, Barth *et al.*³³ developed an efficient method to assess the addition-fragmentation equilibrium coefficient (K_{eq}) for the reversible chain transfer with macro-RAFT CTA. This was done via the following equation, which relies on time-resolved electron paramagnetic resonance (EPR) measurements of the concentration ratio of the macroradicals (R_n in Scheme 3.1; total concentration λ_0) and intermediate radical species (INT-(m,n) in Scheme 3.1; total concentration $[INT]$) after pulsed laser initiation, assuming quasi-equilibrium between addition and fragmentation and negligible cross-termination (*cf.* Chapter 1):

$$K_{eq} = \frac{k_{add}}{k_{frag}} = \frac{[INT]_{eq}}{\lambda_{0,eq}\tau_{0,eq}} \approx \frac{[INT]}{\lambda_0\tau_0} \quad (12)$$

in which $[A]_{eq}$ denotes the corresponding equilibrium concentration of A. Subsequently, after calibration of the EPR equipment for the simultaneous measurement of $[INT]$ and λ_0 , Meiser *et al.* reported values for k_{add} and k_{frag} (and thus C_{tr}) by regression analysis to the obtained experimental concentration profiles.^{34,35} However, PLP equipment is expensive and limited to RAFT CTAs that do not degrade under the imposed ultraviolet laser pulses, and, furthermore, it is worth mentioning that a proper calibration of the EPR can be a tedious task.^{34,35}

To summarize, in Table 3.2, an overview of the above discussed experimental methods to determine the RAFT chain transfer reactivities via analytic models is given, including a listing of the main assumptions and required experimental quantities. Methods to determine $C_{-tr,0}$ are not included in this table as they involve either high-level *ab initio* calculations or parameter fitting to kinetic modeling results. In the next section, the potential of the analytical models outlined in Table 3.2 is re-evaluated based on simulations and their accuracy is mapped for a broad range of reaction conditions in order to provide useful guidelines for the experimentalist.

3.3 *In silico* evaluation of literature models to determine $C_{tr(,0)}$

In this section, first the simulation details and the *in silico* procedure for the simulation of a ‘perfect experiment’ via a complete degenerative RAFT polymerization kinetic model are elaborated. Subsequently, the accuracy of the experimental methods to determine $C_{tr,0}$ and C_{tr} is discussed.

Table 3.2: Overview of the main methods using an analytical model to determine the transfer reactivity in RAFT polymerization.

method	Expression	quantity determined	assumptions	measurement
Mayo ^{a, 6}	$\frac{1}{x_n} = C_{tr,0} \frac{[R_0X]_0}{[M]_0} + \frac{\langle k_t \rangle \lambda_0}{k_p [M]_0}$	$C_{tr,0}$	<ol style="list-style-type: none"> 1. Flory-Schulz distribution 2. very low $C_{tr,0}$ 	<i>regression</i> to data of <i>multiple</i> experiments: x_n via SEC for different $\frac{[R_0X]_0}{[M]_0}$
CLD ^{a, 8-10}	$\frac{d \ln(y_n)}{dn} \approx -C_{tr,0} \frac{[R_0X]}{[M]} + \frac{\langle k_t \rangle \lambda_0}{k_p [M]}$	$C_{tr,0}$	<ol style="list-style-type: none"> 1. PSSA for concentration macroradicals 2. very low $C_{tr,0}$ 	<i>regression</i> to data of <i>multiple</i> experiments: slope of $\ln(y_n)$ via SEC for different $\frac{[R_0X]_0}{[M]_0}$
Moad and coworkers ^{22,23}	$C_{tr,0} \approx \frac{d \ln([R_0X])}{d \ln([M])}$	$C_{tr,0}$	<ol style="list-style-type: none"> 1. degenerative transfer mechanism 2. negligible contribution of $C_{-tr,0}$ 	<i>regression</i> to data of a <i>single</i> experiment: concentration decay of both R_0X and M
Theis <i>et al.</i> ²⁵	$x_n^0 \approx \frac{[M]_0}{C_{tr,0} [R_0X]_0} + 1$	$C_{tr,0}$	<ol style="list-style-type: none"> 1. degenerative transfer mechanism 2. hybrid behavior 	<i>regression</i> to data of a <i>single</i> experiment: x_n vs. x via SEC, extrapolation to $x = 0$ (x_n^0)

Barth <i>et al.</i> ³³	$K_{eq}\tau_0 \approx K_{eq}[R_0X]_0 \approx \frac{[INT]}{\lambda_0}$	$K_{eq} = \frac{k_{add}}{k_{frag}}$	<ol style="list-style-type: none"> 1. no influence of RAFT reactions with R_0X 2. quasi-equilibrium (no cross-termination) 	<i>regression</i> to data of <i>multiple</i> experiments: $\frac{[INT]}{\lambda_0}$ via PLP-EPR for different $[R_0X]_0$
Goto and Fukuda ²¹	$\mathfrak{D} \approx 1 + \frac{1}{x_n} + \frac{2-x}{x C_{tr}}$	C_{tr}^b	<ol style="list-style-type: none"> 1. degenerative transfer mechanism 2. instantaneous initiation 3. no termination 4. no influence of RAFT reactions with R_0X 	<i>regression</i> to data of <i>a single</i> experiment: \mathfrak{D} and x_n via SEC, x
Gao and Zhu ⁴	$\mathfrak{D} \approx \frac{\frac{2B}{A-2} \frac{C_{tr}[R_0X]_0 + B}{C_{tr}[R_0X]_0^2} [(1-x)^2 - (1-x)^A]}{[1-x - (1-x)^A]^2} + \frac{\frac{B^2}{(A-1)[R_0X]_0[M]_0} [1-x - (1-x)^A] - \frac{2B}{[R_0X]_0} x(1-x)}{[1-x - (1-x)^A]^2}$	C_{tr}	<ol style="list-style-type: none"> 1. degenerative transfer mechanism 2. PSSA for macroradicals 3. chain length independent termination 4. no influence of RAFT reactions with R_0X 	<i>regression</i> to data of <i>a single</i> experiment: \mathfrak{D} via SEC, x , k_t and λ_0

^awritten down as applied under RAFT polymerization conditions; for transfer with conventional irreversible CTA: C_{tr} . ^b C_{tr} via post-processing

3.3.1 Simulation of a 'perfect experiment'

All simulations to evaluate the literature models are based on a degenerative transfer scheme for the RAFT polymerization of methyl methacrylate (MMA) at 353 K initiated by azobis(isobutyronitrile) (AIBN; Scheme 3.2 and Appendix E; R_0 equal to I^*). A deterministic modeling technique is selected, which includes the calculation of CLDs of all macrospecies types, *i.e.* macroradicals, dormant species and dead species. The individual continuity equations are simultaneously integrated using the Livermore Solver for Ordinary Differential Equations (LSODA) for chain lengths up to 3000.³⁶ An example of such differential equation with R_0 equal to I^* is shown in Equation (13) for a dormant polymer molecule of chain length n :

$$\frac{1}{V} \frac{d(V[R_n X])}{dt} = -[R_n X] \sum_{m=0}^N k_{tr}^{n,m} [R_m] + [R_n] \sum_{m=0}^N k_{tr}^{n,m} [R_m X] \quad (13)$$

in which V is the reaction volume and $k_{tr}^{n,m}$ the RAFT exchange rate coefficient between macrospecies of chain length n and m . The kinetic parameters used in the simulations in the present work are taken from literature and are listed in Table 3.3. For simplicity, a constant conventional radical initiator efficiency is assumed, which is a reasonable assumption for monomer conversions below 80%.^{37,38} The RAFT exchange by degenerative transfer rate coefficients are varied for the evaluation of the literature models for a wide range of conditions. Chain length and conversion dependent apparent termination kinetics have been implemented explicitly via the $k_{t,app}(n,x)$ surface function determined by Derboven *et al.*³⁹ at 353 K via the RAFT – chain length dependent – termination (RAFT-CLD-T) technique. Termination at this temperature is assumed to occur almost exclusively (99%) via disproportionation, as determined by Johnston-Hall *et al.*^{30,40}

Table 3.3: Rate coefficients at 353 K used in the simulations and benchmark for the *in silico* experiments for RAFT polymerization of MMA initiated by AIBN (R_0 equal to I^*). Assumptions in Appendix E.

Reaction	Rate coefficient	Value at 353 K	Reference
dissociation ^a	k_{dis}	$1.4 \cdot 10^{-4} \text{ s}^{-1}$	41-43
propagation	k_p	$1318 \text{ L mol}^{-1} \text{ s}^{-1}$	44
degenerative chain transfer	$k_{tr,0}, k_{-tr,0}, k_{tr}$	$10^3\text{-}10^5 \text{ L mol}^{-1} \text{ s}^{-1b}$	13
termination by recombination	$0.99 k_t$	RAFT-CLD-T	30,39,40
termination by disproportionation	$0.01 k_t$	RAFT-CLD-T	30,39,40

^aInitiator efficiency $f = 0.7$. ^bDifferent values for the transfer rate coefficients have been scanned for the evaluation of the literature models.

For the *in silico* evaluation of the literature methods to determine the RAFT transfer coefficients $C_{tr,(0)}$, a procedure as depicted in Figure 3.1 is followed. An implemented value for $C_{tr,0}$ or C_{tr} in the complete kinetic model ($C_{tr,(0),IN}$) is compared with the corresponding value obtained by application of the considered analytical literature method to the simulated responses of this model ($C_{tr,(0),OUT}$). The observed deviation between $C_{tr,(0),IN}$ and $C_{tr,(0),OUT}$ is a measure for the accuracy of the considered method. Since the simulated responses are implicitly assumed to be determined with a precision of 100%, this measure reflects the systematic error induced by the model assumptions of the particular method under the considered conditions. It should be emphasized that the other RAFT transfer coefficients that are not determined by the considered method, can have a pronounced influence on the validity of the model assumptions of the considered method and can thus directly affect the induced systematic error.

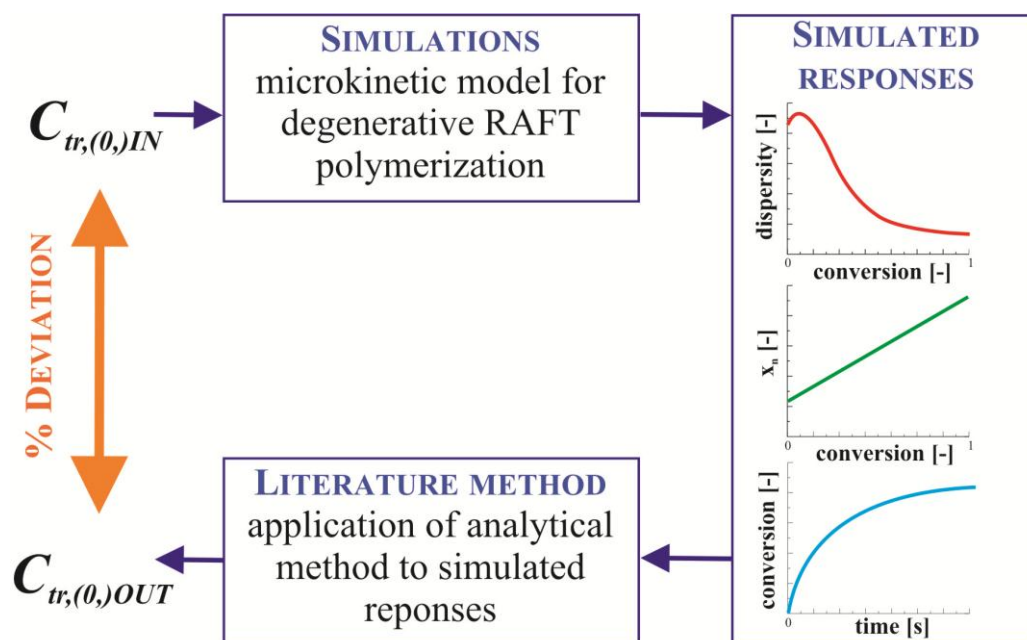


Figure 3.1: Schematic representation of the *in silico* procedure for the evaluation of the analytical literature methods to determine $C_{tr,0}$ or C_{tr} . $C_{tr,(0),IN}$ is the implemented $C_{tr,(0)}$ while $C_{tr,(0),OUT}$ is the value obtained after application of the considered method to the perfect simulated responses.

3.3.2 Methods to determine $C_{tr,0}$

It is generally known that the Mayo method⁶ (Equation (2)) and the CLD method of Gilbert and Clay⁸ and its extension by Moad and coworkers^{9,10} (Equation (3)) are only accurate in case the considered RAFT polymerization reaction shows many FRP characteristics, *i.e.* a minor control over the CLD should be obtained which corresponds to very low values of $C_{tr,0}$ ($C_{tr,0} \ll 1$). Due to their facile application, one of these methods is commonly the method of choice to determine the chain transfer reactivity of xanthates,⁴⁵ as corresponding $C_{tr,0}$ values are usually low. However, in case a value greater than 1 is obtained, it is important to have a notion of the related inherent systematic error. Therefore, in Table 3.4 an evaluation of the Mayo method⁶ and the CLD method⁸⁻¹⁰ is performed for higher values of $C_{tr,0}$ based on the simulated responses of perfect experiments in which 4 different targeted chain lengths (TCL; in the present work referring to the initial molar ratio of R_0X to monomer; 100, 200, 300 and

400) are considered to determine $C_{tr,0}$ by regression of Equation (2)-(3) ($C_{tr,0,OUT}$). The resulting values for $C_{tr,0,OUT}$ are compared with the implemented values ($C_{tr,0,IN}$) to assess the accuracy of the respective method. Values for $C_{tr,0,OUT}$ are determined based on the CLD (x_n only for Mayo method⁶) at $x = 0.01$.

Table 3.4: Evaluation of the Mayo method⁶ (Equation (2)) and the chain length distribution (CLD) method⁸⁻¹⁰ (Equation (3)) for higher values of $C_{tr,0}$. The value of $C_{tr,0}$ implemented in the simulations of the perfect experiments ($C_{tr,0,IN}$) is compared with the value obtained by application of the respective method to the simulated chain length data at $x=0.01$ ($C_{tr,0,OUT}$) and the % deviation compared to the 'real' implemented value is shown. In all simulations $C_{tr,0} = C_{tr} = C_{tr,0,IN}$; $[M]_0 = 9 \text{ mol L}^{-1}$; $[I_2]_0 = 9 \cdot 10^{-3} \text{ mol L}^{-1}$. $C_{tr,OUT}$ from four different TCLs ($= [M]_0/[R_0X]_0$): 100, 200, 300 and 400; corresponding $[R_0X]_0$: 0.09, 0.045, 0.03 and 0.0225 mol L^{-1} respectively. In case no chain length dependency k_t : $k_t = 5 \cdot 10^8 \text{ L mol}^{-1} \text{ s}^{-1}$. Other kinetic parameters in Table 3.3.

entry	varying k_t^a	Mayo method			CLD method	
		$C_{tr,0,IN}$ [-]	$C_{tr,0,OUT}$ [-]	% deviation	$C_{tr,0,OUT}$ [-]	% deviation
1	no	1.0	0.97	3.0	0.99	1.0
2	no	5.0	4.48	10.4	4.70	6.0
3	no	15.0	11.68	22.1	13.27	11.5
4	yes	5.0	4.61	7.8	4.74	5.2

^aConversion and chain length dependency of k_t via RAFT-CLD-T surface function determined by Derboven et al.³⁹

For the simulation results in Table 3.4, the transfer reactivity of macroradicals with the macro-RAFT CTA (C_{tr}) is assumed equal to $C_{tr,0}$ since simulations showed that a variation of the former (up to a factor 10) induces no additional deviation for the Mayo method⁶ and less than 1% for the CLD method.⁸⁻¹⁰ Furthermore, for simplicity, the transfer reactivity of R_0 species with macro-RAFT CTA ($C_{tr,0}$) is also taken equal to $C_{tr,0}$. Both the theoretical results for a constant k_t ($k_t = 5 \cdot 10^8 \text{ L mol}^{-1} \text{ s}^{-1}$; entry 1-3) and chain length dependent termination kinetics (entry 4) are presented, showing only a small influence of the latter on the determination of $C_{tr,0}$. It is clear that in general the CLD method⁸⁻¹⁰ yields more accurate

results and significantly larger deviations are obtained for higher values of $C_{tr,0}$. For completeness it is mentioned here that application of both methods (Equation (2)-(3)) to data at higher monomer conversion (> 0.01) lowers the accuracy, *e.g.* a factor of *ca.* 2 for the deviation of $C_{tr,0,OUT}$ from $C_{tr,0,IN} = 5$ at $x = 0.05$ instead of at $x = 0.01$ for chain length dependent termination kinetics.

As explained above, other methods to determine $C_{tr,0}$ for the RAFT exchange reactions with R_0X were developed by Moad and coworkers²²⁻²⁴ (Equation (8)) and Theis *et al.*²⁵ (Equation (9)). The former method relies on the assumption that the reaction of R_0 species with macro-RAFT CTA can be neglected ($C_{-tr,0}$), while the latter method can only be applied to monomer/RAFT CTA combinations that display a strong hybrid behavior. In Table 3.5, the accuracy of these two methods is evaluated via the simulation of perfect experiments for a range of conditions covering different TCLs and values for the chain transfer reactivity with R_0X , $C_{tr,0}$, in a similar way as done for the construction of Table 3.4 ($C_{tr,0,IN}$ vs. $C_{tr,0,OUT}$). For all the simulation results in Table 3.5 chain length dependent termination kinetics are taken into account, which is shown to induce only minor deviations ($\sim 1\%$) from the approximate case with constant termination rate coefficients based on preliminary simulations. Furthermore, the reactivities of the R_0 ($C_{-tr,0}$) species and the macroradicals (R_i ; C_{tr}) with macro-RAFT CTA are assumed equal to $C_{tr,0}$ at first instance, not to overcomplicate the analysis. The value of C_{tr} again does not affect the obtained $C_{tr,0}$ significantly with typical additional deviations less than 1%, as verified by simulations. In contrast, the value of $C_{-tr,0}$ has a pronounced influence on the accuracy at which $C_{tr,0}$ can be determined, as discussed further.

It is clear from Table 3.5 that the accuracy of the method of Moad and coworkers²²⁻²⁴ (Equation (8)), in which $C_{tr,0}$ is obtained by linear regression of $\ln([R_0X]/[R_0X]_0)$ versus $\ln([M]/[M]_0)$, increases markedly for *lower* values of $C_{tr,0}$ (entry 1-4) and higher TCLs (entry

3, 5, 6). This is in line with expectations as the contribution of R_0 species reacting with macro-RAFT CTA will decrease accordingly and, hence, the underlying assumption for the derivation of Equation (8) will be more closely met.

Table 3.5: Evaluation of the method of Moad and coworkers²²⁻²⁴ (Equation (8)) and the method of Theis *et al.*²⁵ (Equation (9)) to determine $C_{tr,0}$ ($C_{tr,0,OUT}$) in case the reaction of R_0 species with macro-RAFT CTA can be neglected, based on the simulation of perfect experiments. Different targeted chain lengths (TCLs = $[M]_0/[R_0X]_0$) and values for the implemented value for $C_{tr,0}$ ($C_{tr,0,IN}$) are covered. In all simulations $C_{-tr,0} = C_{tr} = C_{tr,0,IN}$. $[M]_0 = 9 \text{ mol L}^{-1}$; $[I_2]_0 = 9 \cdot 10^{-3} \text{ mol L}^{-1}$. For TCL 100, 200 and 300, $[R_0X]_0$ is respectively: 0.09, 0.04 and 0.03 mol L^{-1} . Other kinetic parameters in Table 3.3.

entry	TCL	method Moad and coworkers			method Theis <i>et al.</i>	
		$C_{tr,0,IN}$ [-]	$C_{tr,0,OUT}$ [-]	% deviation	$C_{tr,0,OUT}$ [-]	% deviation
1	100	1.0	0.97	3.0	1.14	14.0
2	100	5.0	4.61	7.8	5.25	5.0
3	100	15.0	12.59	16.1	15.78	5.2
4	100	20.0	15.80	21.0	21.47	7.4
5	200	15.0	13.72	8.5	15.99	6.6
6	300	15.0	14.19	5.4	16.17	7.8

In contrast, when applying the method of Theis *et al.*²⁵ to determine $C_{tr,0}$ from the initial x_n (Equation (9)), a much less pronounced increase for the deviation of $C_{tr,0,OUT}$ from the implemented value ($C_{tr,0,IN}$) is obtained for *higher* transfer reactivities (entry 1-4). The mismatch increases however further with increasing TCL. Except for a low value of $C_{tr,0}$ (entry 1), for which no linear increase of the chain length with conversion is observed anymore as almost FRP behavior results, the method of Theis *et al.*²⁵ is more accurate than the method of Moad and coworkers,²²⁻²⁴ with resulting deviations from $C_{tr,0,IN}$ between 5 and

8% for the studied conditions. However, in practice, also other factors need to be taken into account such as the much lower precision of the SEC measurements to determine the initial number average chain length (> 10%) in comparison with the concentration measurements of monomer and R_0X , which can often be accurately obtained via *e.g.* on-line ^1H -nuclear magnetic resonance (NMR) spectroscopy (*ca.* 5%). Furthermore, if $C_{-tr,0}$ is very small compared to $C_{tr,0}$, Equation (8) (method of Moad and coworkers²²⁻²⁴) becomes an exact equality (*cf.* Chapter 1) and errors on $C_{tr,0}$ will only be determined by the precision of the corresponding concentration measurements for the monomer and R_0X .

On the other hand, a very high value for $C_{-tr,0}$ compared to $C_{tr,0}$ will induce non-linearity in the plot of $\ln([R_0X]/[R_0X]_0)$ versus $\ln([M]/[M]_0)$ as shown in Figure 3.2 (full red line; $C_{-tr,0} = 10 C_{tr,0}$; $C_{tr,0} = 15$; TCL 100), making a reliable determination of $C_{tr,0}$ impossible via Equation (8). Considering a higher TCL will partially resolve this issue as also depicted in Figure 3.2 (dashed blue line; $C_{-tr,0} = 10 C_{tr,0}$; $C_{tr,0} = 15$; TCL 500), however the corresponding inherent deviation from the real value ($C_{tr,0,IN}$) is still 20%. Importantly, the method of Theis *et al.*²⁵ is not significantly affected by the higher $C_{-tr,0}$ values, and yields reasonable deviations of respectively 3% (TCL 100) and 5% (TCL 500).

If a non-linearity as presented by the full red line in Figure 3.2 is observed as a consequence of a high $C_{-tr,0}$, Equation (7) can be alternatively applied to determine simultaneously $C_{tr,0}$ and $C_{-tr,0}$ in which $\frac{d[R_0X]}{d[M]}$ is either calculated based on kinetic modeling results for the considered RAFT polymerization, or, determined experimentally. However, the latter requires accurate time-resolved measurements of $[R_0X]$ and $[M]$ for application of Equation (7), *e.g.* simulations indicated that monitoring $[M]$ and $[R_0X]$ every 1% of monomer conversion and calculating accordingly $\frac{d[R_0X]}{d[M]}$ via $\frac{[R_0X]_2 - [R_0X]_1}{[M]_2 - [M]_1}$ with $[A]_1$ and $[A]_2$ two consecutive concentration

measurements of A , already induces a 10% mismatch between the left-hand-side and the right-hand-side of Equation (7).

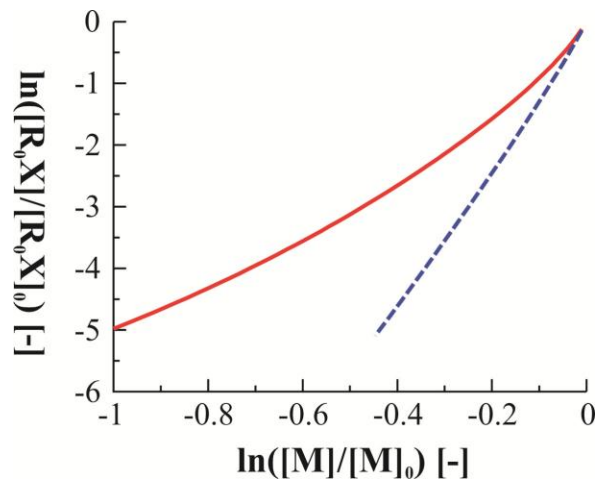


Figure 3.2: Natural logarithm of the concentration ratio of R_0X versus the natural logarithm of the concentration ratio of monomer (Equation (8)) for TCL 100 (full red line) and TCL 500 (dashed blue line) in case the transfer reactivity of the R_0 species with macro-RAFT CTA is high: $C_{-tr,0} = 150$, $C_{tr,0} = 15 = C_{tr}$. $[M]_0 = 9 \text{ mol L}^{-1}$; $[I_2]_0 = 9 \cdot 10^{-3} \text{ mol L}^{-1}$. $[R_0X]_0$ for TCL ($= [M]_0/[R_0X]_0$) 100 and 500 respectively: 0.09 and 0.018 mol L⁻¹. Other kinetic parameters in Table 3.3.

It can thus be concluded based on Table 3.4-5 that a reliable determination of $C_{tr,0}$ is possible via the CLD method (Equation (3)) for low values of $C_{tr,0}$ (< 5) with corresponding deviations only up to 5%. On the other hand, for higher $C_{tr,0}$ values the method of Theis *et al.*²⁵ (Equation (9)) provides a good estimate independent of the transfer reactivity of the R_0 species with macro-RAFT CTA ($C_{-tr,0}$) provided that hybrid behavior occurs. The latter implies that $C_{tr,0}$ cannot be too high (< 100). Furthermore, the method of Theis *et al.* is limited by the precision of the SEC measurements which becomes especially important at low TCLs, as at low conversion SEC polymer peaks can fall outside the calibration region of the instrument. Hence, large extrapolations have to be made to obtain the initial increase in chain length x_n^0 . In case the contribution of $C_{-tr,0}$ is negligible, which can be verified experimentally by a constant $C_{tr,0,OUT}$ for different TCLs, the method of Moad and coworkers²²⁻²⁴ (Equation (8)) is the most effective. Table 3.6 presents a summary of the conditions for which each of the discussed methods provides the most accurate results, and can be used as a guideline for

the experimental chemist. The Mayo method⁶ is not included in this table since its accuracy is in general lower than the CLD method, while similar factors influence its optimal conditions. From Table 3.6 it is clear that no generally applicable method to determine accurate values for $C_{tr,0}$ under a wide range of conditions is available. In particular, for higher values of $C_{tr,0}$ (> 10), current literature models are less accurate. It should be stressed that in case of too high values for $C_{tr,0}$ (> 100), its experimental determination becomes more difficult as R_0X is fully consumed after a few percentages of monomer conversion and no hybrid behavior will occur.

Table 3.6: Summary of the conditions corresponding to the highest accuracy of the discussed analytical literature methods to determine $C_{tr,0}$.^{8-10,22,23,25} The absolute requirement and its corresponding experimental verification are also listed. TCL: targeted chain length, $[M]_0/[R_0X]_0$. Summary of model assumptions for each method in Table 3.2 and detailed discussion in Chapter 1.

method	expression	$C_{tr,0}$ [-]	TCL	absolute requirement	experimental verification
CLD ^a	Eq. (3)	$C_{tr,0} < 5$	n.a. ^b	measurement at low x	broad CLD
Moad ²²⁻²⁴	Eq. (8)	$C_{tr,0} < 100$	high	negligible contribution of $C_{-tr,0}$	linear $\ln([R_0X])$ vs. $\ln([M])$
Theis <i>et al.</i> ²⁵	Eq. (9)	$1 < C_{tr,0} < 100$	low ^c	hybrid behavior	strong initial increase in x_n

^aalways better than Mayo method.^{6,8-10} ^bfor low $C_{tr,0}$ always broad CLD and high chain lengths will be obtained ^cLimited by precision of SEC measurements, for low TCLs peaks can be outside calibration region

3.3.3 Models to determine C_{tr}

Next to $C_{tr,0}$ and $C_{-tr,0}$, also the transfer reactivity of macroradicals with dormant polymer molecules, C_{tr} , influences the observed polymer properties, its contribution depending on the respective relative values. In principle, the above described methods to determine $C_{tr,0}$ developed by Moad and coworkers^{22,23} (Equation (7)-(8)) and Theis *et al.*²⁵ (Equation (9)) could be used to quantify C_{tr} if the RAFT polymerization is started from a macro-RAFT CTA with number average chain length x_n instead of using a conventional R_0X . However, the necessary experimental responses are difficult to access as a proper resolution between the

initial macro-RAFT CTA and the corresponding dormant polymeric species after consecutive additions of monomer is hard to obtain, for both the SEC and concentration measurements.

Alternatively, for a conventional RAFT polymerization started from R_0X , analytical expressions for the polymer dispersity as a function of the monomer conversion were developed from which C_{tr} values can be directly obtained by a comparison with experimental polymer dispersity data.^{4,19-21} However, as these analytical methods are based on expressions for the dispersity of the dormant polymers, they only hold for a well-controlled RAFT polymerization, in which the observed polymer dispersity can be approximated by the one of the dormant polymer. Furthermore, as highlighted before, the derivation of these equations is based on several assumptions which limit the application scope (*cf.* Table 3.2 and Chapter 1). In particular, for the simulation of a perfect experiment with $C_{tr,0} = C_{-tr,0} = C_{tr} = 15$ (TCL 100), both the analytical expressions determined by Goto and Fukuda²¹ (Equation (10); dashed blue line in Figure 3.3) and Gao and Zhu⁴ (Equation (11); dotted red line in Figure 3.3) yield a severe initial overestimation of the actual polymer dispersity (full green line in Figure 3.3a; complete kinetic model), as shown in Figure 3.3a (left axis). Concomitantly, application of Equation (10)-(11) to the simulated polymer dispersity with the full kinetic model to determine the corresponding C_{tr} values results in a strong initial overshoot of the implemented value ($C_{tr,IN}$), as depicted in Figure 3.3b. Both observations can be ascribed to the common model assumption for Equation (10)-(11) that RAFT transfer reactions with R_0X have a negligible influence on the observed polymer properties, which only holds for very high values of $C_{tr,0}$ (> 100). Only at full conversion of R_0X (right axis Figure 3.3a, full green line), the dispersity obtained via the models of Goto and Fukuda²¹ and Gao and Zhu⁴ tend towards the input dispersity values ($C_{tr} = 15$; $C_{tr} = C_{tr,0} = C_{-tr,0}$), and the determined C_{tr} values approach the implemented value of 15 (full green line in Figure 3.3b; $C_{tr,IN}$). Note that from

Figure 3.3 it can also be derived that the method of Gao and Zhu⁴ is more accurate than the method of Goto and Fukuda,²¹ due to less stringent model assumptions.

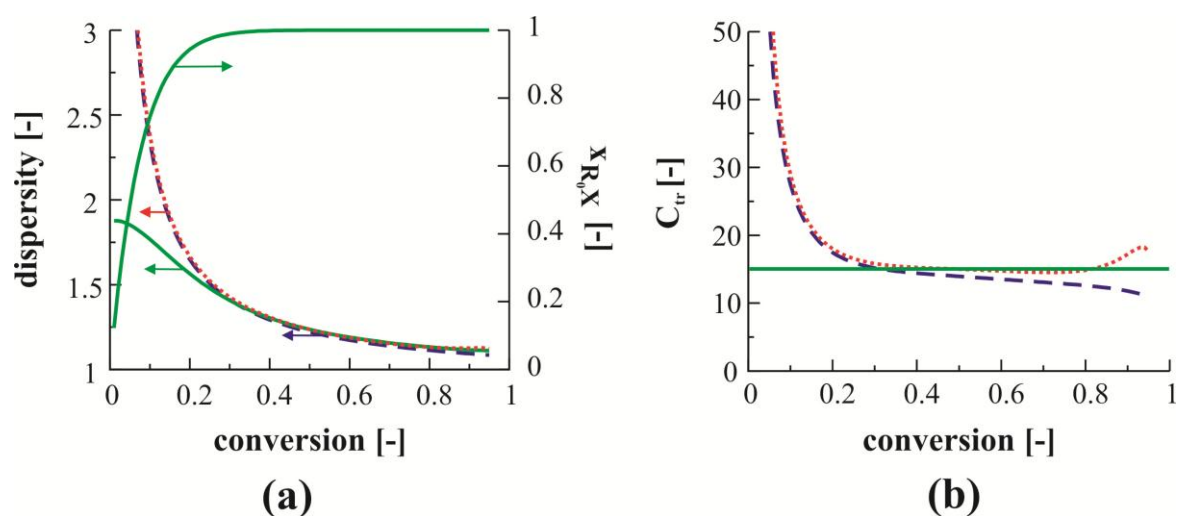


Figure 3.3: (a) Left axis: comparison between the simulated polymer dispersity for a perfect experiment (full green line) and the polymer dispersity obtained by application of the analytical expression of Goto and Fukuda²¹ (dashed blue line; Equation (10)) and Gao and Zhu⁴ (dotted red line; Equation (11)) with $C_{tr} = 15$; right axis: R_0X conversion. (b) Comparison between the implemented C_{tr} value (full green line) and the values for C_{tr} obtained from the application of Equations (10) (dashed blue line) and (11) (dotted red line) to the simulated polymer dispersity profile of the dormant chains. $TCL=100$; $C_{tr} = C_{tr,0} = C_{tr,0} = 15$; $[M]_0 = 9 \text{ mol L}^{-1}$; $[I_2]_0 = 9 \cdot 10^{-3} \text{ mol L}^{-1}$. Other kinetic parameters in Table 3.3.

Although for an equal RAFT exchange reactivity of R_0X and the macro-RAFT CTA the analytical method of Gao and Zhu⁴ yields still acceptable results for C_{tr} as soon as R_0X is fully consumed (Figure 3.3b), the current analytical models do not lead to reliable C_{tr} values if the RAFT exchange reactivity with R_0X ($C_{tr,0}$) is significantly different from that with macro-RAFT CTA (C_{tr}). This is shown in Figure 3.4, which presents the obtained C_{tr} values upon application of Equation (10)-(11) to the simulated polymer dispersity with the full kinetic model ($C_{tr,OUT}$) for a perfect experiment with $C_{tr,0} = C_{-tr,0} = 15$ ($C_{tr,0,IN}$) and $C_{tr} = 30$ ($C_{tr,IN}$) (left axis). Again, both the method of Goto and Fukuda²¹ (dashed blue line) and the one of Gao and Zhu⁴ (dotted red line) yield a strong overshoot of C_{tr} until full conversion of R_0X is obtained (full green line, right axis). Importantly, at full conversion of R_0X , significant deviations ($> 20\%$) from $C_{tr,IN}$ (black square in Figure 3.4) are obtained. It can thus be concluded that the current analytical models for the polymer dispersity in a degenerative

RAFT polymerization fail to provide a valid approximation over a broad range of RAFT transfer reactivities. In general, it can thus be stated that no straightforward experimental method is available to determine the RAFT exchange reactivity with macro-RAFT CTA (C_{tr}).

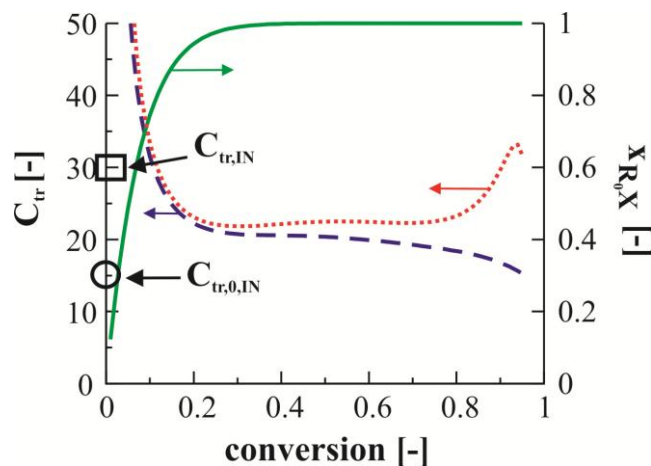


Figure 3.4: Left axis: comparison between the implemented C_{tr} values ($C_{tr,0,IN}$, black circle; $C_{tr,IN}$, black square) and the values for C_{tr} obtained from the application of Equations (10) (dashed blue line) and (11) (dotted red line) to the simulated polymer dispersity profile of the dormant chains. Right axis: R_0X conversion (full green line). $TCL=100$; $C_{tr,0} = C_{-tr,0} = 15$, $C_{tr} = 30$; $[M]_0 = 9 \text{ mol L}^{-1}$; $[I_2]_0 = 9 \cdot 10^{-3} \text{ mol L}^{-1}$. Other kinetic parameters in Table 3.3.

3.4 Conclusions

An evaluation of the currently available analytical methods to determine the transfer reactivities for degenerative RAFT polymerization has been performed based on the simulation of perfect experiments, using a complete kinetic model. No general method is currently available to determine accurate values for either $C_{tr,0}$ or C_{tr} under a wide range of conditions and transfer reactivities. Instead, each method is only effective for a well-defined limited range of conditions which depends on the corresponding model assumptions.

It is shown that a reliable determination of $C_{tr,0}$ is possible via the CLD method (Equation (3)) for low values of $C_{tr,0}$ (< 5). For higher $C_{tr,0}$ values, the method of Theis *et al.*²⁵ (Equation (9)) leads to a good estimate of $C_{tr,0}$ independent of the transfer reactivity of the R_0 species with macro-RAFT CTA ($C_{-tr,0}$), provided that the considered RAFT polymerization exhibits a pronounced hybrid behavior. Furthermore, in case the contribution of $C_{-tr,0}$ is negligible, the

method of Moad and coworkers^{22,23} (Equation (8)) is the most effective as it is based on concentration measurements, which are in general more precise than the SEC measurements required in the method of Theis *et al.*²⁵

Moreover, for the RAFT exchange reactivity with macro-RAFT CTA, C_{tr} , the analytical methods currently available in literature are limited to RAFT polymerizations with equal values for $C_{tr,0}$ and C_{tr} , at full conversion of the initial RAFT CTA. Hence, an important future research task is the development of more detailed analytical models capable of covering a wider range of RAFT exchange reactivities.

3.5 References

- (1) Flory, P. J. *Principles of Polymer Chemistry*; Cornell University Press: Ithaca, 1953.
- (2) Matyjaszewski, K. D., T. P. *Handbook of Radical Polymerization*; John Wiley and Sons: New Jersey, 2002.
- (3) Odian, G. *Principles of Polymerization*; John Wiley and Sons: New Jersey, 2004.
- (4) Gao, X.; Zhu, S. *Journal of Applied Polymer Science* **2011**, *122*, 497-508
- (5) Whitby, G. S. *Synthetic Rubber*; Wiley: New York, 1954.
- (6) Mayo, F. R. *Journal of the American Chemical Society* **1943**, *65*, 2324-2329
- (7) Barner-Kowollik, C.; Russell, G. T. *Progress in Polymer Science* **2009**, *34*, 1211-1259
- (8) Clay, P. A.; Gilbert, R. G. *Macromolecules* **1995**, *28*, 552-569
- (9) Moad, G.; Moad, C. L. *Macromolecules* **1996**, *29*, 7727-7733
- (10) Moad, C. L.; Moad, G.; Rizzardo, E.; Thang, S. H. *Macromolecules* **1996**, *29*, 7717-7726
- (11) Beuermann, S.; Buback, M. *Progress in Polymer Science* **2002**, *27*, 191-254

- (12) Chiefari, J.; Chong, Y. K.; Ercole, F.; Krstina, J.; Jeffery, J.; Le, T. P. T.; Mayadunne, R. T. A.; Meijs, G. F.; Moad, C. L.; Moad, G.; Rizzardo, E.; Thang, S. H. *Macromolecules* **1998**, *31*, 5559-5562
- (13) Barner-Kowollik, C. *Handbook of RAFT Polymerization*; Wiley: Weinheim, 2008.
- (14) Harrisson, S.; Liu, X.; Ollagnier, J.-N.; Coutelier, O.; Marty, J.-D.; Destarac, M. *Polymers* **2014**, *6*, 1437-1488
- (15) Barner-Kowollik, C.; Buback, M.; Charleux, B.; Coote, M. L.; Drache, M.; Fukuda, T.; Goto, A.; Klumperman, B.; Lowe, A. B.; McLeary, J. B.; Moad, G.; Monteiro, M. J.; Sanderson, R. D.; Tonge, M. P.; Vana, P. *Journal of Polymer Science Part a-Polymer Chemistry* **2006**, *44*, 5809-5831
- (16) Moad, G.; Chiefari, J.; Chong, Y. K.; Krstina, J.; Mayadunne, R. T. A.; Postma, A.; Rizzardo, E.; Thang, S. H. *Polymer International* **2000**, *49*, 993-1001
- (17) Moad, G.; Rizzardo, E.; Thang, S. H. *Polymer* **2008**, *49*, 1079-1131
- (18) Favier, A.; Charreyre, M.-T. *Macromolecular Rapid Communications* **2006**, *27*, 653-692
- (19) Muller, A. H. E.; Yan, D. Y.; Litvinenko, G.; Zhuang, R. G.; Dong, H. *Macromolecules* **1995**, *28*, 7335-7338
- (20) Muller, A. H. E.; Zhuang, R. G.; Yan, D. Y.; Litvinenko, G. *Macromolecules* **1995**, *28*, 4326-4333
- (21) Goto, A.; Fukuda, T. *Progress in Polymer Science* **2004**, *29*, 329-385
- (22) Chiefari, J.; Mayadunne, R. T. A.; Moad, C. L.; Moad, G.; Rizzardo, E.; Postma, A.; Skidmore, M. A.; Thang, S. H. *Macromolecules* **2003**, *36*, 2273-2283

- (23) Chong, Y. K.; Krstina, J.; Le, T. P. T.; Moad, G.; Postma, A.; Rizzardo, E.; Thang, S. H. *Macromolecules* **2003**, *36*, 2256-2272
- (24) Moad, G.; Chiefari, J.; Mayadunne, R. T. A.; Moad, C. L.; Postma, A.; Rizzardo, E.; Thang, S. H. *Macromolecular Symposia* **2002**, *182*, 65-80
- (25) Theis, A.; Feldermann, A.; Charton, N.; Stenzel, M. H.; Davis, T. P.; Barner-Kowollik, C. *Macromolecules* **2005**, *38*, 2595-2605
- (26) Coote, M. L. *Journal of Physical Chemistry A* **2005**, *109*, 1230-1239
- (27) Coote, M. L.; Henry, D. J. *Macromolecules* **2005**, *38*, 1415-1433
- (28) Coote, M. L.; Izgorodina, E. I.; Krenske, E. H.; Busch, M.; Barner-Kowollik, C. *Macromolecular Rapid Communications* **2006**, *27*, 1015-1022
- (29) Coote, M. L.; Krenske, E. H.; Izgorodina, E. I. *Macromolecular Rapid Communications* **2006**, *27*, 473-497
- (30) Johnston-Hall, G.; Monteiro, M. J. *Macromolecules* **2007**, *40*, 7171-7179
- (31) Peklak, A. D.; Butte, A.; Storti, G.; Morbidelli, M. *Journal of Polymer Science Part a-Polymer Chemistry* **2006**, *44*, 1071-1085
- (32) Drache, M.; Schmidt-Naake, G. *Macromolecular Symposia* **2007**, *259*, 397-405
- (33) Barth, J.; Buback, M.; Meiser, W.; Vana, P. *Macromolecules* **2010**, *43*, 51-54
- (34) Meiser, W.; Buback, M.; Barth, J.; Vana, P. *Polymer* **2010**, *51*, 5977-5982
- (35) Meiser, W.; Barth, J.; Buback, M.; Kattner, H.; Vana, P. *Macromolecules* **2011**, *44*, 2474-2480
- (36) Petzold, L. *Siam Journal on Scientific and Statistical Computing* **1983**, *4*, 136-148

- (37) Shen, J. C.; Yuan, T.; Wang, G. B.; Yang, M. L. *Makromolekulare Chemie-Macromolecular Chemistry and Physics* **1991**, *192*, 2669-2685
- (38) Beuermann, S.; Buback, M.; Russell, G. T. *Macromolecular Chemistry and Physics* **1995**, *196*, 2493-2516
- (39) Derboven, P.; D'hooge, D. R.; Reyniers, M.-F.; Marin, G. B.; Barner-Kowollik, C. *Macromolecules* **2015**, *48*, 492-501
- (40) Johnston-Hall, G.; Stenzel, M. H.; Davis, T. P.; Barner-Kowollik, C.; Monteiro, M. J. *Macromolecules* **2007**, *40*, 2730-2736
- (41) Braun, D.; Quella, F. *Makromolekulare Chemie-Macromolecular Chemistry and Physics* **1978**, *179*, 387-394
- (42) Korbar, A.; Malavasic, T. *Journal of Thermal Analysis* **1995**, *44*, 1357-1365
- (43) Szafko, J.; Feist, W. *Journal of Polymer Science Part a-Polymer Chemistry* **1995**, *33*, 1637-1642
- (44) Beuermann, S.; Buback, M.; Davis, T. P.; Gilbert, R. G.; Hutchinson, R. A.; Olaj, O. F.; Russell, G. T.; Schweer, J.; van Herk, A. M. *Macromolecular Chemistry and Physics* **1997**, *198*, 1545-1560
- (45) Adamy, M.; van Herk, A. M.; Destarac, M.; Monteiro, M. J. *Macromolecules* **2003**, *36*, 2293-2301

Chapter 4: A novel method to measure degenerative RAFT exchange reactivities: proof of concept and experimental validation

Summary

A novel method is presented to experimentally determine transfer coefficients in degenerative reversible addition fragmentation chain transfer (RAFT) polymerization for both exchange with small RAFT CTA and macro-RAFT CTA based on measurements of the polymer dispersity, including an accurate correction for the diffusional limitations on termination. The method is rigorously tested via the simulation of perfect experiments and is also able to accurately capture for the first time a possible chain length dependency of the transfer or RAFT addition coefficient, an outstanding challenge in the fundamental understanding of RAFT polymerization kinetics up to high conversion. The method is successfully applied to experimental data for azobis(isobutyronitrile) (AIBN) initiated RAFT polymerization of methyl methacrylate (MMA) with cyano-2-propyl dithobenzoate (CPDB) as small RAFT CTA at 353 K. A value of 20 is reported for the exchange with CPDB. For RAFT exchange with the corresponding macro-RAFT CTA an approximate value of 76 is obtained. No chain length dependency is detected for the current experimental dataset.

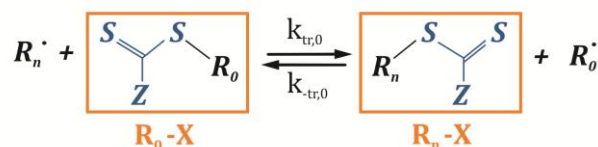
4.1 Introduction

Reversible addition-fragmentation chain transfer (RAFT) polymerization has emerged as the main technique for many precision macromolecular design procedures, due to its versatility and high monomer flexibility.^{1,2} Like any other reversible deactivation radical polymerization (RDRP) or controlled radical polymerization (CRP) technique, control over the polymer properties is established via a reversible capping of macroradicals into dormant macrospecies by addition of a RDRP agent,^{2,3} in this case a RAFT chain transfer agent (CTA). However, the unique feature of RAFT polymerization, discerning itself from other RDRP techniques such as nitroxide mediated and atom transfer radical polymerization, relies on the simultaneous formation of another radical each time a dormant macrospecies (R_nX) is formed, *i.e.* an exchange process takes place via a consecutive addition and fragmentation step (*cf.* Chapter 1 and Chapter 3).¹⁻³ For an efficient RAFT exchange, no rate retardation is observed compared to the corresponding free radical polymerization (FRP),^{2,4,5} making RAFT polymerization an eligible candidate for industrialization of specialty applications.² In contrast, for less efficient RAFT CTA/monomer combinations the RAFT polymerization can be significantly retarded, which has been ascribed to either slow fragmentation of the intermediate radical species formed in the RAFT exchange process and/or cross-termination reactions of the latter species with any other radical in the polymerization mixture.⁴⁻⁸

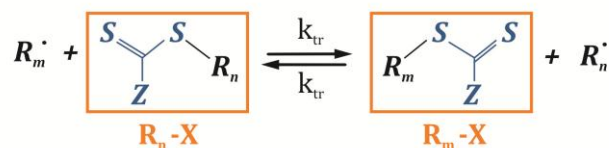
In the absence of the latter slow fragmentation and cross-termination reactions, the RAFT exchange process can be formally described by a degenerative transfer mechanism (*cf.* Appendix E). If the RAFT exchange reactivity of the conventional initiator-derived radicals and the small RAFT CTA-derived species (R_0) is similar or the contribution of the former species can be neglected, three (degenerative) RAFT exchange rate coefficients ($k_{tr,0}$, $k_{-tr,0}$ and k_{tr}) are needed, as shown in Scheme 4.1 (*cf.* Appendix E).^{2,3,5,9,10} Several methods exist in literature to determine the corresponding RAFT transfer coefficients $C_{tr,0}$, $C_{-tr,0}$ and C_{tr} , which

are respectively defined as the ratio of $k_{tr,0}$, $k_{-tr,0}$ and k_{tr} to the intrinsic propagation rate coefficient.^{2,5,9-21} The values of these transfer coefficients are determined by the nature of the RAFT CTA (R_0X ; Scheme 4.1) and can therefore be used as a measure to classify a RAFT CTA according to its suitability for a given monomer.

Degenerative transfer of macroradical R_n with RAFT CTA R_0X



Degenerative transfer of macroradical R_m with macro-RAFT CTA R_nX



Scheme 4.1: Simplified RAFT degenerative transfer mechanism based on the pseudo-steady state assumption for the calculation of the concentration of the intermediate radical species (cf. Appendix E). Only RAFT exchange reactions are shown for simplicity.

Yet, no direct experimental method is currently available to accurately determine these transfer coefficients for a wide range of conditions, as was demonstrated in Chapter 3. Particularly, for C_{tr} the application scope of the available methods, which are mainly based on analytical expressions for the polymer dispersity, is very narrow.^{9,13,14,20,21} Furthermore, none of the current literature models to determine $C_{tr,0}$ or C_{tr} properly account for the influence of diffusional limitations on the termination rate coefficients due to the strong viscosity increase. Also, they all rely on a constant RAFT transfer coefficient, which is in disagreement with for instance Izgorodina and Coote who postulated a strong intrinsic chain length dependency of the addition rate coefficient, and thus possibly for C_{tr} , based on *ab initio* calculations for oligomeric species up to a size of three monomer units.²² In contrast, in earlier experimental work of Moad *et al.* the intrinsic chain transfer reactivity of methyl methacrylate (MMA) dimers, trimers, tetramers and macromonomers under FRP conditions was shown not to depend on the macromonomer chain length, thus questioning these theoretical observations on

the intrinsic chain length dependency.¹⁹ On the other hand, similar to termination, the RAFT addition reaction requires the diffusion of two polymeric species prior to reaction and, hence, RAFT addition/transfer rates can be susceptible to diffusional limitations, and can depend on the conversion and chain length, if the intrinsic reactivity is sufficiently high.²³⁻²⁷ An apparent RAFT transfer reactivity needs to be considered in the latter case.

In this chapter, an improved experimental method is developed to accurately determine $C_{tr,0}$ and C_{tr} based on an analytical expression for the polymer dispersity as a function of monomer conversion. The deficiency of the current literature models (Chapter 3) is eliminated, as chain length and conversion dependent termination and transfer reactivities are considered, and for a wide range of conditions both $C_{tr,0}$ and C_{tr} can be deduced from a single experiment. Proof of concept of the method is first provided based on the simulation of perfect experiments using a detailed degenerative RAFT polymerization kinetic model. It is further shown based on these simulations that the developed method leads to more accurate results compared to literature models. In a final step, the method is applied to experimental RAFT polymerization data reported by Derboven *et al.* for MMA at 353 K with cyano-isopropyl dithiobenzoate (CPDB) as RAFT CTA and initiated by azobis(isobutyronitrile) (AIBN).²⁸ It is demonstrated that for this RAFT polymerization intrinsic/apparent chain length dependencies for the RAFT exchange can be ignored.

4.2 Method section

In this section, an improved method to obtain $C_{tr,0}$ and/or C_{tr} based on an analytical expression for the polymer dispersity profile is developed, with a limited number of assumptions. The model is an extension of the method of Gao and Zhu in which the polymer dispersity is calculated based on the method of moments while assuming a constant termination and transfer reactivity and a negligible contribution of RAFT exchange reactions involving the

small RAFT CTA (R_0X),⁹ strongly limiting its application scope (*cf.* Chapter 3). In the current method, these constraints have been resolved, as discussed in detail below.

For the derivation, the degenerative RAFT polymerization scheme presented in Table 4.1 is assumed, which imposes an equal reactivity of the conventional initiator-derived radicals, I^* , and the R_0 radicals originating from the RAFT CTA R_0X .⁹ The latter assumption holds for identical I^* and R_0 species or if the conventional radical initiator (I_2) concentration is very small compared to the R_0X concentration, a condition typically fulfilled for a controlled RAFT polymerization, as the contribution of reactions with I^* is then negligible.^{2,29} In this reaction scheme, the termination rate coefficient k_t between macroradicals R_n and R_m accounts for contributions of both recombination and disproportionation. Also the influence of diffusional limitations is included by the consideration of apparent termination reactivities. Similarly, a possible chain length/ conversion dependency of the RAFT transfer rate coefficient, denoted in general form as k_{tr}^* in Table 4.1 is taken into account. Note that for chain length values n and/or m equal to zero, k_{tr}^* is equal to $k_{tr,0}$ or $k_{-tr,0}$ (*cf.* Scheme 4.1) and can thus be significantly different from k_{tr} , *i.e.* the RAFT exchange rate coefficient if n and m are larger than zero.

Table 4.1: Degenerative transfer RAFT polymerization scheme used for the model development of in the present work. M : monomer; R_nX : dormant species with chain length n , for $n=0$ small RAFT CTA; I_2 : conventional radical initiator with I^* identical to R_0 ; R_n : macroradical with chain length n ; P : dead polymer species; all rate coefficients can be apparent, i.e. can vary as a function of conversion and chain length of the participating reactants. Assumptions in Appendix E.

Reaction	Equation
Dissociation ^a	$I_2 \xrightarrow{k_d, f} 2R_0$
Propagation	$R_{n-1} + M \xrightarrow{k_p} R_n \quad n = 1, \dots, \infty$
degenerative chain transfer	$R_n + R_mX \xrightleftharpoons{k_{tr}^*} R_nX + R_m \quad n, m = 0, \dots, \infty$
termination	$R_n + R_m \xrightarrow{k_t} (2)P \quad n, m = 0, \dots, \infty$

^a f is the initiator efficiency and takes into account that only a certain fraction of the R_0 radicals generated by decomposition of I_2 will effectively initiate the polymerization

In order to enable an analytical solution for the polymer dispersity \mathcal{D} as a function of monomer conversion and in agreement with the earlier work of Gao and Zhu the moments of the macrospecies need to be defined via the summation for the chain length n from zero to infinity,^{9,20,21} as shown in Equation (1) for the macroradicals (λ_s) and Equation (2) for the dormant polymeric species (τ_s):

$$\lambda_s = \sum_{n=0}^{\infty} n^s [R_n] \quad (1)$$

$$\tau_s = \sum_{n=0}^{\infty} n^s [R_nX] \quad (2)$$

As a consequence, the zeroth order moment of the dormant polymer chains τ_0 is constant and equal to the initial RAFT CTA concentration:

$$\tau_0 = \sum_{n=0}^{\infty} [R_nX] = [R_0X]_0 \quad (3)$$

Assuming a controlled RAFT polymerization, the polymer dispersity \mathfrak{D} at a monomer conversion x can be approximated based on the dormant chain length distribution (CLD):⁹

$$\mathfrak{D} \approx \frac{x_{m,dormant}}{x_{n,dormant}} = \frac{(\tau_0 x_{R_0X}) \tau_2(x)}{[\tau_1(x)]^2} \quad (4)$$

in which $x_{m,dormant}$ and $x_{n,dormant}$ are respectively the mass averaged and number averaged chain length of the dormant polymer. In this expression \mathfrak{D} needs to be corrected with the conversion of the RAFT CTA (x_{R_0X}) as only the dormant polymeric species and not the initial RAFT CTA (R_0X), although included in the calculation of the zeroth moment (Equation (3)), contribute to the dispersity of the dormant polymer (Equation (4)). Importantly, this correction factor is novel and has a pronounced influence on the resulting value for \mathfrak{D} . This is particularly relevant for low to intermediate transfer reactivities of R_0X ($C_{tr,0} < 50$), as in that case the consumption of R_0X will extend over a significant monomer conversion range ($> 20\%$).^{1,2,5,10}

The application of the method of moments also implies the calculation of population weighted or average rate coefficients.^{27,30} In particular, an average apparent termination rate coefficient $\langle k_t \rangle$ is used that corrects for chain length and conversion dependencies due to diffusional limitations. Additionally, the inclusion of R_0 and R_0X in the moments of respectively the macroradicals and dormant macrospecies requires also the consideration of a population weighted RAFT transfer rate coefficient $\langle k_{tr} \rangle$ and thus a population weighted $\langle C_{tr} \rangle$, even if the RAFT transfer rate coefficient is chain length independent. The transfer reactivity of R_0X ($C_{tr,0}$), which is predominantly present at low monomer conversions and corresponding low R_0X conversion, often differs markedly from the reactivity of the corresponding macro-RAFT CTA (C_{tr}), which is the dominant CTA species at higher monomer conversions for which full consumption of R_0X is reached, explaining this need for $\langle k_{tr} \rangle$ and $\langle C_{tr} \rangle$, and inducing inherently a conversion dependency of the latter. However, if $C_{tr,0}$ is very high (> 100), full

conversion of R_0X is reached already at a few percentages of monomer conversion and the value of $\langle C_{tr} \rangle$ can be solely linked to the transfer reactivity of the macro-RAFT CTA (C_{tr}).

Equation (4) can thus be written in general by the following analytic expression:

$$\mathfrak{D}(x) \approx \frac{(\tau_0 x_{R_0X})\tau_2(x)}{[\tau_1(x)]^2} = g(\langle C_{tr} \rangle(x), x) \quad (5)$$

in which g is an analytical function depending on x and $\langle C_{tr} \rangle$. To evaluate $\langle C_{tr} \rangle$ at each x , $g(\langle C_{tr} \rangle(x), x)$ needs to be set equal to the experimentally observed dispersity \mathfrak{D}_{exp} and solved to $\langle C_{tr} \rangle(x)$:

$$\mathfrak{D}_{exp}(x) = g(\langle C_{tr} \rangle(x), x) \quad (6)$$

Clearly, analytical expressions for τ_1 and τ_2 as function of x are required to identify the functional form of g . Expressions for the derivative of τ_1 and τ_2 to x can be obtained based on the pseudo steady-state approximation (PSSA) for λ_1 and λ_2 , following the methodology as developed by Gao and Zhu:⁹

$$\frac{d\tau_1}{dx} = \frac{1 - x + \frac{\langle C_{tr} \rangle \tau_1}{[M]_0}}{\langle k_t \rangle \frac{\lambda_0}{k_p [M]_0} + \frac{\langle C_{tr} \rangle \tau_0}{[M]_0}} \frac{\langle C_{tr} \rangle \tau_0}{1 - x} - \frac{\langle C_{tr} \rangle \tau_1}{1 - x} \quad (7)$$

$$\frac{d\tau_2}{dx} = \langle C_{tr} \rangle \tau_0 \frac{1 + 2 \frac{1 - x + \frac{\langle C_{tr} \rangle \tau_1}{[M]_0}}{\langle k_t \rangle \frac{\lambda_0}{k_p [M]_0} + \frac{\langle C_{tr} \rangle \tau_0}{[M]_0}} + \frac{\langle C_{tr} \rangle \tau_2}{[M]_0 (1 - x)}}{\langle k_t \rangle \frac{\lambda_0}{k_p [M]_0} + \frac{\langle C_{tr} \rangle \tau_0}{[M]_0}} - \frac{\langle C_{tr} \rangle \tau_2}{1 - x} \quad (8)$$

For completeness it is mentioned here that the term $\langle k_t \rangle \frac{\lambda_0}{k_p [M]_0}$ in these equations cannot be neglected compared to the term $\langle C_{tr} \rangle \frac{\tau_0}{[M]_0}$. Such simplification, as previously made by Gao and Zhu,⁹ induces only a minor error for the calculation of τ_1 , however, this error is magnified in the determination of τ_2 and thus the dispersity (*cf.* Equation (5)), as deduced from

simulation results in the present work. Moreover, in Equation (7)-(8) in principle also higher order population weighted averages of the RAFT transfer coefficient should be considered as these equations are based on the first and second order moment of the macroradicals (λ_s) and dormant macrospecies (τ_s).^{27,30} However, as will be demonstrated in the current work, this higher order dependency can be ignored.

To correctly account for a possible conversion dependency of $\langle C_{tr} \rangle$ induced by either a different reactivity of R_0X ($C_{tr,0}$) and the macro-RAFT CTA (C_{tr}), an intrinsic chain length dependency of the RAFT transfer coefficients and/or the influence of diffusional limitations on the latter, a *stepwise integration* of Equation (7) and subsequently Equation (8) needs to be performed as a function of x as shown in Figure 4.1. Accordingly, it is imperative that in each monomer conversion integration interval accurate experimental values are available for $\langle k_t \rangle$ and λ_0 , which can be easily accessed via *e.g.* parallel RAFT – chain length dependent – termination (RAFT-CLD-T) measurements, and k_p which is reported in literature for most monomers (*cf.* Figure 4.1). For a step ($x_0 \rightarrow x$), Equation (7) and (8) can be analytically solved *via e.g.* the mathematics software package Maple 18 with initial conditions $\tau_1 = Q_1$ (mol L⁻¹) and $\tau_2 = Q_2$ (mol L⁻¹) at $x = x_0$. A closed expression for τ_1 (Equation (9)) is obtained and an integral expression for τ_2 (Equation (10)):

$$\tau_1(x) = \frac{\langle C_{tr} \rangle [M]_0 \tau_0 (1-x)}{\langle C_{tr} \rangle B - \tau_0 A} + \frac{(1-x)^D (Q_1 + \frac{\langle C_{tr} \rangle [M]_0 \tau_0 (x_0 - 1)}{\langle C_{tr} \rangle B - \tau_0 A})}{(1-x_0)^D} \quad (9)$$

$$\begin{aligned}
\tau_2(x) = (x-1)^D & \left\{ \frac{Q_2}{(x_0-1)^D} + \right. \\
& \int_{x_0}^x \frac{\langle C_{tr} \rangle [M]_0}{\tau_0 (\langle C_{tr} \rangle + A)^2 (A\tau_0 - B\langle C_{tr} \rangle)} [-2(x_0 - \\
& 1)^{-D} \langle C_{tr}^2 \rangle [M]_0 \tau_0 x_0 + 2(x-1)^{-D} \langle C_{tr}^2 \rangle [M]_0 \tau_0 x + \\
& (x-1)^{-D} A^2 \tau_0^2 - (x-1)^{-D} AB \langle C_{tr} \rangle \tau_0 + \\
& 2(x_0-1)^{-D} A \langle C_{tr} \rangle \tau_0 Q_1 + (x-1)^{-D} A \langle C_{tr} \rangle \tau_0^2 - \\
& 2(x-1)^{-D} A [M]_0 \tau_0 x - 2(x_0-1)^{-D} B \langle C_{tr}^2 \rangle Q_1 - \\
& (x-1)^{-D} B \langle C_{tr}^2 \rangle \tau_0 + 2(x-1)^{-D} B \langle C_{tr} \rangle [M]_0 x + \\
& 2(x_0-1)^{-D} \langle C_{tr}^2 \rangle [M]_0 \tau_0 - 2(x-1)^{-D} \langle C_{tr}^2 \rangle [M]_0 \tau_0 + \\
& \left. 2(x-1)^{-D} A [M]_0 \tau_0 - 2(x-1)^{-D} B \langle C_{tr} \rangle [M]_0 \right] dx \Big\} \tag{10}
\end{aligned}$$

in which $A = \frac{\langle k_t \rangle \lambda_0}{k_p \tau_0}$, $B = \frac{\langle k_t \rangle \lambda_0}{k_p} - \tau_0$, and $D = \frac{C_{tr} A}{C_{tr} + A}$. Solving the integral in Equation (10)

yields a complicated but still analytical expression for $\tau_2(x)$ which holds in the considered conversion interval (Equation (11)):

$$\begin{aligned}
\tau_2(x) = & \\
& (1-x)^D(1-x_0)^{-D} \left[Q_2 + \right. \\
& \left. \frac{\langle C_{tr} \rangle [M]_0 (x-x_0) (2A \langle C_{tr} \rangle \tau_0 Q_1 - 2B \langle C_{tr}^2 \rangle Q_1)}{\tau_0 (\langle C_{tr} \rangle + A)^2 (A\tau_0 - B \langle C_{tr} \rangle)} \right] - \\
& \frac{(1-x)^D \langle C_{tr} \rangle [M]_0}{\tau_0 (\langle C_{tr} \rangle + A)^2 (A\tau_0 - B \langle C_{tr} \rangle)} \left\{ -(1-x_0)^{-D+1} \left[(x-x_0) 2 \langle C_{tr}^2 \rangle [M]_0 \tau_0 + \right. \right. \\
& \left. \left. \frac{A^2 \tau_0^2 - AB \langle C_{tr} \rangle \tau_0 + A \langle C_{tr} \rangle \tau_0^2 - B \langle C_{tr}^2 \rangle \tau_0}{-D+1} \right] + \right. \\
& \left. (1-x_0)^{-D+2} \frac{2 \langle C_{tr}^2 \rangle [M]_0 \tau_0 - 2A [M]_0 \tau_0 + 2B \langle C_{tr} \rangle [M]_0}{-D+2} \right\} + \\
& \frac{\langle C_{tr} \rangle [M]_0 (x-1) (A^2 \tau_0^2 - AB \langle C_{tr} \rangle \tau_0 + A \langle C_{tr} \rangle \tau_0^2 - B \langle C_{tr}^2 \rangle \tau_0)}{\tau_0 (\langle C_{tr} \rangle + A)^2 (A\tau_0 - B \langle C_{tr} \rangle) (-D+1)} + \\
& \frac{\langle C_{tr} \rangle [M]_0 (x-1)^2 (2 \langle C_{tr}^2 \rangle [M]_0 \tau_0 - 2A [M]_0 \tau_0 + 2B \langle C_{tr} \rangle [M]_0)}{\tau_0 (\langle C_{tr} \rangle + A)^2 (A\tau_0 - B \langle C_{tr} \rangle) (-D+2)}
\end{aligned} \tag{11}$$

The analytical expression for \mathfrak{D} at each x can be obtained by application of Equation (5), using the expressions for $\tau_1(x)$ and $\tau_2(x)$ in respectively Equation (9) and Equation (11), taking into account that τ_0 is constant. A comparison with the experimental dispersity \mathfrak{D}_{exp} at each monomer conversion x via Equation (6) leads to a non-linear equation in $\langle C_{tr} \rangle(x)$. This equation can be numerically solved for a given monomer conversion interval to directly obtain $\langle C_{tr} \rangle(x)$ from the measured \mathfrak{D}_{exp} provided that accurate (experimental) values for all necessary input quantities (k_p , x_{R_0X} , $\langle k_t \rangle$ and λ_0) are available. In the present work, the standard Newton-Raphson shooting algorithm³¹ is used taking into account an appropriate convergence criterion. Particularly, at full consumption of R_0X , the variation of the polymer dispersity becomes less pronounced and the corresponding non-linear equation in $\langle C_{tr} \rangle(x)$ (Equation (6)) exhibits a very small derivative in the proximity of its root. Hence, scatter in \mathfrak{D}_{exp} or small inaccuracies in the analytical expression for $\mathfrak{D}(x)$ will be magnified into large

deviations for the corresponding $\langle C_{tr} \rangle(x)$ upon solution of Equation (6). This can be identified by the comparison of the solutions via three different convergence criteria:

- *convergence criterion A*, i.e. the one used in the original Newton-Raphson method:

$$\frac{\Delta\langle C_{tr} \rangle(x)}{\langle C_{tr} \rangle(x)} \leq 0.01 \quad (12)$$

- *convergence criterion B*:

$$\frac{\mathfrak{D}(x) - \mathfrak{D}_{exp}}{\mathfrak{D}_{exp}} \leq 0.01 \quad (13)$$

- *convergence criterion C*:

$$\frac{\mathfrak{D}(x) - \mathfrak{D}_{exp}}{\mathfrak{D}_{exp}} \leq 0.05 \quad (14)$$

in which $\Delta\langle C_{tr} \rangle$ is the difference between the $\langle C_{tr} \rangle$ values obtained in two consecutive iteration steps. More details on the solution procedure via the Newton-Raphson method can be found in Appendix F.

Hence, starting at $x_0 = 0$ with $\tau_1(0) = Q_1 = 0 \text{ mol L}^{-1}$ and $\tau_2(0) = Q_2 = 0 \text{ mol L}^{-1}$ eventually $\langle C_{tr} \rangle$ is obtained in the complete monomer conversion range via the stepwise integration procedure shown in Figure 4.1. In each monomer conversion interval, accurate values for \mathfrak{D}_{exp} and additional input values for $\langle k_t \rangle$, k_p , λ_0 and x_{R_0X} need to be available to evaluate τ_1 and τ_2 at the considered monomer conversion x in order to solve Equation (6) for $\langle C_{tr} \rangle(x)$ and to calculate updated values for Q_1 and Q_2 for the consecutive integration interval, using the obtained $\langle C_{tr} \rangle(x)$ value. A proposed experimental protocol complementary to Figure 4.1 can be found in Appendix G. Importantly, if only the determination of the RAFT transfer reactivity of the RAFT CTA ($C_{tr,0}$) is aimed at, in principle, the developed method allows to

determine $C_{tr,0}$ via one single experimental data point at very low monomer conversion, on the condition that dedicated analysis is performed, as explained also in Appendix G.

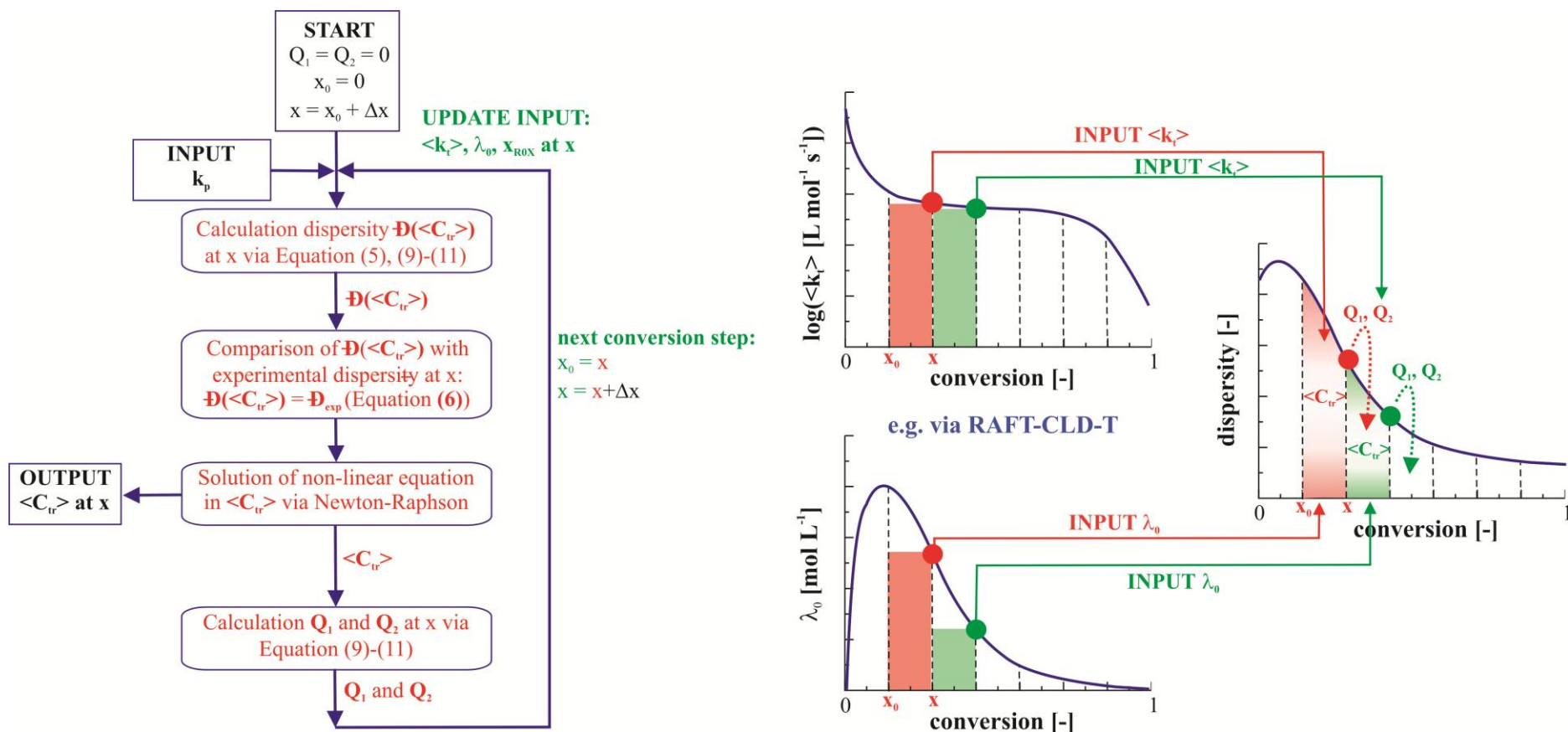


Figure 4.1: Summary of the methodology developed in the present work to determine $\langle C_{tr} \rangle$ as function of conversion via a flow chart, including input parameters (left figure) and schematic representation of the stepwise integration procedure (right figure). In red and green two consecutive integration intervals for the conversion are indicated. Q_1 and Q_2 calculated at the conversion separating both intervals are used as initial conditions in the next integration interval (Equation (9)-(11)).

4.3 Results and discussion

In what follows, proof of concept is provided for the developed method in the present work to determine both $C_{tr,0}$ and C_{tr} by the simulation of perfect experiments covering a wide range of theoretical transfer reactivities. In particular, the inherent ability of the method to assess for the first time a possible chain length dependency of the RAFT transfer reactivity, due to intrinsic chain length effects and/or the influence of diffusional limitations, is also evaluated *in silico*. Unless stated otherwise the simulated perfect experiments are based on data for every 1% of monomer conversion. Finally, the developed method is applied to experimental RAFT polymerization data at 353 K for MMA with CPDB as RAFT CTA and AIBN as conventional radical initiator reported by Derboven *et al.*²⁸

4.3.1 Proof of concept by the simulation of perfect experiments

To demonstrate the reliability of the developed method, it is applied to four different test cases with increasing variation in the kinetic parameters for RAFT exchange and selecting MMA as monomer. In particular, in the final case the RAFT transfer coefficients are theoretically assumed to vary with conversion due to a strong intrinsic/apparent chain length dependency. It should be reminded that the outcome of the method is an average RAFT transfer coefficient $\langle C_{tr} \rangle$ (Equation (5)), which is at the start of the RAFT polymerization almost exclusively governed by the RAFT exchange reactivity with R_0X ($C_{tr,0}$) while at full conversion of the latter the transfer reactivity of macroradicals with macro-RAFT CTA (C_{tr}) dominates. Perfect experiments are simulated via the procedure elaborated in Chapter 3 and the corresponding conditions are summarized in Table 4.2. The values of the RAFT transfer coefficients in Table 4.2 used for the *in silico* evaluation are based on literature values for different R_0X /MMA combinations.^{5,10,12,13,23,32}

Table 4.2: Conditions of the performed *in silico* experiments. Different targeted chain lengths (TCLs) and values for the implemented value for $C_{tr,0}$ ($C_{tr,0,IN}$), $C_{-tr,0}$ ($C_{-tr,0,IN}$) and C_{tr} ($C_{tr,IN}$) (theoretical RAFT CTAs) are covered. Case 1: entry 1; Case 2: entry 2-6; Case 3: entry 7-8. $[M]_0 = 9 \text{ mol L}^{-1}$; $[I_2]_0 = 9 \cdot 10^{-3} \text{ mol L}^{-1}$; $[R_0X]_0$ for TCL 100, 200, 300 and 500: respectively 0.09, 0.045, 0.03 and 0.018 mol L^{-1} .

	entry	TCL	$C_{tr,0,IN}$ [-]	$C_{-tr,0,IN}$ [-]	$C_{tr,IN}$ [-]
case 1	1	100	15.0	15.0	15.0
	2	100	15.0	15.0	30.0
	3	200	15.0	15.0	30.0
case 2	4	300	15.0	15.0	30.0
	5	100	1.0	1.0	10.0
	6	100	20.0	20.0	120.0
case 3	7	100	15.0	150.0	30.0
	8	500	15.0	150.0	30.0
case 4	9	100	120 ^a	120 ^a	120 ^a
	10	100	20	20	120 ^a

^achain length and conversion dependency for RAFT exchange using parameters composite k_r -model for MMA³³

Test case 1: $C_{tr,0,IN} = C_{-tr,0,IN} = C_{tr,IN}$

First, the simplified situation of an equal transfer reactivity for all species involved in the RAFT exchange reactions is considered ($C_{tr,0,IN} = C_{-tr,0,IN} = C_{tr,IN}$; case 1). For a TCL of 100 and $C_{tr,0,IN} = C_{-tr,0,IN} = C_{tr,IN} = 15$ (entry 1 in Table 4.2), in Figure 4.2a the obtained $\langle C_{tr} \rangle$ as function of the monomer conversion x are shown using the original Newton-Raphson method (full blue line, *convergence criterion A*) and the modified ones based on a convergence

criterion for the difference between the analytical and experimental dispersity instead of for $\langle C_{tr} \rangle$ (dashed green line, *convergence criterion B*, 1% deviation; dotted red line, *convergence criterion C*, 5% deviation). Initially, the implemented value of 15, which is marked by a black circle on the $\langle C_{tr} \rangle$ axis is perfectly predicted by the solution via *convergence criterion A* (full blue line), whereas at higher monomer conversion a slight overestimation results due to an enhanced effect of inaccuracies of the analytical expression for $\mathcal{D}(x)$ (Equation (5)), as highlighted previously (*cf.* also Appendix F).

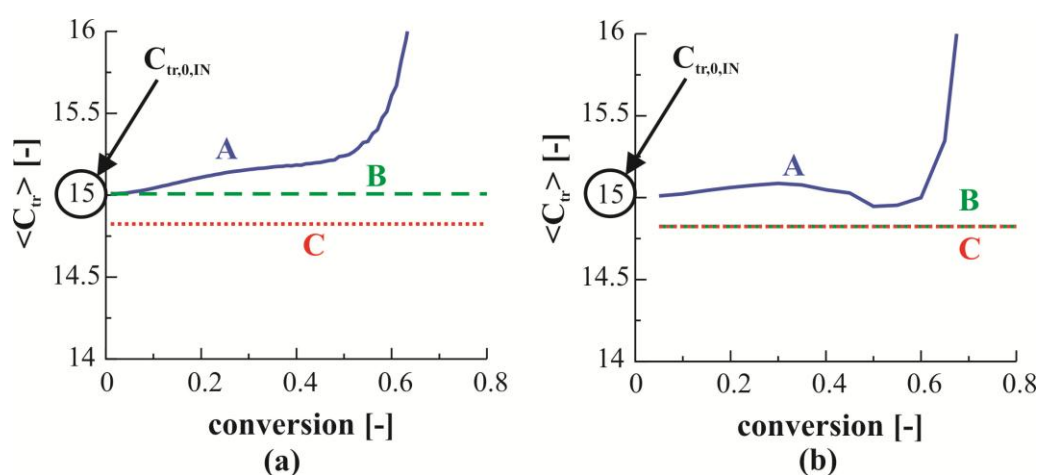


Figure 4.2: $\langle C_{tr} \rangle$ as function of the monomer conversion obtained by solution of Equation (5)-(6) using the original Newton-Raphson convergence criterion (full blue line, convergence criterion A, Equation (12)) and the additional modified convergence criterion B (dashed green line, 1% deviation, Equation (13)) and C (dotted red line, 5% deviation, Equation (14)) which are only used for sensitivity purpose, for TCL 100; $C_{tr,0} = C_{-tr,0} = C_{tr} = 15 = C_{tr,0,IN}$ (black circle) (a) Data points every 1% monomer conversion. (b) Data points every 5% monomer conversion; conditions: entry 1 in Table 4.2; other kinetic parameters from Chapter 3.

This is confirmed by the solutions with *convergence criterion B* and *C*, as shown by respectively the dashed green line and the dotted red line in Figure 4.2a. Based on the modified convergence criteria *B* and *C*, the inherent slight deviation for solution *A* can be compensated for and less than 1.5% deviation is obtained from the implemented value of $\langle C_{tr} \rangle$ ($C_{tr,0} = C_{-tr,0} = C_{tr} = 15 = C_{tr,0,IN}$; black circle in Figure 4.2) over the complete x region. Similarly, the consideration of 5 times less data points (every 5% conversion instead of every 1% conversion), which is more likely for a realistic experimental situation in which size

exclusion chromatography (SEC) measurements are involved, also leads to only very small deviations for $\langle C_{tr} \rangle$ from the implemented value, as shown in Figure 4.2b for *convergence criterion A* (full blue line) and the corresponding modified *convergence criterion B* and *C* (dashed green line and dotted red line coincide).

In Figure 4.3 it is shown that the corresponding polymer dispersity profile calculated by the analytical expression for $\mathcal{D}(x)$ in Equation (5) using the $\langle C_{tr} \rangle$ values from *convergence criterion A* in Figure 4.2a (full blue line; Equation (12)), coincides with the simulated dispersity of the dormant polymer chains (dashed orange line coinciding with full blue line), and at low monomer conversion x also with the total polymer dispersity (dotted black line). A slight mismatch between the latter and the dispersity of the dormant chains is although obtained at high x . However, this is covered by the use of *convergence criterion B* and *C* to determine $\langle C_{tr} \rangle$, demonstrating the robustness of the developed method, which is particularly relevant for its application to experimental data as it is always the total polymer dispersity that will be measured. It should be stressed that the precision of polymer dispersity measurements via SEC is significantly lower than the one for concentration measurements via ^1H – nuclear magnetic resonance (NMR) or Fourier transform infrared (FTIR) spectroscopy, on which the method of Moad and coworkers is based to determine $C_{tr,0}$ (*cf.* Chapter 3). A scatter in the experimental polymer dispersity data of 20% is to be expected, while only 5% for the concentration measurements. This could significantly affect the reliability of the $\langle C_{tr} \rangle$ data obtained via the proposed method, which can be verified by the additional consideration of the *convergence criterion B* and *C*, unveiling the sensitivity of $\langle C_{tr} \rangle$ for small variations in \mathcal{D}_{exp} .

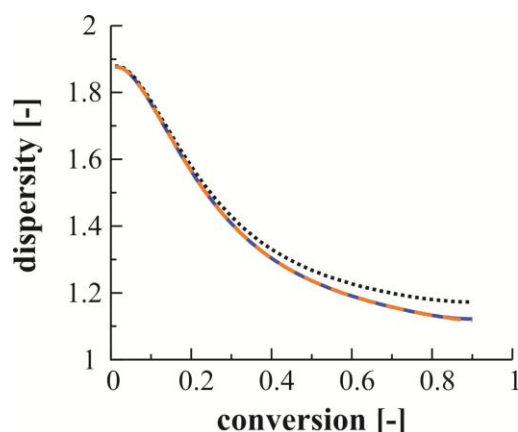


Figure 4.3: Comparison between the dispersity profile calculated by the analytical expression for $\mathfrak{D}(x)$ in Equation (5) using the $\langle C_{tr} \rangle$ values from convergence criterion A (full blue line, Equation (12)), the simulated total polymer dispersity (dotted black line) and the simulated dispersity of the dormant chains (dashed orange line coinciding with full blue line) as a function of (monomer) conversion for TCL 100 (\mathfrak{D}_{exp} in Equation (6)); $C_{tr,0} = C_{-tr,0} = C_{tr} = 15$; conditions: entry 1 in Table 4.2; other kinetic parameters from Chapter 3.

Test case 2: $C_{tr,0,IN} = C_{-tr,0,IN} < C_{tr,IN}$

For the second test case, the transfer reactivity of the macroradicals with the macro-RAFT CTA (C_{tr}) is assumed higher than the RAFT exchange reactivities with R_0X ($C_{tr,0}$ and $C_{-tr,0}$), which are still assumed to be equal (entry 2-6 in Table 4.2; case 2). At first, a variation of the TCL is considered between 100 and 300 for $C_{tr,0,IN} = C_{-tr,0,IN} = 15$ and $C_{tr,IN} = 30$, as shown in Figure 4.4a-c (entry 2-4 in Table 4.2). It is clear that for all TCLs the calculated $\langle C_{tr} \rangle$ values via *convergence criterion A* (full blue line) accurately represent the initial transfer reactivity with R_0X at the start of the polymerization ($C_{tr,0,IN} = 15$; black circle in Figure 4.4a-c). Moreover, the exchange reactivity of macroradicals with macro-RAFT CTA ($C_{tr,IN} = 30$; black square in Figure 4.4a-c) is also obtained at full R_0X conversion, which is indicated by the vertical grey line (black cross for point on full blue line). Respective deviations of $\langle C_{tr} \rangle$ from $C_{tr,0,IN}$ and $C_{tr,IN}$ are less than 1 and 4%.

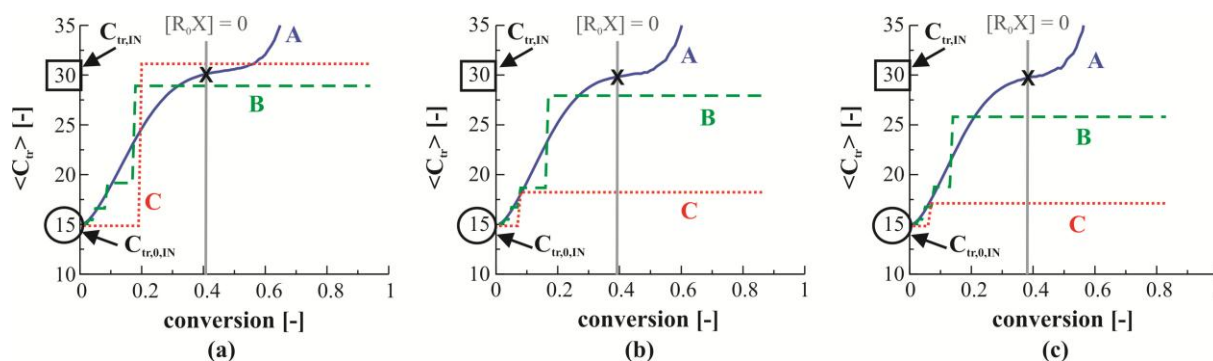


Figure 4.4: $\langle C_{tr} \rangle$ as function of the monomer conversion obtained by solution of Equation (5)-(6) using the original Newton-Raphson convergence criterion (full blue line, convergence criterion A, Equation (12)) and the additional modified convergence criterion B (dashed green line, 1% deviation, Equation (13)) and C (dotted red line, 5% deviation, Equation (14)) which are only used for sensitivity purpose, for (a) TCL 100; entry 2 in Table 4.2 (b) TCL 200; entry 3 in Table 4.2 and (c) TCL 300; entry 4 in Table 4.2. $C_{tr,0} = C_{-tr,0} = 15 = C_{tr,0,IN}$ (black circle), $C_{tr} = 30 = C_{tr,IN}$ (black square). Vertical grey line indicates full conversion of R_0X , black cross is intersection point with full blue line. Simulated data points every 1% monomer conversion. Other kinetic parameters from Chapter 3.

However, the additional solutions for $\langle C_{tr} \rangle$ based on convergence criterion B (dashed green line, Equation (13)) and C (dotted red line, Equation (14)) only yield accurate values for $C_{tr,0}$, indicative of a lower reliability of the values for $\langle C_{tr} \rangle$ obtained at higher x (full blue line) upon an actual experimental application. The closer the three solutions approach each other, the more reliable the obtained $\langle C_{tr} \rangle$ values are, as a small variation of the polymer dispersity will only induce a small corresponding variation in $\langle C_{tr} \rangle$ and, hence, the influence of e.g. model inaccuracies or experimental scatter will be limited. This is clearly the case at low x (Figure 4.4a-c; $x < 0.2$), which was also highlighted by Gao and Zhu⁹ who found that the influence of the transfer reactivity on the polymer dispersity is the largest at low monomer conversions.

A similar conclusion can be drawn from a variation of the RAFT transfer reactivities with still the constraint $C_{tr,0,IN} = C_{-tr,0,IN}$ (case 2) as shown in Figure 4.5a-b (entry 5-6 in Table 4.2). Again, $C_{tr,0}$ is accurately determined at the start of the RAFT polymerization with less than 2% deviation between $C_{tr,0,IN}$ and the calculated $\langle C_{tr} \rangle$ (black circle for value of $C_{tr,0,IN}$, Figure 4.5a-b), whereas the value of C_{tr} (black square for value of $C_{tr,IN}$, Figure 4.5a) is only obtained

via the application of *convergence criterion A* (full blue line) at full conversion of R_0X (Figure 4.5a; black cross is intersection point). The strong discrepancy between the full blue line (*convergence criterion A*) and the dashed green (*convergence criterion B*) and dotted red line (*convergence criterion C*) at the latter conversion point demonstrates that the obtained value for C_{tr} is highly sensitive to fluctuations in the experimentally observed polymer dispersity profile. Moreover, for very low values of $C_{tr,0}$ (Figure 4.5b; $C_{tr,0,IN} = 1$), full R_0X conversion is not reached and, hence, C_{tr} cannot be determined by the proposed method.

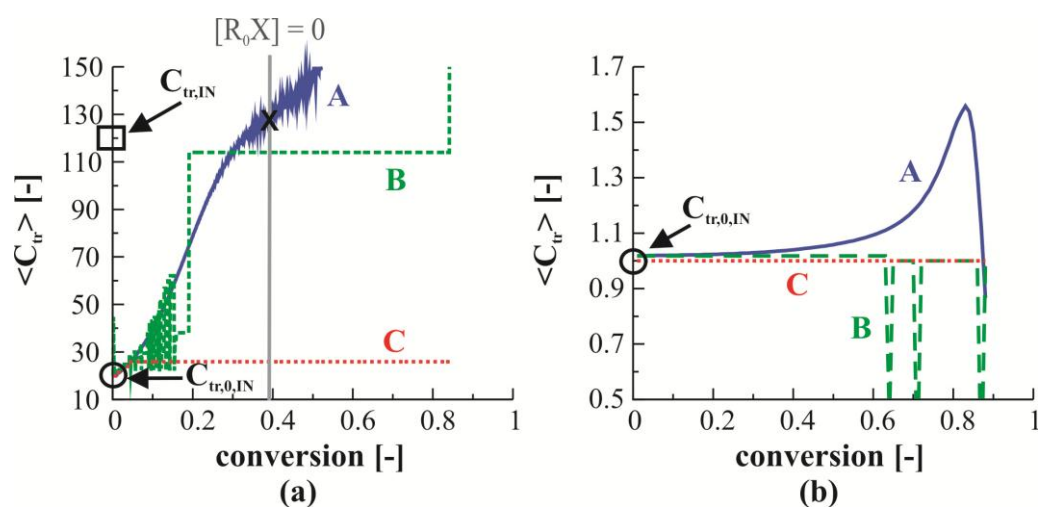


Figure 4.5: $\langle C_{tr} \rangle$ as function of the monomer conversion obtained by solution of Equation (5)-(6) using the original Newton-Raphson convergence criterion (full blue line, convergence criterion A, Equation (12)) and the additional modified convergence criterion B (dashed green line, 1% deviation, Equation (13)) and C (dotted red line, 5% deviation, Equation (14)) which are only used for sensitivity purpose, for TCL 100. (a) $C_{tr,0} = C_{tr,0} = 20 = C_{tr,0,IN}$ (black circle), $C_{tr} = 120$ (black square); entry 6 in Table 4.2. (b) $C_{tr,0} = C_{tr,0} = 1 = C_{tr,0,IN}$ (black circle), $C_{tr} = 10 = C_{tr,IN}$; entry 5 in Table 4.2. Vertical grey line indicates full conversion of R_0X (only in a). Other kinetic parameters from Chapter 3.

Test case 3: $C_{tr,0,IN} > C_{tr,0,IN}$

Importantly, for a high transfer reactivity of the R_0 species with the macro-RAFT CTA ($C_{tr,0}$), which is the third considered test case (entry 7-8 in Table 4.2; case 3), only high TCLs lead to a reliable determination of $C_{tr,0}$, as shown in Figure 4.6a-b for $C_{tr,IN} = 30$, $C_{tr,0,IN} = 15$ and $C_{tr,0,IN} = 150$. For a TCL of 100 (entry 7 in Table 4.2), initially a deviation of 7% from $C_{tr,0}$ ($C_{tr,0,IN} = 15$; black circle in Figure 4.6a) is obtained for $\langle C_{tr} \rangle$, which is reduced to less than

3% for TCL 500 ($C_{tr,0,IN}$; black circle in Figure 4.6b; entry 8 in Table 4.2). Furthermore, from the $\langle C_{tr} \rangle$ data obtained by application of *convergence criterion A*, i.e. the original Newton-Raphson numeric solution of Equation (5)-(6), for a TCL of 500 (full blue line in Figure 4.6b), C_{tr} is determined at full R_0X conversion with deviations of less than 11% ($C_{tr,IN}$; black square in Figure 4.6b; black cross is intersection point). However, the high sensitivity of $\langle C_{tr} \rangle$ to small variations in the observed polymer dispersity should be highlighted as indicated by the mismatch between the dashed green line and red dotted line in Figure 4.6b.

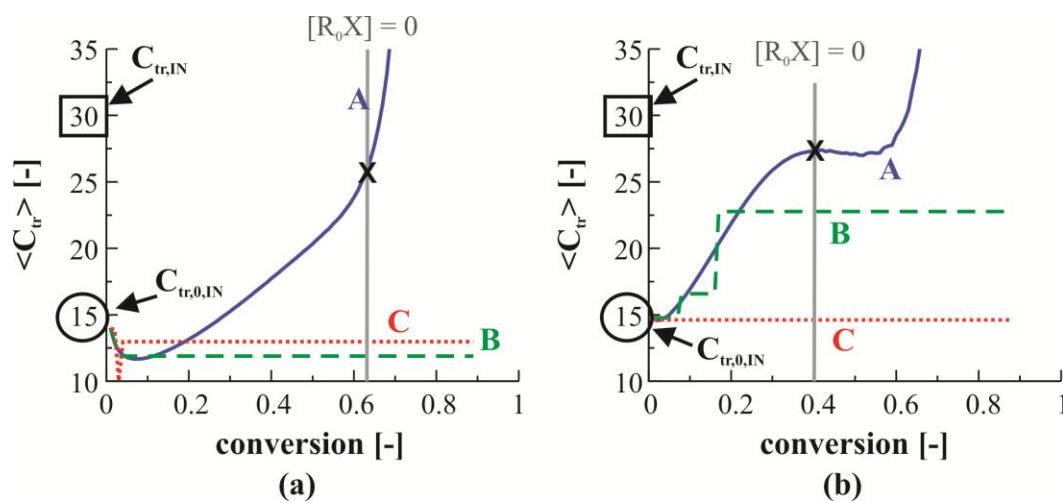


Figure 4.6: $\langle C_{tr} \rangle$ as function of the monomer conversion obtained by solution of Equation (5)-(6) using the original Newton-Raphson convergence criterion (full blue line, convergence criterion A, Equation (12)) and the additional modified convergence criterion B (dashed green line, 1% deviation, Equation (13)) and C (dotted red line, 5% deviation, Equation (14)) which are only used for sensitivity purpose, for (a) TCL 100; entry 7 in Table 4.2 and (b) TCL 500; entry 8 in Table 4.2. $C_{tr,0} = 15 = C_{tr,0,IN}$ (black circle), $C_{tr,0} = 150$, $C_{tr} = 30 = C_{tr,IN}$ (black square). Vertical grey line indicates full conversion of R_0X (black cross is intersection point with full blue line). Other kinetic parameters from Chapter 3.

In general, from the discussed test cases 1-3 it can be concluded that the method developed in the present work is an accurate way to determine $C_{tr,0}$ by means of polymer dispersity data at the start of the polymerization. Importantly, only a single reliable measurement of the polymer dispersity at low monomer conversion is needed for an accurate determination of $C_{tr,0}$, even for high values of $C_{tr,0}$ provided that a sufficiently high TCL is considered (case 3) and values for the other input quantities are available, as explained in Appendix F. As is clear from Table 4.3, the proposed method exhibits an increased accuracy for $C_{tr,0}$ determination

compared to the other literature techniques by Moad and coworkers^{12,13} and Theis *et al.*¹⁶ which were extensively discussed in Chapter 3. In particular, using the developed method, the deviations of the calculated $\langle C_{tr} \rangle$ from the implemented $C_{tr,0,IN}$ (deviation 3) are significantly lower than those for the corresponding methods of Moad and coworkers^{12,13} (deviation 1) and Theis *et al.*¹⁶ (deviation 2) for all considered conditions in test cases 1 and 2. For a strong influence of $C_{-tr,0}$, *i.e.* test case 3, a high TCL should be considered in order to obtain accurate values for $C_{tr,0}$ ($< 3\%$ deviation from $C_{tr,0,IN}$) via the method developed in this work, which is also a prerequisite for the application of the method of Moad and coworkers^{12,13} for these conditions exhibiting however much higher deviations (20%; *cf.* Chapter 3). Importantly, the lower precision of the SEC measurements to determine the polymer dispersity for application of the proposed method compared to the concentration measurements in the method of Moad and coworkers,^{12,13} does not affect the accuracy of the obtained $C_{tr,0}$ data to a significant extent indicated by the coinciding of the solutions using the different *convergence criteria A-C*.

Table 4.3: *In silico* comparison of the accuracy of the different literature methods to determine $C_{tr,0}$ with the corresponding accuracy of the developed method in the present work. % deviation of the resulting value for $C_{tr,0}$ from the implemented value $C_{tr,0,IN}$ for the method of Moad^{12,13} (% deviation 1), the method of Theis *et al.*¹⁶ (% deviation 2) and the method presented in the current work (% deviation 3). Different targeted chain lengths (TCLs) and values for $C_{tr,0,IN}$ are covered. $[M]_0 = 9 \text{ mol L}^{-1}$; $[I_2]_0 = 9 \cdot 10^{-3} \text{ mol L}^{-1}$. $[R_0X]_0$ for TCL 100, 200 and 300: respectively 0.09, 0.045 and 0.03 mol L^{-1} . Other kinetic parameters from Chapter 3.

entry	TCL	$C_{tr,0,IN}$ [-]	% deviation 1	% deviation 2	% deviation 3 (this work)
1	100	1.0	3.0	14.0	< 2
2	100	15.0	16.1	5.2	< 2
3	100	20.0	21.0	7.4	< 1
4	200	15.0	8.5	6.6	< 1
5	300	15.0	5.4	7.8	< 1

Test case 4: chain length dependent RAFT transfer reactivity

Since the possibility of an intrinsic/apparent chain length dependency of k_{add} can currently not be discarded as highlighted above, the sensitivity of the proposed method for chain length dependent RAFT exchange kinetics is assessed *in silico*. Two different hypothetical examples are considered with, for illustration purposes, only a strong theoretical chain length dependency. In the first example, it is assumed that *all* transfer reactivities ($C_{tr,0}$, $C_{-tr,0}$ and C_{tr}) are equal and chain length dependent, which implies the impact of chain length dependencies from the start of the RAFT polymerization. Such strong impact is in practice very unlikely but a good testing case for a theoretical evaluation of the proposed method. In the second example, the RAFT exchange reactions with R_0X are assumed to be characterized by chain length independent kinetics ($C_{tr,0}$ and $C_{-tr,0}$ are constant) while C_{tr} is still chain length

dependent, which is a more realistic situation in case chain length dependency would be an issue.

For both examples, an arbitrary variation of the relevant transfer reactivities with conversion and chain length is assumed based on the composite k_t model determined by Johnston-Hall *et al.* for MMA.^{23,33} This dependency is implemented explicitly (*i.e.* for each $k_{tr}^{n,m}(x)$ individually) with an initial theoretical value for C_{tr} of 120 at $x = 0$ and $x_n = 1$. For simplicity, a geometric mean model has been assumed to determine $k_{tr}^{n,m}(x)$ for $n \neq m$. In the second example the transfer reactivities for the RAFT reactions with R_0X are however assumed to be chain length independent, as explained above, and also lower than the initial C_{tr} : $C_{tr,0,IN} = C_{tr,0,IN} = 20$, so that their influence on the calculated $\langle C_{tr} \rangle$ can also be properly assessed *in silico*. In Figure 4.7, the *in silico* procedure that has been applied to evaluate the sensitivity of the proposed method to detect chain length dependent RAFT exchange kinetics is summarized.

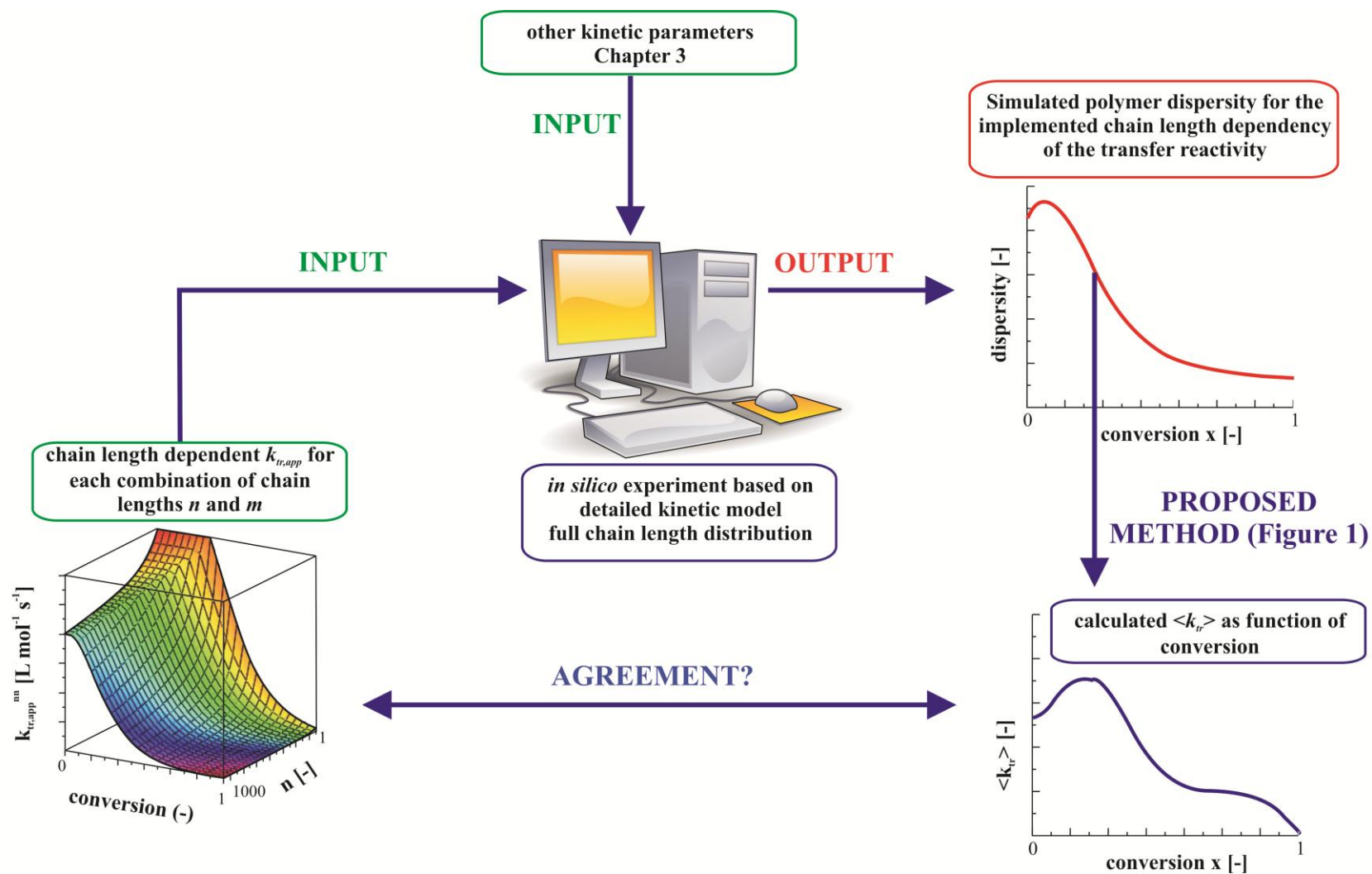


Figure 4.7: *In silico* procedure applied to assess the sensitivity of the developed methodology (Figure 4.1) for possible chain length dependent RAFT transfer kinetics.

In Figure 4.8a-b, the calculated $\langle C_{tr} \rangle$ profile from solution of Equation (6) using the original Newton-Raphson convergence criterion (*convergence criterion A*, full blue line) is shown together with the additional solutions for $\langle C_{tr} \rangle$ obtained by using the modified *convergence criterion B* (dashed green line) and *C* (dotted red line) for example 1 (Figure 4.8a) and 2 (Figure 4.8b). Also, the implemented theoretical variation of the transfer reactivity of the macrospecies based on the number average chain length x_n is shown for each monomer conversion x by the dashed-dotted black line. Importantly, for both examples the theoretical chain length dependency of the RAFT transfer reactivity is well captured by the calculated $\langle C_{tr} \rangle$ based on *convergence criterion A* (full blue line vs. dashed-dotted black line), albeit after a certain delay for example 2 (Figure 4.8b). This delay can be attributed to the dominance of the RAFT transfer reactions with R_0X with a constant reactivity (full R_0X conversion indicated by the vertical grey line) at the lower x . Moreover, for this example in which the RAFT reactions with R_0X are characterized by a different transfer reactivity ($C_{tr,0,IN} = C_{-tr,0,IN} = 20$), the chain length dependency of the RAFT exchange reactivity C_{tr} does not interfere with the accurate determination of $C_{tr,0}$ via the method developed in the present work (black circle in Figure 4.8b; $C_{tr,0,IN} = 20$). In contrast, for the first theoretical example, in which also deliberately RAFT transfer reactions involving R_0X are assumed chain length dependent, the implemented theoretical value for the transfer coefficient of 120 at $x = 0$ and $x_n = 1$ can only be obtained after extrapolation, similar to *e.g.* RAFT-CLD-T experiments.^{33,34}

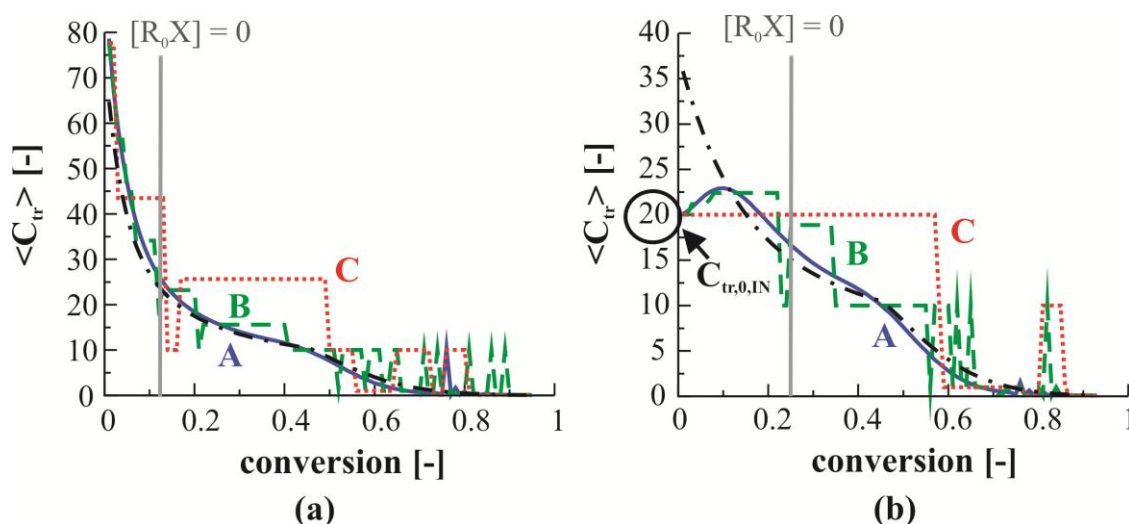


Figure 4.8: $\langle C_{tr} \rangle$ as function of the monomer conversion obtained by solution of Equation (5)-(6) using the original Newton-Raphson convergence criterion (full blue line, convergence criterion A, Equation (12)) and the additional modified convergence criterion B (dashed green line, 1% deviation, Equation (13)) and C (dotted red line, 5% deviation, Equation (14)) which are only used for sensitivity purpose, for TCL 100 and a chain length dependent RAFT transfer reactivity in case (a) all transfer coefficients are equal and chain length dependent (example 1), (b) $C_{tr,0} = C_{-tr,0} = 20 = C_{tr,0,IN}$ (black circle) are chain length independent, only chain length dependent C_{tr} (example 2). Chain length dependency of k_{tr} based on the composite k_t model determined by Johnston-Hall et al. for MMA^{23,33} and implemented explicitly with initial value of $C_{tr} = 120$ at $x = 0$ and chain length 1. Dashed-dotted black line is theoretical ‘observed’ variation of the RAFT transfer reactivity based on the number average chain length x_n . $[M]_0 = 9 \text{ mol L}^{-1}$; $[R_0X]_0 = 9 \cdot 10^{-2} \text{ mol L}^{-1}$; $[I_2]_0 = 9 \cdot 10^{-3} \text{ mol L}^{-1}$. Other kinetic parameters from Chapter 3.

In general, care should be taken about the reliability of the obtained results, as indicated by the discrepancy between the solutions based on the different convergence criteria A-C (Equation (12)-(14)) after full R_0X conversion (full blue line vs. dashed green and dotted red line in Figure 4.8a-b), however, the same trend is still observed. Hence, for a strong chain length dependency of the transfer reactivity, as implemented for the simulation of the perfect experiments in Figure 4.8a-b, for the first time, the method developed in the present work allows a quantification of the corresponding intrinsic/apparent transfer reactivity in case accurate experimental data would be available for the complete RAFT polymerization reaction. In Figure 4.9a-b, the corresponding polymer dispersity profiles are shown for both example cases (full blue line) together with the dispersity obtained assuming chain length independent RAFT transfer kinetics (dashed green line). Higher dispersities are obtained for

the complete conversion range in case of a chain length dependent RAFT transfer reactivity. Moreover, from the start of the polymerization onwards, higher dispersities are also obtained for example 2 (Figure 4.9b) even though it is characterized by a chain length independent $C_{tr,0}$ and $C_{-tr,0}$, indicating that C_{tr} already significantly interferes with the period before full R_0X conversion. Furthermore, when the transfer reactivity approaches zero at higher x , an additional increase of the dispersity results, which is intuitively clear as it implies more FRP character.

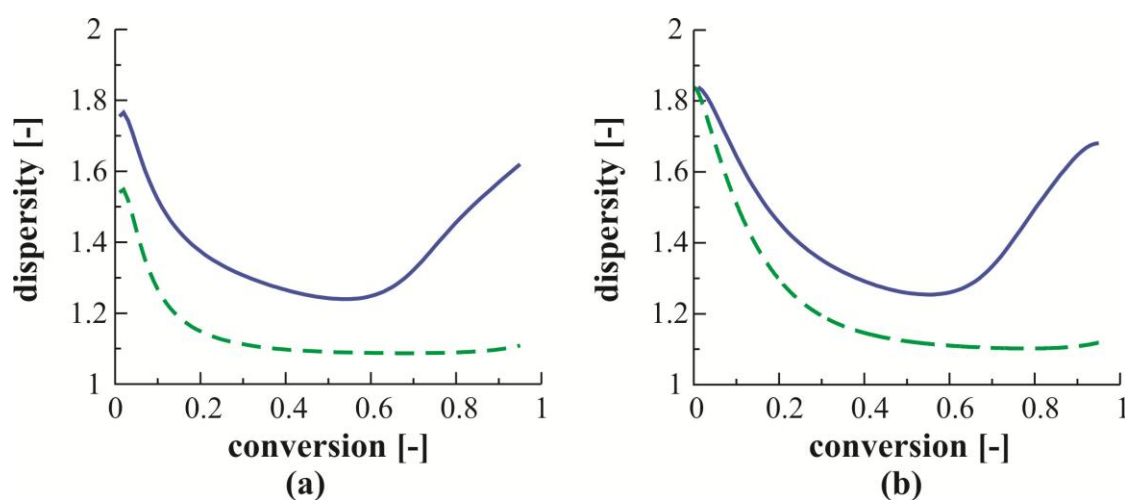


Figure 4.9: Comparison between the simulated polymer dispersity profile for the case of chain length dependent (full blue line) and chain length independent (dashed green line) RAFT transfer kinetics for TCL 100 (a) all transfer coefficients are equal and chain length dependent (example 1), (b) $C_{tr,0} = C_{-tr,0} = 20 = C_{tr,0,IN}$ (black circle) are chain length independent, only chain length dependent C_{tr} (example 2). Chain length dependency of k_{tr} based on the composite k_t model determined by Johnston-Hall et al. for MMA^{23,33} and implemented explicitly with initial value of $C_{tr} = 120$ at $x = 0$ and chain length 1. $[M]_0 = 9 \text{ mol L}^{-1}$; $[R_0X]_0 = 9 \cdot 10^{-2} \text{ mol L}^{-1}$; $[I_2]_0 = 9 \cdot 10^{-3} \text{ mol L}^{-1}$. Other kinetic parameters from Chapter 3.

From the test cases 2-4 in this proof of concept study it can thus be concluded that, besides the accurate determination of $C_{tr,0}$, the methodology developed in the present work allows also to access an approximate value for C_{tr} at complete depletion of R_0X – even for relatively high $C_{-tr,0}$ – of which the reliability is indicated by the solutions for $\langle C_{tr} \rangle$ based on three different convergence criteria A-C (Equation (12)-(14)). Moreover, if the RAFT transfer coefficient varies throughout the polymerization reaction due to a strong intrinsic/apparent

chain length dependency, the developed method allows to accurately quantify the corresponding transfer coefficient at each instant during the RAFT polymerization.

4.3.2 RAFT polymerization of MMA with CPDB as RAFT CTA at 353 K

As stated previously, for an actual application of the developed method, next to the experimental polymer dispersity, additional accurate input values for $\langle k_t \rangle$, k_p , λ_0 and x_{R_0X} need to be available for a reliable determination of $\langle C_{tr} \rangle$, making it an ideal complement to for instance RAFT-CLD-T experiments in which $\langle k_t \rangle$, λ_0 are directly accessed via differential scanning calorimetric measurements.^{33,34} A suggested experimental protocol can be found in Appendix G in which all input parameters are discussed separately. Furthermore, in this appendix, a procedure is given to determine $C_{tr,0}$ via one single experimental data point in which λ_0 is determined from the initial slope of the monomer conversion profile. The results of the application of such protocol are also included in this section. For the experimental validation of the developed method, the RAFT-CLD-T data at 353 K for MMA with CPDB as RAFT CTA and AIBN as conventional radical initiator reported by Derboven *et al.*²⁸ are used. Since no conversions of R_0X (CPDB) were however determined experimentally in that study, x_{R_0X} is calculated from x_n data and the known concentrations of monomer and conventional radical initiator.

Rearrangement of the expression for x_n proposed by Moad and coworkers, if termination exclusively occurs by disproportionation (Equation (15)), leads to x_{R_0X} :^{12,13}

$$x_n = \frac{[M]_0 - [M]}{([R_0X]_0 - [R_0X]) + 2f([I_2]_0 - [I_2])} \quad (15)$$

$$\frac{[R_0X]_0 - [R_0X]}{[R_0X]_0} = x_{R_0X} = \frac{[M]_0 - [M]}{x_n [R_0X]_0} - \frac{2f([I_2]_0 - [I_2])}{[R_0X]_0} \quad (16)$$

Importantly, the validity of Equation (16) has been confirmed by simulations. For example, as shown in Figure 4.10 (entry 1 in Table 4.8), no discrepancy is observed between the simulated conversion of R_0X (full blue line) and the one calculated via Equation (16) (dashed red line).

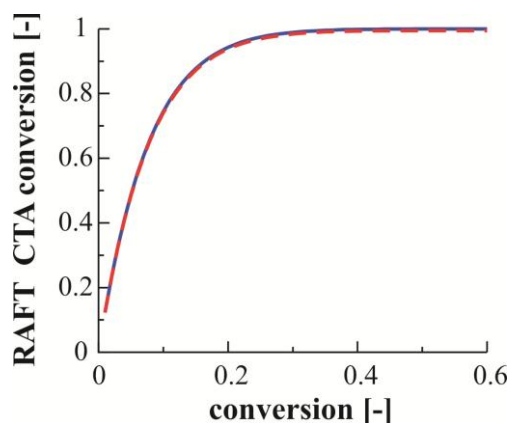


Figure 4.10: Comparison between the simulated RAFT CTA conversion (full blue line; full kinetic model) and the one calculated via Equation (16) (dashed red line) as a function of (monomer) conversion for TCL 100; $C_{tr} = C_{tr,0} = C_{-tr,0} = 15$; Entry 1 in Table 4.2; other kinetic parameters from Chapter 3.

As highlighted in the previous section, the choice of the TCL to determine reliable values for $\langle C_{tr} \rangle$ depends on the importance of the RAFT exchange reactions of R_0 species with macro-RAFT CTA ($C_{-tr,0}$). Therefore the effect of the TCL is first studied. For a low TCL of 60, a plot of $\ln([R_0X]/[R_0X]_0)$ versus $\ln([M]/[M]_0)$ shows a non-linear behavior (Figure 4.11; dashed black line is added to guide the eye), indicative of a high $C_{-tr,0}$ value, as discussed in Chapter 3. Indeed, in agreement with the previous results by the simulation of perfect experiments (Figure 4.6a), application of the proposed method to the experimental dispersity profile in Figure 4.12a (TCL = 60) yields an initial decrease of $\langle C_{tr} \rangle$ followed by a steep increase for the solution based on the original Newton-Raphson *convergence criterion A* (blue squares), diverging significantly from the solutions for $\langle C_{tr} \rangle$ using *convergence criterion B* (green triangles; based on 1% deviation) and *C* (red circles; based on 5% deviation) as shown in Figure 4.12b. Note that the measured dispersity profile is corresponding to a controlled RAFT polymerization and, hence, a strong chain length dependency for the RAFT exchange is very unlikely (*cf.* Figure 4.9).

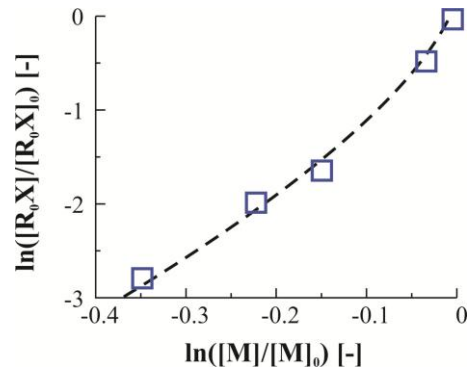


Figure 4.11: $\ln([M]/[M]_0)$ vs. $\ln([R_0X]/[R_0X]_0)$ based on experimental data for the RAFT polymerization of MMA with CPDB as RAFT CTA and AIBN as conventional radical initiator (dashed black line is a trend-line for eye-guidance only). $[R_0X]/[R_0X]_0$ calculated via Equation (16). 353 K; $[MMA]_0:[CPDB]_0:[AIBN]_0 = 60:1:0.033$.

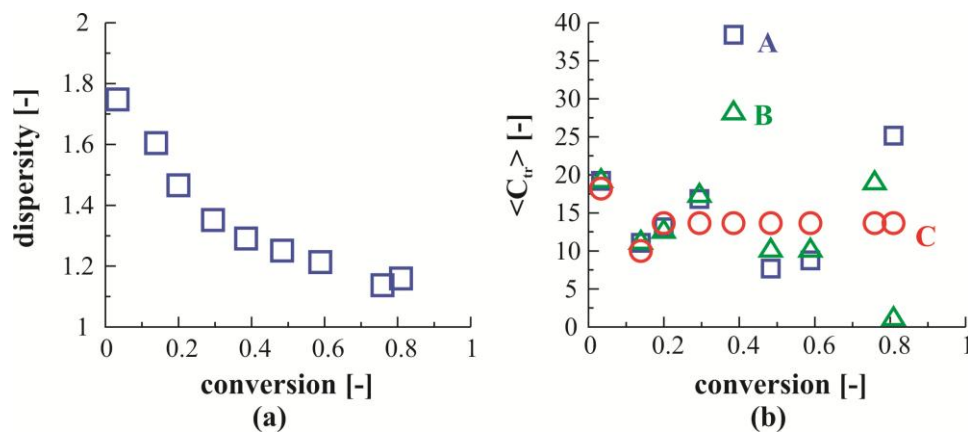


Figure 4.12: Experimental polymer dispersity as a function of (monomer) conversion (a) and corresponding $\langle C_{tr} \rangle$ as function of the monomer conversion obtained by solution of Equation (5)-(6) using the original Newton-Raphson convergence criterion (blue squares, convergence criterion A, Equation (12)) and the additional modified convergence criterion B (green triangles, 1% deviation, Equation (13)) and C (red circles, 5% deviation, Equation (14)) which are only used for sensitivity purpose, (b) for the RAFT polymerization of MMA with CPDB as RAFT CTA and AIBN as conventional radical initiator. 353 K; $[MMA]_0:[CPDB]_0:[AIBN]_0 = 60:1:0.033$; a higher TCL should be considered (Figure 4.13) for the accurate determination of $C_{tr,0}$ and C_{tr} .

For an accurate determination of $C_{tr,0}$ and C_{tr} high TCLs should be thus considered, as in that case negligible interference of the high RAFT exchange reactivity of the R_0 species occurs for the calculation of $\langle C_{tr} \rangle$ (cf. Figure 4.6b vs. Figure 4.6a). Therefore, three high TCLs of respectively 713, 741 and 997 are selected from the experimental dataset of Derboven *et al.*²⁸ For each experiment, the polymer dispersity profile and the corresponding calculated $\langle C_{tr} \rangle$ values using the three different convergence criteria A-C via the method developed in the present work are shown in respectively Figure 4.13-15a and b. In accordance with the

conclusions drawn from the *in silico* proof of concept study in the previous section, a high reliability is obtained at low monomer conversion as evident from the coinciding calculated $\langle C_{tr} \rangle$ values based on the three different convergence criteria (A, blue squares; B, green triangles; C, red circles). As demonstrated *in silico*, the corresponding $\langle C_{tr} \rangle$ values at the first data point thus correspond to $C_{tr,0}$ and are listed in Table 4.4 (“ $C_{tr,0}$ 3”). For comparison, also the method of Moad and coworkers^{12,13} (Figure 4.12-14c; Equation (8) in Chapter 3) and Theis *et al.*¹⁶ (Equation (9) in Chapter 3) are applied to the considered experimental data to obtain values for $C_{tr,0}$, as also summarized in Table 4.4 (respectively “ $C_{tr,0}$ 1” and “ $C_{tr,0}$ 2”).

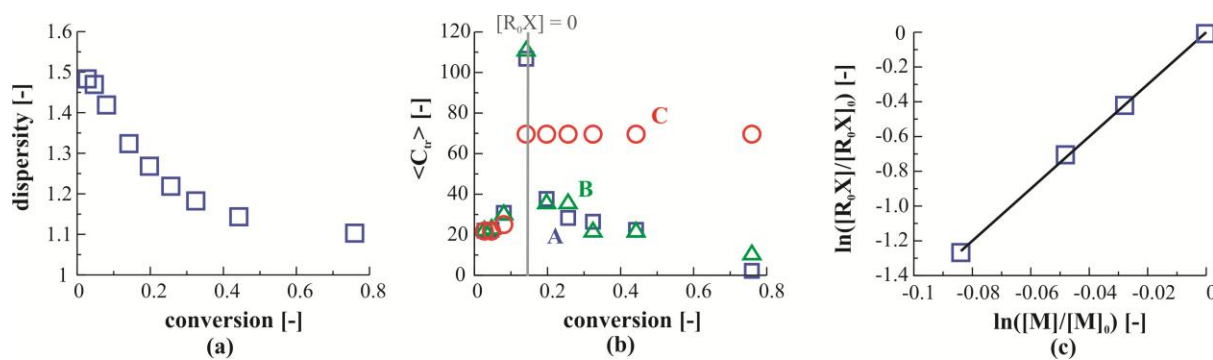


Figure 4.13: Experimental polymer dispersity as a function of (monomer) conversion (a) and corresponding $\langle C_{tr} \rangle$ as function of the monomer conversion obtained by solution of Equation (5)-(6) using the original Newton-Raphson convergence criterion (blue squares, convergence criterion A, Equation (12)) and the additional modified convergence criterion B (green triangles, 1% deviation, Equation (13)) and C (red circles, 5% deviation, Equation (14)) which are only used for sensitivity purpose, (b) and $\ln([M]/[M]_0)$ vs. $\ln([R_0X]/[R_0X]_0)$ data (c) for the RAFT polymerization of MMA with CPDB as RAFT CTA and AIBN as conventional radical initiator. 353 K; $[MMA]_0:[CPDB]_0:[AIBN]_0 = 713:1:0.12$. $[R_0X]/[R_0X]_0$ calculated via Equation (16), full black line is obtained via linear regression: $y(x) = 15.00 x$.

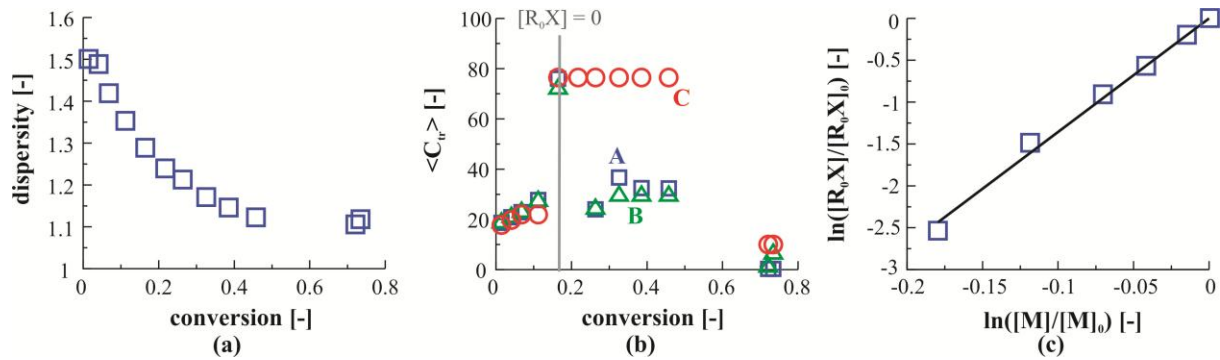


Figure 4.14: Experimental polymer dispersity as a function of (monomer) conversion (a) and corresponding $\langle C_{tr} \rangle$ as function of the monomer conversion obtained by solution of Equation (5)-(6) using the original Newton-Raphson convergence criterion (blue squares, convergence criterion A, Equation (12)) and the additional modified convergence criterion B (green triangles, 1% deviation, Equation (13)) and C (red circles, 5% deviation, Equation (14)) which are only used for sensitivity purpose, (b) and $\ln([M]/[M]_0)$ vs. $\ln([R_0X]/[R_0X]_0)$ data (c) for the RAFT polymerization of MMA with CPDB as RAFT CTA and AIBN as initiator. 353 K; $[MMA]_0:[CPDB]_0:[AIBN]_0 = 741:1:0.1$. $[R_0X]/[R_0X]_0$ calculated via Equation (16), full black line is obtained via linear regression: $y(x) = 13.57 x$.

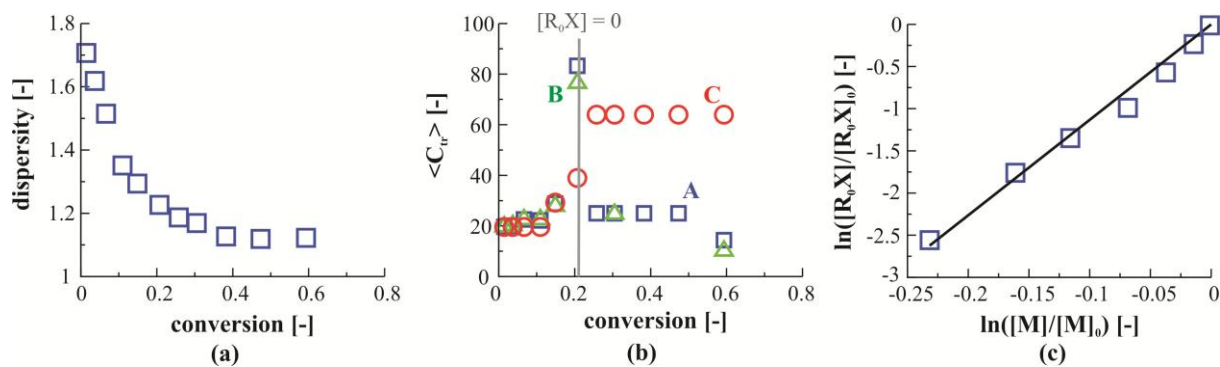


Figure 4.15: Experimental polymer dispersity as a function of (monomer) conversion (a) and corresponding $\langle C_{tr} \rangle$ as function of the monomer conversion obtained by solution of Equation (5)-(6) using the original Newton-Raphson convergence criterion (blue squares, convergence criterion A, Equation (12)) and the additional modified convergence criterion B (green triangles, 1% deviation, Equation (13)) and C (red circles, 5% deviation, Equation (14)) which are only used for sensitivity purpose, (b) and $\ln([M]/[M]_0)$ vs. $\ln([R_0X]/[R_0X]_0)$ data (c) for the RAFT polymerization of MMA with CPDB as RAFT CTA and AIBN as initiator. 353 K; $[MMA]_0:[CPDB]_0:[AIBN]_0 = 997:1:0.125$. $[R_0X]/[R_0X]_0$ calculated via Equation (16), full black line is obtained via linear regression: $y(x) = 11.32 x$.

Clearly, the scatter in $C_{tr,0}$ values is the lowest for the proposed method in the present work resulting in an average value for $C_{tr,0}$ of 20, which is significantly higher than the ones obtained by the other methods. In agreement with the results of the *in silico* evaluation of literature methods to determine the RAFT transfer coefficients in Chapter 3, further inspection of Table 4.4 again highlights that the method of Moad and coworkers^{12,13} inherently

underestimates $C_{tr,0}$ in case the contribution of $C_{-tr,0}$ cannot be neglected, and, the method of Theis *et al.*¹⁶ exhibits the least error for lower TCLs ($C_{tr,0} = 21.6$ for TCL 60). Note that accurate measurements of the R_0X concentration instead of its calculation from Equation (16) will increase the accuracy of both the method of Moad and coworkers^{12,13} and the one presented in the current work.

Table 4.4: Comparison of the values for $C_{tr,0}$ obtained via the method of Moad^{12,13} ($C_{tr,0}$ 1; Equation (8) in Chapter 3), the method of Theis *et al.*¹⁶ ($C_{tr,0}$ 2; Equation (9) in Chapter 3), and the method developed in the present work ($C_{tr,0}$ 3) based on experimental data for the RAFT polymerization of MMA at 353 K with CPDB as RAFT CTA and AIBN as initiator.²⁸ Entry 1-4 correspond to Figures 4.12-15. Different targeted chain lengths (TCLs) are considered. Mean value and maximum deviation for $C_{tr,0}$ determined by each method are also shown.

entry	TCL	$C_{tr,0}$ 1 [-]	$C_{tr,0}$ 2 [-]	$C_{tr,0}$ 3 [-]
1	60	— ^a	21.6	19.2
2	713	15.0	14.1	22.0
3	741	13.6	13.4	18.6
4	997	11.3	16.0	19.6
mean value:		13.3	16.3	19.9
maximum deviation [%]:		15.0	32.7	10.8

^aDetermination of $C_{tr,0}$ is not possible for TCL 60 due to non-linearity as shown in Figure 4.11

Importantly, if only the first experimental data point is used to determine $C_{tr,0}$ via the simple protocol described in Appendix G, exactly the same values are obtained (< 1% deviation) as if the full methodology would be followed (Figure 4.13-15; Table 4.4 “ $C_{tr,0}$ 3”). Hence, the loss of accuracy for the values of the total radical concentration λ_0 , induced by the simplified protocol for one-point measurements (*cf.* Appendix G), has a negligible influence on the

calculated $\langle C_{tr} \rangle$ value. The proposed methodology thus enables a rapid experimental screening of small RAFT CTAs for a given monomer system.

Furthermore, for all three considered high TCLs (entry 2-4 in Table 4.4), a reliable increase of $\langle C_{tr} \rangle$ is obtained until full conversion of R_0X is reached (marked by the vertical grey line) as the solutions for $\langle C_{tr} \rangle$ using convergence criteria A-C coincide. Hence, it can be safely deduced that C_{tr} is higher than $C_{tr,0}$. On the other hand, at higher conversions the $\langle C_{tr} \rangle$ values should be considered less reliable as they are more sensitive to small scatter in the experimental data, as evidenced by the systematic discrepancy between the three solutions. At the point of full R_0X conversion, values for C_{tr} between 76 and 110 are obtained for the three different TCLs. Importantly, at TCL equal to 741 the $\langle C_{tr} \rangle$ values for the three different convergence criteria coincide at complete consumption of R_0X , which indicates that the corresponding value of 76 is a reliable estimate for the RAFT transfer reactivity of the macro-RAFT CTA (C_{tr}). However, a valuable confidence interval cannot be provided, as for the other two TCLs no such coinciding of the three solutions is obtained. Note that the use of the solutions based on *convergence criterion B* and *C* are thus of high-added value as they allow a true evaluation of the reliability of the method for a given set of conditions.

Finally, it can be deduced from Figure 4.13-15 that a chain length and conversion dependency of C_{tr} is very unlikely. Not only are the measured dispersity values very low, as already indicated above, but also no clear decreasing trend is observed for the three solutions as would be expected for such dependency based on the theoretical evaluations in the previous section (*cf.* Figure 4.8).

4.4 Conclusions

An improved method to determine RAFT transfer coefficients has been developed in which the transfer reactivities are obtained by numeric solution of an analytical expression for the

polymer dispersity as a function of monomer conversion, including apparent termination kinetics and a possible intrinsic/apparent chain length dependency of the RAFT addition rate coefficient.

The presented method is validated *in silico* as a more accurate way to determine $C_{tr,0}$ compared to current literature models, which value can in principle be obtained from one single reliable measurement of the polymer dispersity at low monomer conversion, even for high values of $C_{tr,0}$ provided that a sufficiently high TCL is considered. Importantly, also a value for C_{tr} and its possible chain length dependency can be accessed from the same experiment at higher monomer conversions. The reliability of the measurements can be directly deduced via the consideration of additional convergence criteria for the numeric solution procedure.

Application of the presented methodology to experimental data for RAFT polymerization of MMA at 353 K with CPDB as RAFT CTA leads to a value for $C_{tr,0}$ of 20, whereas other literature methods are clearly less reliable. For C_{tr} an approximate value of 76 is obtained and no chain length dependency is detected for the current experimental dataset.

4.5 References

- (1) Chiefari, J.; Chong, Y. K.; Ercole, F.; Krstina, J.; Jeffery, J.; Le, T. P. T.; Mayadunne, R. T. A.; Meijs, G. F.; Moad, C. L.; Moad, G.; Rizzardo, E.; Thang, S. H. *Macromolecules* **1998**, *31*, 5559-5562
- (2) Barner-Kowollik, C. *Handbook of RAFT Polymerization*; Wiley: Weinheim, 2008.
- (3) Matyjaszewski, K. D., T. P. *Handbook of Radical Polymerization*; John Wiley and Sons: New Jersey, 2002.

- (4) Barner-Kowollik, C.; Buback, M.; Charleux, B.; Coote, M. L.; Drache, M.; Fukuda, T.; Goto, A.; Klumperman, B.; Lowe, A. B.; McLeary, J. B.; Moad, G.; Monteiro, M. J.; Sanderson, R. D.; Tonge, M. P.; Vana, P. *Journal of Polymer Science Part a-Polymer Chemistry* **2006**, *44*, 5809-5831
- (5) Moad, G.; Chiefari, J.; Chong, Y. K.; Krstina, J.; Mayadunne, R. T. A.; Postma, A.; Rizzardo, E.; Thang, S. H. *Polymer International* **2000**, *49*, 993-1001
- (6) Coote, M. L. *Journal of Physical Chemistry A* **2005**, *109*, 1230-1239
- (7) Coote, M. L.; Izgorodina, E. I.; Krenske, E. H.; Busch, M.; Barner-Kowollik, C. *Macromolecular Rapid Communications* **2006**, *27*, 1015-1022
- (8) Coote, M. L.; Krenske, E. H.; Izgorodina, E. I. *Macromolecular Rapid Communications* **2006**, *27*, 473-497
- (9) Gao, X.; Zhu, S. *Journal of Applied Polymer Science* **2011**, *122*, 497-508
- (10) Moad, G.; Chiefari, J.; Mayadunne, R. T. A.; Moad, C. L.; Postma, A.; Rizzardo, E.; Thang, S. H. *Macromolecular Symposia* **2002**, *182*, 65-80
- (11) Barth, J.; Buback, M.; Meiser, W.; Vana, P. *Macromolecules* **2010**, *43*, 51-54
- (12) Chiefari, J.; Mayadunne, R. T. A.; Moad, C. L.; Moad, G.; Rizzardo, E.; Postma, A.; Skidmore, M. A.; Thang, S. H. *Macromolecules* **2003**, *36*, 2273-2283
- (13) Chong, Y. K.; Krstina, J.; Le, T. P. T.; Moad, G.; Postma, A.; Rizzardo, E.; Thang, S. H. *Macromolecules* **2003**, *36*, 2256-2272
- (14) Goto, A.; Fukuda, T. *Progress in Polymer Science* **2004**, *29*, 329-385

-
- (15) Meiser, W.; Barth, J.; Buback, M.; Kattner, H.; Vana, P. *Macromolecules* **2011**, *44*, 2474-2480
- (16) Theis, A.; Feldermann, A.; Charton, N.; Stenzel, M. H.; Davis, T. P.; Barner-Kowollik, C. *Macromolecules* **2005**, *38*, 2595-2605
- (17) Clay, P. A.; Gilbert, R. G. *Macromolecules* **1995**, *28*, 552-569
- (18) Mayo, F. R. *Journal of the American Chemical Society* **1943**, *65*, 2324-2329
- (19) Moad, C. L.; Moad, G.; Rizzardo, E.; Thang, S. H. *Macromolecules* **1996**, *29*, 7717-7726
- (20) Muller, A. H. E.; Yan, D. Y.; Litvinenko, G.; Zhuang, R. G.; Dong, H. *Macromolecules* **1995**, *28*, 7335-7338
- (21) Muller, A. H. E.; Zhuang, R. G.; Yan, D. Y.; Litvinenko, G. *Macromolecules* **1995**, *28*, 4326-4333
- (22) Izgorodina, E. I.; Coote, M. L. *Macromolecular Theory and Simulations* **2006**, *15*, 394-403
- (23) Johnston-Hall, G.; Monteiro, M. J. *Macromolecules* **2007**, *40*, 7171-7179
- (24) Peklak, A. D.; Butte, A. *Macromolecular Theory and Simulations* **2006**, *15*, 546-562
- (25) Peklak, A. D.; Butte, A.; Storti, G.; Morbidelli, M. *Journal of Polymer Science Part a-Polymer Chemistry* **2006**, *44*, 1071-1085
- (26) Wang, A. R.; Zhu, S. P. *Macromolecular Theory and Simulations* **2003**, *12*, 196-208
- (27) D'hooge, D. R.; Reyniers, M.-F.; Marin, G. B. *Macromolecular Reaction Engineering* **2013**, *7*, 362-379

(28) Derboven, P.; D'hooge, D. R.; Reyniers, M.-F.; Marin, G. B.; Barner-Kowollik, C. *Macromolecules* **2015**, *48*, 492-501

(29) Favier, A.; Charreyre, M.-T. *Macromolecular Rapid Communications* **2006**, *27*, 653-692

(30) D'hooge, D. R.; Reyniers, M.-F.; Stadler, F. J.; Dervaux, B.; Bailly, C.; Du Prez, F. E.; Marin, G. B. *Macromolecules* **2010**, *43*, 8766-8781

(31) Householder, A. S. *Principles of Numerical Analysis*; McGraw-Hill: New York, 1953.

(32) Moad, G.; Rizzardo, E.; Thang, S. H. *Polymer* **2008**, *49*, 1079-1131

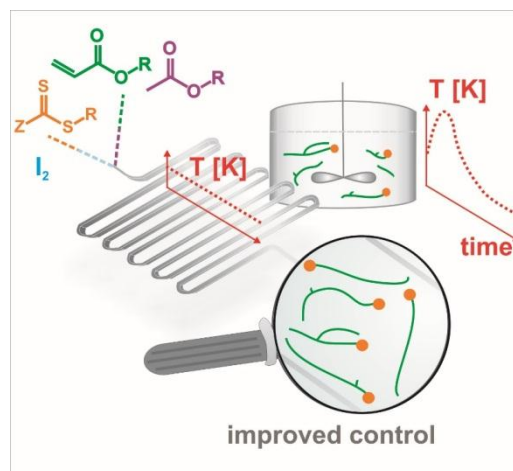
(33) Johnston-Hall, G.; Stenzel, M. H.; Davis, T. P.; Barner-Kowollik, C.; Monteiro, M. J. *Macromolecules* **2007**, *40*, 2730-2736

(34) Vana, P.; Davis, T. P.; Barner-Kowollik, C. *Macromolecular Rapid Communications* **2002**, *23*, 952-956

Chapter 5: Improved livingness and control over branching in RAFT polymerization of acrylates: could microflow synthesis make the difference?

Summary

The superior capabilities of structured microreactors over batch reactors are demonstrated for the reversible addition-fragmentation chain transfer (RAFT) solution polymerization of *n*-butyl acrylate with the aid of simulations, explicitly accounting for the chain length distribution of all macrospecies types. Since perfect isothermicity can be established in a microreactor less side products due to backbiting and subsequent β -scission of the tertiary radicals are formed compared to the batch operation, in which ineffective heat removal leads



to an undesirable temperature spike. For a given RAFT chain transfer agent (CTA), additional microstructural control results under microflow conditions by optimizing the reaction temperature, lowering the dilution degree or decreasing the initial molar ratio of monomer to RAFT CTA. This work has been accepted for publication in *Macromolecular Rapid Communications* 2015, DOI: 10.1002/marc.201500357

5.1 Introduction

Over the past 15 years, structured microreactors have emerged as a standardized tool to safely handle highly exothermic reactions and unstable intermediates in the realm of (bio)chemical research developments.¹⁻³ Miniaturization of the reactor size to the μL range enlarges significantly the heat exchanging surface area per unit of volume, allowing exquisite temperature control and thus prevents the undesirable formation of local hot spots. Together with efficient radial mixing, it can be expected that side product formation is suppressed, outperforming the corresponding batch operation.² The previous features also highlight the propensity of microreactors for reliable intrinsic kinetic measurements.^{4,5} Moreover, due to an excellent modularity, microreactor technology allows an elegant lab-scale realization of a wide spectrum of chemical syntheses^{1-3,6-8} and subsequent analyses.⁹

However, for less reactive processes and high pressure drops, as typically encountered in viscous media, microreactors are not always beneficial, and their use should be decided on a case-by-case basis.^{10,11} In particular, the highly exothermic radical solution polymerization of acrylates exhibits markedly better-defined average polymer properties in microreactors, both in the absence and presence of a reversibly deactivating agent.¹²⁻¹⁵ For example, Vandenberg et al.¹⁶ could synthesize in a microreactor at 373 K multiblock copolymers consisting of five different acrylate blocks via reversible addition-fragmentation chain transfer (RAFT) polymerization, an important reversible deactivation radical polymerization (RDRP) or previously called controlled radical polymerization (CRP) technique. In contrast, only three such blocks could be obtained with reasonable dispersity in the corresponding batch process.¹⁶ Importantly, an extensive control over the polyacrylate microstructure is essential when targeting advanced macromolecular architectures¹⁷ or site-specific functionality in, for instance, the automotive coating industry¹⁸⁻²¹ and block copolymer self-assembly.²²

It should be emphasized that the microstructure of polyacrylates is complex, as branching points and unsaturations can be formed during the synthesis. It is commonly accepted that both in free radical polymerization (FRP) and RDRP of acrylates tertiary mid-chain radicals (MCRs) are formed via intra- and intermolecular chain transfer to polymer, as unequivocally deduced from nuclear magnetic resonance studies.²³⁻²⁹ Subsequent slow tertiary propagation leads to the formation of short (SCB) and long chain branches (LCB), whereas at elevated temperatures (> 343 K) β -scission of the tertiary radicals results in the creation of macromonomers (MMs).³⁰ The latter yield additional branching points upon macropropagation.³¹⁻³³ Since high branching levels alter the gelation behavior,^{27,34} a thorough understanding of the factors influencing branch formation is crucial for advanced product design. In particular, the switch from FRP to RDRP allows to reduce the number of branching points per incorporated monomer unit, i.e. the cumulative branching fraction f_{branch} ,²⁴ which is predominantly affected by SCB formation

Based on simulations of atom transfer radical polymerization (ATRP), Reyes and Asua³⁵ claimed that these lower f_{branch} values in RDRP are caused by the lower macroradical transient lifetime since deactivation can occur. Later, Konkolewicz et al.^{36,37} applied the concept of competitive equilibria to highlight that factors such as the dilution degree and the tertiary (de)activation reactivity also determine the ATRP branching level.³⁶ On the other hand, Ballard et al.³⁸ claimed that an unconventional hypo-exponential reaction probability density distribution is required to explain the reduced branching in RAFT polymerization.

In the present work it is demonstrated that conventional kinetics can be used to describe the complex RAFT polymerization of acrylates in which branching is shown to be inherently reduced, even in the absence of RAFT exchange of the MCRs. Moreover, the superior design capabilities of microreactors over batch reactors are elucidated, highlighting in particular the relevance of isothermicity for advanced polymer synthesis.

5.2 Experimental section

For solution RAFT polymerization of *n*BuA in a structured microreactor (volume: 19.5 μ L; a detailed description can be found in reference [16]) using 2-(dodecylthiocarbonothioylthio)propionic acid (DoPAT), butyl acetate (50 wt%; solvent) and azobis(isobutyronitrile) (AIBN), Vandenberg et al.¹⁶ recently reported isothermal experimental data on number average molar mass (M_n) and dispersity at 373 K. A targeted chain length (TCL; $[n\text{BuA}]_0:[\text{DoPAT}]_0$) of 10 and 80 was considered with the former being the targeted block length for a subsequent multiblock copolymer synthesis. As the objective of the present work is to explain the enhanced performance of microreactors for macromolecular design, comparative experiments in an EASY MAX lab-scale batch reactor (both 20 mL and 40 mL) with integrated temperature monitoring were performed for the highest TCL ($[n\text{BuA}]_0:[\text{DoPAT}]_0:[\text{AIBN}]_0=80:1:0.05$; 50 wt% solvent; set temperature: 373 K; reference conditions). A non-isothermicity resulted with a sharp temperature rise of *ca.* 30 K (black diamonds in Figure 5.1a). A detailed discussion on the analysis is found in the Supporting Information.

5.2.1 Materials

n-Butyl acrylate (*n*BuA; 99% pure) was purchased from Acros Organics and deinhibited over a column of activated basic alumina prior to use. Azobis(isobutyronitrile) (AIBN; 98% pure) was purchased from Sigma-Aldrich and recrystallized twice from ethanol prior to use. 2-(dodecylthiocarbonothioylthio)propionic acid (DoPAT) was synthesized according to a literature procedure.³⁹ Butyl acetate was obtained from Sigma Aldrich and used without further purification.

5.2.2 Experimental procedure of the batch reaction (TCL 80)

A reagent mixture of *n*BuA (10 g; 0.078 moles), DoPAT (0.34 g; $9.75 \cdot 10^{-4}$ moles) and butyl acetate (solvent; 10 g; 0.061 moles) with a total volume of 19 mL was added to a 100 mL

reactor of an EasyMax 102 advanced synthesis workstation (Mettler Toledo) and degassed by nitrogen purging for 15 min. The reactor temperature was set at 373 K and the magnetic stirrer speed at 200 rpm, and on-line temperature monitoring of the reaction mixture was initiated. The solid-state thermostat covers a temperature range from -40 °C to 180 °C and does not imply the use of cumbersome oil or ice baths, or bulky cryostats. All data is directly stored for evaluation or report preparation. As soon as the set-temperature was reached, on-line Fourier transform infrared (FTIR) monitoring was started and a degassed solution of AIBN (0.008 g; $4.88 \cdot 10^{-5}$ moles) in 1 mL butyl acetate was added to the EasyMax batch reactor with a gas-tight glass syringe. The butyl acrylate concentration was followed via FTIR for 15 minutes after which the reactor was opened and the reaction quenched by addition of a methanol/hydroquinone solution and exposure to air. The results obtained via the EasyMax 102 batch reactor set-up used in the present work are found in Appendix H and can be considered as a lower limit for the deviation from the isothermal microreactor data in comparison with the use of conventional laboratory flasks and thermostatic oil baths, as was originally done in the experimental comparative study of Vandenberg *et al.*¹⁶ aiming at multi-block copolymers in batch and in a microflow.

5.2.3 Experimental procedure of the microreactor reaction (TCL 80)

In a typical procedure, a reagent mixture of *n*BuA (1.00 g; $7.802 \cdot 10^{-3}$ moles), AIBN (0.8 10^{-3} g; $5 \cdot 10^{-6}$ moles), DoPAT (0.034 g; $9.8 \cdot 10^{-5}$ mol) and butyl acetate (solvent; 1 g; $6.1 \cdot 10^{-3}$ moles) was added into a sealed Schlenk tube. The schlenk tube was subjected to 3 freeze-pump-thaw cycles, and subsequently inserted into the glovebox. The schlenk tube was opened and two 1-mL gastight syringes were filled with the reagent mixture. By using the Labtrix[®] Start R2.2 system, fitted with a glass microreactor (3227, reactor volume = 19.5 μ L), the degassed solution was pumped into the reactor. Reaction samples were subsequently analyzed with SEC, ¹H NMR and ESI-MS immediately after collection. In order to prevent clogging of

the microreactor, for a TCL of 80 conversions were limited to 80%. A detailed description of the microreactor set-up used can be found in Vandenberg *et al.*¹⁶

5.2.4 Characterization

The disappearance of *n*BuA in time was recorded via on-line FTIR measurements using a ReactIRTM 15 instrument (Mettler Toledo) with a flexible silverhalide (6 mm x 1.5 m) attenuated total reflection (ATR) probe. The absorbance peaks corresponding to the =CH₂ deformation at a wavelength of 810 cm⁻¹ and the =CH₂ twist at 1410 cm⁻¹ were used to calculate the *n*BuA conversion as they do not overlap with solvent peaks. The baseline was corrected for at a wavelength of 1561 cm⁻¹. Both peaks yield identical conversion profiles (Figure 5.1a, red dots). The final conversion after quenching of the reaction was checked via gravimetric analysis.

Size exclusion chromatography (SEC) measurements were performed on a Tosoh EcoSEC HLC-8320GPC, operated by PSS WinGPC software, comprising of an autosampler, a PSS guard column SDV (50 x 7.5 mm²), followed by three PSS SDV analytical linear XL (5 μm, 300 x 7.5 mm²) columns thermostated at 40 °C (column molecular weight range: 1 x 10² – 1 x 10⁶ g·mol⁻¹), and a differential refractive index detector (Tosoh EcoSEC RI) using THF as the eluent with a flow rate of 1 mL min⁻¹ with toluene as flow marker. Calibration was performed using linear narrow polystyrene (PS) standards from PSS Laboratories in the range of 4.7 x 10² - 7.5 x 10⁶ g·mol⁻¹. For the analysis, MHKS parameters of *Pn*BuA ($\alpha = 0.7$, $K = 12.2 \times 10^{-5} \text{ dL}\cdot\text{g}^{-1}$, THF 40 °C) were applied.⁴⁰ The SEC calibration range implies that for a TCL of 10 only at higher conversions reliable data on the chain length distribution can be obtained.

Electron spray ionization mass spectroscopy (ESI-MS) was performed using an LTQ Orbitrap Velos Pro mass spectrometer (ThermoFischer Scientific) equipped with an atmospheric

pressure ionization source operating in the nebulizer assisted electro spray mode. The instrument was calibrated in the m/z range 220-2000 using a standard solution containing caffeine, MRFA and Ultramark 1621. A constant spray voltage of 5 kV was used and nitrogen at a dimensionless auxiliary gas flow-rate of 5 and a dimensionless sheath gas flow-rate of 10 were applied. The S-lens RF level, the gate lens voltage, the front lens voltage and the capillary temperature were set to 50 %, -90 V, -8.5 V, and 275°C respectively. A 250 μL aliquot of a polymer solution with concentration of 10 $\mu\text{g mL}^{-1}$ was injected. A mixture of THF and methanol (THF:MeOH = 3:2), all HPLC grade, were used as solvent. For the ESI-MS measurements only samples with a molar mass below 5000 g mol^{-1} are considered as only in that case reliable quantitative information about the RAFT CTA functionality can be obtained. The recorded ESI-MS spectra can be found in Appendix H.

5.3 Model details

Solution RAFT polymerization of *n*BuA is modeled considering the reactions listed in Table 5.1. For simplicity, a degenerative scheme is assumed to describe the RAFT exchange⁴¹ and at first instance (Figure 5.1-3b) no RAFT exchange of MCRs is considered, as their impact can be expected to be limited (*cf.* section Kinetic parameters). Chain transfer to dormant and dead polymer are negligible as preliminary simulations indicated that the contribution of their products is below 1 mol%, even at high conversion. Hence, in the present work MCRs are only formed by backbiting (reaction 5 in Table 5.1). For clarity in Appendix I a reaction scheme is included which provides the chemical pathways for the formation and disappearance reactions of the MCRs. Thermal degradation reactions of the trithiocarbonyl moiety are not considered in the kinetic model based on experimental studies in literature and the low reaction times (~ 10 min).^{42,43} For all simulations in the present work, only literature values for the kinetic parameters have been used without further tuning to the experimental data.

Table 5.1: Reactions for simulation of solution RAFT polymerization of nBuA. Secondary/tertiary nature: superscript S/T; M: monomer, R₀X: initial RAFT CTA, I: conventional initiator fragment, R_i/R_iX/P_i: radical/dormant/dead macrospecies with chain length i; MM: macromonomer; f: efficiency; Arrhenius parameters: Table I.1 in Appendix I.

Reaction	Equation
dissociation	$I_2 \xrightarrow{k_{dis,f}} 2I$
chain initiation	$M + \begin{cases} I \\ R_0 \end{cases} \xrightarrow{k_{p0}} R_1$
propagation	$M + \begin{cases} R_i^S \\ R_i^T \end{cases} \xrightarrow{k_p^{S/T}} R_{i+1}$
chain transfer to monomer	$M + \begin{cases} R_i^S \\ R_i^T \end{cases} \xrightarrow{k_{trM}^{S/T}} P_i + R_1^S$
backbiting	$R_i^S \xrightarrow{k_{bb}} R_i^T \quad i > 3$
β -scission	$\begin{cases} R_i^T \xrightarrow{k_\beta} R_j^S + MM_{i-j} \\ R_i^T \xrightarrow{k_\beta} MM_j + R_{i-j}^S \\ i > 3, \quad j < i - 1 \end{cases}$
macropropagation	$MM_j + \begin{cases} R_i^S \\ R_i^T \end{cases} \xrightarrow{k_{p,macro}^{S/T}} R_{i+j}^T$
degenerative transfer with RAFT CTA ^a	$\begin{cases} R_i^S \\ R_i^T \end{cases} + R_0X \xrightleftharpoons{k_{tr}^{S/T,S}} \begin{cases} R_i^S X \\ R_i^T X \end{cases} + R_0$
degenerative transfer with macro-RAFT CTA ^a	$\begin{cases} R_i^S \\ R_i^T \end{cases} + \begin{cases} R_i^S X \\ R_j^T X \end{cases} \xrightleftharpoons{k_{tr}^{S/T,S/T}} \begin{cases} R_i^S X \\ R_i^T X \end{cases} + \begin{cases} R_i^S \\ R_j^T \end{cases}$
termination by recombination ^b	$\begin{cases} R_i^S \\ R_i^T \\ R_0 \end{cases} + \begin{cases} R_i^S \\ R_j^T \\ R_0 \end{cases} \xrightarrow{k_{tc,app}^{S/T,S/T}} P_{i+j}$

^a $k_{tr}^{TS} = 0 \text{ L mol}^{-1} \text{ s}^{-1}$ except for illustration purposes in Figure 5.3c-d. ^bApparent rate coefficients to account for diffusional limitations (*cf.* section Kinetic parameters).

To calculate the evolution of the species concentrations an explicit deterministic modeling technique is selected, which includes the calculation of the chain length distributions (CLDs) of all macrospecies types (*e.g.* mid-chain radicals (MCRs), end-chain radicals (ECRs), secondary dormant species, ...). The individual continuity equations are simultaneously integrated using the Livermore Solver for Ordinary Differential Equations (LSODA) for chain lengths up to 3000.⁴⁴ This allows in particular a rigorous implementation of backbiting and subsequent β -scission reactions which require respectively ECRs and MCRs with a minimal chain length of 4. For the polymer population, the fraction of macrospecies with RAFT CTA and C=C functionality are denoted as F_X and F_{MM} , respectively (*cf.* Figure 5.1e).

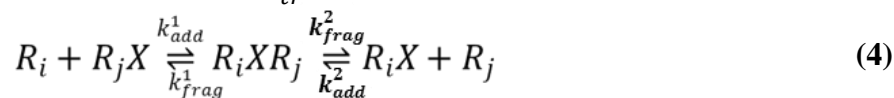
The microreactor can be assumed to be operated under isothermal conditions¹⁶ and can be modeled as a stationary plug flow reactor (no backmixing), as confirmed by the manufacturer Chemtrix who recorded the residence time distribution via tracer pulse experiments for the considered flow range.⁴⁵ The corresponding model equation as illustrated for the secondary dormant macrospecies is given by Equation (1), in which i represents the chain length, c the concentration [mol m^{-3}], \bar{v} the average fluid velocity [m s^{-1}], N the maximum chain length considered in the kinetic model and z the spatial coordinate of the reactor [m]. For the batch reactor, on the other hand, the recorded temperature variation in Figure 5.1a (black diamonds; set temperature 373 K) has been implemented in the kinetic model. For completeness, also the batch model equation for the secondary dormant species is presented below (Equation (2)) in which t is the reaction time [s] and V the reactor volume [m^3]. Note that for the construction of Equation (1) and (2) for simplification no RAFT exchange with tertiary macrospecies was assumed (see further). The simulation of the different influences on the branching level and the RAFT CTA functionality is performed for a microreactor at a lower polymerization temperature of 343 K.

$$\bar{v} \frac{d(c_{R_i-X})}{dz} = -c_{R_i-X} \sum_{i=1}^N k_{tr}^{i,j} c_{R_j} + c_{R_i} \sum_{i=1}^N k_{tr}^{i,j} c_{R_j-X} \quad \left[\frac{\text{mol}}{\text{m}^3 \text{ s}} \right] \quad (1)$$

$$\frac{1}{V} \frac{d(Vc_{R_i-X})}{dt} = -c_{R_i-X} \sum_{i=1}^N k_{tr}^{i,j} c_{R_j} + c_{R_i} \sum_{i=1}^N k_{tr}^{i,j} c_{R_j-X} \quad \left[\frac{\text{mol}}{\text{m}^3 \text{ s}} \right] \quad (2)$$

5.4 Kinetic parameters

In Table I.1 in Appendix I, the literature Arrhenius parameters for all the considered reactions in the kinetic model are listed together with their value at 373 K and the corresponding literature reference. The rate coefficients for the transfer reactions of the degenerative RAFT model (k_{tr}) given by Equation (3) are calculated based on the general RAFT addition-fragmentation scheme (Equation (4)) via Equation (5) which follows from the pseudo-steady state assumption for the intermediate radical R_iXR_j .⁴¹



$$k_{tr} = \frac{k_{add}^1 k_{frag}^2}{k_{frag}^1 + k_{frag}^2} \quad (5)$$

In a first stage (Figure 5.1-8b), it is assumed that tertiary radicals cannot undergo RAFT exchange with secondary dormant species ($k_{tr}^{TS} = 0 \text{ L mol}^{-1} \text{ s}^{-1}$) and, hence, no tertiary dormant species can be formed. This simplification is based on the rationale that addition of a tertiary macroradical to the carbon-sulphur double bond is significantly retarded compared to its secondary counterpart, and furthermore fragmentation towards the initial reactants (R_i^T, R_jX) is favored due to the enhanced stability of the tertiary radical species. Even though the values for the rate coefficients of the other RAFT exchange reactions involving tertiary

species are different from zero ($k_{tr}^{TT}, k_{tr}^{ST} \neq 0$), they have no effect since no tertiary dormant species are present throughout the polymerization reaction ($k_{tr}^{TS} = 0 \text{ L mol}^{-1} \text{ s}^{-1}$).

In a second stage (Figure 5.8c-14), a sensitivity analysis is performed for the effect of the RAFT exchange reactivity on the resulting polymer microstructure. This also involves an evaluation of the impact of the RAFT exchange reactions involving tertiary macrospecies ($k_{tr}^{TS}, k_{tr}^{TT}, k_{tr}^{ST} \neq 0 \text{ L mol}^{-1} \text{ s}^{-1}$; Figure 5.3c-d). For simplicity, the limiting case in which both secondary and tertiary radicals have the same reactivity for RAFT exchange is considered. In general, the activation energy of the transfer coefficients is taken equal to zero since in case of equal fragmentation rate coefficients ($k_{frag}^1 = k_{frag}^2$) Equation (5) simplifies to $k_{tr} = 0.5 k_{add}^1$, and the addition reaction has an activation energy close to zero.^{46,47}

For the reactions in which a tertiary macroradical undergoes chain transfer to monomer and propagation with macromonomer, the rate coefficients have been adopted from the secondary counterparts, though, multiplied by a constant factor similar to the work of Wang et al.³² This factor is assumed to be the ratio of the tertiary to the secondary propagation rate coefficient. Propagation rate coefficients for the initiator fragments ($I, R_0; k_{pl}, k_{p0}$) of both the conventional free radical initiator (I_2) and the RAFT CTA (R_0X) have been assumed 10 times higher than the macroradical propagation rate coefficient (k_p).^{48,49} For termination, diffusional limitations are accounted for via the composite k_t model using literature parameters.^{50,51}

5.5 Results and discussion

Whether a radical polymerization benefits from being conducted in a microreactor or not has been the subject of an ongoing scientific debate grounded mostly on experimental studies.¹²⁻¹⁶ However, more recently, some theoretical studies have been performed for non-acrylate monomers and considering simplified reaction schemes.⁵²⁻⁵⁴ In the present work, RAFT solution polymerization of *n*BuA is modeled with a detailed formal reaction scheme (Table

5.1) in a batch and microreactor to elucidate the advantages of the latter, focusing on the optimization of the microreactor conditions towards an improved control over f_{branch} and RAFT CTA functionality.

Figure 5.1 illustrates the simulated effect of the experimentally observed non-isothermicity in batch (black diamonds Figure 5.1a; set-temperature: 373 K; TCL=80) on the average polymer properties (Figure 5.1b-e; dotted red lines). In general, the observed experimental trends (Figure 5.1a-c,e) are well captured by the simulation results for which only literature values for the kinetic parameters were used (*cf.* Appendix I). An inferior control over the polymer microstructure is obtained compared to the isothermal microreactor simulation results (full red lines; 373 K; TCL=80). In particular, at high conversion, a clear discrepancy results between the microreactor and the batch reactor data both theoretically and experimentally (batch: full red circles; microflow: open red triangles). More specifically, the temperature spike in batch induces higher dispersities (Figure 5.1c), higher f_{branch} values (Figure 5.1d), and much lower RAFT CTA functionalities (Figure 5.1e; F_X , left axis) at high conversion.

These low F_X values jeopardize further macromolecular design, explaining directly why a higher number of acrylate blocks could be synthesized under microflow conditions.¹⁶ Due to isothermicity in a microreactor less side products are formed compared to the batch operation in which the temperature spike induces a higher importance of the highly activated backbiting and β -scission reactions (*cf.* Appendix I). In agreement with Guillaneuf et al.³¹ the loss of RAFT CTA functionality is mainly caused by the latter reactions (~ 90 %), as shown in Figure 5.1e via the simulated macromonomer fraction F_{MM} (right axis). The reduced relevance of β -scission under microflow conditions is also confirmed in the simulated number CLDs. For example, for a TCL of 80 at a conversion of 0.80 clearly fewer short chains are formed via β -scission (Figure 5.1f, full vs. dotted red line).

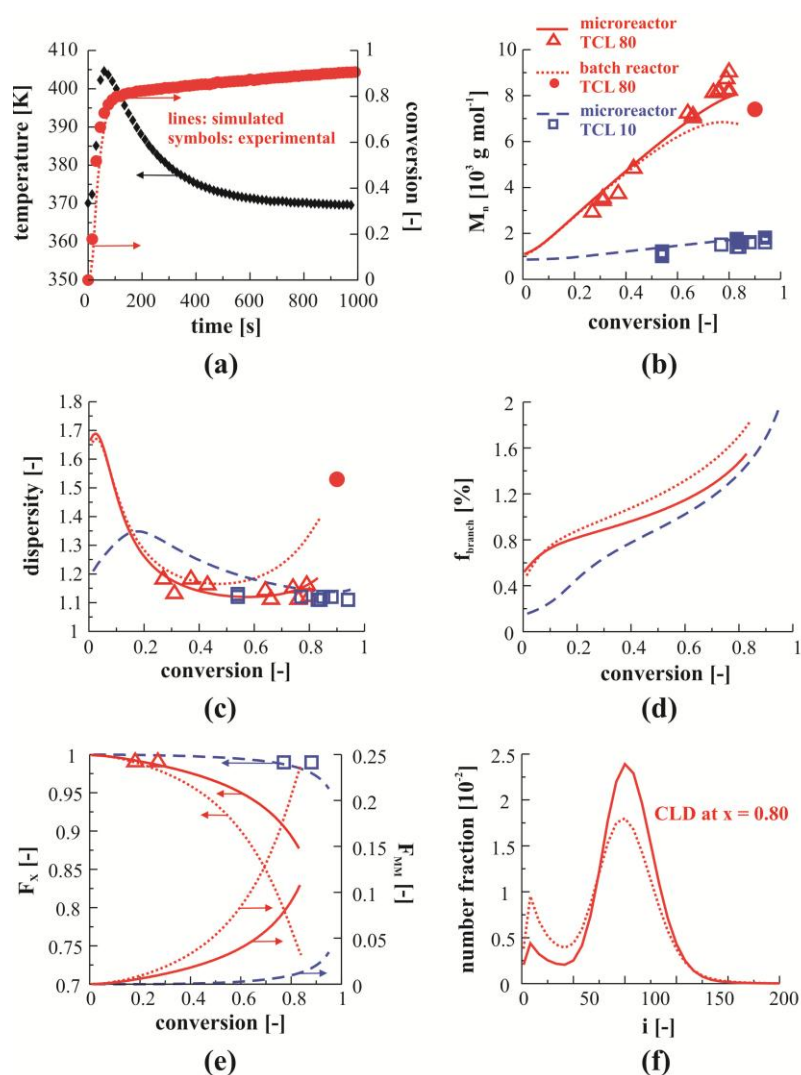


Figure 5.1: (a) Experimental batch temperature (black diamonds) and conversion (red dots) evolution and simulated conversion profile (dotted red line) under reference conditions ($[nBuA]_0:[DoPAT]_0:[AIBN]_0=80:1:0.05$; 50 m% solvent; TCL 80; set temperature: 373 K) (b)-(c) Comparison between simulated and experimental number average molar mass M_n (b) and dispersivity (c) profile for the reference conditions in batch (dotted red line vs. full red circle) and under microflow (full red line vs. open red triangles), and an additional condition under microflow (TCL 10; dashed blue line vs. open blue squares) (d)-(e) Simulated cumulative branching fraction (f_{branch}), number average macroradical chain length ($x_{n,R}$), RAFT CTA functionality (F_X) (also experimental data) and macromonomer fraction (F_{MM}) as a function of conversion for a TCL of 80 in batch (dotted red lines) and under microflow (full red lines), and for a TCL of 10 under microflow (dashed blue lines) (f) Comparison between simulated chain length distribution (CLD) under reference conditions in batch (dotted red line) and microflow (full red line) at a conversion of 0.8. Kinetic parameters in Table I.1 in Appendix I. Kinetic model: Equation (1)-(2) and Table 5.1. TCL defined as $[nBuA]_0/[DoPAT]_0$.

In order to explain the superior polyacrylate properties obtained in an isothermal microreactor compared to a batch reactor characterized by a temperature spike, the reaction probabilities of the secondary (Figure 5.2a-d) and tertiary (Figure 5.2e,f) macroradicals are considered. Figure

5.2a-b show that the probabilities of the secondary radical for propagation (full line; prop), RAFT exchange (dashed line; exch) and side reactions (dotted line; side) are similar in both the micro- and batch reactor. However, when studying the contributions of the different side reactions as depicted in Figure 5.2c-d, it is clear that despite a lower probability for termination reactions (dashed line; term), in a batch reactor (Figure 5.2d) the probabilities for backbiting (full line; backb) and macropropagation (dotted line; macrop) are significantly higher than in a microreactor (Figure 5.2c). The greater contribution of backbiting at elevated temperatures is explained by its high activation energy compared to the other competing reactions (*cf.* Table I.1 in Appendix I). Similarly for the tertiary radicals (Figure 5.2e-f), β -scission has the highest activation energy (*cf.* Table I.1 in Appendix I). Hence, in the non-isothermal batch reaction, β -scission (dotted line; β -sc) of the tertiary macroradicals is favored over termination (full line; termT) and other tertiary side reactions (dashed line; other). Since both backbiting and subsequent β -scission are the dominant side reaction pathways for respectively the secondary and tertiary macroradicals, a high contribution of short chains results causing the high dispersity values in batch. Moreover, the high backbiting probability leads to more branch formation.

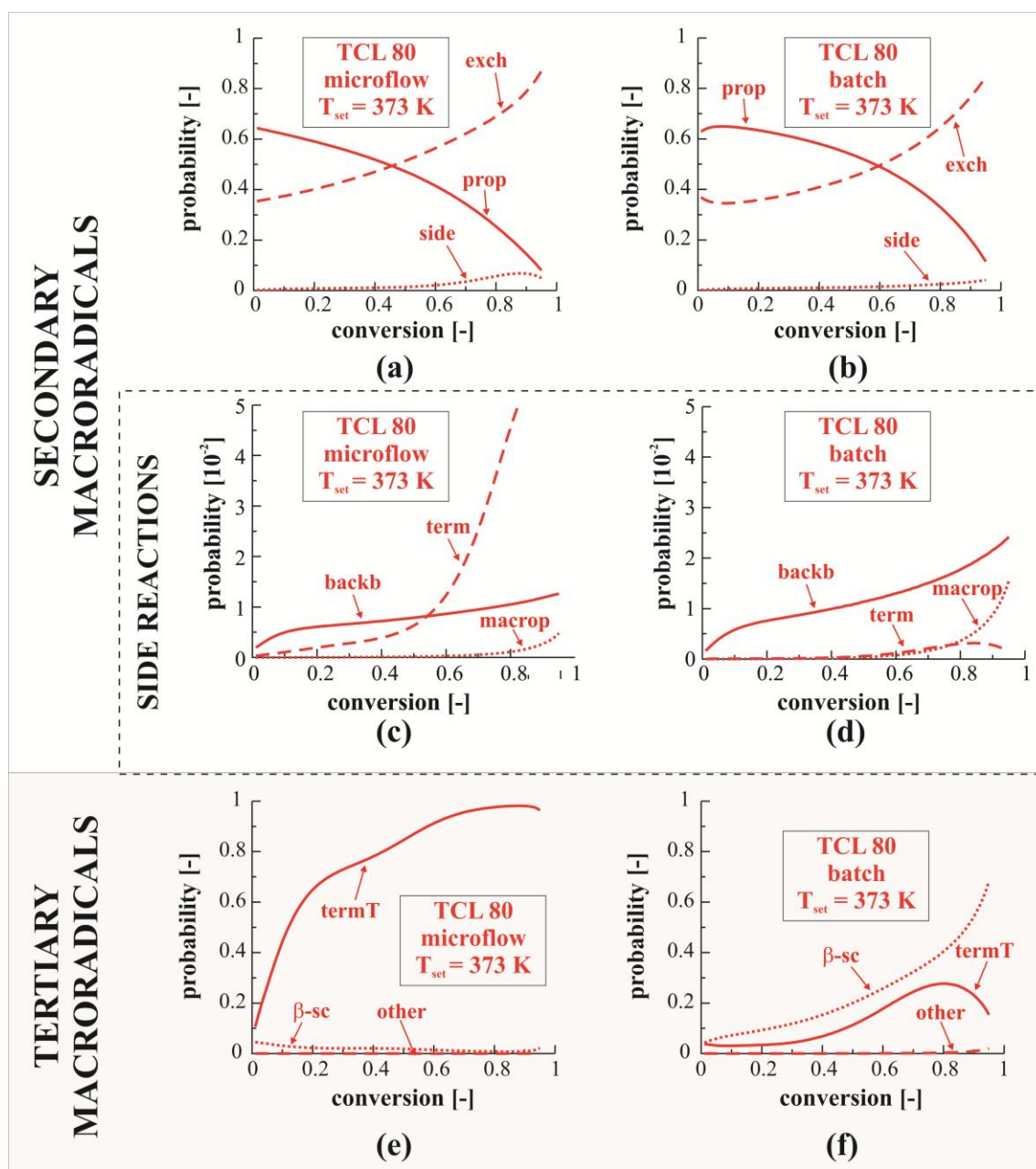


Figure 5.2: (a)-(b) Simulated reaction probabilities for propagation (full line; prop), RAFT exchange (dashed line; exch) and all side reactions (dotted line; side) of the secondary radicals in an isothermal microreactor (a) and a non-isothermal batch reactor (b) with a set-temperature T_{set} of 373 K. (c)-(d) Simulated reaction probabilities for backbiting (full line; backb), termination (dashed line; term) and macropropagation (dotted line; macrop) of the secondary radicals in the microreactor (c) and the batch reactor (d). (e)-(f) Simulated reaction probabilities for termination (full line; termT), β -scission (dotted line; β -sc) or other side reactions (dashed line; other) of the tertiary radicals in microflow (e) and in batch (f); All simulations are performed under the reference conditions: $([nBuA]_0:[DoPAT]_0:[AIBN]_0 = 80:1:0.05; 50 \text{ wt\% solvent; TCL 80})$. Kinetic parameters in Table I.1 in Appendix I. Kinetic model: Equation (1)-(2) and Table 5.1. TCL defined as $[nBua]_0/[DoPAT]_0$.

A further improvement of the polyacrylate properties can be obtained by optimizing the microreactor conditions, which requires a detailed insight into all competitive reactions, focusing in particular on the control over branch formation (f_{branch}) and functionality conservation (F_X). For instance, an increase of the initial RAFT CTA concentration, and thus decrease of TCL, yields significantly lower f_{branch} values (TCL 10 vs. 80 in Figure 5.1b-e; 373 K; simulations: dashed blue vs. full red lines; experimental data: open blue squares vs. open red triangles). As shown in Figure 5.3, a first reason for this reduction in branching with decreasing TCL is a lower backbiting probability (Figure 5.3c-d, full blue vs. full red line) due to a faster RAFT exchange of secondary end-chain radicals (ECRs; Figure 5.3a-b, dashed blue vs. dashed red line), whereas a second reason is a higher importance of oligomeric radicals incapable of backbiting ($i < 4$) due to a lower number average chain length ($x_{n,R}$) which is clearly seen in Figure 5.3c by the more pronounced decrease of the backbiting probability (full blue line) at low conversion. Note that these observations are in agreement with the recent modeling results of Ballard et al.⁵⁵ for FRP with high initial amounts of conventional CTA and the simulated f_{branch} are in the expected range of literature values.³⁸ Similarly, a significantly higher RAFT CTA functionality results for a lower TCL, due to a higher secondary RAFT exchange rate and lower probability for backbiting and subsequent β -scission, as is clear from Figure 5.1e (dashed blue, TCL 10 vs. full red line, TCL 80).

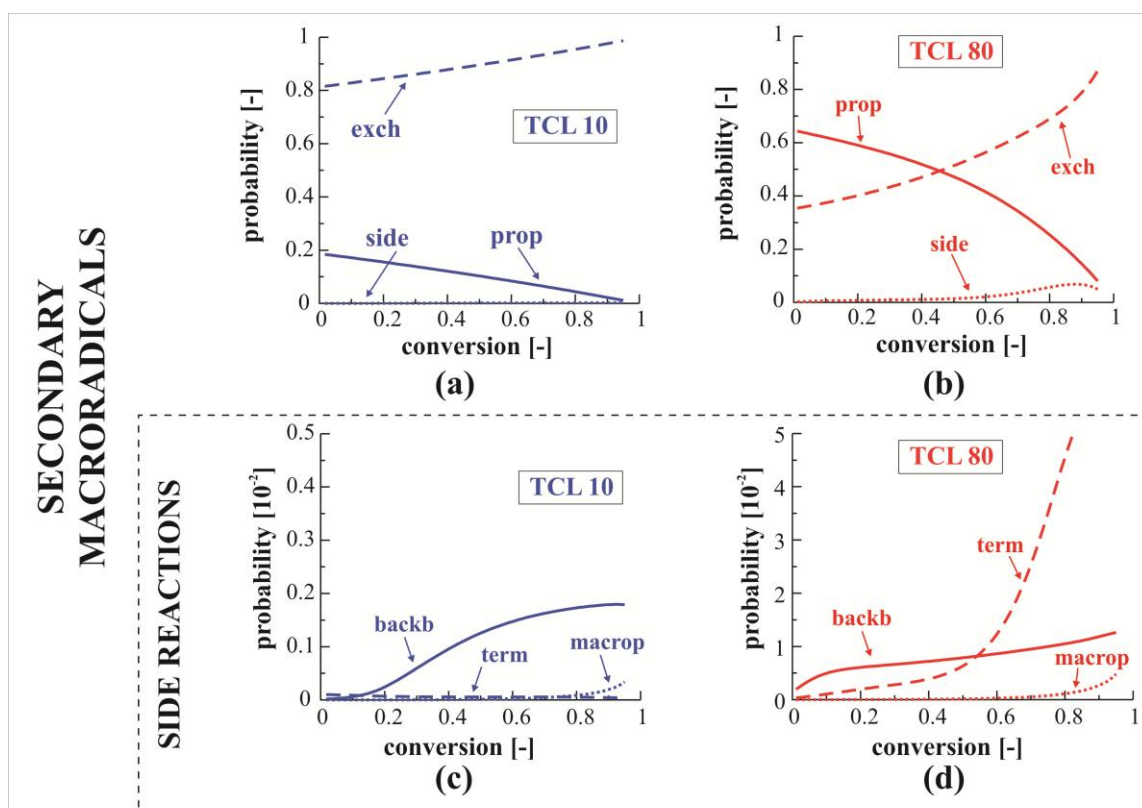


Figure 5.3: (a)-(b) Simulated reaction probabilities for propagation (full line; prop), RAFT exchange (dashed line; exch) and all side reactions (dotted line; side) of the secondary radicals in an isothermal microreactor at 373 K for TCL 10 (a; blue lines) and TCL 80 (b; red lines). (c)-(d) Simulated reaction probabilities for backbiting (full line; backb), termination (dashed line; term) and macropropagation (dotted line; macrop) of the secondary radicals at 373 K for TCL 10 (c; blue lines) and TCL 80 (d; red lines). Note that the scale of the ordinate is different for (c) and (d). All simulations are performed under the conditions: $[DoPAT]_0:[AIBN]_0 = 1:0.05$; 50 wt% solvent). Kinetic parameters in Table I.1 in Appendix I. Kinetic model: Equation (1)-(2) and Table 5.1. TCL defined as $[nBua]_0/[DoPAT]_0$.

In accordance with the aforementioned discussion on the effect of non-isothermicity in a batch reactor, a lowering of the polymerization temperature in the microreactor leads to an additional improvement of f_{branch} and F_X , as shown in Figure 5.4 (373 K: full red line (reference case) vs. 343 K: dashed red line). As highlighted before, the higher activation energy for backbiting and β -scission in comparison with respectively secondary and tertiary propagation explains this trend. Also, from Figure 5.5a-b it is clear that at a lower temperature of 343 K, the probability of the secondary radicals for RAFT exchange (dashed line; exch) is higher, as it is non-activated (Table I.1 in Appendix I), and consequently the total contribution of side reactions (dotted line; side) is much smaller than at 373 K.

Moreover, an additional decrease of the dilution degree also positively affects f_{branch} and F_x , since monomolecular backbiting is less affected by dilution compared to the competitive bimolecular reactions, in agreement with the ATRP simulations of Konkolewicz et al.³⁶ This is also demonstrated in Figure 5.4 for a TCL of 80 (343 K) and dilution degrees of 50% (dashed red line; reference case) and 25% (dashed-dotted red line). Furthermore, Figure 5.6 shows that the probability for backbiting of the secondary radicals (Figure 5.6c-d; full line; backb) decreases for more concentrated polymerization mixtures (d vs. c), while the probabilities for secondary propagation (Figure 5.6a-b; prop; full line) and RAFT exchange (Figure 5.6a-b; exch; dashed line) remain the same. It should however be kept in mind that in a microreactor the minimal degree of dilution is in practice determined by the viscosity of the reaction mixture as clogging could occur.

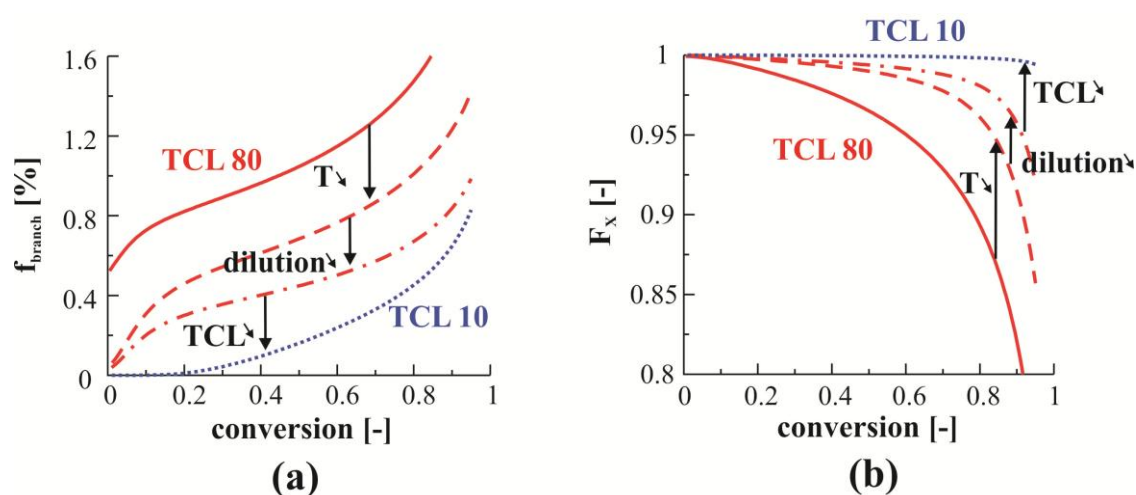


Figure 5.4: Summary of the positive impact of the microreactor conditions on the control over (a) branching level f_{branch} and (b) RAFT CTA functionality F_x . Top to bottom in (a) and vice versa in (b): a decrease of the polymerization temperature (373 to 343 K, TCL 80, $[M]_0$: 3.5 (50 wt% solvent); full to dashed red line), an additional lowering of the dilution degree ($[M]_0$: 3.5 to 5.25 M (25 wt% solvent)), dashed to dashed-dotted red line) and an additional lowering of TCL (TCL 80, to 10, dotted blue line). Kinetic parameters in Table I.1 in Appendix I. Kinetic model: Equation (1)-(2) and Table 5.1. TCL defined as $[nBua]_0/[DoPAT]_0$.

Hence, it can be concluded that the temperature, dilution degree and TCL are important microreactor conditions for microstructural control, as illustrated by the arrows in Figure 5.2 (TCL 10: blue dotted line; 343 K; 25 wt% solvent). For completeness, in Appendix J the

effect of the TCL on the polyacrylate microstructure and different reaction probabilities is illustrated for a larger range (TCL 10 – 200) at 343 K.

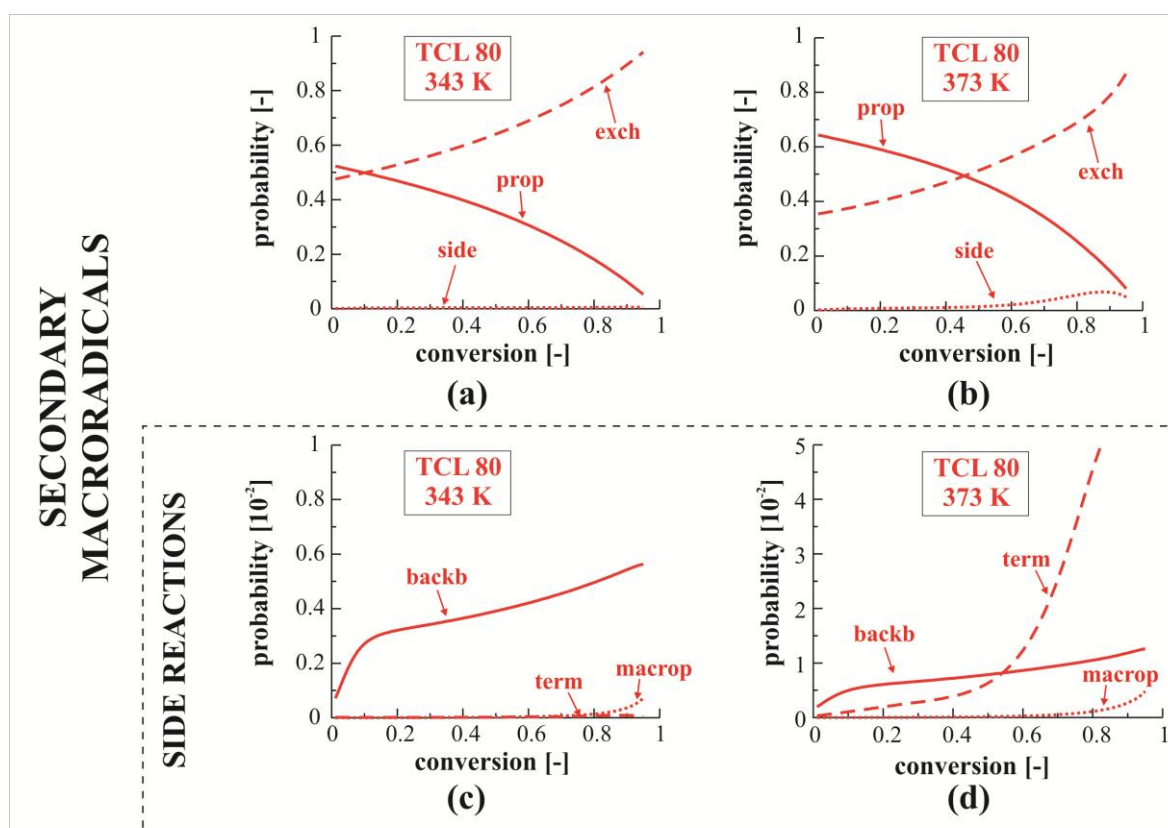


Figure 5.5: (a)-(b) Simulated reaction probabilities for propagation (full line; prop), RAFT exchange (dashed line; exch) and all side reactions (dotted line; side) of the secondary radicals in an isothermal microreactor at 343 K (a) and 373 K (b). (c)-(d) Simulated reaction probabilities for backbiting (full line; backb), termination (dashed line; term) and macropropagation (dotted line; macrop) of the secondary radicals at 343 K (c) and 373 K (d). Note that the scale of the ordinate is different for (c) and (d). All simulations are performed under the reference conditions: $([nBuA]_0:[DoPAT]_0:[AIBN]_0 = 80:1:0.05; 50 \text{ wt\% solvent; TCL } 80)$. Kinetic parameters in Table I.1 in Appendix I. Kinetic model: Equation (1)-(2) and Table 5.1. TCL defined as $[nBuA]_0/[DoPAT]_0$.

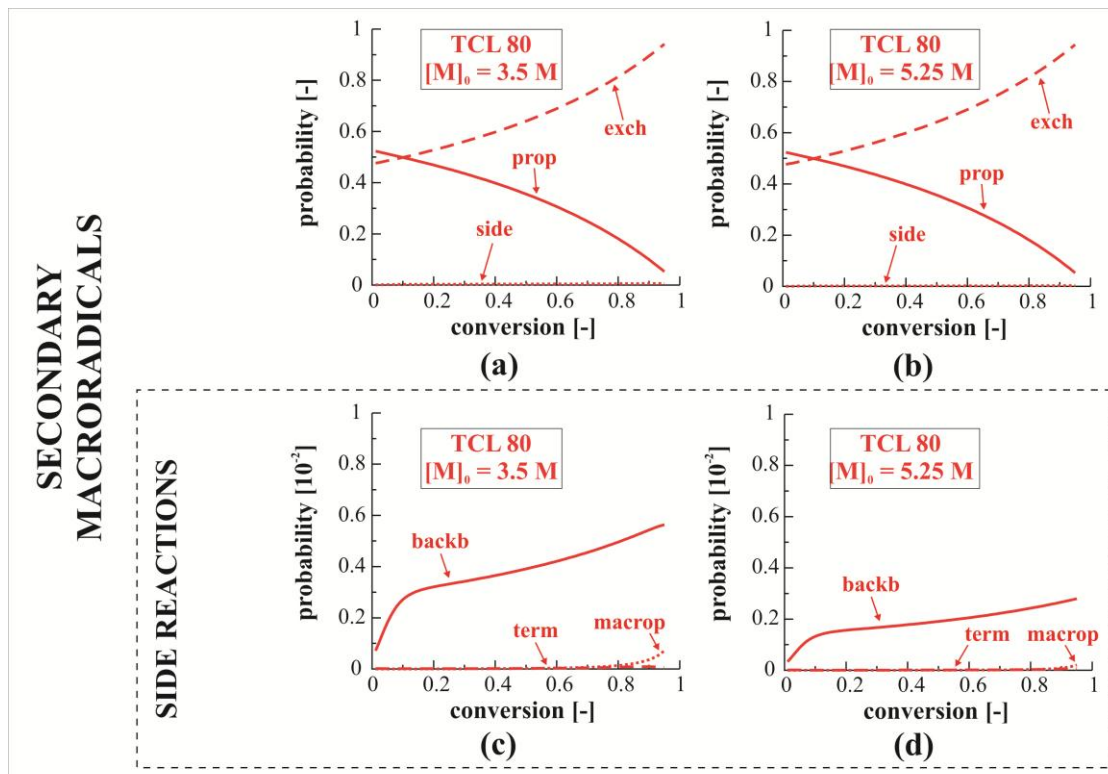


Figure 5.6: (a)-(b) Simulated reaction probabilities for propagation (full line; prop), RAFT exchange (dashed line; exh) and total side reactions (dotted line; side) of the secondary radicals in an isothermal microreactor at 343 K in solution (a, $[M]_0 = 3.5 \text{ M}$ and b, $[M]_0 = 5.25 \text{ M}$). (c)-(d) Simulated reaction probabilities for backbiting (full line; backb), termination (dashed line; term) and macropagation (dotted line; macrop) of the secondary radicals in solution (c, $[M]_0 = 3.5 \text{ M}$ and d, $[M]_0 = 5.25 \text{ M}$). All simulations are performed under the reference conditions: ($[n\text{BuA}]_0:[\text{DoPAT}]_0:[\text{AIBN}]_0 = 80:1:0.05$; TCL 80). Kinetic parameters in Table I.1 in Appendix I. Kinetic model: Equation (1)-(2) and Table 5.1. TCL defined as $[n\text{Bua}]_0/[\text{DoPAT}]_0$.

It should be noted that, alternatively, the branching content can be represented by the average number of branches per chain as illustrated in Figure 5.7, which is the equivalent of Figure 5.4a. This allows a classification of process conditions toward a targeted microstructure in a different manner (*cf.* also Appendix K). It is clear that the same factors that reduce f_{branch} also reduce the number of branches per chain.

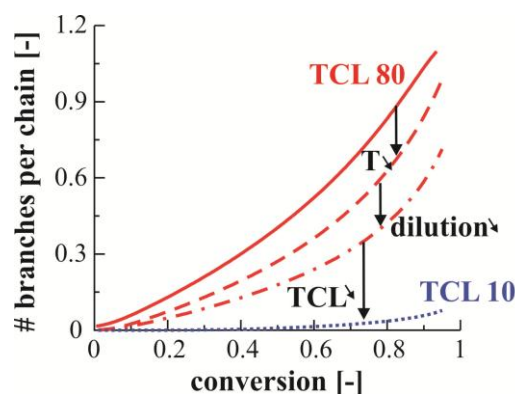


Figure 5.7: Similar to Figure 5.4a but now for the number (#) of branches per chain instead of the cumulative branching fraction (f_{branch}). Top to bottom: a decrease of the polymerization temperature (373 to 343 K, TCL 80, $[M]_0$: 3.5 (50 wt% solvent); full to dashed red line), an additional lowering of the dilution degree ($[M]_0$: 3.5 to 5.25 M (25 wt% solvent)), dashed to dashed-dotted red line) and an additional lowering of TCL (TCL 80, to 10, dotted blue line). Kinetic parameters in Table I.1 in Appendix I. Kinetic model: Equation (1)-(2) and Table 5.1. TCL defined as $[nBua]_0/[DoPAT]_0$.

Finally, to evaluate the sensitivity of the polymer microstructure obtained in a microreactor for the RAFT exchange reactivity, simulations are performed at 343 K for a TCL of 80 in which the corresponding rate coefficients for the ECRs (k_{tr}^{SS} , k_{tr}^{ST} in Table 5.1) and MCRs (k_{tr}^{TS} , k_{tr}^{TT} in Table 5.1) are varied (Figure 5.8). For a higher k_{tr}^{SS} , significantly lower f_{branch} and higher F_X values result, as shown in Figure 5.8a-b for $k_{tr}^{SS} = 3 \cdot 10^3$ (dotted purple line), $3 \cdot 10^4$ (dashed-dotted green line), $3 \cdot 10^5$ (dashed orange line), and $3 \cdot 10^6$ (full red line, Table 5.1) $L \cdot mol^{-1} \cdot s^{-1}$, still neglecting RAFT exchange with MCRs ($k_{tr}^{TS} = 0 \cdot L \cdot mol^{-1} \cdot s^{-1}$). Raising k_{tr}^{SS} increases the secondary RAFT exchange rate, which causes a decrease of the contribution of side reactions (dotted line in Figure 5.9a-b; side), for which backbiting (full line in Figure 5.9c-d; backb) is clearly the dominant reaction pathway. The lower tertiary radical concentration induces also a lower reaction rate for the subsequent β -scission. Hence, both a reduction of f_{branch} and an increase in F_X are obtained if the RAFT agent is characterized by a higher k_{tr}^{SS} (Figure 5.8a-b). This observation agrees with the claim of Reyes and Asua³⁵ that in RDRP a reduced f_{branch} can be related to a shorter transient ECR lifetime as compared to FRP.

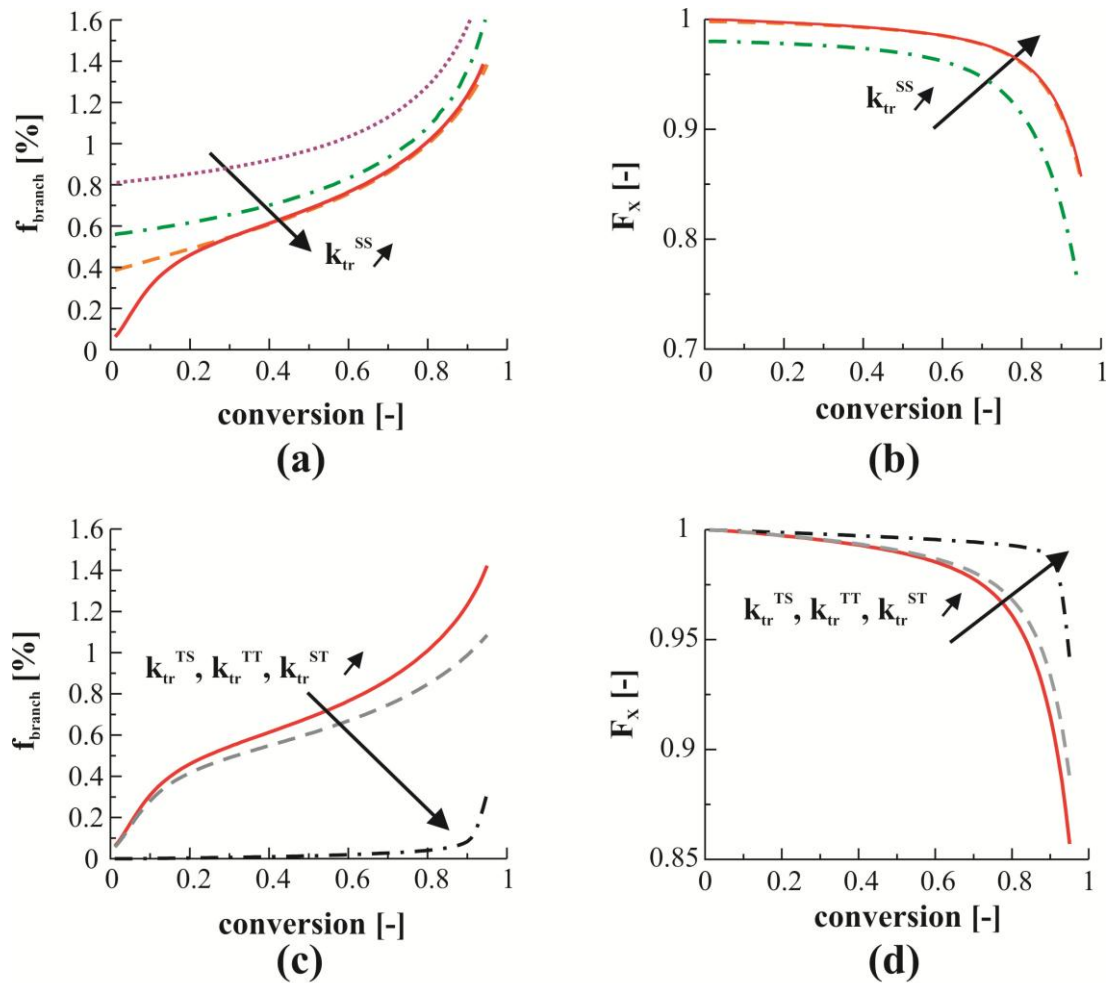


Figure 5.8: Simulated cumulative branching fractions (a,c) and RAFT CTA functionalities (b, d) at 343 K under reference conditions ($[n\text{BuA}]_0:[\text{RAFT CTA}]_0:[\text{AIBN}]_0=80:1:0.05$; 50 wt% solvent; TCL 80) (a)-(b) Influence of $k_{\text{tr}}^{\text{SS}}$: $k_{\text{tr}}^{\text{SS}} = 3 \times 10^6 \text{ L mol}^{-1} \text{ s}^{-1}$ (full red line, reference case), $k_{\text{tr}}^{\text{SS}} = 3 \times 10^5 \text{ L mol}^{-1} \text{ s}^{-1}$ (dashed orange line); $k_{\text{tr}}^{\text{SS}} = 3 \times 10^4 \text{ L mol}^{-1} \text{ s}^{-1}$ (dashed-dotted green line); $k_{\text{tr}}^{\text{SS}} = 3 \times 10^3 \text{ L mol}^{-1} \text{ s}^{-1}$ (dotted purple line) (c)-(d) Theoretical evaluation of the effect of RAFT exchange of tertiary radicals for TCL 80: $k_{\text{tr}}^{\text{TS}} = 3 \times 10^6 \text{ L mol}^{-1} \text{ s}^{-1}$ (dashed-dotted black line and $k_{\text{tr}}^{\text{TS}} = 3 \times 10^2 \text{ L mol}^{-1} \text{ s}^{-1}$ (dashed grey line) versus $k_{\text{tr}}^{\text{TS}} = 0 \text{ L mol}^{-1} \text{ s}^{-1}$ (full red line; reference case). Kinetic parameters in Table I.1 in Appendix I. Kinetic model: Equation (1)-(2) and Table 5.1. TCL defined as $[n\text{Bua}]_0/[\text{RAFT CTA}]_0$.

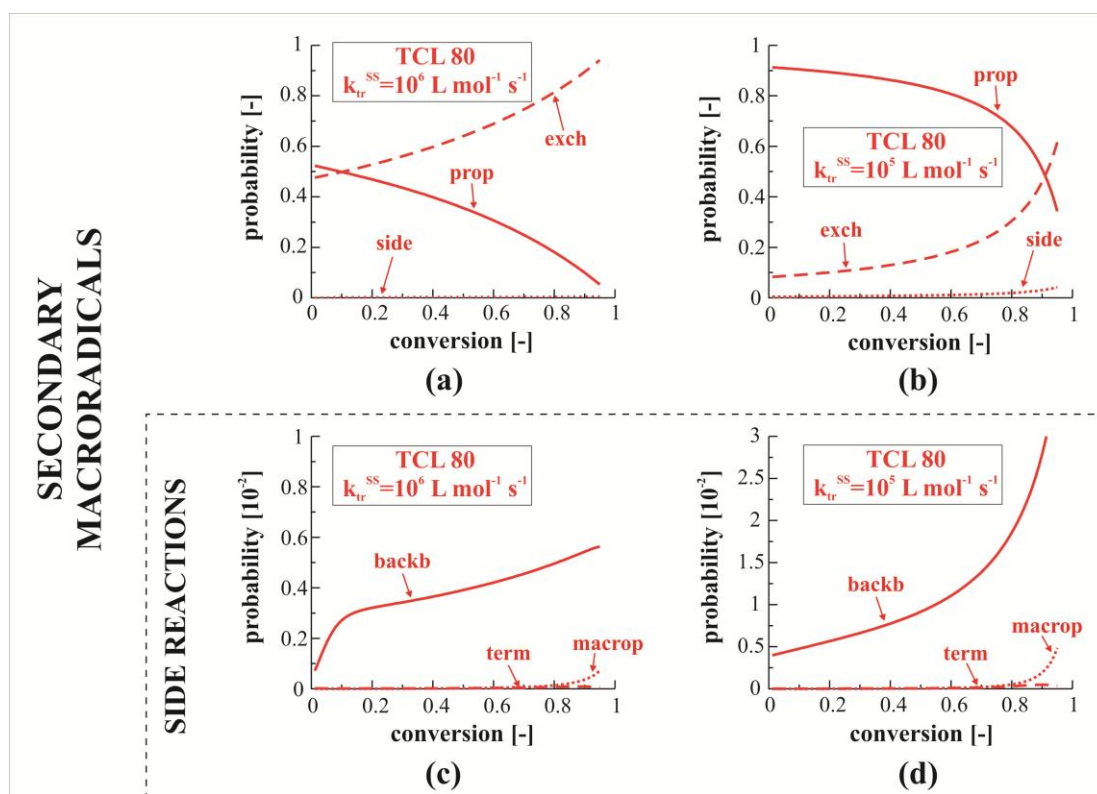


Figure 5.9: (a)-(b) Simulated reaction probabilities for propagation (full line; prop), RAFT exchange (dashed line; excl) and all side reactions (dotted line; side) of the secondary radicals in an isothermal microreactor at 343 K for $k_{tr}^{SS} = 10^6 \text{ L mol}^{-1} \text{ s}^{-1}$ and $k_{tr}^{SS} = 10^5 \text{ L mol}^{-1} \text{ s}^{-1}$. (c)-(d) Simulated reaction probabilities for backbiting (full line; backb), termination (dashed line; term) and macropropagation (dotted line; macrop) of the secondary radicals for $k_{tr}^{SS} = 10^6 \text{ L mol}^{-1} \text{ s}^{-1}$ and $k_{tr}^{SS} = 10^5 \text{ L mol}^{-1} \text{ s}^{-1}$. Note that the scale of the ordinate is different for (c) and (d). All simulations are performed under the reference conditions: $([nBuA]_0:[RAFT\ CTA]_0:[AIBN]_0 = 80:1:0.05; 50 \text{ wt\% solvent; TCL 80})$. Kinetic parameters in Table I.1 in Appendix I. Kinetic model: Equation (1)-(2) and Table 5.1. TCL defined as $[nBua]_0/[RAFT\ CTA]_0$.

Moreover, a similar reasoning holds if RAFT exchange of MCRs would not be negligible ($k_{tr}^{ST} \neq 0 \text{ L mol}^{-1} \text{ s}^{-1}$). An increase of the latter RAFT exchange reactivity ($k_{tr}^{TS}, k_{tr}^{ST}, k_{tr}^{TT}$ from $0 \text{ L mol}^{-1} \text{ s}^{-1}$, Figure 5.10a,c to $10^2 \text{ L mol}^{-1} \text{ s}^{-1}$, Figure 5.10b,d) induces no significant change in the relative probabilities for propagation (full line in Figure 5.10a-b; prop), RAFT exchange (dashed line in Figure 5.10a-b; excl) and side reactions (dotted line in Figure 5.10a-b; Figure 5.10c-d; side) of the secondary radicals. However, due to participation of the tertiary macroradicals in the RAFT exchange process (dashed line in Figure 5.10f; exclT), the

probabilities for tertiary propagation (full line in Figure 5.10e-f; propT) and side reactions (β -scission, termination; dotted line in Figure 5.10e-f; sideT) are lowered, which leads respectively to an additional reduction of f_{branch} and an increase in F_X . These effects on f_{branch} and F_X are theoretically shown in Figure 5.8c-d for $k_{tr}^{TS}, k_{tr}^{ST}, k_{tr}^{TT} = 0$ (full red line; Table 5.1), $3 \cdot 10^2$ (dashed grey line), and $3 \cdot 10^6$ (dashed-dotted black line) $\text{L mol}^{-1} \text{s}^{-1}$. Furthermore, in agreement with the ATRP kinetic modeling study of Konkolewicz *et al.*³⁶ for *n*BuA, an imbalance between the backbiting and tertiary propagation rate is established due to the participation of MCRs in the RAFT activation/deactivation process as shown in Figure 5.11 since the timescale for tertiary propagation becomes substantially larger than the timescale for tertiary RAFT exchange. In addition, in Figure 5.12, the corresponding effect of RAFT exchange of the tertiary macrospecies (k_{tr}^T ; $k_{tr}^T = k_{tr}^{TS} = k_{tr}^{ST} = k_{tr}^{TT}$) on the key polymer properties is illustrated at 343 K. Although the influence of k_{tr}^T on f_{branch} is pronounced even for low values of k_{tr}^T (Figure 5.9c), a significant effect on the dispersity and the RAFT end-group functionality (F_X) is only observed for very high values of k_{tr}^T , whereas the number average molar mass is not influenced much.

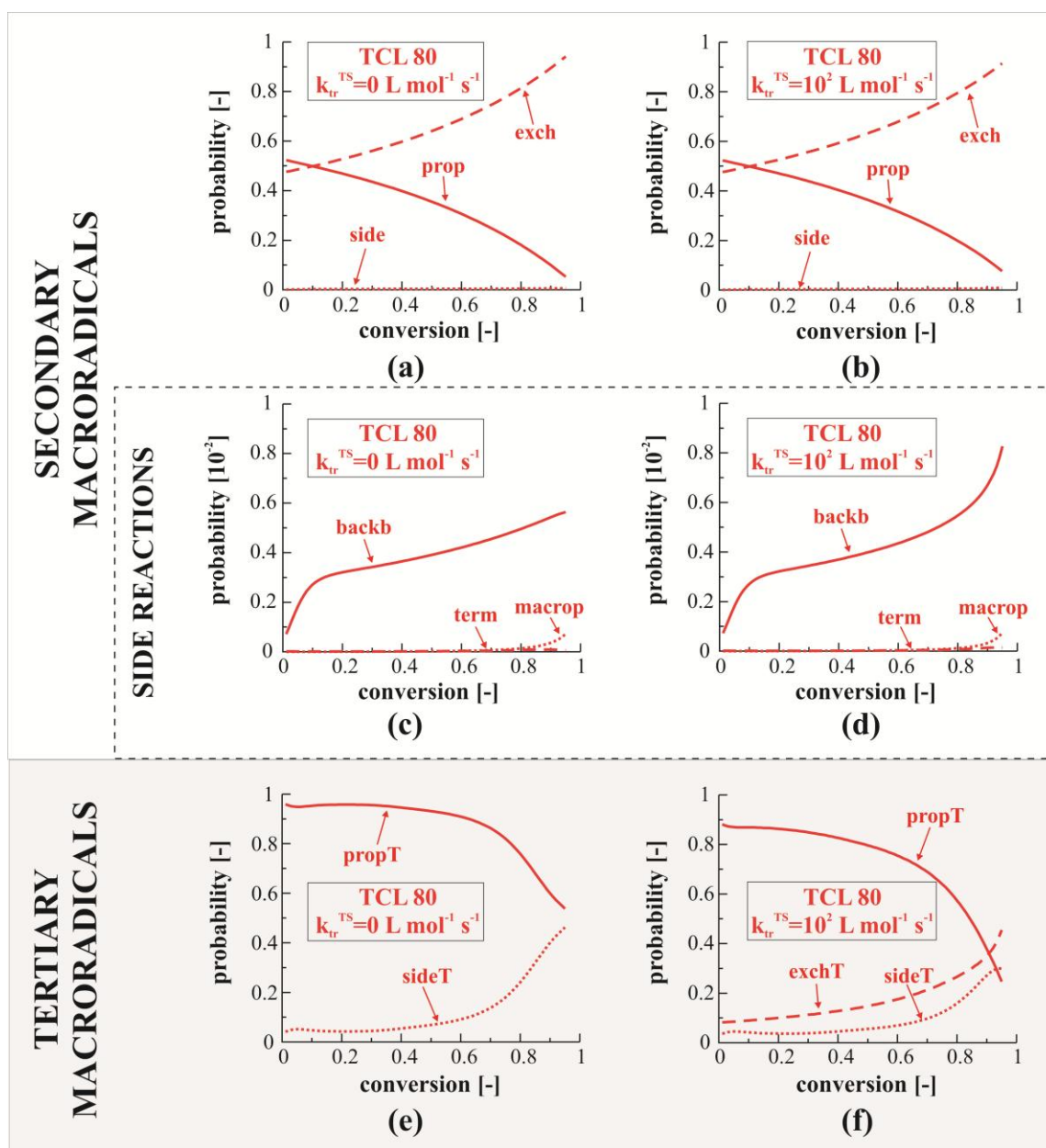


Figure 5.10: (a)-(b) Simulated reaction probabilities for propagation (full line; prop), RAFT exchange (dashed line; exch) and total side reactions (dotted line; side) of the secondary radicals in an isothermal microreactor at 343 K for $k_{tr}^{TS} = k_{tr}^{ST} = k_{tr}^{TT} = 0 \text{ L mol}^{-1} \text{ s}^{-1}$ (a) and $k_{tr}^{TS} = k_{tr}^{ST} = k_{tr}^{TT} = 10^2 \text{ L mol}^{-1} \text{ s}^{-1}$ (b). (c)-(d) Simulated reaction probabilities for backbiting (full line; backb), termination (dashed line; term) and macropropagation (dotted line; macrop) of the secondary radicals for $k_{tr}^{TS} = k_{tr}^{ST} = k_{tr}^{TT} = 0 \text{ L mol}^{-1} \text{ s}^{-1}$ (c) and $k_{tr}^{TS} = k_{tr}^{ST} = k_{tr}^{TT} = 10^2 \text{ L mol}^{-1} \text{ s}^{-1}$ (d). (e)-(f) Simulated reaction probabilities for termination (full line; termT), β -scission (dotted line; β -sc) or other side reactions (dashed line; other) of the tertiary radicals for $k_{tr}^{TS} = k_{tr}^{ST} = k_{tr}^{TT} = 0 \text{ L mol}^{-1} \text{ s}^{-1}$ (e) and $k_{tr}^{TS} = k_{tr}^{ST} = k_{tr}^{TT} = 10^2 \text{ L mol}^{-1} \text{ s}^{-1}$ (f); All simulations are performed under the reference conditions: $([n\text{BuA}]_0:[\text{RAFT CTA}]_0:[\text{AIBN}]_0=80:1:0.05; 50 \text{ wt}\% \text{ solvent}; \text{TCL } 80)$. Kinetic parameters in Table I.1 in Appendix I. Kinetic model: Equation (1)-(2) and Table 5.1. TCL defined as $[n\text{BuA}]_0/[\text{RAFT CTA}]_0$.

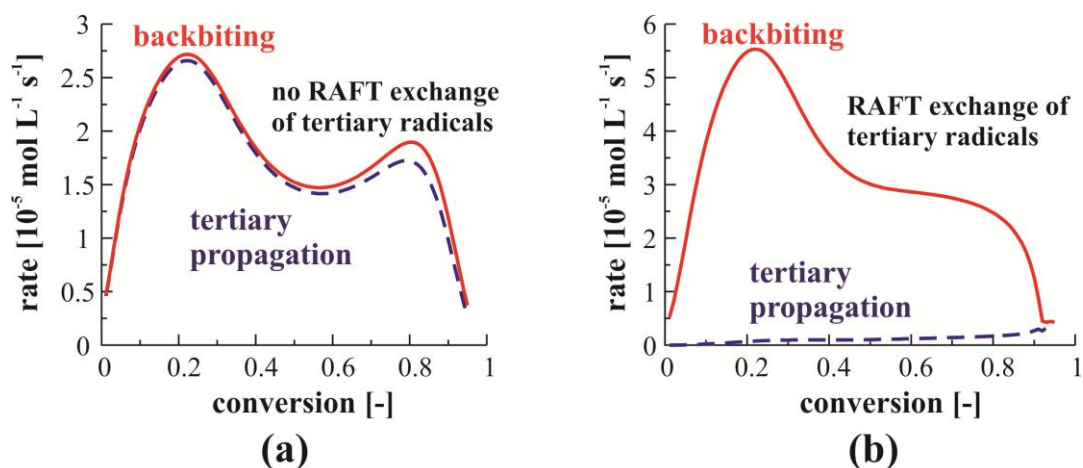


Figure 5.11: Comparison between the backbiting rate and the rate of tertiary propagation for reference conditions ($[nBuA]_0:[RAFT\ CTA]_0:[AIBN]_0=80:1:0.05$; 50 wt% solvent; TCL 80; 343 K) without ($k_{tr}^T = 0\ L\ mol^{-1}s^{-1}$) (a) and with ($k_{tr}^T = 10^6\ L\ mol^{-1}s^{-1}$) (b) RAFT exchange reactions of the tertiary radicals. Kinetic parameters in Table I.1 in Appendix I. Kinetic model: Equation (1)-(2) and Table 5.1.

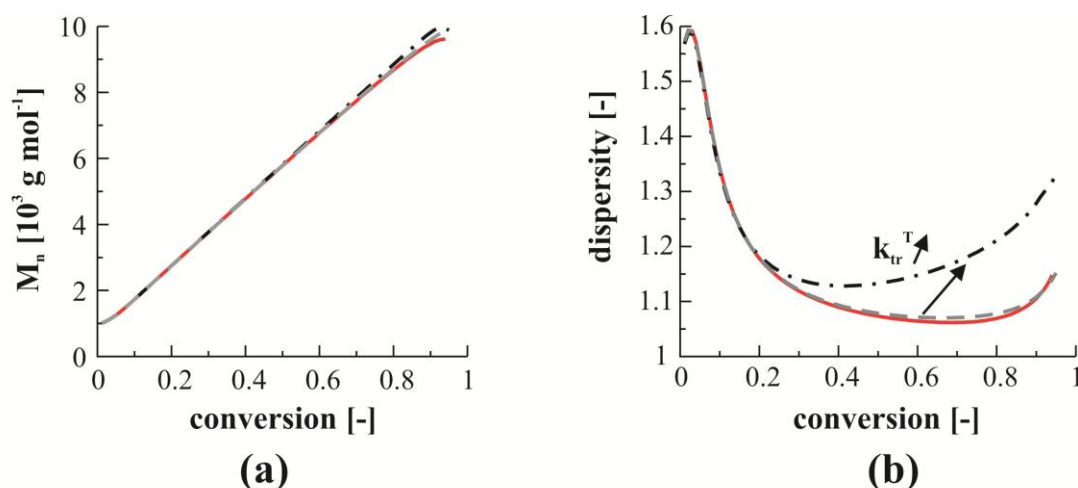


Figure 5.12: Effect of the inclusion of RAFT exchange reactions for the tertiary radicals on number average chain length (a, M_n) and the polymer dispersity (b) at 343 K under reference conditions ($[nBuA]_0:[RAFT\ CTA]_0:[AIBN]_0=80:1:0.05$; 50 wt% solvent; TCL 80). In the simulations, all the transfer rate coefficients for RAFT exchange of the tertiary radicals are assumed to be equal ($k_{tr}^{TS} = k_{tr}^{ST} = k_{tr}^{TT} = k_{tr}^T$) with the corresponding rate coefficient for the secondary radicals as the upper limiting value (k_{tr}^{SS} ; dashed red line in a-b). The lower limit ($k_{tr}^T = 0$) corresponds to the full red line in a-b. The dashed grey line represents $k_{tr}^T = 10^2\ L\ mol^{-1}s^{-1}$ and the dashed-dotted black line corresponds to $k_{tr}^T = 10^6\ L\ mol^{-1}s^{-1}$. Kinetic parameters in Table I.1 in Appendix I. Kinetic model: Equation (1)-(2) and Table 5.1.

Furthermore, Figure 5.13 shows how the conversion-time profile is affected by a variation of k_{tr}^T . Similarly as for the average polymer properties, no significant influence of the tertiary

RAFT exchange reactivity on the conversion profile is obtained for rate coefficients up to 10^2 $\text{L mol}^{-1} \text{s}^{-1}$ which corresponds with the tertiary propagation reactivity (*cf.* Table I.1 in Appendix I). A further increase of the tertiary exchange reactivity (above the tertiary propagation reactivity) induces a rate acceleration as the corresponding secondary radical concentration (λ_0) becomes slightly higher (Figure 5.13b; dashed black line versus full red line). This is caused by the corresponding higher conversion rate of tertiary macroradicals into secondary (macro)radicals by RAFT exchange reactions of the former with secondary dormant polymeric species or initial RAFT CTA, whereas for a lower tertiary RAFT exchange reactivity (from zero up to 10^2 $\text{L mol}^{-1} \text{s}^{-1}$) this conversion rate was dominated by the (slower) tertiary propagation reaction. Besides a higher secondary radical concentration, this phenomenon also induces a lower tertiary macroradical concentration (λ_0^T), as also shown in Figure 5.13b (dashed-dotted black line versus dotted red line).

Importantly, in practice, the RAFT exchange reactivity of tertiary radicals with secondary dormant polymeric species or initial RAFT CTA is expected to be significantly smaller than the corresponding secondary RAFT exchange reactivity (*cf.* Section ‘Kinetic Parameters’). Therefore, the discussed rate acceleration is very unlikely to be encountered for a real physical system. For completeness, it is shown via Figure 5.14 that also at a higher temperature of 373 K, a variation of the tertiary RAFT exchange reactivity from zero to 10^2 $\text{L mol}^{-1} \text{s}^{-1}$ does not significantly affect the simulated polymer properties and conversion profile, which enables a direct comparison with the data in Figure 5.1. This justifies the model assumption that at first instance the impact of RAFT exchange reactions involving tertiary macrospecies can be neglected.

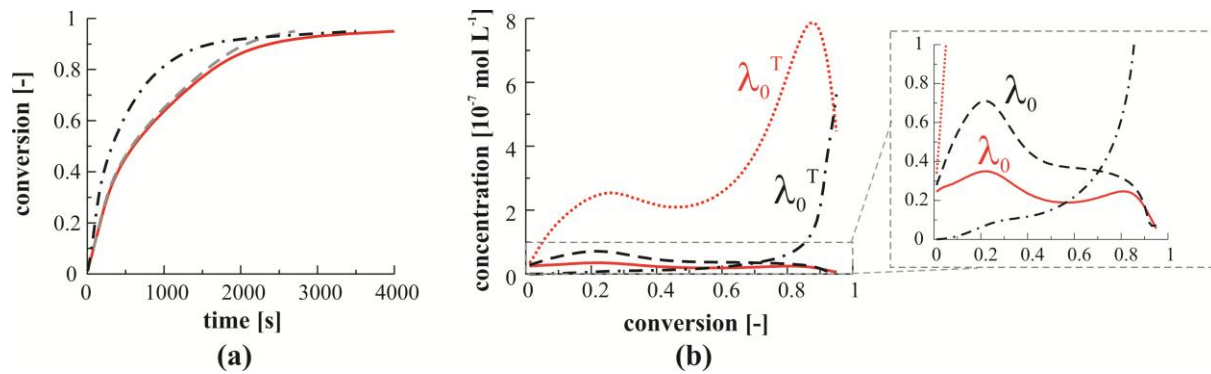


Figure 5.13: (a) Effect of the inclusion of RAFT exchange reactions for the tertiary radicals on the conversion profile at 343 K under reference conditions ($[n\text{BuA}]_0:[\text{RAFT CTA}]_0:[\text{AIBN}]_0=80:1:0.05$; 50 wt% solvent; TCL 80). In the simulations, all the transfer rate coefficients for RAFT exchange of the tertiary radicals are assumed to be equal ($k_{\text{tr}}^{\text{TS}} = k_{\text{tr}}^{\text{ST}} = k_{\text{tr}}^{\text{TT}} = k_{\text{tr}}^{\text{T}}$) with the corresponding rate coefficient for the secondary radicals as the upper limiting value. The lower limit ($k_{\text{tr}}^{\text{T}} = 0$) corresponds to the full red line. The dashed grey line represents $k_{\text{tr}}^{\text{T}} = 10^2 \text{ L mol}^{-1}\text{s}^{-1}$ and the dashed-dotted black line corresponds to $k_{\text{tr}}^{\text{T}} = 10^6 \text{ L mol}^{-1}\text{s}^{-1}$. (b) Comparison of the corresponding secondary and tertiary radical concentrations for the limiting situations: $k_{\text{tr}}^{\text{T}} = 0$ (full red line, λ_0 ; dotted red line, λ_0^{T}) and $k_{\text{tr}}^{\text{T}} = 10^6 \text{ L mol}^{-1}\text{s}^{-1}$ (dashed black line, λ_0 ; dashed-dotted black line, λ_0^{T}). The smaller figure on the right is an inset added for clarity. Other kinetic parameters in Table I.1 in Appendix I. TCL defined as $[n\text{BuA}]_0/[\text{RAFT CTA}]_0$.

Hence, it can be deduced that also the RAFT CTA type affects the degree of microstructural control, at least to a limited extent. Note that the number of branches per chain is affected in a similar way as f_{branch} by the degree of RAFT exchange of the secondary and tertiary macroradicals as shown in Appendix K.

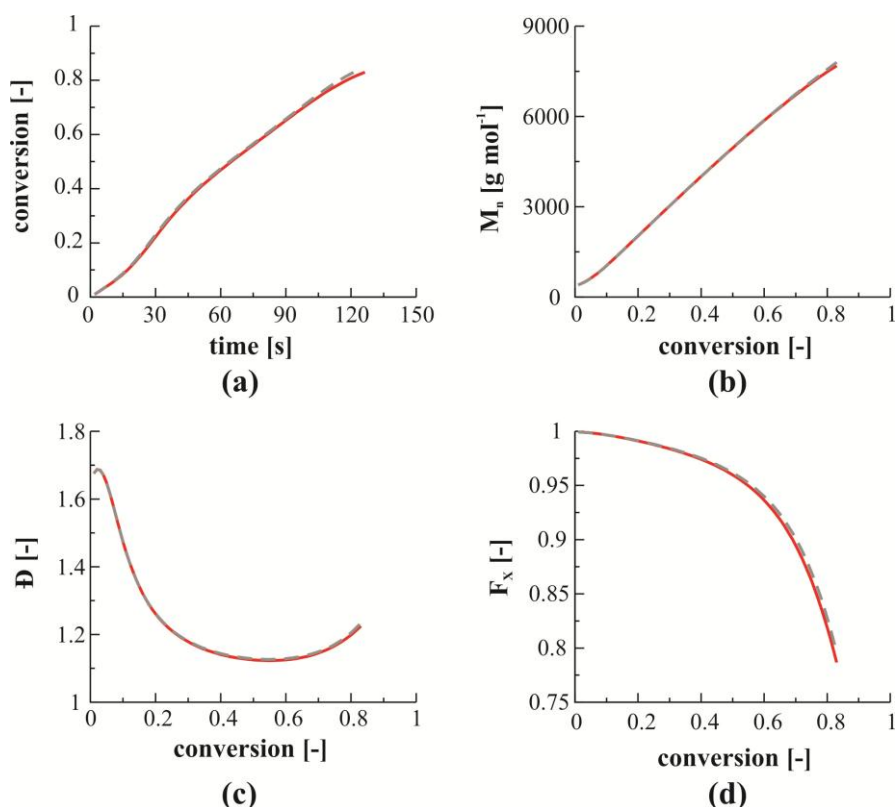


Figure 5.14: Effect of the inclusion of RAFT exchange reactions for the tertiary radicals on the conversion profile (a) and the polymer properties (b)-(d) at 373 K under reference conditions ($[n\text{BuA}]_0:[\text{RAFT CTA}]_0:[\text{AIBN}]_0=80:1:0.05$; 50 wt% solvent; TCL 80). In the simulations, all the transfer rate coefficients for RAFT exchange of the tertiary radicals are assumed to be equal ($k_{tr}^{TS} = k_{tr}^{ST} = k_{tr}^{TT} = k_{tr}^T$). The lower limit ($k_{tr}^T = 0$) corresponds to the full red line in a-d and the dashed grey line represents $k_{tr}^T = 10^2 \text{ L mol}^{-1} \text{ s}^{-1}$. Other kinetic parameters in Table I.1 in Appendix I. TCL defined as $[n\text{BuA}]_0/[\text{RAFT CTA}]_0$.

5.6 Conclusions

A deterministic kinetic model is developed to simulate and understand the kinetics of solution RAFT polymerization of *n*BuA, both in a lab-scale batch reactor and a microreactor at a set-temperature of 373 K. The isothermicity of the microreactor is the reason for the superior control over polymer properties compared to the batch reactor, in which the recorded temperature spike results in an increased contribution of side products. Moreover, in a microreactor for a given RAFT CTA, the branching level and loss of functionality can be significantly reduced by lowering the TCL, temperature and dilution degree. The simulations thus confirm that microreactors are ideally suited for advanced macromolecular design involving acrylate monomers, including the synthesis of well-defined block copolymers.

Importantly, detailed kinetic analysis also allows to determine unambiguously the different underlying causes for the effect of the microreactor conditions on the cumulative branching content and the degree of livingness.

5.7 References

- (1) Wegner, J.; Ceylan, S.; Kirschning, A. *Chemical Communications* **2011**, *47*, 4583-4592
- (2) Jensen, K. F. *Chemical Engineering Science* **2001**, *56*, 293-303
- (3) Mason, B. P.; Price, K. E.; Steinbacher, J. L.; Bogdan, A. R.; McQuade, D. T. *Chemical Reviews* **2007**, *107*, 2300-2318
- (4) Moore, J. S.; Jensen, K. F. *Angewandte Chemie-International Edition* **2014**, *53*, 470-473
- (5) Mozharov, S.; Nordon, A.; Littlejohn, D.; Wiles, C.; Watts, P.; Dallin, P.; Girkin, J. M. *Journal of the American Chemical Society* **2011**, *133*, 3601-3608
- (6) Sahoo, H. R.; Kralj, J. G.; Jensen, K. F. *Angewandte Chemie-International Edition* **2007**, *46*, 5704-5708
- (7) Hartman, R. L.; Naber, J. R.; Buchwald, S. L.; Jensen, K. F. *Angewandte Chemie-International Edition* **2010**, *49*, 899-903
- (8) Palde, P. B.; Jamison, T. F. *Angewandte Chemie-International Edition* **2011**, *50*, 3525-3528
- (9) Haven, J. J.; Vandenbergh, J.; Junkers, T. *Chemical Communications* **2015**, *51*, 4611-4614
- (10) Valera, F. E.; Quaranta, M.; Moran, A.; Blacker, J.; Armstrong, A.; Cabral, J. T.; Blackmond, D. G. *Angewandte Chemie-International Edition* **2010**, *49*, 2478-2485

- (11) Poe, S. L.; Cummings, M. A.; Haaf, M. R.; McQuade, D. T. *Angewandte Chemie-International Edition* **2006**, *45*, 1544-1548
- (12) Bally, F.; Serra, C. A.; Hessel, V.; Hadziioannou, G. *Macromolecular Reaction Engineering* **2010**, *4*, 543-561
- (13) Iwasaki, T.; Yoshida, J. *Macromolecules* **2005**, *38*, 1159-1163
- (14) Rosenfeld, C.; Serra, C.; Brochon, C.; Hadziioannou, G. *Chemical Engineering Science* **2007**, *62*, 5245-5250
- (15) Hornung, C. H.; Guerrero-Sanchez, C.; Brasholz, M.; Saubern, S.; Chiefari, J.; Moad, G.; Rizzardo, E.; Thang, S. H. *Organic Process Research & Development* **2011**, *15*, 593-601
- (16) Vandenberg, J.; Ogawa, T. d. m.; Junkers, T. *Journal of Polymer Science Part a-Polymer Chemistry* **2013**, *51*, 2366-2374
- (17) Li, X.; Wang, W.-J.; Li, B.-G.; Zhu, S. *Macromolecular Reaction Engineering* **2014**, n/a-n/a
- (18) Chan, N.; Meuldijk, J.; Cunningham, M. F.; Hutchinson, R. A. *Industrial & Engineering Chemistry Research* **2013**, *52*, 11931-11942
- (19) Zhang, X.; Xia, J. H.; Matyjaszewski, K. *Macromolecules* **2000**, *33*, 2340-2345
- (20) Boschmann, D.; Vana, P. *Macromolecules* **2007**, *40*, 2683-2693
- (21) Wang, W.; Hutchinson, R. A. *Macromolecular Reaction Engineering* **2008**, *2*, 199-214
- (22) Mai, Y.; Eisenberg, A. *Chemical Society Reviews* **2012**, *41*, 5969-5985
- (23) Lovell, P. A.; Shah, T. H.; Heatley, F. *Polymer Communications* **1991**, *32*, 98-103

- (24) Ahmad, N. M.; Britton, D.; Heatley, F.; Lovell, P. A. *Macromolecular Symposia* **1999**, *143*, 231-241
- (25) Ahmad, N. M.; Charleux, B.; Farcet, C.; Ferguson, C. J.; Gaynor, S. G.; Hawket, B. S.; Heatley, F.; Klumperman, B.; Konkolewicz, D.; Lovell, P. A.; Matyjaszewski, K.; Venkatesh, R. *Macromolecular Rapid Communications* **2009**, *30*, 2002-2021
- (26) Ahmad, N. M.; Heatley, F.; Lovell, P. A. *Macromolecules* **1998**, *31*, 2822-2827
- (27) Plessis, C.; Arzamendi, G.; Leiza, J. R.; Schoonbrood, H. A. S.; Charmot, D.; Asua, J. M. *Macromolecules* **2000**, *33*, 5041-5047
- (28) Heatley, F.; Lovell, P. A.; Yamashita, T. *Macromolecules* **2001**, *34*, 7636-7641
- (29) Junkers, T.; Barner-Kowollik, C. *Journal of Polymer Science Part a-Polymer Chemistry* **2008**, *46*, 7585-7605
- (30) Junkers, T.; Koo, S. P. S.; Davis, T. P.; Stenzel, M. H.; Barner-Kowollik, C. *Macromolecules* **2007**, *40*, 8906-8912
- (31) Guillaneuf, Y.; Gigmes, D.; Junkers, T. *Macromolecules* **2012**, *45*, 5371-5378
- (32) Wang, W.; Nikitin, A. N.; Hutchinson, R. A. *Macromolecular Rapid Communications* **2009**, *30*, 2022-2027
- (33) Zorn, A. M.; Junkers, T.; Barner-Kowollik, C. *Macromolecules* **2011**, *44*, 6691-6700
- (34) Plessis, C.; Arzamendi, G.; Alberdi, J. M.; Agnely, M.; Leiza, J. R.; Asua, J. M. *Macromolecules* **2001**, *34*, 6138-6143
- (35) Reyes, Y.; Asua, J. M. *Macromolecular Rapid Communications* **2011**, *32*, 63-67

- (36) Konkolewicz, D.; Sosnowski, S.; D'hooge, D. R.; Szymanski, R.; Reyniers, M.-F.; Marin, G. B.; Matyjaszewski, K. *Macromolecules* **2011**, *44*, 8361-8373
- (37) Konkolewicz, D.; Krys, P.; Matyjaszewski, K. *Accounts of Chemical Research* **2014**, *47*, 3028-3036
- (38) Ballard, N.; Rusconi, S.; Akhmatkaya, E.; Sokolovski, D.; de la Cal, J. C.; Asua, J. M. *Macromolecules* **2014**, *47*, 6580-6590
- (39) Ferguson, C. J.; Hughes, R. J.; Nguyen, D.; Pham, B. T. T.; Gilbert, R. G.; Serelis, A. K.; Such, C. H.; Hawket, B. S. *Macromolecules* **2005**, *38*, 2191-2204
- (40) Penzel, E.; Goetz, N. *Angewandte Makromolekulare Chemie* **1990**, *178*, 201-208
- (41) Barner-Kowollik, C. *Handbook of RAFT polymerization*; Wiley-VCH: Weinheim, 2008.
- (42) Postma, A.; Davis, T. P.; Moad, G.; O'Shea, M. S. *Macromolecules* **2005**, *38*, 5371-5374
- (43) Zhou, Y. W.; He, J. P.; Li, C. X.; Hong, L. X.; Yang, Y. L. *Macromolecules* **2011**, *44*, 8446-8457
- (44) Petzold, L. *Siam Journal on Scientific and Statistical Computing* **1983**, *4*, 136-148
- (45) Wiles, C. S., Charl. Characterisation of Labtrix 32XX devices. Chemtrix BV; 2012.
- (46) Coote, M. L.; Izgorodina, E. I.; Krenske, E. H.; Busch, M.; Barner-Kowollik, C. *Macromolecular Rapid Communications* **2006**, *27*, 1015-1022
- (47) Coote, M. L.; Krenske, E. H.; Izgorodina, E. I. *Macromolecular Rapid Communications* **2006**, *27*, 473-497
- (48) Heuts, J. P. A.; Russell, G. T. *European Polymer Journal* **2006**, *42*, 3-20

- (49) Heuts, J. P. A.; Russell, G. T.; Smith, G. B. *Australian Journal of Chemistry* **2007**, *60*, 754-764
- (50) Barth, J.; Buback, M.; Russell, G. T.; Smolne, S. *Macromolecular Chemistry and Physics* **2011**, *212*, 1366-1378
- (51) Junkers, T.; Theis, A.; Buback, M.; Davis, T. P.; Stenzel, M. H.; Vana, P.; Barner-Kowollik, C. *Macromolecules* **2005**, *38*, 9497-9508
- (52) Cortese, B.; Noel, T.; de Croon, M. H. J. M.; Schulze, S.; Klemm, E.; Hessel, V. *Macromolecular Reaction Engineering* **2012**, *6*, 507-515
- (53) Mandal, M. M.; Serra, C.; Hoarau, Y.; Nigam, K. D. P. *Microfluidics and Nanofluidics* **2011**, *10*, 415-423
- (54) Gao, Z.; He, J. *Macromolecular Reaction Engineering* **2015**, DOI: 10.1002/mren.201400061
- (55) Ballard, N.; de la Cal, J. C.; Asua, J. M. *Macromolecules* **2015**, *48*, 987-993

Chapter 6: General conclusions and future outlook

6.1 General conclusions

In this PhD thesis, kinetic modeling is applied to accurately describe reversible addition-fragmentation chain transfer (RAFT) polymerization, an important reversible deactivation radical polymerization (RDRP) technique, in order to obtain fundamental insight into the process and radical polymerization in general. Despite the broad industrial exploitation of conventional free radical polymerization (FRP), still crucial fundamental knowledge about the interplay between diffusional limitations, due to the increasing viscosity along the course of the polymerization, and the intrinsic reaction kinetics, is lacking. A fundamental description of physical transport limitations requires the consideration of ‘apparent’ kinetics at the micro-scale. In particular, termination reactions are characterized by a strong apparent reactivity.

As demonstrated in Chapter 1, accurate intrinsic and/or apparent rate coefficients are required for a proper model-based design of radical polymerization. Direct experimental measurement of these rate coefficients is recommended and has important merits in the determination of reliable propagation rate coefficients via pulsed laser polymerization (PLP) techniques and of reliable apparent *homo*-termination rate coefficients via PLP and the RAFT – chain length dependent – termination (RAFT-CLD-T) technique. Yet, in FRP, termination is dominated by *short-long*-termination reactions, for which neither an experimental protocol nor data were available and only simplified theoretical models could be applied for model-based design. Furthermore, for RAFT polymerization, which is due to its monomer versatility, mild reaction conditions, and absence of a catalyst one of the most promising RDRP techniques, reliable quantification of the different addition-fragmentation rate coefficients remains a fundamental bottleneck, hampering its industrial application.

Therefore, in the present work, novel methodologies (Chapter 2-4) have been developed to (i) reliably quantify all apparent termination rate coefficients, using RAFT polymerization as a kinetic tool and (ii) to determine for a degenerative RAFT polymerization mechanism the transfer reactivity of the initial RAFT chain transfer agent (CTA) and macro-RAFT agent, based on analytical expressions for the average polymer properties. Detailed deterministic simulations of RAFT polymerization have been employed to evaluate current literature models and provide proof of concept for the methods proposed in this PhD thesis after which they have been successfully applied to own experimental data for RAFT polymerization of methyl methacrylate (MMA) with cyano isopropyl dithiobenzoate (CPDB) as RAFT CTA and initiated by azobis(isobutyronitrile) (AIBN) at 353 K.

In Chapter 2, a generic and flexible experimental framework, based on the straightforward RAFT-CLD-T technique, is presented that not only allows to obtain reliable absolute apparent *homo*-termination coefficients but also the very first measurement of apparent *short-long*-termination rate coefficients under well-defined RAFT polymerization conditions. The generic nature of the framework is evidenced by its capability to quantify the influence of the polymer matrix, an important dynamic variable in any polymerization process. In line with previous theoretical postulations, the experimental results show that the diffusivity of the *short-chain* macroradicals dominates the *short-long*-termination reactivity. Furthermore, data analysis unveils compelling evidence for the deficiency of the currently used simplified mean models. It is, however, shown that in the studied intermediate MMA conversion range with limited matrix effects, the observed average polymer properties (*e.g.* end-group functionality) can still be approximated by these models. It should be stressed that the proposed generic methodology opens new perspectives to determine the complexity of radical polymerization kinetics and finally close the hiatus of diffusion theories to describe the diffusion of long and short macrospecies.

In Chapter 3, the analytical methods currently available in literature to determine the RAFT transfer coefficients for degenerative RAFT polymerization are re-evaluated based on the simulation of perfect experiments and their accuracy is mapped for a broad range of reaction conditions in order to provide useful guidelines for the experimentalist. It is found that no general method is available to determine accurate values for either $C_{tr,0}$ or C_{tr} under a wide range of conditions. Instead, each method is only effective for a well-defined limited range of conditions which depends on the corresponding model assumptions. Moreover, it is shown that for the RAFT exchange reactivity with macro-RAFT CTA, C_{tr} , the analytical methods currently available in literature are limited to RAFT polymerizations with equal values for $C_{tr,0}$ and C_{tr} , at full conversion of the RAFT CTA. Hence, an important future research task is the development of more detailed analytical models capable of covering a wider range of RAFT exchange reactivities.

This deficiency is redressed in Chapter 4, in which an improved method to determine RAFT transfer coefficients has been developed. In this method, the transfer reactivities are obtained by numeric solution of an analytical expression for the polymer dispersity as a function of monomer conversion, including apparent termination kinetics and a possible intrinsic/apparent chain length dependency of the RAFT addition rate coefficient. The presented method is validated *in silico* as a more accurate way to determine $C_{tr,0}$ compared to current literature models, which value can in principle be obtained from one single reliable measurement of the polymer dispersity at low monomer conversion, even for high values of $C_{tr,0}$ provided that a sufficiently high TCL is considered. Importantly, also a value for C_{tr} and its possible chain length dependency can be accessed from the same experiment at higher monomer conversions. Furthermore, the reliability of the measurements can be directly deduced via the consideration of additional convergence criteria for the numeric solution procedure. Application of the presented methodology to experimental data for RAFT

polymerization of MMA at 353 K with CPDB as RAFT CTA has led to a value for $C_{tr,0}$ of 19.85 ± 1.49 , whereas other literature methods are shown to be less reliable. For C_{tr} an approximate value of 76 is obtained and no chain length dependency is detected for the current experimental dataset.

Finally, in Chapter 6 the strength of a detailed kinetic modeling approach is illustrated by the simulation of the more complex solution RAFT polymerization of *n*-butyl acrylate in a batch and microreactor at a set-temperature of 373 K, demonstrating the cause for the better control of the polymer microstructure obtained in the latter reactor. It is found that the isothermicity of the microreactor is the reason for the superior control over polymer properties compared to the batch reactor, in which the recorded temperature spike results in an increased contribution of side products. Moreover, in a microreactor for a given RAFT CTA, the branching level and loss of functionality can be significantly reduced by lowering the TCL, temperature and dilution degree. The simulations thus confirm that microreactors are ideally suited for advanced macromolecular design involving acrylate monomers, including the synthesis of well-defined block copolymers. Importantly, detailed kinetic analysis also allows to determine unambiguously the fundamental underlying causes for the effect of the microreactor conditions on the cumulative branching content and the degree of livingness. For the first time, a complete understanding of the reduced short chain branching in acrylate polymerization under RDRP conditions is thus obtained.

6.2 Future outlook

The developed methodologies in Chapter 2 and 4 are general and can be applied to other vinylic monomers than MMA for which the degenerative transfer mechanism is valid, *i.e.* if the RAFT addition-fragmentation reactions do not significantly influence the total net production rate of radicals. In particular, the presented protocols in these chapters should be

considered as turnkey methods to determine on the one hand accurate values for both the apparent *homo*- and *short-long*-termination rate coefficients for the considered monomer, and on the other hand reliable values for the transfer coefficients of the considered (macro-)RAFT CTA/monomer system, including a possible chain length dependency.

A first desirable extension would be the application of the extended RAFT-CLD-T technique presented in Chapter 2 to determine apparent *short-long*-termination rate coefficients for MMA at 353 K under a broader range of conditions, as only four different conditions were considered in the current work in which a significant effort went to the necessary accurate description of the corresponding apparent *homo*-termination reactivity. In particular, the consideration of conditions with a larger difference between the chain lengths of the two macroradical populations in the polymerization mixture during the extended RAFT-CLD-T experiments is desired, as they tend even more towards the situation typically encountered in FRP. If in those specific cases the findings of the present work that the diffusion of the short chains determines the termination reactivity are still confirmed, a further improvement of the kinetic description of FRP could be established. However, it should be born in mind that in the application of the extended RAFT-CLD-T method for these conditions a pronounced matrix effect is expected to occur for which a proper correction factor needs to be determined, as explained in Chapter 2. Next, after a large variation of *short-long*-conditions has been covered, a re-evaluation of current diffusion theories would be possible which could have significant impact on the current understanding of apparent radical polymerization kinetics.

Secondly, it would be of high fundamental value to apply the developed protocol to determine accurate *homo*- and *short-long*-termination rate coefficients to other reaction temperatures as this directly influences the viscosity of the reaction mixture and hence the mobility of the polymer chains. Similarly, the screening of other monomers with different corresponding chain flexibility would be of high scientific value. Ideally, a library of retrieved diffusion

parameters should be established for different monomer types. Also the termination of two different homopolymer chains to form a block copolymer chain could be assessed, based on the developed method.

Another direct extension of the work in this PhD thesis would be the application of the methodology developed in Chapter 4 to determine the RAFT chain transfer reactivity to other RAFT CTA/monomer systems, in order to enable a proper classification of the latter. Such database can be a useful guide both for experimentalists working with RAFT polymerization and polymer reaction engineers. Moreover, the screening of other monomer systems and RAFT polymerization conditions could allow to confirm, for the first time experimentally, a chain length dependency of the transfer reactivity with the macro-RAFT CTA, which is shown to be accurately accessed by the developed method.

Finally, microreactor technology could be further used to determine experimental data for radical polymerization processes characterized by a high exothermicity, provided that the viscosity increase is still acceptable. Model-based design, as performed in Chapter 5, can subsequently be applied to the obtained isothermal data, opening the pathway to more efficient and tailored next-generation copolymers.

Appendix A: Modification of the RAFT-CLD-T equation for *homo*-termination

In the paragraph below, the modification of the RAFT-CLD-T equation to determine *homo*-termination rate coefficients in case the chain length distribution of the macroradicals is accounted for is discussed in detail. In particular, it is explained why a correction (Equation (9) in Chapter 2 with b a value of 1 instead of 2) is necessary in case the dispersity changes from a value of 1 to ~ 1 . In order to exclude any ambiguities, the derivation starts from the rate expression for a general elementary reaction. Gradually, the level of complexity is increased until eventually the case considering the full (non-monodisperse) chain length distribution, as encountered in an actual RAFT-CLD-T *homo*-termination experiment, is discussed.

A.1 Reaction rates for a general elementary reaction

The IUPAC definition of elementary reactions states that for a general irreversible chemical reaction as given by:¹



for a closed system the reaction rate r under constant-volume conditions is linked to the individual net disappearance rates as follows:^{2,3}

$$r = -\frac{1}{a} \frac{d[A]}{dt} = -\frac{1}{b} \frac{d[B]}{dt} = \frac{1}{p} \frac{d[P]}{dt} = \frac{1}{q} \frac{d[Q]}{dt} \quad (\text{A2})$$

In addition, based on the mass-action law of Gulberg and Waage⁴ it follows that the reaction rate is also given by:

$$r = k[A]^a[B]^b \quad (\text{A3})$$

Hence, for the basic reaction in which a , b and p are equal to one and q equals zero ($A + B \xrightarrow{k_1} P$; reference case 1), the reaction rate is given by:

$$r = -\frac{d[A]}{dt} = -\frac{d[B]}{dt} = \frac{d[P]}{dt} = k_1[A][B] \quad (\text{A4})$$

Furthermore, for the basic reaction in which a equals to two, q equals to one and all other coefficients are zero ($2A \xrightarrow{k_2} Q$; reference case 2), it holds:

$$r = -\frac{1}{2} \frac{d[A]}{dt} = \frac{d[Q]}{dt} = k_2[A]^2 \quad (\text{A5})$$

or equivalently:

$$\frac{d[A]}{dt} = -2k_2[A]^2 \quad (\text{A6})$$

A.2 Reaction rates for isolated termination by recombination reactions

When studying a single *short-long*-termination by recombination reaction $R_i + R_j \xrightarrow{k_t^{ij}} P_{i+j}$ with $i \neq j$, it follows based on Equation (A4) (example of reference case 1) that:

$$\frac{d[R_i]}{dt} = -k_t^{ij}[R_i][R_j] \quad (\text{A7})$$

Similarly, based on Equation (A5) (example of reference case 2) it follows for a single *homo*-termination by recombination reaction $2R_i \xrightarrow{k_t^{ii}} P_{2i}$ that:

$$\frac{d[R_i]}{dt} = -2k_t^{ii}[R_i]^2 \quad (\text{A8})$$

A.3 Termination by recombination reaction rates for simple case of chain length distribution involving only two chain lengths

A. Correct description

For simplicity, a macroradical distribution is first considered consisting of only two neighboring chain lengths, namely 100 and 101. Clearly, this distribution is very narrow though a dispersity not exactly equal to one is obtained. The continuity equations for both macroradicals R_{100} and R_{101} can be combined for the calculation of the contribution of termination reactions to the change of the total radical concentration $[R_{tot}]$ as follows:

$$\begin{aligned} \frac{d[R_{tot}]}{dt} &= \frac{d([R_{100}] + [R_{101}])}{dt} = \frac{d[R_{100}]}{dt} + \frac{d[R_{101}]}{dt} & \text{(A9)} \\ &= \dots + (-2 k_t^{100,100} [R_{100}]^2 - k_t^{100,101} [R_{100}][R_{101}]) \\ &\quad + (-2 k_t^{101,101} [R_{101}]^2 - k_t^{100,101} [R_{100}][R_{101}]) \end{aligned}$$

Note that a factor 2 is used for termination reactions involving identical species/chain lengths. The ellipsis in Equation (A9) and all subsequent equations (until Equation (A22)) refer to the missing terms in the considered continuity equation originating from *e.g.* propagation or chain initiation. Rearrangement leads to:

$$\frac{d[R_{tot}]}{dt} = \dots - 2 k_t^{100,100} [R_{100}]^2 - 2 k_t^{100,101} [R_{100}][R_{101}] - 2 k_t^{101,101} [R_{101}]^2 \quad \text{(A10)}$$

Hence, the expression for the average observed termination rate coefficient becomes:

$$\langle k_t \rangle = \frac{2 k_t^{100,100} [R_{100}]^2 + 2 k_t^{100,101} [R_{100}][R_{101}] + 2 k_t^{101,101} [R_{101}]^2}{([R_{100}] + [R_{101}])^2} \quad \text{(A11)}$$

taking into account that:

$$\frac{d[R_{tot}]}{dt} = \frac{d([R_{100}] + [R_{101}])}{dt} = \dots - \langle k_t \rangle ([R_{100}] + [R_{101}])^2 \quad \text{(A12)}$$

Note that it can be expected that at a given polymer mass fraction, the value of $k_t^{100,100}$ is very close to the one of $k_t^{100,101}$ and $k_t^{101,101}$ as the chain lengths involved are identical or differ only by one unit. Equation (A10) can thus be approximately rewritten as:

$$\frac{d[R_{tot}]}{dt} \approx \dots - 2 k_t^{100,100} [R_{100}]^2 - 2 k_t^{100,100} [R_{100}][R_{101}] - 2 k_t^{100,100} [R_{101}]^2 \quad (\text{A13})$$

B. Simplified description

In case the original RAFT-CLD-T technique is followed, *i.e.* assuming a dispersity of one, a mistake is made, as illustrated via the following equations. Suppose all macroradicals can be treated as chains terminating as if they were chains possessing a chain length of 100, it follows that the total radical concentration changes by termination according to:

$$\frac{d[R_{tot}]}{dt} \approx \dots - 2 k_t^{100,100} [R_{tot}]^2 \quad (\text{A14})$$

which implies:

$$\langle k_t \rangle \approx 2 k_t^{100,100} \quad (\text{A15})$$

but also:

$$\begin{aligned} \frac{d[R_{tot}]}{dt} &= \frac{d([R_{100}] + [R_{101}])}{dt} \approx \dots - 2 k_t^{100,100} ([R_{100}] + [R_{101}])^2 \\ &= \dots - 2 k_t^{100,100} ([R_{100}]^2 + 2[R_{100}][R_{101}] + [R_{101}]^2) \end{aligned} \quad (\text{A16})$$

and thus:

$$\frac{d[R_{tot}]}{dt} \approx \dots - 2 k_t^{100,100} [R_{100}]^2 - 4 k_t^{100,100} [R_{100}][R_{101}] - 2 k_t^{100,100} [R_{101}]^2 \quad (\text{A17})$$

Equation (A17) clearly **differs** from Equation (A13), because the latter equation does not contain a factor of 4 for the cross-term between R_{100} and R_{101} . Hence, Equation (A17) is inherently limited. It would only be correct if the dispersity is exactly equal to one ($[R_{101}]=0$).

As will be shown below, the induced error becomes even higher if more than 2 chain lengths are present, which can be expected under RAFT polymerization conditions.

A.4 Termination by recombination reaction rates for general case of chain length distribution involving N chain lengths

A. Correct description

For a macroradical distribution with N chain lengths, the change of the total radical concentration considering only the termination terms is obtained by summation for all chain lengths i of Equation (A18), which gives the net disappearance rate for one single macroradical with chain length i :

$$\frac{d[R_i]}{dt} = \dots - 2k_t^{ii}[R_i]^2 - \sum_{j=1, (i \neq j)}^{\infty} k_t^{ij}[R_i][R_j] \quad (\text{A18})$$

$$\begin{aligned} \frac{d[R_{tot}]}{dt} &= \frac{d \sum_{i=1}^{\infty} [R_i]}{dt} = \dots - \langle k_t \rangle [R_{tot}]^2 & (\text{A19}) \\ &= \dots - \sum_{i=1}^N 2 k_t^{ii} [R_i]^2 - \sum_{i=1}^N \sum_{j=1}^i 2 k_t^{ij} [R_i][R_j] \\ &= \dots - \sum_{i=1}^N 2 k_t^{ii} [R_i]^2 - \sum_{i=1}^N \sum_{j=1, (i \neq j)}^N k_t^{ij} [R_i][R_j] \end{aligned}$$

Assuming a relatively narrow distribution (with number average chain length i^*) it follows that approximately it holds that:

$$\begin{aligned}
\frac{d[R_{tot}]}{dt} &= \dots - \langle k_t \rangle [R_{tot}]^2 & \text{(A20)} \\
&\approx \dots - 2 k_t^{i^*i^*} \sum_{i=1}^N [R_i]^2 - k_t^{i^*i^*} \sum_{i=1}^N \sum_{j=1, (i \neq j)}^N [R_i][R_j] \\
&= \dots - k_t^{i^*i^*} \sum_{i=1}^N [R_i]^2 - k_t^{i^*i^*} \sum_{i=1}^N \sum_{j=1}^N [R_i][R_j]
\end{aligned}$$

Since the contribution of cross-termination is **dominant** as they outnumber by far the homo-termination terms, the first term on the right hand side for the homo-termination terms can be neglected so that the total radical concentration $\sum_{i=1}^{\infty} [R_i]$ can be directly incorporated in an elegant way as follows:

$$\begin{aligned}
\frac{d[R_{tot}]}{dt} &= \frac{d \sum_{i=1}^N [R_i]}{dt} \approx \dots - k_t^{i^*i^*} \sum_{i=1}^N \sum_{j=1}^N [R_i][R_j] & \text{(A21)} \\
&= \dots - k_t^{i^*i^*} \left(\sum_{i=1}^N [R_i] \right) \left(\sum_{j=1}^N [R_j] \right) = -k_t^{i^*i^*} \left(\sum_{i=1}^N [R_i] \right)^2 \\
&= \dots - k_t^{i^*i^*} [R_{tot}]^2
\end{aligned}$$

B. Simplified description

On the contrary, when a dispersity of one is assumed, as is the case for the original RAFT-CLD-T technique, the following equation results:

$$\begin{aligned}
\frac{d[R_{tot}]}{dt} &\approx \dots - 2 k_t^{i^*i^*} [R_{tot}]^2 & \text{(A22)} \\
&= \dots - 2 k_t^{i^*i^*} \sum_{i=1}^N [R_i]^2 - 2 k_t^{i^*i^*} \sum_{i=1}^N \sum_{j=1, (i \neq j)}^N [R_i][R_j]
\end{aligned}$$

From a comparison between the correct Equation (A20) and the false Equation (A22), it is clear that the use of Equation (A22) leads to an underestimation of the average termination rate coefficient $\langle k_t \rangle$. Note that the number of incorrect cross-terms between R_i and R_j ($i \neq j$),

$\langle \frac{N}{2} \rangle$, increases more rapidly than the number of correct *homo*-termination terms, N . Hence, the error increases when N increases. For example, for 20 distinct chain lengths, 20 *homo*-termination terms are correct but 360 cross-terms are incorrect by a factor 2. Even for the case of an ideal Poisson distribution of the macroradicals, as is the case in PLP experiments, application of Equation (A22) yields a deviation of 97% from the correct absolute value of $k_t^{i^*i^*}$.

In Equation (A21) instead, the error is in the *homo*-termination terms instead of in the *short-long*-termination terms, the latter far outnumbering the former, greatly attenuating the error. This modification is in agreement with earlier work of D'hooge *et al.*⁵ and a recent recommendation of Szymanski⁶ in which, for simplicity, the conversion and chain length dependency of the termination rate coefficient was ignored. Note that the removal of this factor 2 implies the update of Equation (A23) (original RAFT-CLD-T equation; Equation (9) in main text with $b=2$) to Equation (A24) (Equation (9) in main text with $b=1$):

$$k_t^{i^*i^*}(t) \approx \langle k_t \rangle (t) = \frac{r_{ini} - \frac{d}{dt} \left[\frac{r_{prop}(t)}{k_p([M]_0 - \int_0^t r_{prop}(t) dt)} \right]}{2 \left[\frac{r_{prop}(t)}{k_p([M]_0 - \int_0^t r_{prop}(t) dt)} \right]^2} \quad (\text{A23})$$

$$k_t^{i^*i^*}(t) \approx \langle k_t \rangle (t) = \frac{r_{ini} - \frac{d}{dt} \left[\frac{r_{prop}(t)}{k_p([M]_0 - \int_0^t r_{prop}(t) dt)} \right]}{\left[\frac{r_{prop}(t)}{k_p([M]_0 - \int_0^t r_{prop}(t) dt)} \right]^2} \quad (\text{A24})$$

A.5 References

- (1) Muller, P. *Pure Appl Chem* 1994, 66, 1077-1184

-
- (2) Connors, K. A. *Chemical Kinetics*; VCH Publishers: New York, 1990.
- (3) Marin, G. B. Y., G. S. *Kinetics of Chemical Reactions*; Wiley-VCH: Weinheim, 2011.
- (4) Waage, P.; Gulberg, C. M. *J Chem Educ* 1986, 63, 1044-1047
- (5) D'Hooge, D. R.; Reyniers, M. F.; Marin, G. B. *Macromol React Eng* 2009, 3, 185-209
- (6) Szymanski, R. *Macromolecular Theory and Simulations* 2011, 20, 8-12

Appendix B: Detailed discussion on the determination of the RAFT-CLD-T *homo*-termination surface (Figure 2.4)

B.1 Limited impact of volume contraction during RAFT-CLD-T measurement of homo-termination rate coefficients

The calculation of the volume contraction during the polymerization is based on the following densities of MMA (ρ_{MMA}) and PMMA (ρ_{PMMA}) calculated at a T of 80 °C:^{1,2}

$$\rho_{PMMA} = 1.188 - 1.34 * 10^{-4} T - 0.91 * 10^{-6} T^2$$

$$\rho_{MMA} = 0.8721 \text{ g mL}^{-1}$$

In general, Equation (9) in Chapter 2 should be further modified to account for this effect, as Equation (10) in Chapter 2 should be:

$$\frac{1}{V} \frac{d[R_{tot}V]}{dt} = r_{ini} - \langle k_t \rangle [R_{tot}]^2 \quad (\text{B1})$$

and thus:

$$\begin{aligned} \frac{d[R_{tot}]}{dt} &= r_{ini} - \langle k_t \rangle [R_{tot}]^2 - \frac{[R_{tot}]}{V} \frac{dV}{dt} \\ &= 2fk_d[I_2] - \langle k_t \rangle [R_{tot}]^2 - \frac{[R_{tot}]}{V} \frac{dV}{dt} \end{aligned} \quad (\text{B2})$$

Also the continuity equation to calculate the initiator concentration $[I_2]$ needs a correction:

$$\frac{1}{V} \frac{d[I_2V]}{dt} = -k_d[I_2] \quad (\text{B3})$$

yielding:

$$[I_2] = \frac{V_0}{V} [I_2]_0 e^{-k_d t} \quad (\text{B4})$$

The corrected RAFT-CLD-T equation becomes:

$$\langle k_t \rangle (t) \quad (\text{B5})$$

$$= \frac{\frac{V_0}{V} [I_2]_0 e^{-k_{at}} - \frac{d}{dt} \left[\frac{r_{prop}(t)}{k_p ([M]_0 - \int_0^t r_{prop}(t) dt)} \right] - \frac{1}{V} \left[\frac{r_{prop}(t)}{k_p ([M]_0 - \int_0^t r_{prop}(t) dt)} \right] \frac{dV}{dt}}{\left[\frac{r_{prop}(t)}{k_p ([M]_0 - \int_0^t r_{prop}(t) dt)} \right]^2}$$

The influence of this volume contraction on the termination rate coefficients as obtained via the RAFT-CLD-T technique is however limited for intermediate polymer mass fractions, but becomes significant (> 10 % deviation) when exceeding a polymer mass fraction of 0.5. This is illustrated in Figure B.1 which plots the ratio of the calculated *homo*-termination rate coefficient with (Equation (B5)) and without inclusion of the volume contraction (Equation (9) in Chapter 2) for a conventional *homo*-termination RAFT-CLD-T experiment (blue line) and a modified *homo*-termination RAFT-CLD-T experiment containing also a certain amount of dead PMMA standard (red line; see further). In the present work, all the presented data have been corrected for this volume contraction during the polymerization reaction by application of Equation (B5).

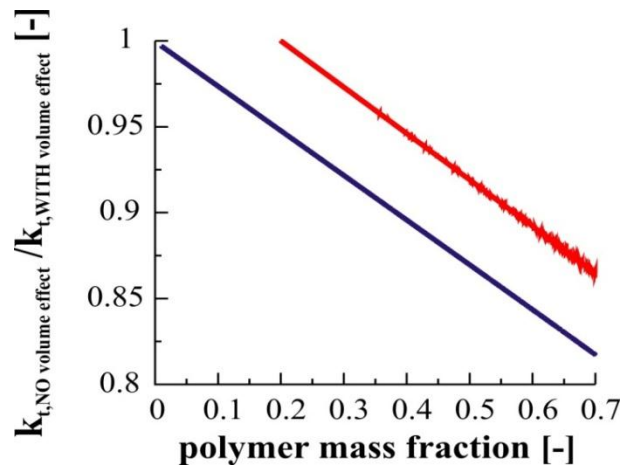
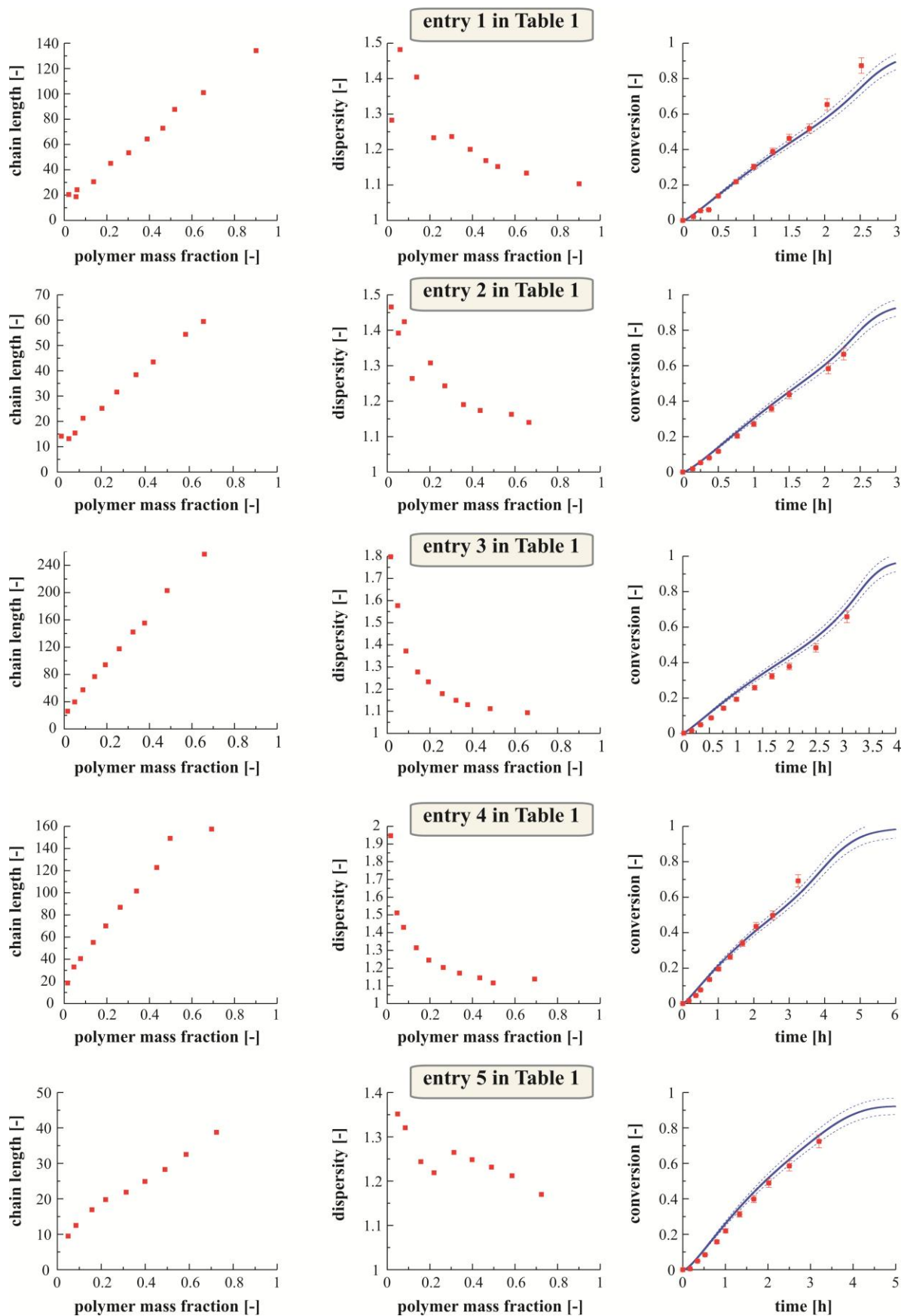
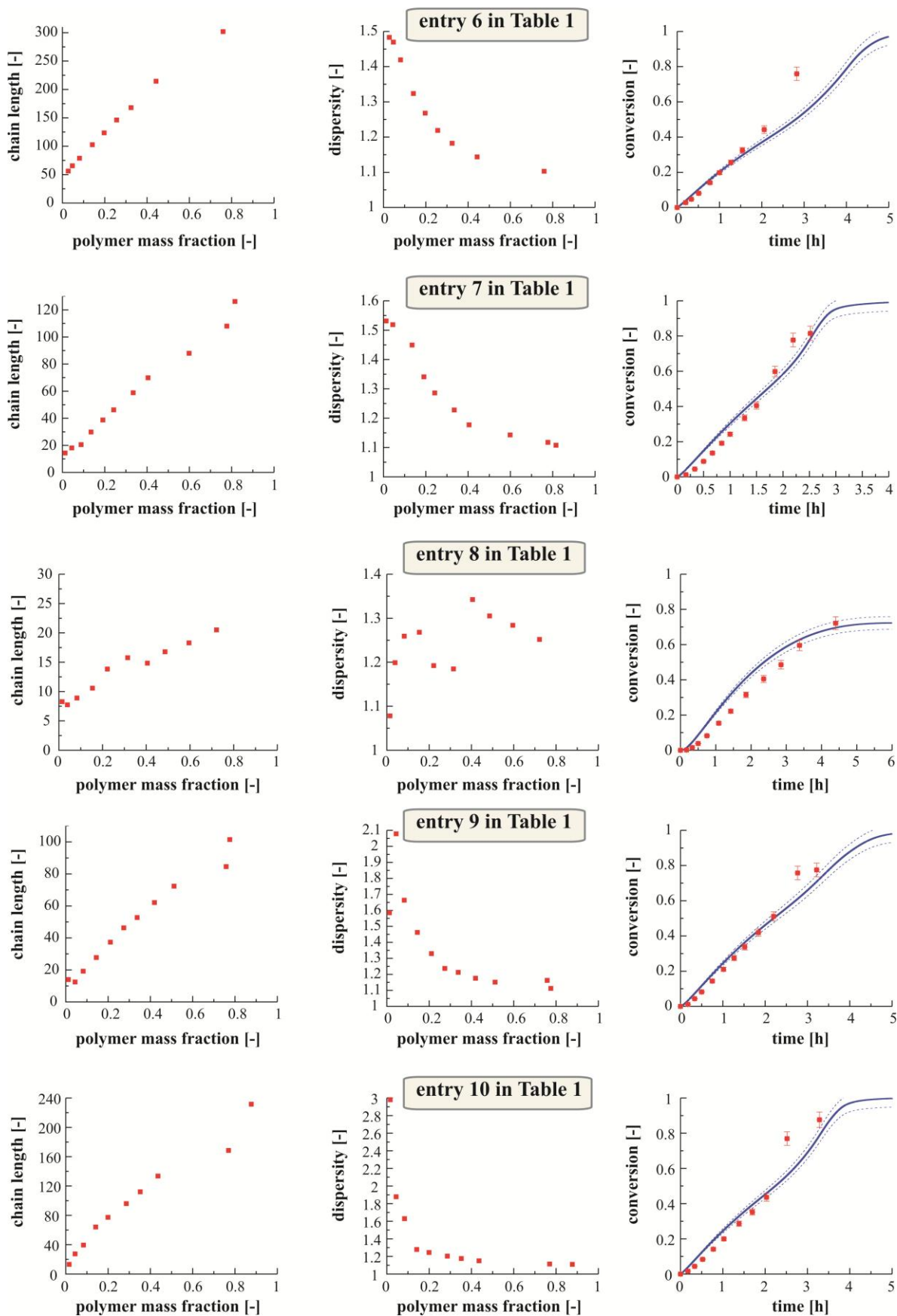


Figure B.1: Influence of volume contraction on the *homo*-termination rate coefficient. Ratio of value obtained via the RAFT-CLD-T technique through Equation (9) in Chapter 2, i.e. without any volume effect taken into account, to the value obtained with Equation (B5), i.e. with inclusion of the volume contraction; conditions: entry 7 in Table 2.1 (blue line) and entry 17 in Table 2.1 (red line).

B.2 Reliability of RAFT-CLD-T homo-termination experimental data

In accordance with the IUPAC guideline^{3,4} that for each k_t measurement the corresponding polymer matrix should be specified, and to prove the reliability of the performed k_t -measurements and consequently the fitted $k_t^{i^*i^*}$ surface function, in Figure B.2 for all RAFT-CLD-T *homo*-termination experiments the chain length, dispersity and conversion data are plotted. For the latter, both the on-line DSC results (full blue line) and off-line ¹H-NMR data (red squares) are shown together with their respective scatter.





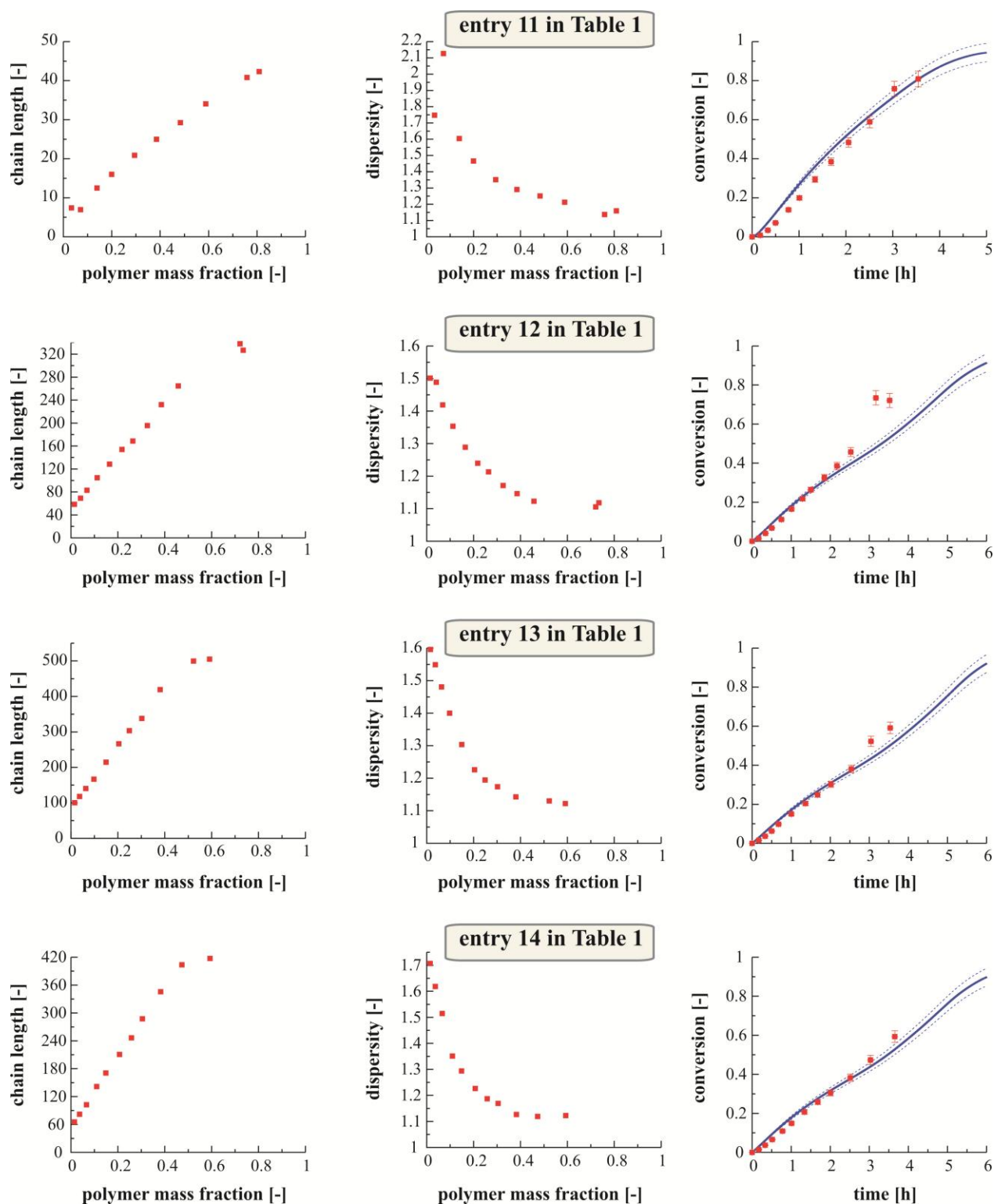


Figure B.2: Number average chain length (left), dispersity (middle) and conversion data (right) for all performed RAFT-CLD-T homo-termination experiments: entry 1-14 in Table 2.1 in Chapter 2. For the conversion results, both the on-line DSC (full blue line) and the off-line $^1\text{H-NMR}$ data (red squares) are shown together with their respective error.

B.3 Propagation of uncertainty analysis (Figure 2.4b in Chapter 2)

The propagated uncertainty on the input parameters of the RAFT-CLD-T method when processing the DSC data to obtain the average termination rate coefficients is calculated via the following general formula:⁵

$$[\Delta g(x_1, x_2, x_3, \dots, x_N, C)]^2 = \sum_{i=1}^N \left(\frac{\delta g}{\delta x_i} \right)^2 (\Delta x_i)^2 \quad (\text{B6})$$

in which g is a certain function of the input parameters x_i and a constant C . Δ refers to the uncertainty on that specific function or parameter. Note that this equation only holds in case the errors in the parameters x_i are random and independent, the latter implying that the covariance between all the parameters is zero.

Starting from the input parameters and their uncertainty in Table 2.3 in Chapter 2, for each single calculation in the processing of the DSC results, Equation (B6) is applied to calculate the corresponding propagated error. Commonly applied derivatives of Equation (B6) are:

$$[\Delta(x_1 + x_2 + C)]^2 = (\Delta x_1)^2 + (\Delta x_2)^2 \quad (\text{B7})$$

$$\left[\frac{\Delta \left(\frac{x_1 x_2}{x_3 x_4} \right)}{\left(\frac{x_1 x_2}{x_3 x_4} \right)} \right]^2 = \left(\frac{\Delta x_1}{x_1} \right)^2 + \left(\frac{\Delta x_2}{x_2} \right)^2 + \left(\frac{\Delta x_3}{x_3} \right)^2 + \left(\frac{\Delta x_4}{x_4} \right)^2 \quad (\text{B8})$$

$$\frac{\Delta(x_1^n)}{x_1^n} = |n| \left(\frac{\Delta x_1}{x_1} \right) \quad (\text{B9})$$

B.4 Regression of the improved homo-termination surface (Figure 2.4c in Chapter 2)

After the calculated propagated error for each RAFT-CLD-T homo-termination experiment (Figure 2.4b in Chapter 2) has been added as a random scatter to the corresponding

determined *homo*-termination rate coefficients (Figure 2.4a), a surface regression is performed using the TableCurve 3D software package, yielding an improved *homo*-termination surface that accounts for the uncertainty on the RAFT-CLD-T input parameters.

The surface equation is:

$$z = a + bx + c\ln(y) + dx^2 + e[\ln(y)]^2 + fx\ln(y) + gx^3 + h[\ln(y)]^3 + ix[\ln(y)]^2 + jx^2\ln(y) \quad (\text{B10})$$

in which x is the polymer mass fraction, y represents $\log(i^*)$ and z corresponds to $\log(k_t^{i^*t^*})$. In Table B.1, the parameters appearing in Equation (S38) and their respective t -values and 95% confidence intervals are listed. One should take however care when using this surface in its extrapolated regions for which no benchmark with experimental data is available. Hence, the valid region of the determined improved *homo*-termination surface is:

polymer mass fraction (x): 0.05 – 0.70 ; $\log(i^*)$ (y): 0.93 – 2.80

It can be concluded that all estimated parameters are significant and the global significance of the regression is high (F -value = 32776 \gg $F_{tabulated}=1.88$), as also confirmed by the drop lines in Figure 2.4c in Chapter 2, which reflect only minor deviations between the experimental data points and the fitted surface function (R^2 -value = 0.984).

Table B.1: Parameters of the surface function (Equation (B10)) and their respective *t*-values and 95% confidence intervals.

parameter	value	<i>t</i> -value	95% confidence limits	
			-95%	+95%
a	8.399	1101.987	8.383	8.413
b	-2.182	-32.211	-2.315	-2.049
c	-1.239	-37.546	-1.303	-1.174
d	3.916	21.269	3.555	4.276
e	1.565	18.549	1.399	1.730
f	2.879	22.940	2.633	3.125
g	-1.679	-9.854	-2.013	-1.345
h	-1.214	-16.841	-1.355	-1.072
i	0.730	4.721	0.427	1.033
j	-7.964	-45.558	-8.307	-7.622

B.5 References

- (1) Mark, J. E. *Physical Properties of Polymers Handbook*; American Institute of Physics: New York, 1996
- (2) Fan, W.; Zhou, Q.; Sun, J.; Zhang, S. J. *J Chem Eng Data* **2009**, *54*, 2307-2311
- (3) Junkers, T.; Theis, A.; Buback, M.; Davis, T. P.; Stenzel, M. H.; Vana, P.; Barner-Kowollik, C. *Macromolecules* **2005**, *38*, 9497-9508
- (4) Buback, M.; Egorov, M.; Gilbert, R. G.; Kaminsky, V.; Olaj, O. F.; Russell, G. T.; Vana, P.; Zifferer, G. *Macromol Chem Phys* **2002**, *203*, 2570-2582
- (5) Ku, H. H. *Journal of Research of the National Bureau of Standards Section C-Engineering and Instrumentation* **1966**, *C 70*, 263

Appendix C: Details on the quantification of matrix effects for the homotermination rate coefficients

C.1 Consistency of the modified RAFT-CLD-T homo-termination experiments to quantify the influence of matrix effects

Similar to the conventional RAFT-CLD-T *homo*-termination experiments (Figure B.2), in Figure C.1 the chain length, dispersity and polymer mass fraction data are shown for all the performed modified RAFT-CLD-T *homo*-termination experiments (entry 15-19 in Table 2.1 in Chapter 2). Data are only considered as long as there is a good agreement between the conversion measured via on-line DSC analysis and off-line $^1\text{H-NMR}$ spectroscopy in the parallel sampling experiment.

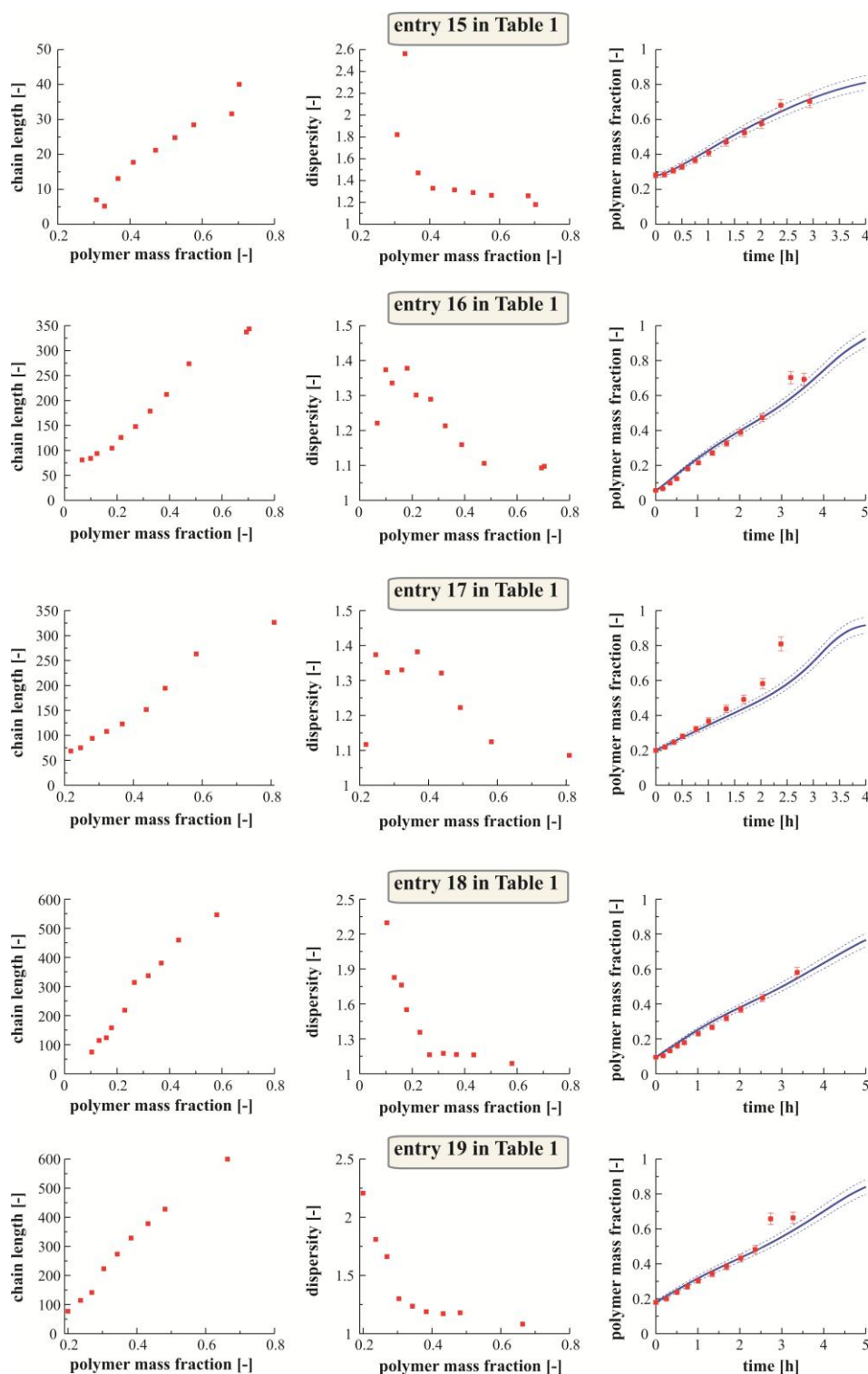


Figure C.1: Number average chain length of the terminating radicals (left), dispersity (middle) and total polymer mass fraction data (right) for all the modified RAFT-CLD-T homo-termination experiments (entry 15-19 in Table 2.1 in Chapter 2) to quantify the matrix effects, i.e. in the presence of a certain amount of dead PMMA standard. For the conversion results, both the on-line DSC (full blue line) and the off-line $^1\text{H-NMR}$ data (red squares) are shown together with their respective error, similar to Figure B.2.

C.2 Regression of the surface function to evaluate the effect of the polymer matrix (Figure 2.11c in Chapter 2)

In order to quantify the influence of the polymer matrix on the *homo*-termination rate coefficients, the ratio of *homo*-termination rate coefficients obtained in the presence of a certain amount of PMMA standard ($k_{t,NU}^{ii}$) to the corresponding *homo*-termination rate coefficients derived from the *homo*-termination surface in Figure 2.4c ($k_{t,U}^{ii}$) in Chapter 2 is considered. Due to the addition of the PMMA standard to the RAFT polymerization mixture for the modified RAFT-CLD-T experiments, two new degrees of freedom are introduced: the polymer mass fraction of PMMA standard, $w_{p,ST}$, and the chain length of the PMMA standard, i_{ST} . Since the mass average chain length j_m^* of the polymer matrix determines together with the total polymer mass fraction w_p the dynamic viscosity of the sample mixture, the surface regression is performed to the ratio between $k_{t,NU}^{ii}$ and $k_{t,U}^{ii}$ as a function of the w_p and $\log(j_m^*)$. Hence, it is assumed that the polymer matrix can be represented by its mass average chain length j_m^* and w_p .

The fitted surface function is shown in Figure C.2 and a top view is presented in Figure 2.11c in Chapter 2. From this surface it is clear that for higher chain lengths (and thus higher j_m^*) the ratio between $k_{t,NU}^{ii}$ and $k_{t,U}^{ii}$ fluctuates around 1 (green zone in Figure C.2) and the influence of the polymer matrix can thus be safely neglected. On the other hand for low chain lengths (low j_m^*) a significant effect of the polymer matrix is observed. Note that the interpolated surface is only an approximate function that enables the observation of certain trends for the considered conditions. Due to the strong fluctuations, the R^2 -value is rather low (0.453) and the deviation from the fitted surface function is indicated by drop lines. As indicated in Chapter 2, this surface function should not be used in its outer regions where no benchmark with experimental data is available. However, it should be remembered that it suffices for the considered short-long termination experiments.

For completeness, the equation of the fitted surface function and its parameter statistics are given below (Equation (C1) and Table C.1).

$$z = a + b[\ln(x)]^2 + \frac{c}{y^{1.5}} + de^{-y} \quad (\text{C1})$$

in which x is the total polymer mass fraction, y is equal to $\log(j_m^*)$ and z corresponds to $k_{t,NU}^{ii}/k_{t,U}^{ii}$. All estimated parameters are significant and the global significance of the regression is high (F -value = 385 \gg $F_{tabulated} = 1.88$)

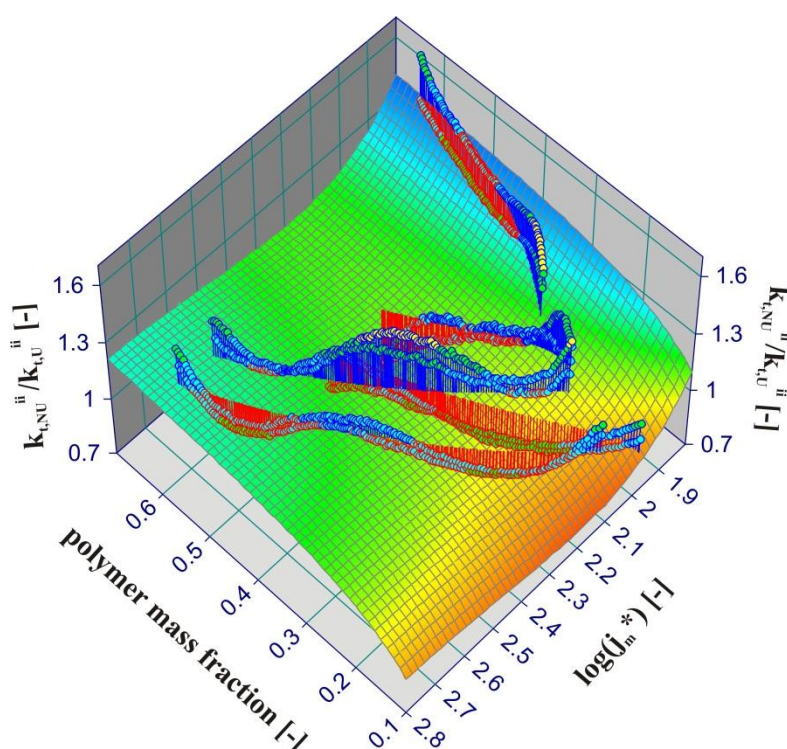


Figure C.2: Quantification of a possible effect of the polymer matrix on k_t^{ii} by the ratio of the homo-termination rate coefficient obtained via the RAFT-CLD-T technique in the presence of dead PMMA standard (non-uniform polymer matrix; $k_{t,NU}^{ii}$), to the homo-termination rate coefficient assuming a uniform polymer matrix as determined from the surface function in Figure 2.4c in Chapter 2 ($k_{t,U}^{ii}$); j_m^* : the mass average chain length of the polymer matrix.

Table C.1: Parameters of the surface function (Equation (C1)) and their respective *t*-values and 95% confidence intervals.

parameter	value	<i>t</i> -value	95% confidence limits	
			-95%	+95%
a	-5.186	-14.049	-5.910	-4.462
b	-0.062	-12.222	-0.072	-0.052
c	65.098	16.844	57.517	72.680
d	-123.010	-16.588	-137.657	-108.542

Appendix D: Detailed discussion of the RAFT-CLD-T *short-long-termination* experiments

D.1 Derivation of CTA conversion from SEC traces in RAFT-CLD-T *short-long-termination* experiments

In a *short-long-termination* experiment, the polymer matrix initially consists only of macro-RAFT CTA while during the course of the reaction, the molar fraction of conventional RAFT CTA-derived dormant species increases, and consequently two dormant populations with different average chain length result as shown in Figure D.1 (yellow and blue peak; entry 21 in Table 2.1 in Chapter 2). Eventually, when the conventional RAFT CTA is fully consumed, the molar ratio between the two dormant populations equals the initial molar ratio between the conventional RAFT CTA and the macro-RAFT CTA. Hence, after deconvolution of the SEC-traces from the *short-long-termination* experiments, a comparison between the ratio of the area of the two individual peaks (yellow and blue area in Figure D.1) and the initial molar ratio of conventional RAFT CTA to macro-RAFT CTA, yields the conventional RAFT CTA conversion (red squares in Figure D.1). Figure D.1 illustrates this for three different times during a *short-long-termination* experiment. In case of unequal transfer coefficients, from the previous section it follows that also the time variation of f_I can be directly assessed from the ratio between the individual peak areas (green triangles in Figure D.1).

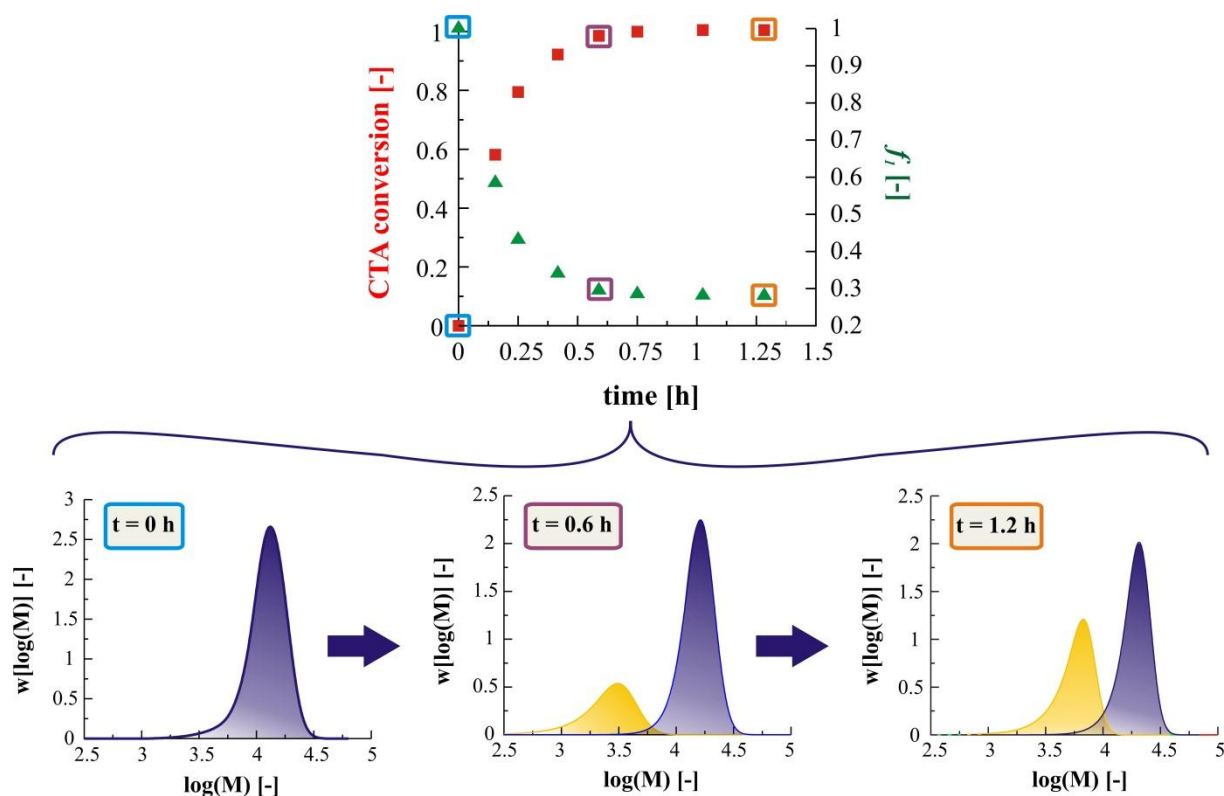


Figure D.1: Evolution of the molar mass distribution of both the short chain (yellow) and long chain (blue) dormant population during a short-long-termination experiment. The depicted individual peaks are obtained after deconvolution of the SEC-trace at three different times for entry 21 in Table 2.1 in Chapter 2. Also, the calculation of the conventional RAFT CTA conversion (red squares) and concomitant f_1 value (green triangles; in case assumed time dependent) is illustrated.

D.2 Propagated error on the measured short-long-termination rate coefficients

In order to quantify the extent of error on $k_t^{S^*L^*}$, again a complete error propagation analysis has been performed which showed that erroneous *observed* average termination rate coefficients measured via DSC or non-reliable *homo*-termination rate coefficients deduced from the $k_t^{i^*i^*}$ surface function (Figure 2.4c) have a huge impact on the accuracy of $k_t^{S^*L^*}$. Taking into account the errors on all the parameters in Table 2.3 in Chapter 2, an arbitrary error of 10% on f_1 and the confidence intervals of $k_t^{L^*L^*}$ and $k_t^{S^*S^*}$, a maximum scatter of one order of magnitude results for $k_t^{S^*L^*}$, due to the nature of Equation (8) in Chapter 2, as shown in Figure D.2 (dotted fuchsia line). However, the latter is a severe *overestimation* of the real error since the parameters in Table 2.3 in Chapter 2 have a similar influence on both the $\langle k_t \rangle$ and $k_t^{L^*L^*}$ and $k_t^{S^*S^*}$, and the experimental procedures in the RAFT-CLD-T *homo*- and *short*-

long-termination experiments are nearly identical. Hence, a better estimate for the error on the experimental *short-long*-termination rate coefficients is obtained by taking into account only the error on f_I and an additional error on the initiator efficiency covering the differences in matrix composition between $\langle k_t \rangle$, $k_t^{L^*L^*}$ and $k_t^{S^*S^*}$, resulting in a relative error of 50% on $k_t^{S^*L^*}$ (dashed fuchsia line in Figure D.2). This is comparable to the error on the *homo*-termination rate coefficients (*cf.* Chapter 2).

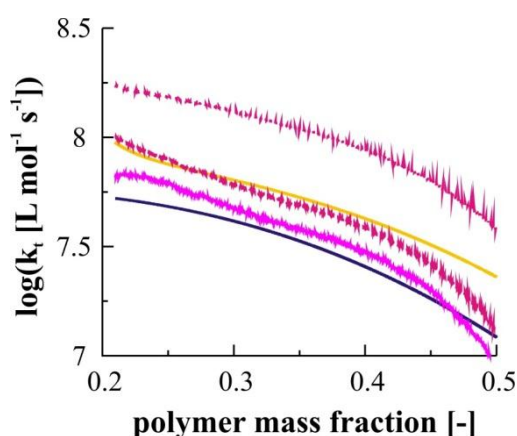


Figure D.2: Short-long-termination rate coefficient (full fuchsia line) plotted together with an estimate of its actual error (dashed fuchsia line) and the maximum error (dotted top fuchsia line; overestimation of error) calculated via a propagation of error analysis. The corresponding homo-termination rate coefficients $k_t^{L^*L^*}$ (full blue line) and $k_t^{S^*S^*}$ (full yellow line) are also shown.

D.3 Verification of the reliability of the short-long-termination data

Similar to the RAFT-CLD-T *homo*-termination experiments, the excellent agreement between the polymer mass fraction obtained via on-line DSC analysis (full blue line) and those measured by $^1\text{H-NMR}$ for a parallel off-line sampling experiment (red dots) for all performed short-long-termination experiments (entry 20-23 in Table 2.1 in Chapter 2) as shown in Figure D.3, is an absolute necessity to exclude systematic errors when coupling off-line $^1\text{H-NMR}$ and SEC ($w_{p,i}$) data with the on-line DSC based $\langle k_t(t) \rangle$ data. Moreover, the accuracy of these off-line $^1\text{H-NMR}$ and SEC ($w_{p,i}$) data has been confirmed by additional reproducibility check experiments as shown in Figure D.4 and indicated in Figure D.3 by the

red error bars. Additionally, it should be stressed that each DSC analysis has been performed at least in duplicate and only minor deviations between the resulting $\langle k_t(t) \rangle$ data were observed as shown in Figure D.5 (full green line and dashed red line). For similar reasons as the RAFT-CLD-T *homo*-termination experiments, neither the first 5% of conversion nor data above a polymer mass fraction of 0.7 will be considered. Finally, it is important to note that the $k_t^{L^*L^*}$ and $k_t^{S^*S^*}$ are within the non-extrapolated region of the *homo*-termination surface for all performed *short-long*-termination experiments, as verified in Figure D.6.

For completion, for entry 20-23 in Table 2.1 in Chapter 2 also the evolution of the number average chain length and dispersity versus the polymer mass fraction is included in Figure D.7, in accordance with IUPAC guidelines to provide details of the corresponding polymer matrix when reporting termination rate coefficients.

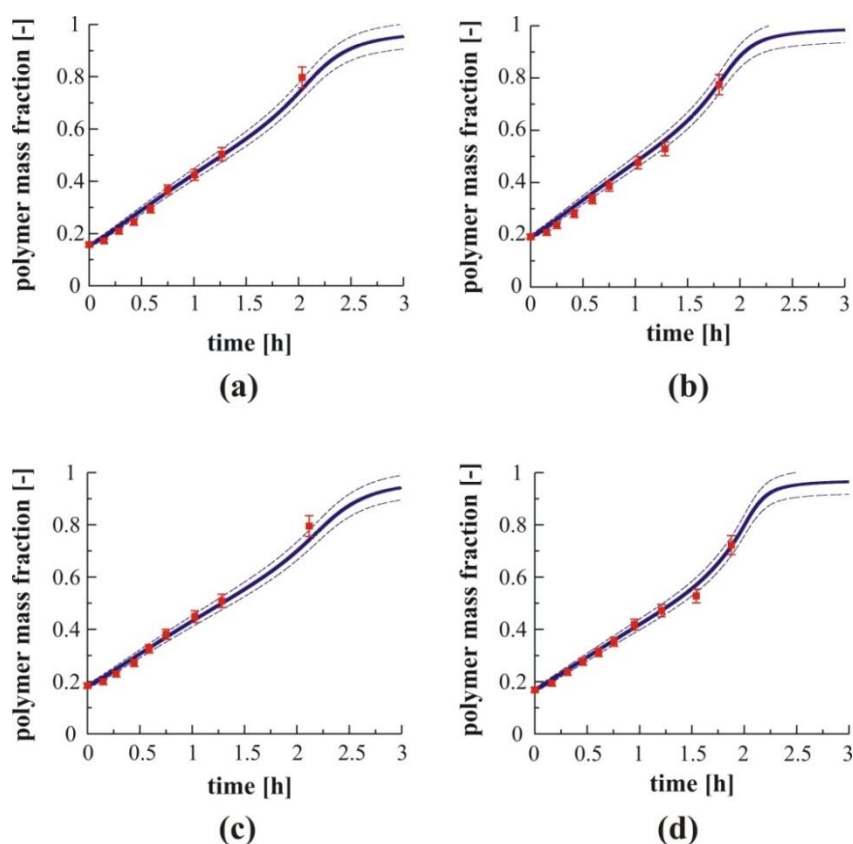


Figure D.3: Good agreement between polymer mass fraction data obtained via DSC (full blue lines) and $^1\text{H-NMR}$ sampling data (red points). 5% error for $^1\text{H-NMR}$ data (red error bars) and on-line DSC data are also indicated (dashed blue lines); conditions: entry 20-23 (a-d) in Table 2.1 in Chapter 2.

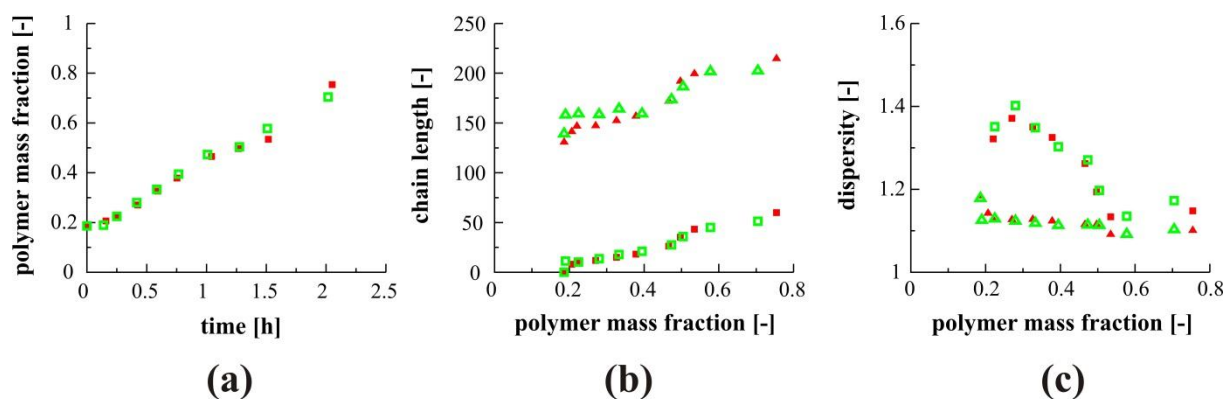


Figure D.4: Reproducibility of the RAFT-CLD-T short-long-termination experiments. Sampling data: (a) polymer mass fraction vs time; (b) number average chain length vs polymer mass fraction; (c) dispersity vs polymer mass fraction; Excellent agreement is obtained. Conditions: $[MMA]_0/[CTA_{tot}]_0 = 90$; $[CTA_{tot}]_0/[AIBN]_0 = 17$; $[macro-RAFT CTA]_0/[CTA_{tot}]_0 = 0.15$; initial CL macro-RAFT CTA = 140.

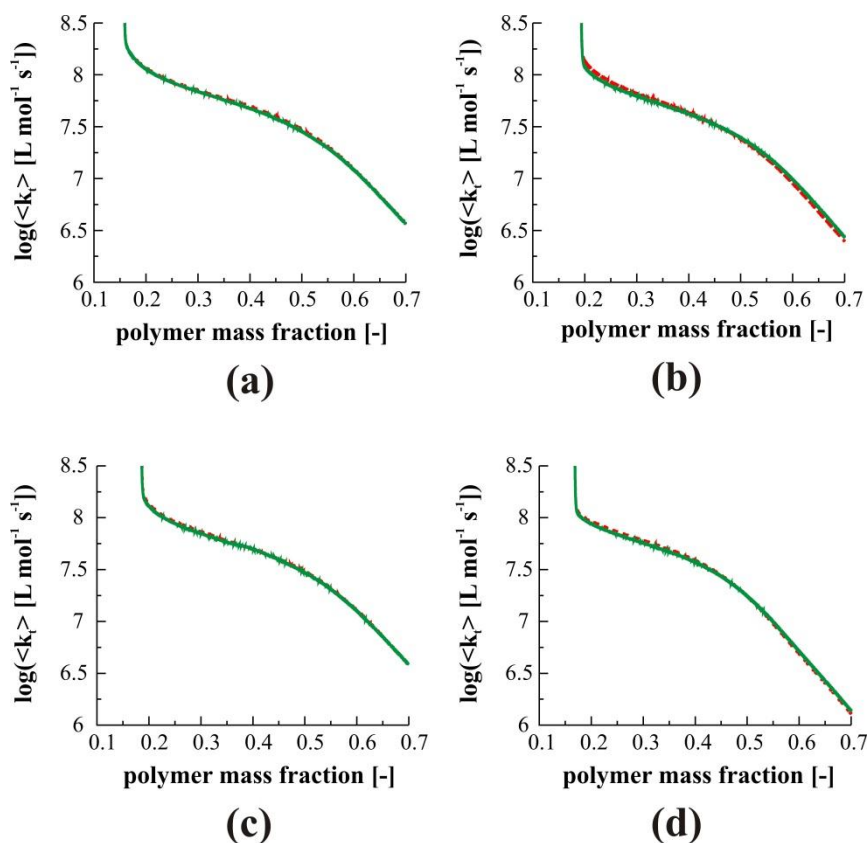


Figure D.5: Observed (overall) termination rate coefficient $\langle k_t \rangle$ measured via DSC (full green line) and its duplicate analysis (dashed red line), which almost coincide for the polymer mass fraction range of the short-long-termination experiments; conditions: entry 20-23 (a-d) in Table 2.1 in Chapter 2.

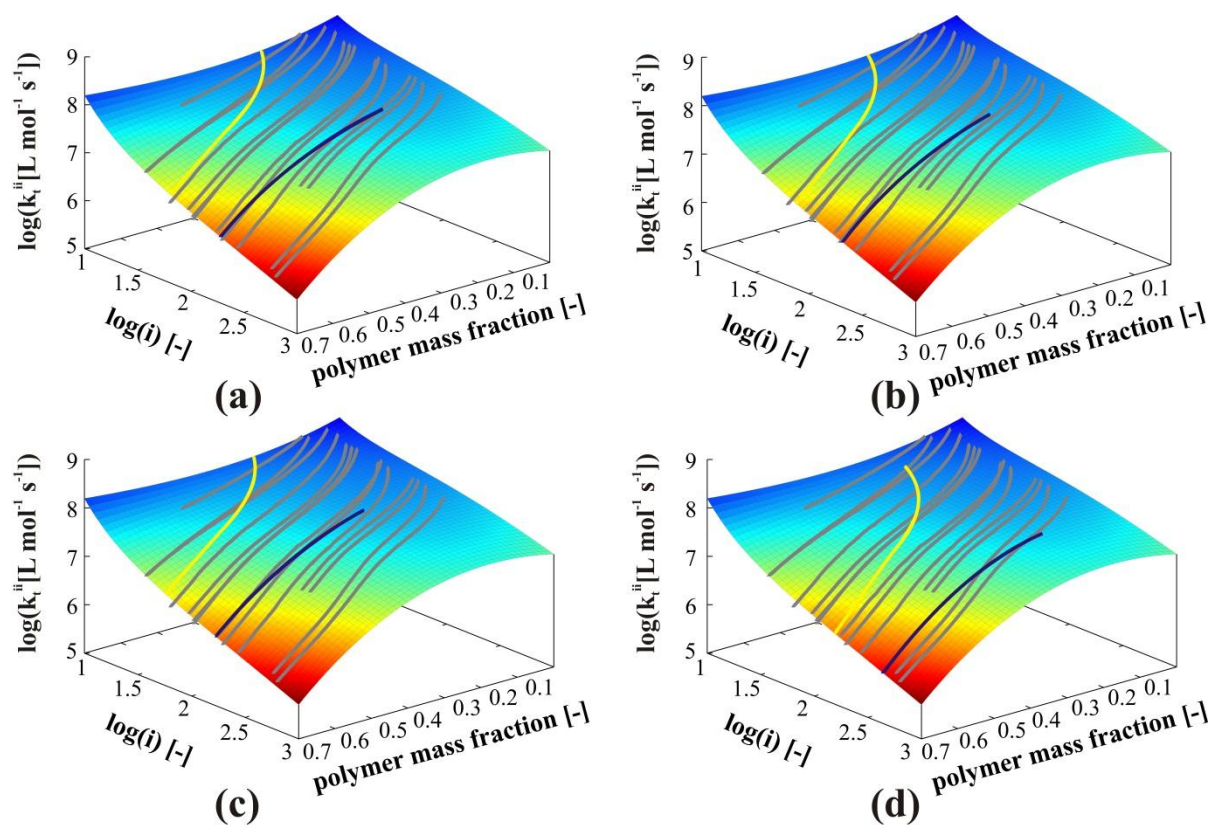


Figure D.6: Visual verification that the homo-termination rate coefficients $k_t^{S^*S^*}$ (full yellow line) and $k_t^{L^*L^*}$ (full blue line) are derived from the non-extrapolated region of the homo-termination surface (Equation (B10)) for all considered short-long-termination conditions (a-d): entry 20-23 in Table 2.1 in Chapter 2.

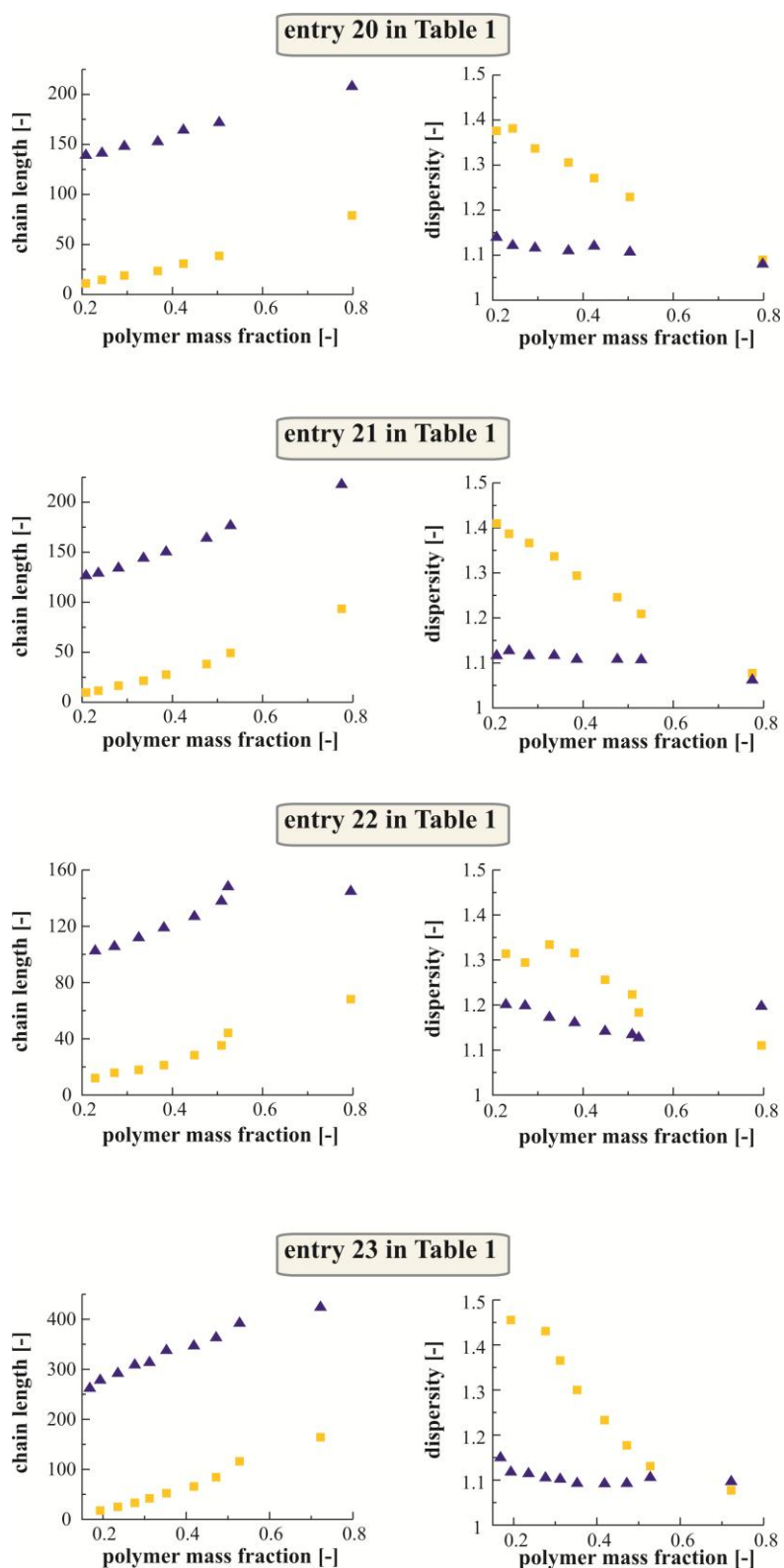


Figure D.7: Chain length and dispersity data for the performed short-long-termination experiments; entry 20-23 in Table 2.1 in Chapter 2. Yellow represents the short chain and blue the long chain distribution.

D.4 Overview of all short-long-termination results

Figure 2.13c in Chapter 2 is reproduced in Figure D.8a-d for all performed *short-long*-termination experiments (entry 20-23 in Table 2.1 in Chapter 2). Additionally, also $k_t^{S^*L^*}$ based on a time-dependent f_I value is plotted (full green line). Only at low polymer mass fractions a difference between the dotted fuchsia line ($k_t^{S^*L^*}$ based on constant f_I) and the green line ($k_t^{S^*L^*}$ based on variable f_I) can be observed. For all short-long-termination conditions $k_t^{S^*L^*}$ is approximately situated in between $k_t^{S^*S^*}$ (full yellow line) and $k_t^{L^*L^*}$ (full blue line), as predicted by diffusion theory.

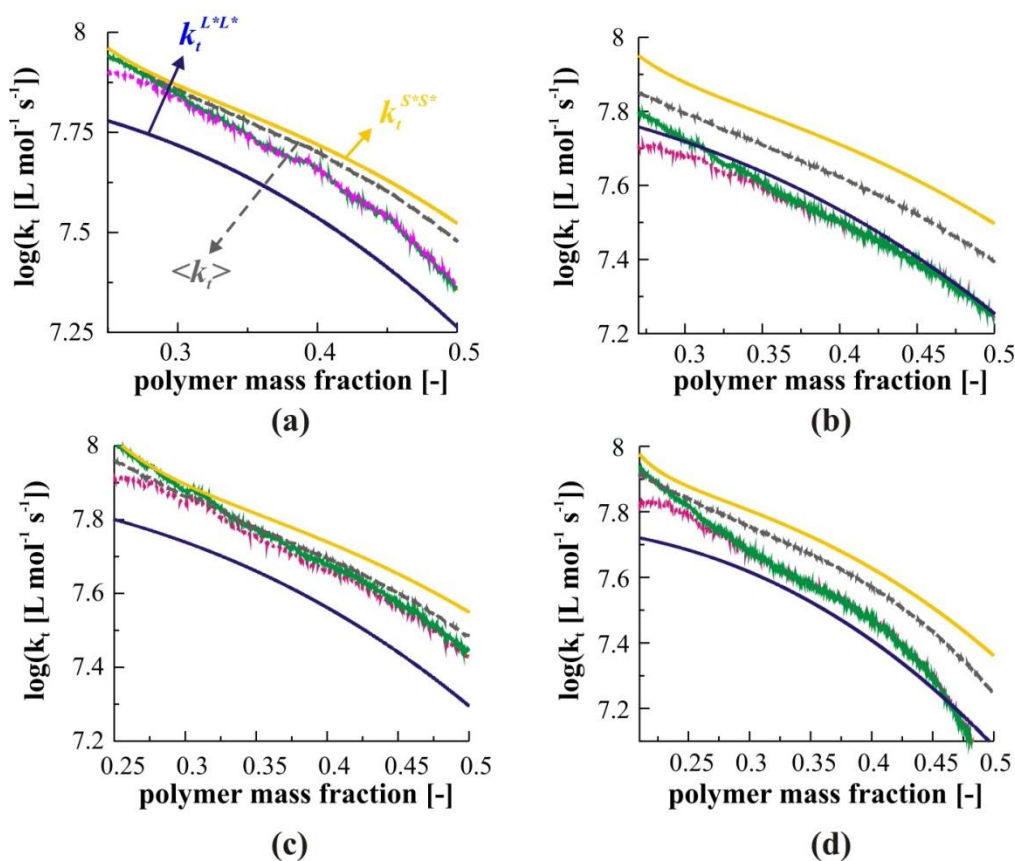


Figure D.8: (a)-(d) $k_t^{S^*L^*}$ based on a constant (dotted fuchsia line) and a variable (full green line) f_I versus the polymer mass fraction for entry 20-23 in Table 2.1 in Chapter 2. $\langle k_t \rangle$ (dashed grey line), $k_t^{S^*S^*}$ (full yellow line) and $k_t^{L^*L^*}$ (full blue line) are also plotted. (a) is similar to Figure 2.13c and 17a in Chapter 2.

Also, Figure 2.17b in Chapter 2 is reproduced in Figure D.9a-d for all performed *short-long*-termination experiments (entry 20-23 in Table 2.1 in Chapter 2). Next to $k_t^{S^*L^*}$ based on a

constant f_1 (dotted fuchsia line), also $k_t^{S^*L^*}$ based on a variable f_1 is shown (full green line). It is clear that a variable f_1 induces an even bigger deviation from the simplified mean models, both with regards to the slope and the absolute values of $k_t^{S^*L^*}$. Hence, the conclusions drawn from Figure 2.17b in Chapter 2 are even enhanced in case f_1 is time dependent. However, it should be remembered that from a relatively low polymer mass fraction onwards a constant f_1 value can be used. At a certain polymer mass fraction indicated by the dashed grey line, the slope of $k_t^{S^*L^*}$ becomes equal to the one of the simplified mean models and the termination behavior is no longer dominated by the diffusion of the short chain radicals, instead a mean behavior results.

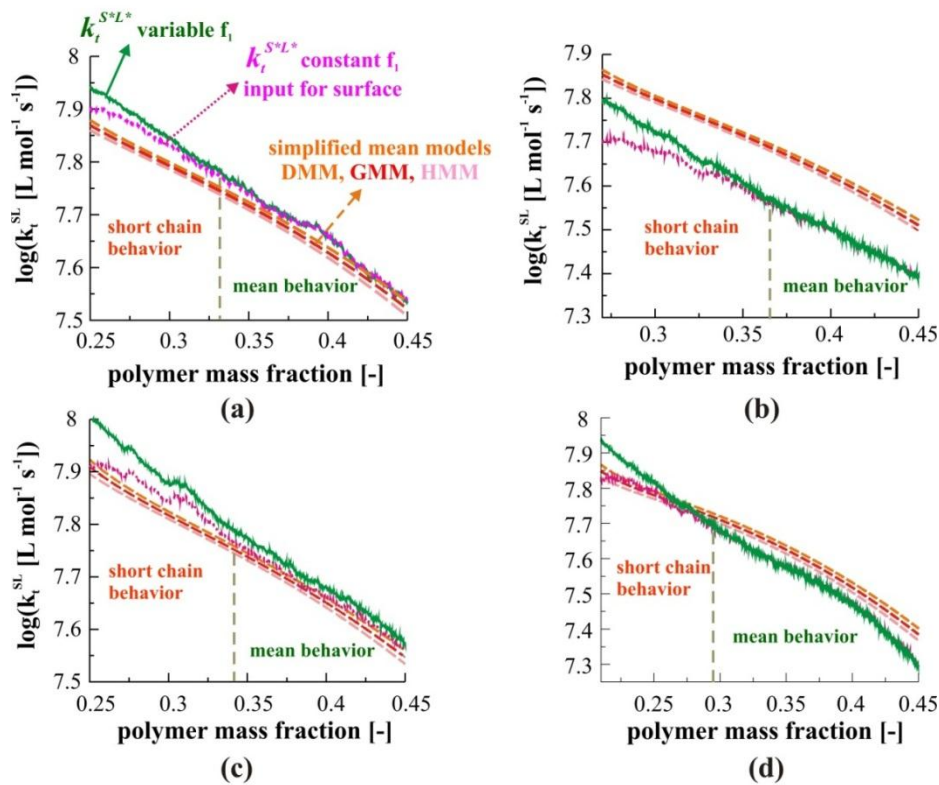


Figure D.9: Comparison between $k_t^{S^*L^*}$ and the simplified mean models for entry 20-23 in Table 2.1 in Chapter 2 (a-d): diffusion mean model (DMM; dashed orange line), geometric mean model (GMM; dashed red line) and harmonic mean model (HMM; dashed pink line). A mismatch is observed for both the slope and the absolute values at low polymer mass fractions. A time dependent f_1 induces an even bigger deviation. At a certain polymer mass fraction indicated by the dashed grey line, the slope of $k_t^{S^*L^*}$ becomes equal to the one of the simplified mean models and the termination behavior is no longer dominated by the diffusion of the short chain radicals, instead a mean behavior results.

Further evidence for the deficiency of the simplified mean models is provided by a simultaneous evaluation of all the *short-long-termination* results (entry 20-23 in Table 2.1 in Chapter 2) in Figure D.10. Clearly, the green surfaces which are obtained via regression to the measured *short-long-termination* data assuming a constant f_i (fuchsia lines) cannot be represented by the red surfaces which are constructed via a regression to the corresponding predictions of the currently used simplified mean models (Figure D.10a, DMM; D10b, GMM; D10c, HMM). For lower chain lengths, the DMM still provides a reasonable description of the true *short-long-termination* reactivity (Figure D.10a) indicating a dominance of translational diffusion of the short chain radicals. It is clear that current simplified theories to describe the *short-long-termination* reactivity fail.

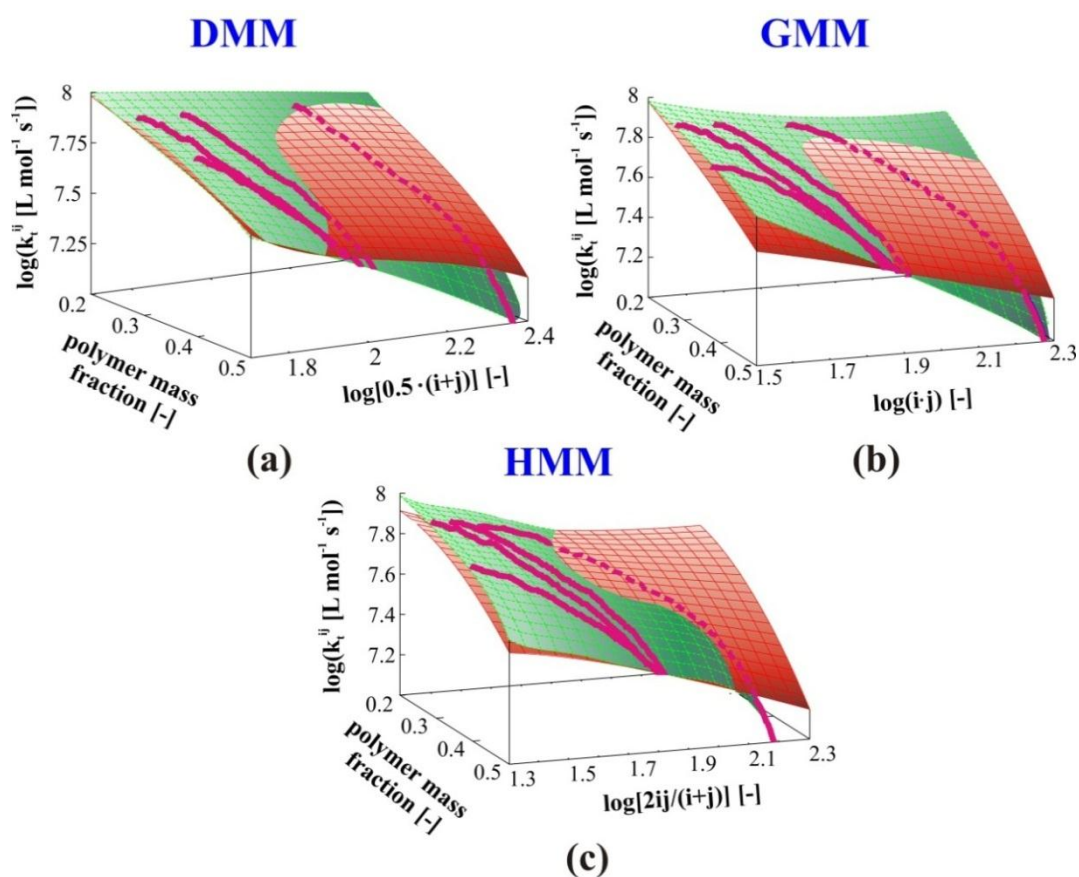


Figure D.10: Comparison between surface function (green surface) fitted to experimental $k_t^{S^*L^*}$ data for specific chain length combinations and polymer mass fractions (full fuchsia lines; entry 20-23 in Table 2.1 in Chapter 2; constant f_i) and the surface (red) as obtained considering a diffusion mean model (DMM; (a)), a geometric mean model (GMM; (b)) or a harmonic mean model (HMM; (c)). Clearly, a significant mismatch is obtained in case the simplified mean models are applied.

For completeness, the equations and regression characteristics of the green surfaces fitted to the measured *short-long*-termination data are presented below.

Comparison with DMM:

The surface equation is:

$$z = \frac{a + bx + cy}{1 + dx + ex^2 + fx^3 + gy} \quad (\mathbf{D1})$$

in which x is the polymer mass fraction, y represents $\log[0.5(S^*+L^*)]$ and z corresponds to $\log(k_t^{S^*L^*})$. In Table D.1, the parameters appearing in Equation (D1) and their respective t -values and 95% confidence intervals are listed. One should take however care when using this surface in its extrapolated regions for which no benchmark with experimental data is available. Hence, the valid region of the obtained surface is:

polymer mass fraction (x): 0.22 – 0.5 ; $\log[0.5(S^*+L^*)]$ (y): 1.75 – 2.37

It can be concluded that all estimated parameters are significant and the global significance of the regression is high (F -value = 9498 \gg $F_{tabulated}=1.88$; R^2 -value = 0.99).

Table D.1: Parameters of the surface function (Equation (D1)) and their respective t -values and 95% confidence intervals.

parameter	value	t -value	95% confidence limits	
			-95%	+95%
a	8.540	53.580	8.226	8.853
b	-9.740	-2.634	-17.019	-2.462
c	-0.933	-1.368	-2.275	0.409
d	-0.933	-1.999	-1.852	-0.014
e	-0.567	-1.604	-1.263	0.129
f	0.407	1.138	-0.297	1.111
g	-0.099	-1.094	-0.277	0.079

Comparison with GMM:

The surface equation is:

$$z = \frac{a + bx + c \ln(y)}{1 + dx + e \ln(y) + f [\ln(y)]^2} \quad (\mathbf{D2})$$

in which x is the polymer mass fraction, y represents $\log(\sqrt{S^*L^*})$ and z corresponds to $\log(k_t^{S^*L^*})$. In Table D.2, the parameters appearing in Equation (D2) and their respective t -values and 95% confidence intervals are listed. The valid region of the obtained surface is:

polymer mass fraction (x): 0.22 – 0.5 ; $\log(\sqrt{S^*L^*})$ (y): 1.54 – 2.28

It can be concluded that all estimated parameters are significant and the global significance of the regression is high (F -value = 10418 \gg $F_{tabulated}=1.88$; R^2 -value = 0.99).

Table D.2: Parameters of the surface function (Equation (D2)) and their respective t -values and 95% confidence intervals.

parameter	value	t -value	95% confidence limits	
			-95%	+95%
a	8.363	121.893	8.227	8.498
b	-5.713	-5.130	-7.905	-3.521
c	-5.237	-5.901	-6.983	-3.490
d	-0.674	-4.713	-0.955	-0.392
e	-0.521	-5.945	-0.693	-0.348
f	-0.094	-3.353	-0.150	-0.039

Comparison with HMM:

The surface equation is:

$$z = a + bx^3 + \frac{cx}{\ln(x)} + \frac{d}{\ln(x)} + ey^{1.5} + fy^2 \ln(y) + gy^{2.5} + hy^3 \quad (\mathbf{D3})$$

in which x is the polymer mass fraction, y represents $\log\left(\frac{0.5 S^* L^*}{S^* + L^*}\right)$ and z corresponds to $\log(k_t^{S^* L^*})$. In Table D.3, the parameters appearing in Equation (D3) and their respective t -values and 95% confidence intervals are listed. The valid region of the obtained surface is:

polymer mass fraction (x): 0.22 – 0.5 ; $\log\left(\frac{0.5 S^* L^*}{S^* + L^*}\right)$ (y): 1.32 – 2.19

It can be concluded that all estimated parameters are significant and the global significance of the regression is high (F -value = 13814 \gg $F_{tabulated}=1.88$; R^2 -value > 0.99).

Table D.3: Parameters of the surface function (Equation (D3)) and their respective t -values and 95% confidence intervals.

parameter	value	t -value	95% confidence limits	
			-95%	+95%
a	503.343	19.220	451.798	554.888
b	31.518	9.236	24.801	38.234
c	13.732	1.327	11.121	16.344
d	-5.040	-10.571	-5.979	-4.102
e	-18979.843	-18.877	-20958.798	-17000.888
f	-16641.334	-18.868	-18377.307	-14905.361
g	20721.076	18.877	18560.524	22881.627
h	-2236.346	-18.903	-2469.204	-2003.488

D.5 Simulation details

All the RAFT-CLD-T simulations performed in the present work are based on an in-house deterministic code including all chain length dependent population balance equations using the kinetic parameters specified in Table 2.3. The continuity equations, which allow to simulate the concentrations of the species involved, are simultaneously integrated using the numeric LSODA solver (*i.e.* Livermore Solver for Ordinary Differential Equations)¹ and hence, full chain length distributions are directly accessed. The simulation of the RAFT-CLD-

T *short-long* experiments are done in a similar fashion as Lovestead *et al.*;^{2,3} at a certain time during the simulation of a conventional RAFT polymerization usually preset by specification of the chain length, monomer, conventional RAFT CTA and initiator are added to the virtual reaction mixture. In order to enable the simulation of specific *short-long*-termination conditions, the concentrations of the macro-RAFT CTA, conventional RAFT CTA, monomer and initiator are first rescaled. From that moment onwards, the RAFT-CLD-T *in silico short-long*-experiment starts and a simultaneous growth of two macroradical populations result. Both macrospecies populations are implemented as different entities and hence, no constraints are present for their mutual transfer reactions, as is the case in the PREDICI simulations of Lovestead *et al.*^{2,3}

D.6 References

- (1) Petzold, L. Siam Journal on Scientific and Statistical Computing 1983, 4, 136-148
- (2) Lovestead, T. M.; Davis, T. P.; Stenzel, M. H.; Barner-Kowollik, C. Macromolecular Symposia 2007, 248, 82-93
- (3) Lovestead, T. M.; Theis, A.; Davis, T. P.; Stenzel, M. H.; Barner-Kowollik, C. Macromolecules 2006, 39, 4975-4982

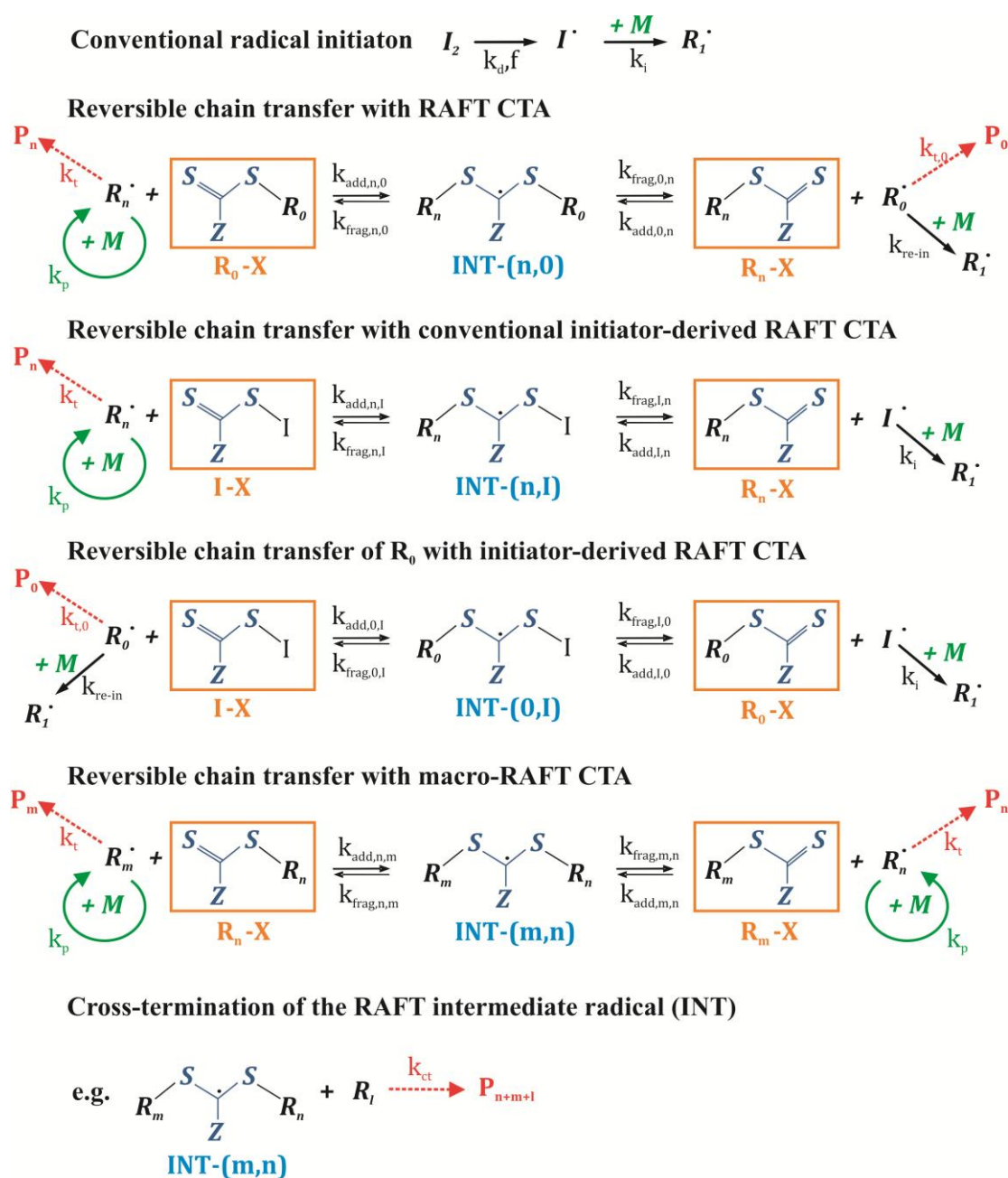
Appendix E: Full RAFT polymerization scheme and approximation via degenerative transfer mechanism

In this appendix, both the full RAFT polymerization scheme and its approximation by the degenerative transfer mechanism are discussed, focusing on the RAFT exchange reactions. A further simplification of the degenerative transfer mechanism commonly applied in kinetic studies (also throughout Chapter 3) is presented and its assumptions regarding the rate coefficients are listed. Finally, the derivation of the expression for the RAFT transfer rate coefficients in the degenerative mechanism is given.

E.1 Full RAFT polymerization scheme

In RAFT polymerization, a complex reaction scheme is established¹ as shown in Scheme E.1 with main focus on the different addition-fragmentation reactions. If the reactivity of the conventional radical initiator-derived (I^*) and RAFT CTA-derived (R_0) radicals is different, all addition and fragmentation reactions are characterized by a different rate coefficient.²⁻⁵ In particular, for the reversible chain transfer with macro-RAFT CTA (*cf.* bottom Scheme E.1), the addition rate coefficients $k_{add,n,m}$ and $k_{add,m,n}$, and the fragmentation rate coefficients $k_{frag,n,m}$ and $k_{frag,m,n}$ will be different in case they are chain length dependent, either intrinsic or apparent via diffusional limitations.⁶⁻⁹ However, for a well-controlled RAFT polymerization, and thus low dispersity of the chain length distribution (CLD), at each conversion x the RAFT polymer matrix can be approximately characterized by a single chain length so that $m(x) \approx n(x)$, and thus, $k_{add,n,m} \approx k_{add,m,n}$ and $k_{frag,n,m} \approx k_{frag,m,n}$. In case of chain length independent addition-fragmentation kinetics, always $k_{add,n,m} = k_{add,m,n}$ and $k_{frag,n,m} = k_{frag,m,n}$. In Scheme E.1, termination reactions are assumed to occur for simplicity only by disproportionation and possible “cross-termination” reactions of the RAFT intermediate radical species (INT), with itself or with propagating species, by recombination.^{10,11} Note that for the conventional radical

initiator-derived radicals no termination reactions are shown as they are comprised in the conventional radical initiator efficiency f , which by definition thus not accounts for reactions with RAFT CTA species.^{12,13}

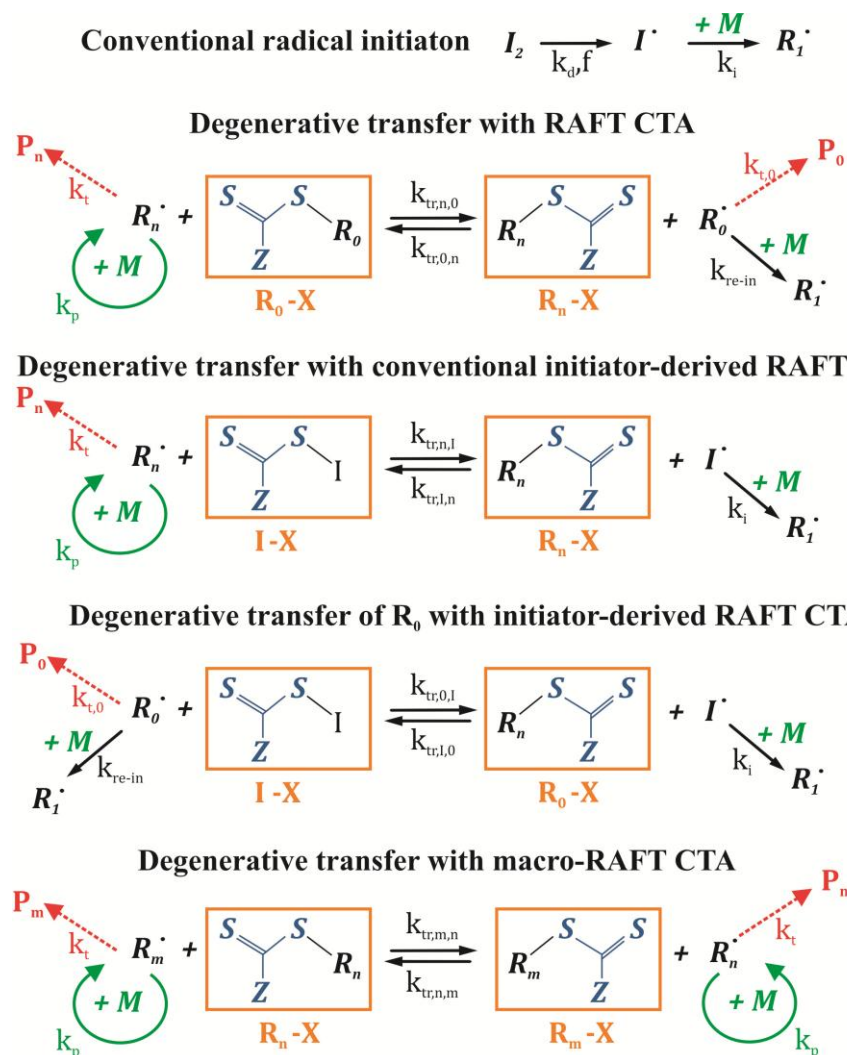


Scheme E.1: Full RAFT polymerization reaction mechanism focusing on addition-fragmentation reactions. Termination (red arrows) and propagation reactions (green arrows) are only shown in a conceptual way; efficiency f only defined for FRP reactions.

E.2 Degenerative transfer mechanism

E.1.1 Reaction scheme

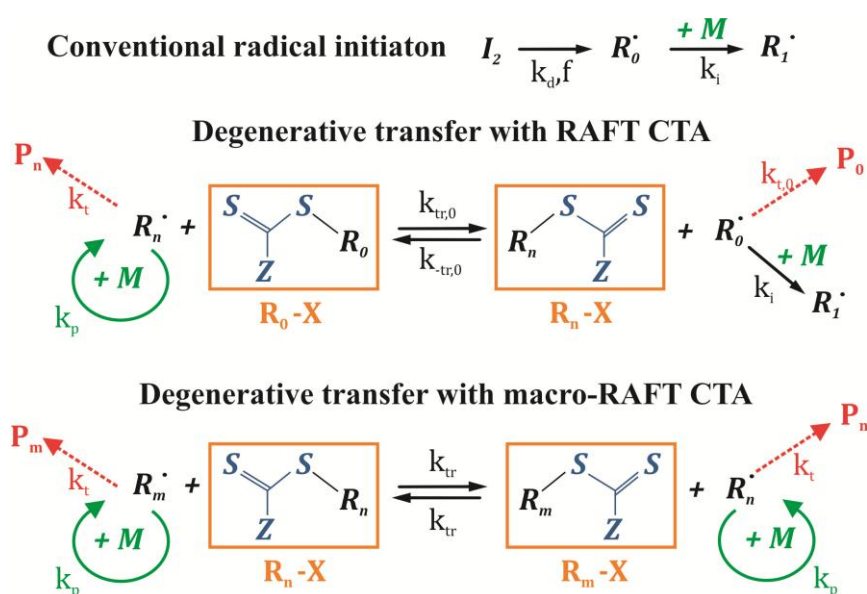
For an efficient exchange of the propagating radicals with the RAFT CTA (R_0X), the conventional radical initiator-derived RAFT CTA (IX) and the macro-RAFT CTA (R_nX), it has been shown that a degenerative transfer mechanism can safely be assumed.^{2,11} This scheme does not explicitly take into account the RAFT intermediate radicals (INT in Scheme E.1). Instead, only direct (formal) exchange reactions between propagating radicals and RAFT species are considered, ignoring any side reaction with the RAFT intermediate radical. In Scheme E.2, the equivalent of Scheme E.1 is shown in case a degenerative transfer mechanism is assumed. Each RAFT exchange reaction is characterized by a different RAFT transfer rate coefficient k_{tr} , which is an “apparent rate coefficient” which implicitly corrects for the addition/fragmentation mechanism (see further). Similarly to Scheme E.1, only in case of chain length independent RAFT transfer kinetics or a well-controlled RAFT polymerization, $k_{tr,m,n}$ can be assumed equal to $k_{tr,n,m}$.



Scheme E.2: Degenerative transfer mechanism for RAFT polymerization, focusing on the RAFT exchange reactions. Termination (red arrows) and propagation reactions (green arrows) are only shown in a conceptual way. $n, m \geq 1$.

However, for many kinetic RAFT polymerization kinetic studies, Scheme E.2 is further simplified to Scheme E.3 by neglecting the reactivity difference between the conventional initiator-derived (I^\cdot) and RAFT CTA-derived (R_0) radicals.^{5,11,14-18} Yet, since in RAFT polymerization conventional radical initiator concentrations are typically much lower (often a factor 10 or higher) than those for R_0X , the contribution of conventional initiator-derived radicals in Scheme E.2 will be small, justifying *a priori* the transition from Scheme E.2 to Scheme E.3, without consideration of a possible difference in reactivities. Moreover, in case the I^\cdot and R_0 species are identical, which is often the case for azobis(isobutyronitrile) (AIBN) initiated RAFT polymerizations, Scheme E.3 is formally equivalent to Scheme E.2. In

Scheme E.3, only three different RAFT transfer rate coefficients, *i.e.* $k_{tr,0}$, $k_{-tr,0}$ and k_{tr} , have to be considered, since it is also assumed that the degenerative transfer with macro-RAFT CTA obeys chain length independent transfer kinetics or relates to a well-controlled RAFT polymerization (see discussion above). All the methods outlined in Chapter 3 to determine the transfer reactivity in RAFT polymerization are based on Scheme E.3. Therefore, in Table E.1 an overview is given of the assumptions made for the RAFT transfer rate coefficients when approximating the full degenerative transfer scheme (Scheme E.2) by Scheme E.3.



Scheme E.3: Further simplified degenerative transfer mechanism for RAFT polymerization, focusing on the RAFT exchange reactions. Termination (red arrows) and propagation reactions (green arrows) are only shown in a conceptual way. $n, m \geq 0$; used in Chapter 3 and most RAFT polymerization kinetic studies; influence of conventional radical initiator molecules is neglected.

Table E.1: Overview of the assumptions made for the RAFT transfer rate coefficients in case the transition is made from Scheme E.2 to Scheme E.3: no distinction made between I^* and R_0 .

rate coefficient in Scheme E.2	reactants	products	value in Scheme E.3
$k_{tr,n,0}$	$R_n + R_0X$	$R_nX + R_0$	$k_{tr,0}$
$k_{tr,0,n}$	$R_0 + R_nX$	$R_0X + R_n$	$k_{-tr,0}$
$k_{tr,n,I}$	$R_n + IX$	$R_nX + I^*$	$k_{tr,0}$
$k_{tr,I,n}$	$I^* + R_nX$	$IX + R_n$	$k_{-tr,0}$
$k_{tr,0,I}$	$R_0 + IX$	$R_0X + I^*$	– ^a
$k_{tr,I,0}$	$I^* + R_0X$	$IX + R_0$	– ^a
$k_{tr,n,m}$	$R_n + R_mX$	$R_nX + R_m$	k_{tr}
$k_{tr,m,n}$	$R_m + R_nX$	$R_mX + R_n$	k_{tr}

^aIn case no distinction is made between R_0 and I^* , the reaction products are equal to the reactants. Therefore, the reaction is not included in the kinetic model.

E.2.1 Derivation of the expressions for $k_{tr,0}$, $k_{-tr,0}$ and k_{tr}

In this section, the expressions are derived for the RAFT transfer rate coefficients in Scheme E.3, *i.e.* $k_{tr,0}$, $k_{-tr,0}$ and k_{tr} , based on the pseudo-steady-state assumption (PSSA) for the calculation of the concentration of the RAFT intermediate species. An analogous methodology can be applied to determine all the RAFT transfer rate coefficients in Scheme E.2.

For the reversible chain transfer with the RAFT CTA in Scheme E.1 the continuity equation for the intermediate radical species R_nXR_0 becomes:

$$\begin{aligned} \frac{d[R_nXR_0]}{dt} = & k_{add,n,0}[R_n][R_0X] - k_{frag,n,0}[R_nXR_0] - k_{frag,0,n}[R_nXR_0] \\ & + k_{add,0,n}[R_0][R_nX] \end{aligned} \quad (\text{E1})$$

Based on the quasi-steady-state assumption for the calculation of the concentration of R_nXR_0 it follows that:

$$[R_nXR_0] = \frac{k_{add,n,0}[R_n][R_0X] + k_{add,0,n}[R_nX][R_0]}{k_{frag,n,0} + k_{frag,0,n}} \quad (\text{E2})$$

Using this expression for the concentration of R_nXR_0 the continuity equation for R_0X based on the full RAFT addition-fragmentation mechanism in Scheme E.1 becomes:

$$\frac{d[R_0X]}{dt} = -k_{add,n,0}[R_n][R_0X] + k_{frag,n,0}[R_nXR_0] \quad (\text{E3})$$

$$\begin{aligned} \frac{d[R_0X]}{dt} = & -k_{add,n,0}[R_n][R_0X] \\ & + k_{frag,n,0} \frac{k_{add,n,0}[R_n][R_0X] + k_{add,0,n}[R_nX][R_0]}{k_{frag,n,0} + k_{frag,0,n}} \end{aligned} \quad (\text{E4})$$

$$\begin{aligned} \frac{d[R_0X]}{dt} = & -k_{add,n,0} \frac{k_{frag,0,n}}{k_{frag,n,0} + k_{frag,0,n}} [R_n][R_0X] \\ & + k_{add,0,n} \frac{k_{frag,n,0}[R_nX][R_0]}{k_{frag,n,0} + k_{frag,0,n}} \end{aligned} \quad (\text{E5})$$

On the other hand, when considering the simplified degenerative transfer mechanism (Scheme E.2), the continuity equation for R_0X is given by:

$$\frac{d[R_0X]}{dt} = -k_{tr,0}[R_n][R_0X] + k_{-tr,0}[R_nX][R_0] \quad (\text{E6})$$

Hence, expressions for $k_{tr,0}$ and $k_{-tr,0}$ are readily obtained by comparison of Equation (E5) and (E6):

$$k_{tr,0} = k_{add,n,0} \frac{k_{frag,0,n}}{k_{frag,n,0} + k_{frag,0,n}} \quad (\text{E7})$$

$$k_{-tr,0} = k_{add,0,n} \frac{k_{frag,n,0}}{k_{frag,n,0} + k_{frag,0,n}} \quad (\text{E8})$$

Similarly, an expression for the transfer rate coefficient for RAFT exchange of macroradicals with a macro-RAFT CTA can be derived (Scheme E.3 vs. Scheme E.1):

$$k_{tr} = k_{add,m,n} \frac{k_{frag,n,m}}{k_{frag,m,n} + k_{frag,n,m}} \quad (\text{E9})$$

E.3 References

- (1) Chiefari, J.; Chong, Y. K.; Ercole, F.; Krstina, J.; Jeffery, J.; Le, T. P. T.; Mayadunne, R. T. A.; Meijs, G. F.; Moad, C. L.; Moad, G.; Rizzardo, E.; Thang, S. H. *Macromolecules* 1998, *31*, 5559-5562
- (2) Moad, G.; Chiefari, J.; Chong, Y. K.; Krstina, J.; Mayadunne, R. T. A.; Postma, A.; Rizzardo, E.; Thang, S. H. *Polymer International* 2000, *49*, 993-1001
- (3) Moad, G.; Chiefari, J.; Mayadunne, R. T. A.; Moad, C. L.; Postma, A.; Rizzardo, E.; Thang, S. H. *Macromolecular Symposia* 2002, *182*, 65-80
- (4) Coote, M. L.; Izgorodina, E. I.; Krenske, E. H.; Busch, M.; Barner-Kowollik, C. *Macromolecular Rapid Communications* 2006, *27*, 1015-1022
- (5) Drache, M.; Schmidt-Naake, G. *Macromolecular Symposia* 2007, *259*, 397-405
- (6) Wang, A. R.; Zhu, S. P. *Macromolecular Theory and Simulations* 2003, *12*, 196-208
- (7) Izgorodina, E. I.; Coote, M. L. *Macromolecular Theory and Simulations* 2006, *15*, 394-403
- (8) Peplak, A. D.; Butte, A. *Macromolecular Theory and Simulations* 2006, *15*, 546-562
- (9) D'hooge, D. R.; Reyniers, M.-F.; Marin, G. B. *Macromolecular Reaction Engineering* 2013, *7*, 362-379

- (10) Barner-Kowollik, C.; Buback, M.; Charleux, B.; Coote, M. L.; Drache, M.; Fukuda, T.; Goto, A.; Klumperman, B.; Lowe, A. B.; McLeary, J. B.; Moad, G.; Monteiro, M. J.; Sanderson, R. D.; Tonge, M. P.; Vana, P. *Journal of Polymer Science Part a-Polymer Chemistry* 2006, 44, 5809-5831
- (11) Barner-Kowollik, C. *Handbook of RAFT Polymerization*; Wiley: Weinheim, 2008.
- (12) Odian, G. *Principles of Polymerization*; John Wiley and Sons: New Jersey, 2004.
- (13) Matyjaszewski, K. D., T. P. *Handbook of Radical Polymerization*; John Wiley and Sons: New Jersey, 2002.
- (14) Chiefari, J.; Mayadunne, R. T. A.; Moad, C. L.; Moad, G.; Rizzardo, E.; Postma, A.; Skidmore, M. A.; Thang, S. H. *Macromolecules* 2003, 36, 2273-2283
- (15) Chong, Y. K.; Krstina, J.; Le, T. P. T.; Moad, G.; Postma, A.; Rizzardo, E.; Thang, S. H. *Macromolecules* 2003, 36, 2256-2272
- (16) Gao, X.; Zhu, S. *Journal of Applied Polymer Science* 2011, 122, 497-508
- (17) Goto, A.; Fukuda, T. *Progress in Polymer Science* 2004, 29, 329-385
- (18) Johnston-Hall, G.; Monteiro, M. J. *Macromolecules* 2007, 40, 7171-7179

Appendix F: the Newton-Raphson method to solve non-linear equations and its modification used in Chapter 4

In this appendix, the Newton-Raphson method to solve non-linear equations is explained, as it is applied in the methodology developed in Chapter 4 to determine the degenerative RAFT transfer reactivity based on an experimental polymer dispersity profile. An additional modification of the original convergence criterion is also discussed below.

F.1 Original Newton-Raphson method

The Newton-Raphson method is a numeric ‘shooting’ method to find the root x_0 of a non-linear equation $f(x)$.¹⁻³ The term ‘shooting’ refers to the fact that it starts from an initial guess of the root and subsequently updates this initial guess every iteration step until convergence with the real root is obtained.

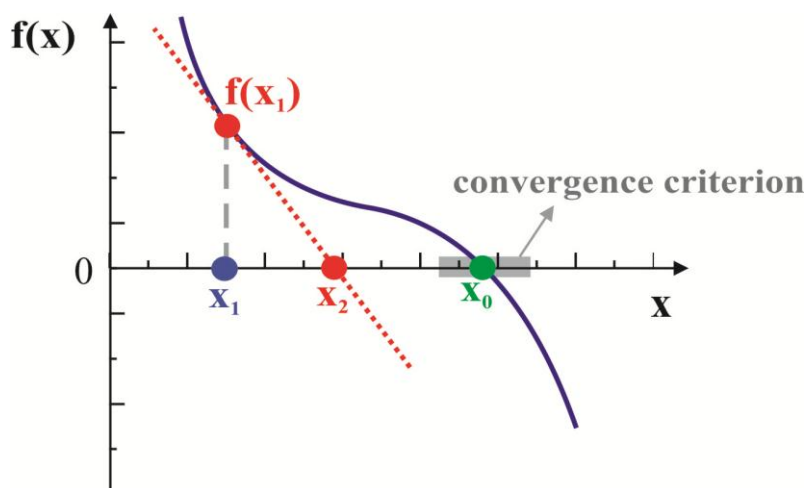


Figure F.1: Principle of the Newton-Raphson method to find the root x_0 of a non-linear function (full blue line). Based on the tangent line to the function in x_1 (dotted red line), a new estimate for the root is obtained, x_2 , until x_0 is reached

The Newton-Raphson method is based on the principle that for a given estimate of the root x_1 (blue point in Figure F.1), the x – intercept of the tangent line to the function $f(x)$ at x_1 (dotted red line in Figure F.1) will be in general a better approximation for the root (green dot in

Figure F.1; x_0) than the original guess x_1 as shown in Figure F.1. An iteration procedure is thus established until a preset convergence criterion for proximity to the root is met.

Based on the equation for a straight line with as slope $f'(x_1)$ that intercepts with the abscis at x_2 ($f(x_2) = 0$) (red dotted line in Figure F.1), an expression for the update of the x -value, *i.e.* x_2 , is found:

$$x_2 = x_1 - \frac{f(x_1)}{f'(x_1)} \quad (\text{F1})$$

If at a certain step (*e.g.* n^*) in the iterative procedure $\frac{f(x_{n^*})}{f'(x_{n^*})}$ is smaller than the predefined convergence criterion (grey zone in Figure F.1), x_{n^*} can be seen as x_0 , *i.e.*, the root of the non-linear function $f(x)$.

F.2 Application to methodology presented in Chapter 4 to determine the RAFT transfer reactivity assuming a degenerative RAFT reaction scheme

In Figure F.2, the use of the Newton-Rhapson method is illustrated for the determination of the RAFT transfer reactivity via the methodology presented in Chapter 4. The non-linear function of which the root, *i.e.* the population averaged RAFT transfer reactivity $\langle C_{tr} \rangle$, needs to be found is the difference between the calculated dispersity $\mathbb{D}(\langle C_{tr} \rangle)$ via the analytical expressions derived in Chapter 4, and the experimental dispersity at the considered conversion. If convergence is reached at a particular conversion step (convergence criterion denoted with ' ϵ '; in Chapter 4 a deviation of 1% is used), the obtained value for $\langle C_{tr} \rangle$ will serve as an initial guess for the solution of the non-linear equation $f(\langle C_{tr} \rangle) = 0$ in the next conversion step.

However, at higher monomer conversions for which the variation of the polymer dispersity becomes less pronounced, a significant overshoot of $\langle C_{tr} \rangle$ occurs, as indicated in Chapter 4. This is due to the shape of the non-linear curve of which the root needs to be found: $f(\langle C_{tr} \rangle) =$

0. In particular, for such monomer conversions, in the close proximity of the root, the derivative of $f(\langle C_{tr} \rangle)$ becomes very small (*cf.* Figure F.3) so that small deviations in $f(\langle C_{tr} \rangle)$ cause very large variations in $\langle C_{tr} \rangle$. Hence, small inaccuracies in the analytical expression for $\mathfrak{D}(\langle C_{tr} \rangle)$ will shift the corresponding root $\langle C_{tr} \rangle$ of the function $f(\langle C_{tr} \rangle)$ towards substantially higher values, which can be determined by using *convergence criterion A*.

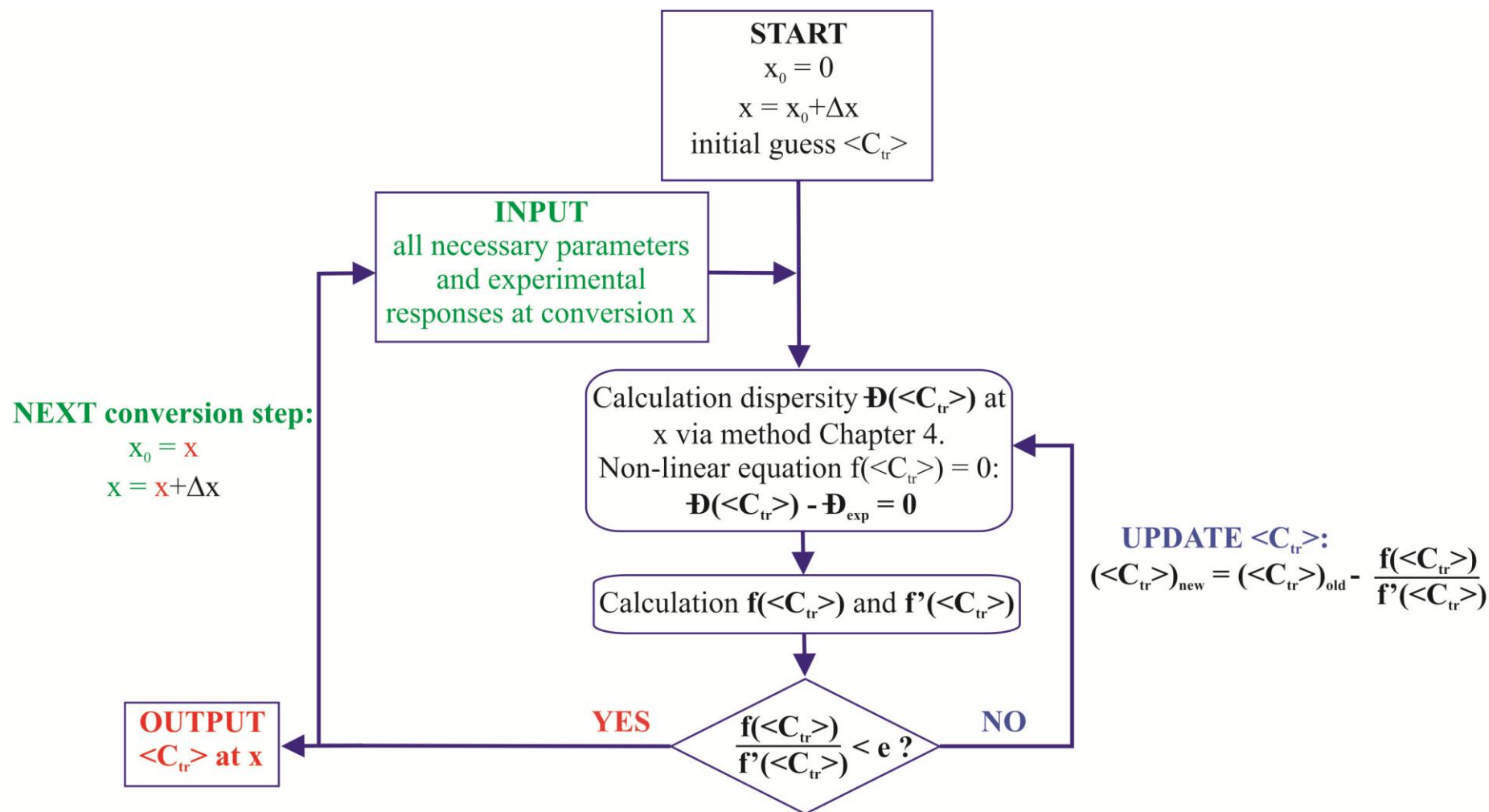


Figure F.2: Newton-Raphson procedure applied in the methodology developed in Chapter 4 to determine the RAFT chain transfer reactivity $\langle C_{tr} \rangle$ based on a comparison between experimental dispersity data (\mathcal{D}_{exp}) and calculated dispersity data via analytical expressions ($\mathcal{D}(\langle C_{tr} \rangle)$); blue lines in figures in Chapter 4).

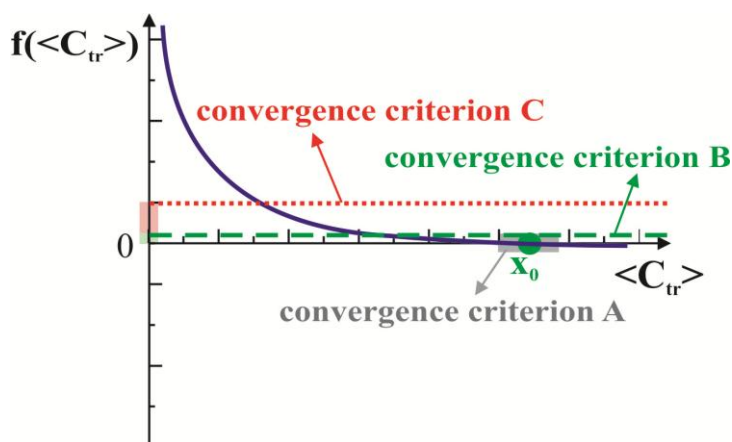


Figure F.3: Shape of the non-linear equation $f(\langle C_{tr} \rangle)$ obtained in the methodology developed in Chapter 4 to determine the RAFT chain transfer reactivity based on a comparison between experimental dispersity data (\mathcal{D}_{exp}) and calculated dispersity data via analytical expressions ($\mathcal{D}(\langle C_{tr} \rangle)$). The convergence criterion of the original Newton-Raphson method (convergence criterion A) is indicated in grey. The additional modified convergence criteria B and C are highlighted in respectively green and red (Equation (F2)).

Therefore, besides the original Newton-Raphson convergence criterion for $\langle C_{tr} \rangle$ based on the ratio of $f(\langle C_{tr} \rangle)$ and $f'(\langle C_{tr} \rangle)$ (convergence criterion A), two additional convergence criteria B and C are defined (Figure F.3) that terminate the numerical iteration procedure if the calculated dispersity $\mathcal{D}(\langle C_{tr} \rangle)$ at the considered iteration step lies within 1% (green line in Figure F.3) and respectively 5% (red line in Figure F.3) from the experimental dispersity \mathcal{D}_{exp} :

$$\frac{\mathcal{D}(\langle C_{tr} \rangle) - \mathcal{D}_{exp}}{\mathcal{D}_{exp}} = \frac{f(\langle C_{tr} \rangle)}{\mathcal{D}_{exp}} \leq 1\% \text{ or } 5\% \quad (\text{F2})$$

Furthermore, in order to increase the stability of the modified Newton-Raphson method, the root of the function (x_0 , green; Figure F.3) is always approached starting from the same initial guess (no update of the initial guess occurs). In addition, for each integration step in the methodology developed in Figure F.3 it is always tested first whether the $\langle C_{tr} \rangle$ value obtained in the previous step already meets the convergence criterion in Equation (F2). If so, no update of the $\langle C_{tr} \rangle$ value in that integration step is performed and the subsequent step is considered. As is clear from Figure F.3, the additional convergence criteria B and C for the calculation of $\langle C_{tr} \rangle$ provide insight into the reliability of the obtained $\langle C_{tr} \rangle$ values. If the solutions for $\langle C_{tr} \rangle$ based on the three different convergence criteria A-C deviate strongly

from each other (*cf.* Figure F.3), possible experimental scatter for \mathcal{D}_{exp} will have a significant effect on the derived $\langle C_{tr} \rangle$ value and hence the reliability of the latter will be poor. In Figure F.4, the modified Newton-Raphson procedure using the modified convergence criteria B and C is shown.

F.3 References

- (1) Newton, I. *De Methodus Fluxionum et Serierum infinitorum*. 1664-1671.
- (2) Raphson, J. *Analysis aequationum universalis*. London 1690.
- (3) Householder, A. S. *Principles of Numerical Analysis*; McGraw-Hill: New York, 1953.

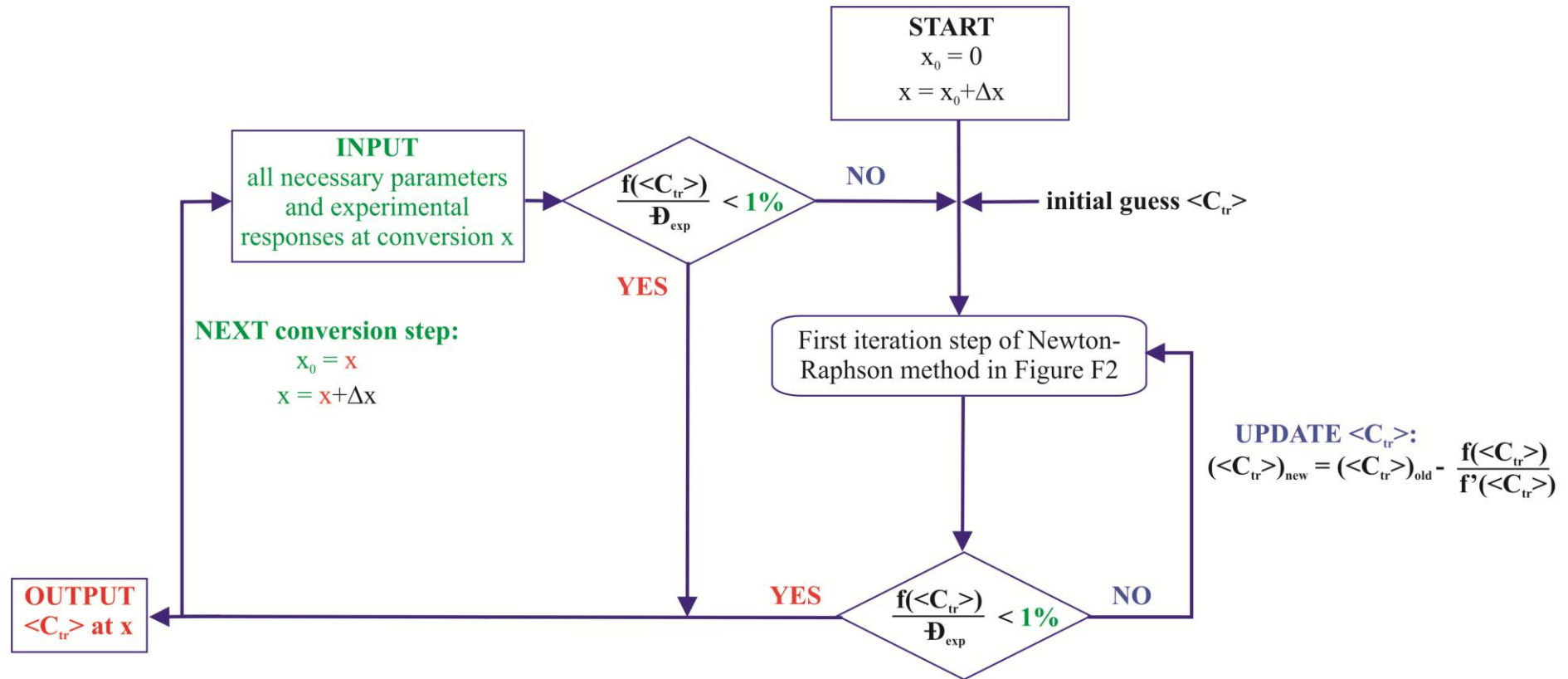


Figure F.4: Modification of the convergence criterion of the Newton-Raphson procedure applied in the methodology developed in Chapter 4 to assess the sensitivity of the calculated $\langle C_{tr} \rangle$ for small fluctuations in the polymer dispersity values. Modified convergence criteria B and C are given by Equation (F2). Only procedure for 1% deviation is shown.

Appendix G: Experimental protocol for reliable measurement of the transfer reactivity in reversible addition-fragmentation chain transfer (RAFT) polymerization

As highlighted in Chapter 4, the proposed methodology relies on the accurate knowledge of several quantities as input, *i.e.* the average termination ($\langle k_t \rangle$) and propagation (k_p) rate coefficient, the total radical concentration (λ_0) and the RAFT chain transfer agent conversion (x_{R_0X}). For each conversion at which a reliable value for the population averaged RAFT transfer reactivity $\langle C_{tr} \rangle$ is desired via the developed method, $\langle k_t \rangle$, k_p , λ_0 and x_{R_0X} need to be precisely known. Each of them will be discussed separately after which two possible experimental protocols are suggested.

G.1 Propagation reactivity

Via pulsed laser polymerization (PLP) – size exclusion chromatography (SEC) accurate values for k_p for a range of monomers have been already determined,¹ and, even for acrylate monomers, correction factors have been introduced to account for the lower propagation reactivity of the tertiary radicals,²⁻⁴ allowing the application of the developed methodology. Furthermore, the reported intrinsic chain length dependency of the propagation reactivity for low chain lengths ($CL < 10$)^{5,6} will only interfere with the obtained results if low targeted chain lengths (defined as $[M]_0/[I]_0$) are considered. In general, the highest accuracy of the proposed method is obtained for high TCLs (*cf.* Chapter 4) with consequently a negligible influence of this intrinsic chain length dependency of k_p . Diffusional limitations due to the increasing viscosity throughout a radical polymerization experiment have been shown to only interfere with the propagation reactivity at very high conversions ($x > 0.8$).^{7,8}

G.2 Termination reactivity

Similar to the case of propagation, the termination reactivity has been widely studied for an extended range of monomers.^{9,10} However, in contrast to propagation, termination is greatly affected by diffusional limitations due its high intrinsic reactivity. Hence, an apparent termination rate coefficient needs to be considered which changes throughout the course of the polymerization reaction. Via both PLP-based techniques and the RAFT – chain length dependent – termination (RAFT-CLD-T) method, the chain length and conversion dependency of the termination rate coefficients has been accurately mapped into a surface function $\langle k_t(n,x) \rangle$ which depends both on the chain length n and the conversion x , and this for several monomers.⁹ Since for RAFT polymerizations, typically a good control over the chain length distribution (CLD) is established, the polymerization mixture can be assumed to be characterized by a single chain length n at each conversion x .^{11,12} Hence, the literature reported surface function $\langle k_t(n,x) \rangle$ for the considered monomer can be safely used.¹³ Only for low transfer reactivities ($C_{tr,0} < 5$) care should be taken as a broader CLD will be obtained, leading to less reliable results.

G.3 RAFT CTA conversion

Several experimental methods are available to monitor the RAFT CTA conversion x_{R_0X} . Spectroscopic analysis techniques based on UV absorption or ¹H nuclear magnetic resonance (¹H-NMR) are commonly applied to directly measure the concentration decay of R_0X .¹⁴⁻¹⁷ On the other hand, indirect methods based on the evolution of the chain length also yield a reliable estimate for x_{R_0X} ,¹⁴ albeit with a slight loss of accuracy as the corresponding SEC measurements are less precise. In Chapter 4, x_{R_0X} is determined via the indirect method for the evaluation of the transfer reactivity for the RAFT polymerization of methyl methacrylate with cyano-isopropyl dithiobenzoate at 353 K (Equation (15)-(16) in Chapter 4).

G.4 Total radical concentration

The determination of the total radical concentration λ_0 is less straight forward and goes hand in hand with the proposed experimental protocol in the next section. Direct measurement of the total radical concentration is difficult and requires expensive equipment, *e.g.* electron paramagnetic resonance spectroscopy,¹⁸⁻²⁰ for which calibration for absolute concentration measurements can be a tedious task. On the other hand, indirect methods enable a simple determination of λ_0 , based on the measurement of the polymerization rate r_{pol} :

$$r_{pol} = -\frac{d[M]}{dt} = k_p[M]\lambda_0 \quad (\text{G1})$$

$$\lambda_0 = \frac{r_{pol}}{k_p[M]} \quad (\text{G2})$$

in which $[M]$ is the monomer concentration (mol L^{-1}). The polymerization rate can be easily accessed as a function of conversion via isothermal differential scanning calorimetric (DSC) measurements as performed when applying the RAFT-CLD-T technique.¹⁶ In addition, a very easy way to calculate the polymerization rate is by determining the slope of the conversion-time profile:

$$r_{pol} = -\frac{d[M]}{dt} = [M]_0 \frac{d\left(\frac{[M]_0 - [M]}{[M]_0}\right)}{dt} = [M]_0 \frac{dx}{dt} \quad (\text{G3})$$

in which $[]_0$ denotes the initial concentration (mol L^{-1}). Via Equation (G2) a value for λ_0 is again obtained. In order to apply Equation (G3) highly time-resolved conversion measurements are required to be able to accurately determine the slope of the conversion-time profile. Therefore, Equation (G3) is often only applied to the start of the polymerization reaction as typically a linear increase of the conversion with time is initially obtained and, hence, no on-line monitoring of the conversion is required. For an accurate measurement of the first conversion point x_0 at time t_0 , in principle, the polymerization rate can be calculated as:

$$r_{pol} = [M]_0 \frac{x_0}{t_0} \quad (\text{G4})$$

If at the time t_0 (conversion x_0) also an accurate measurement of the dispersity and x_{R_0X} , and accurate input parameters for k_p and $\langle k_t \rangle$ are available, the value of $C_{tr,0}$ can be accurately determined from one single experimental data point, as shown in Chapter 4.

G.5 Experimental protocol

Based on the discussion in the previous section on the determination of the total radical concentration, two experimental protocols can be identified for (i) the determination of $\langle C_{tr} \rangle$ for the complete conversion region, and (ii) the determination of $\langle C_{tr} \rangle$ ($= C_{tr,0}$) at the start of the RAFT polymerization.

G.1.1 Determination of $\langle C_{tr} \rangle$ for the complete conversion region

In order to apply the developed methodology in the present work for the complete conversion region of the considered RAFT polymerization, two parallel experiments for the *same RAFT polymerization mixture* need to be performed. One in which the conversion or the polymerization rate is monitored on-line (**a**) with a sufficiently high time-resolution (e.g. DSC, FTIR) and another parallel one in which samples are taken (**b**) to measure the dispersity and chain length via SEC. It is recommended to also verify the agreement between the sampling experiment and the on-line experiment by an additional off-line conversion analysis of the samples taken, as highlighted before in the work of Derboven *et al.*¹³ Ideally, the same conversion for a given time should be obtained in both experiments. The different steps that need to be taken to obtain values for $\langle C_{tr} \rangle$ via the method in the current work after successfully performing the parallel experiments (**a**) and (**b**) are presented below:

Step1: Calculation of the total radical concentration from x or r_{pol} measured in the on-line experiment (**a**) via Equation (G1)-(G3) at the times of the samples taken in experiment (**b**).

Step 2: Calculation of x_{R_0X} from either on-line concentration measurements or indirect methods based on the SEC measurements of the samples in experiment (b) (cf. Equation (15)-(16) in Chapter 3).

Step 3: Calculation of $\langle k_t \rangle$ from available surface functions in literature at the specific conversion and chain length of each sampling point in experiment (b), and look for a reliable value of k_p in the scientific literature.¹ RAFT-CLD-T or PLP based data for $\langle k_t \rangle$ and k_p are recommended above kinetic data from stationary experiments.^{9,21}

Step 4: Calculation of $\langle C_{tr} \rangle$ via the method proposed in the present work (cf. Chapter 4, Figure 4.1). For each conversion, the comparison of the solution obtained via three different convergence criteria will provide a notion of the reliability of the obtained results.

G.2.1 Determination of $\langle C_{tr} \rangle$ at the start of the RAFT polymerization, i.e. $C_{tr,0}$

The procedure to determine $C_{tr,0}$ via application of the presented methodology in Chapter 4 at the start of the considered RAFT polymerization, is much easier and only involves one experiment in which in principle only one sample needs to be taken at low conversion x_0 at time t_0 . For this single sample, the CLD, x and x_{R_0X} need to be measured via the appropriate method in order to allow the determination of $C_{tr,0}$ via the methodology of Chapter 4, as explained by the stepwise procedure below.

Step 1: Calculation of the total radical concentration from r_{pol} being the initial slope of the conversion profile (Equation (G4)) via Equation (G2).

Step 2: Calculation of x_{R_0X} from either concentration measurements of the RAFT CTA or indirect methods based on the SEC measurement of the sample (cf. Equation (15)-(16) in Chapter 4).

Step 3: Calculation of $\langle k_t \rangle$ from available surface functions in literature at the specific conversion x_0 and corresponding chain length determined from the SEC measurement, and look for a reliable value of k_p in the scientific literature.¹ RAFT-CLD-T or PLP based data for $\langle k_t \rangle$ and k_p are recommended above kinetic data from stationary experiments.^{9,21}

Step 4: Calculation of $\langle C_{tr} \rangle$ via the method proposed in the present work (*cf.* Chapter 4, Figure 4.1). For each conversion, the comparison of the solution obtained via three different convergence criteria will provide a notion of the reliability of the obtained value for $C_{tr,0}$.

G.6 References

- (1) Beuermann, S.; Buback, M. *Progress in Polymer Science* **2002**, *27*, 191-254
- (2) Junkers, T.; Theis, A.; Buback, M.; Davis, T. P.; Stenzel, M. H.; Vana, P.; Barner-Kowollik, C. *Macromolecules* **2005**, *38*, 9497-9508
- (3) Theis, A.; Davis, T. P.; Stenzel, M. H.; Barner-Kowollik, C. *Macromolecules* **2005**, *38*, 10323-10327
- (4) Theis, A.; Feldermann, A.; Charton, N.; Davis, T. P.; Stenzel, M. H.; Barner-Kowollik, C. *Polymer* **2005**, *46*, 6797-6809
- (5) Heuts, J. P. A.; Russell, G. T. *European Polymer Journal* **2006**, *42*, 3-20
- (6) Heuts, J. P. A.; Russell, G. T.; Smith, G. B. *Australian Journal of Chemistry* **2007**, *60*, 754-764
- (7) Achilias, D. S. *Macromolecular Theory and Simulations* **2007**, *16*, 319-347
- (8) D'hooge, D. R.; Reyniers, M.-F.; Marin, G. B. *Macromolecular Reaction Engineering* **2013**, *7*, 362-379

- (9) Barner-Kowollik, C.; Russell, G. T. *Progress in Polymer Science* **2009**, *34*, 1211-1259
- (10) Johnston-Hall, G.; Monteiro, M. J. *Journal of Polymer Science Part a-Polymer Chemistry* **2008**, *46*, 3155-3173
- (11) Chiefari, J.; Chong, Y. K.; Ercole, F.; Krstina, J.; Jeffery, J.; Le, T. P. T.; Mayadunne, R. T. A.; Meijs, G. F.; Moad, C. L.; Moad, G.; Rizzardo, E.; Thang, S. H. *Macromolecules* **1998**, *31*, 5559-5562
- (12) Barner-Kowollik, C. *Handbook of RAFT Polymerization*; Wiley: Weinheim, 2008.
- (13) Derboven, P.; D'hooge, D. R.; Reyniers, M.-F.; Marin, G. B.; Barner-Kowollik, C. *Macromolecules* **2015**, *48*, 492-501
- (14) Chiefari, J.; Mayadunne, R. T. A.; Moad, C. L.; Moad, G.; Rizzardo, E.; Postma, A.; Skidmore, M. A.; Thang, S. H. *Macromolecules* **2003**, *36*, 2273-2283
- (15) Chong, Y. K.; Krstina, J.; Le, T. P. T.; Moad, G.; Postma, A.; Rizzardo, E.; Thang, S. H. *Macromolecules* **2003**, *36*, 2256-2272
- (16) Vana, P.; Davis, T. P.; Barner-Kowollik, C. *Macromolecular Rapid Communications* **2002**, *23*, 952-956
- (17) Moad, G.; Chiefari, J.; Mayadunne, R. T. A.; Moad, C. L.; Postma, A.; Rizzardo, E.; Thang, S. H. *Macromolecular Symposia* **2002**, *182*, 65-80
- (18) Shen, J. C.; Yuan, T.; Wang, G. B.; Yang, M. L. *Makromolekulare Chemie-Macromolecular Chemistry and Physics* **1991**, *192*, 2669-2685
- (19) Meiser, W.; Barth, J.; Buback, M.; Kattner, H.; Vana, P. *Macromolecules* **2011**, *44*, 2474-2480

(20) Meiser, W.; Buback, M.; Barth, J.; Vana, P. *Polymer* **2010**, *51*, 5977-5982

(21) Barner-Kowollik, C.; Buback, M.; Egorov, M.; Fukuda, T.; Goto, A.; Olaj, O. F.; Russell, G. T.; Vana, P.; Yamada, B.; Zetterlund, P. B. *Progress in Polymer Science* **2005**, *30*, 605-643

Appendix H: Additional experimental data for the RAFT polymerization of *n*BuA

H.1 Batch measurements for different reactor volumes

The batch reaction was performed with a set-temperature of 373 K for two different reaction volumes, *i.e.* 20 mL and 40 mL. In both reactors a temperature rise of *ca.* 35 °C was observed in the first 45 seconds of the reaction and accordingly the recorded conversion profile are identical. Furthermore, the obtained final polymer properties are identical for both the 20 mL and 40 mL batch reactor as shown in Table H.1 taken into account the precision of the corresponding measurement technique (conversion gravimetrically; M_n and \bar{D} via SEC).

Table H.1: Comparison between the final polymer properties obtained in a batch reactor with a reaction volume of 20 mL and 40 mL at 373.15 K.

reactor volume (mL)	conversion (-)	M_n (g mol ⁻¹)	\bar{D} (-)
20	90	7400	1.53
40	95	6900	1.53

H.2 ESI-MS spectra

The ESI-MS spectra are shown in Figure H.1-2 for two different TCLs (TCL 10, Figure H.1; TCL 80, Figure H.2) in order to quantify experimentally the RAFT CTA functionality. For each TCL two different conversions are considered as indicated on the respective figure. However, it should be emphasized again (cf. Section 1) that for the ESI-MS measurements only samples with a molar mass below 5000 g mol⁻¹ are considered as only in that case reliable quantitative information about the RAFT CTA functionality can be obtained. Figure H.1-2b-c show that for the considered conversions the ESI-MS spectra only show polymer species that contain a RAFT end-group which implies that the RAFT CTA functionality is > 99%.

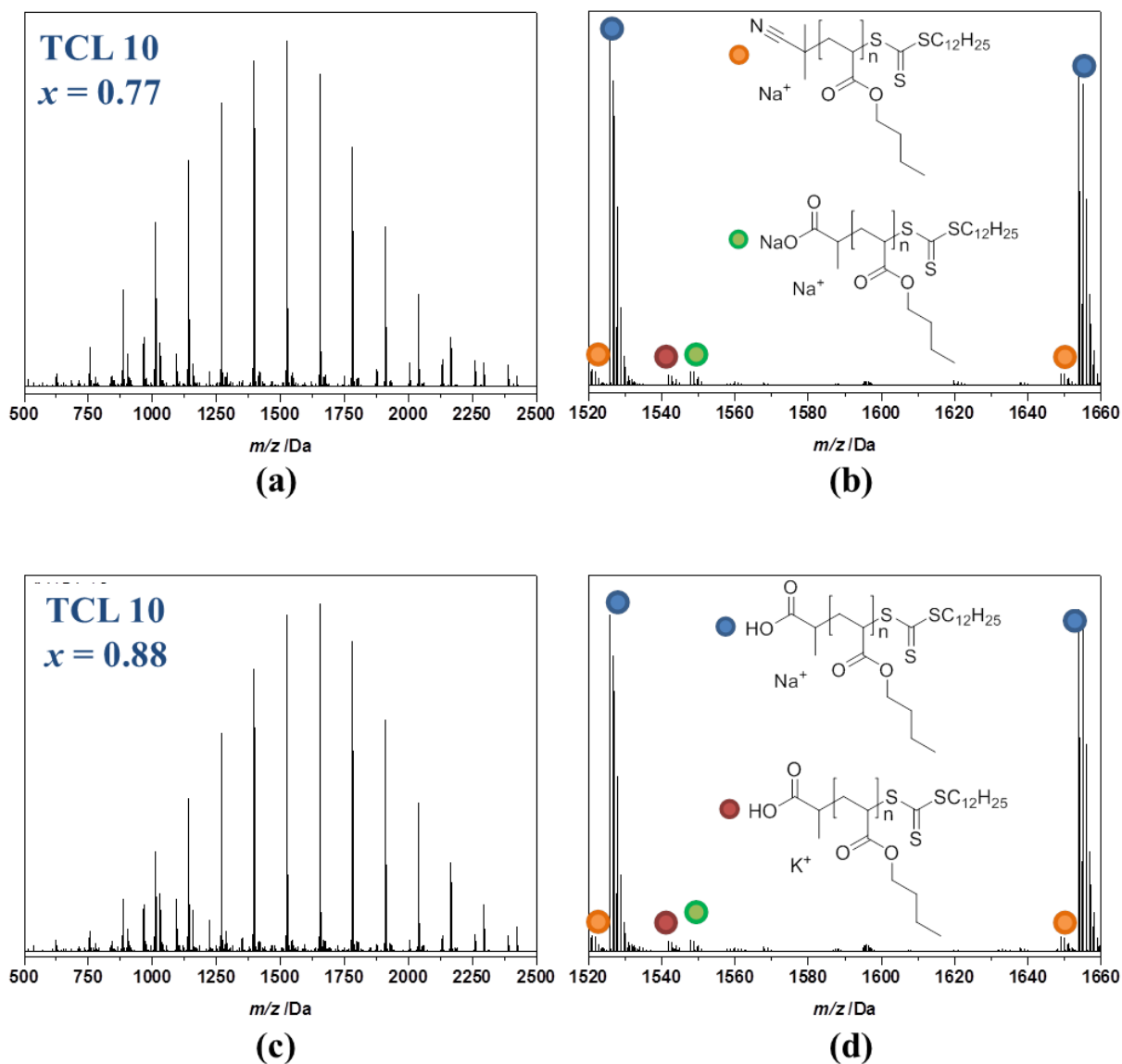


Figure H.1: ESI-MS spectra for $[n\text{BuA}]_0:[\text{DoPAT}]_0:[\text{AIBN}]_0=10:1:0.05$; 50 wt% solvent; TCL 10 for monomer conversions $x=0.77$ and $x=0.88$. **(b)** and **(d)** are an inset of respectively **(a)** and **(c)**. Via a color code the observed polymer products are indicated. Only polymer species containing a RAFT end-group are discerned.

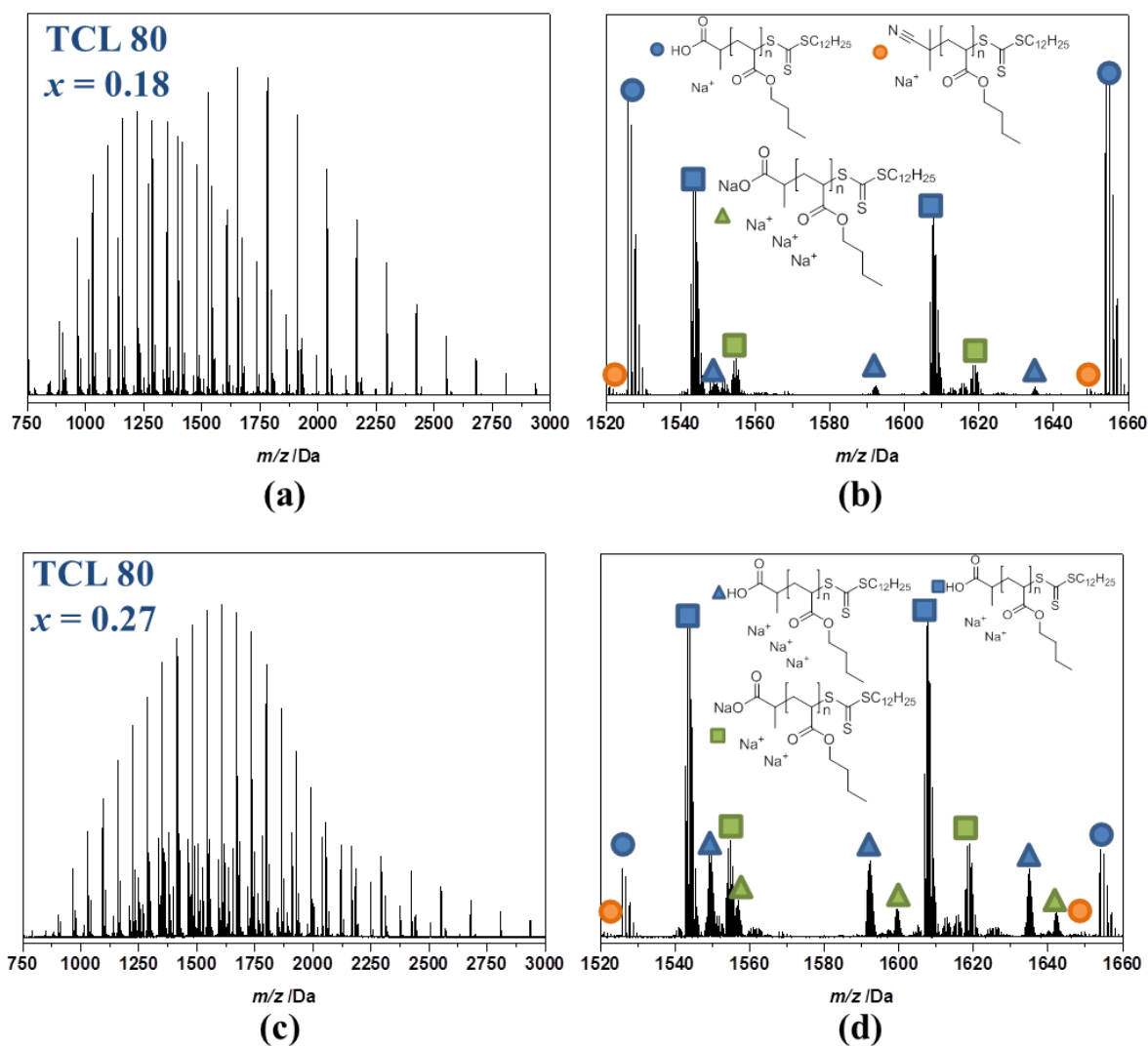


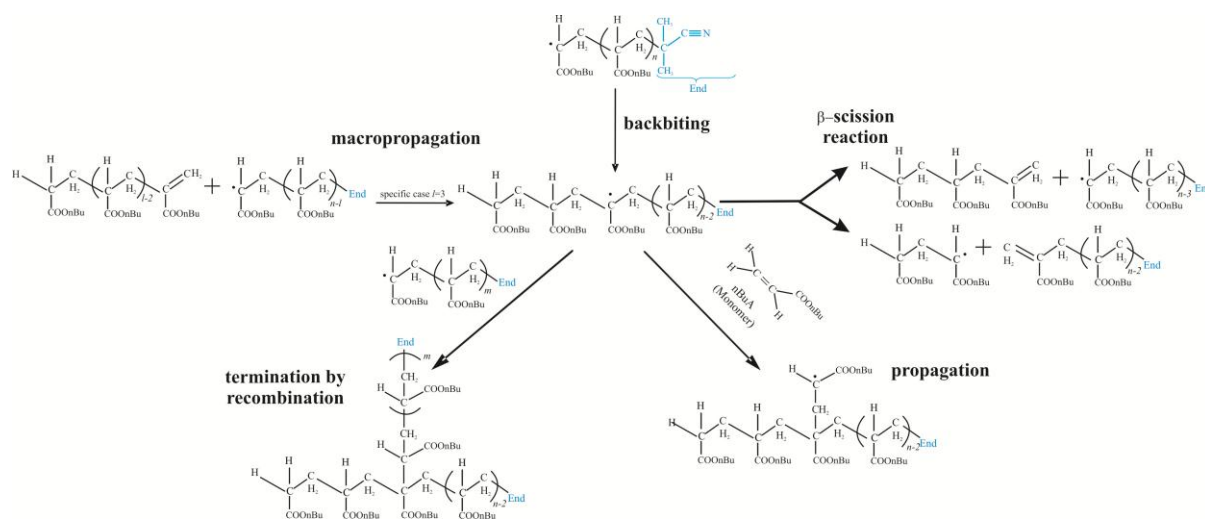
Figure H.2: ESI-MS spectra for $[n\text{BuA}]_0:[\text{DoPAT}]_0:[\text{AIBN}]_0=80:1:0.05$; 50 wt% solvent; TCL 10; for monomer conversions $x=0.18$ and $x=0.27$. (b) and (d) are an inset of respectively (a) and (c). Via a color code the observed polymer products are indicated. Only polymer species containing a RAFT end-group are discerned.

Appendix I: Kinetic parameters for the RAFT polymerization of *n*-butyl acrylate and reaction scheme for the MCRs

Table I.1: Reactions for simulation of reversible addition-fragmentation chain transfer (RAFT) polymerization of *n*-butyl acrylate (*n*BuA). Secondary/tertiary nature of macrospecies denoted by superscript *S/T*; *M*: monomer, *R*₀*X*: initial RAFT chain transfer agent (CTA), *I*: conventional initiator fragment, *R*_{*i*}/*R*_{*i*}*X*/*P*_{*i*}: macroradical/dormant/dead species with chain length *i*; *MM*: macromonomer; *f*: efficiency; Arrhenius parameters are listed in the third (*A*, pre-exponential factor) and fourth (*E*_a, activation energy) column; the fifth column contains the value of the corresponding rate coefficient at 373 K; the sixth column is the literature reference. RAFT specific reactions are highlighted in grey.

reaction	equation	A [L mol ⁻¹ s ⁻¹ or s ⁻¹]	E_a [kJ mol ⁻¹]	value at 373 K	ref
dissociation	$I_2 \xrightarrow{k_{dis,f}} 2I$	1.82 10 ¹⁵	129.3	1.44 10 ³	1,2
chain initiation	$I + M \xrightarrow{k_{pl}} R_1$	2.21 10 ⁸	17.9	7.01 10 ⁵	3
re-initiation	$R_0 + M \xrightarrow{k_{p0}} R_1$	2.21 10 ⁸	17.9	7.01 10 ⁵	3
propagation	$R_i + M \xrightarrow{k_p^S} R_{i+1}$	2.21 10 ⁷	17.9	7.01 10 ⁴	3
	$R_i^T + M \xrightarrow{k_p^T} R_{i+1}$	1.25 10 ⁶	29.5	9.52 10 ¹	4,5
backbiting	$R_i \xrightarrow{k_{bb}} R_i^T$	7.41 10 ⁷	32.7	2.02 10 ³	6
chain transfer to monomer	$R_i + M \xrightarrow{k_{trM}^S} P_i + R_1$	2.9 10 ⁵	32.6	8.15	7
	$R_i^T + M \xrightarrow{k_{trM}^T} P_i + R_1$	4.06 10 ²	32.6	1.10 10 ⁻²	7,8
macropropagation	$R_i + MM_j \xrightarrow{k_{p,macro}^S} R_{i+j}^T$	9.06 10 ⁶	17.9	3.85 10 ⁴	9
	$R_i^T + MM_j \xrightarrow{k_{p,macro}^T} R_{i+j}^T$	5.13 10 ⁵	29.5	3.90 10 ¹	8,9
β -scission	$R_i^T \xrightarrow{k_\beta} R_j + MM_{i-j}$	8.6 10 ¹⁰	71.5	8.43	10
	$R_i^T \xrightarrow{k_\beta} MM_j + R_{i-j}$ $i > 3, j < i - 1$				

degenerative transfer with RAFT CTA	$R_i + R_0X \xrightarrow{k_{tr}^{SS}} R_iX + R_0$	$3.0 \cdot 10^6$	0	$3.0 \cdot 10^6$	11-13
	$R_i^T + R_0X \xrightarrow{k_{tr}^{TS}} R_i^TX + R_0$	$3.0 \cdot 10^6$	0	$3.0 \cdot 10^6$	11-13
	$R_0 + R_iX \xrightarrow{k_{tr}^{SS}} R_0X + R_i$	$3.0 \cdot 10^6$	0	$3.0 \cdot 10^6$	11-13
	$R_0 + R_i^TX \xrightarrow{k_{tr}^{ST}} R_0X + R_i^T$	$3.0 \cdot 10^6$	0	$3.0 \cdot 10^6$	11-13
degenerative transfer with macro-RAFT CTA	$R_i + R_jX \xrightarrow{k_{tr}^{SS}} R_iX + R_j$	$3.0 \cdot 10^6$	0	$3.0 \cdot 10^6$	11-13
	$R_i^T + R_jX \xrightarrow{k_{tr}^{TS}} R_i^TX + R_j$	$3.0 \cdot 10^6$	0	$3.0 \cdot 10^6$	11-13
	$R_i + R_j^TX \xrightarrow{k_{tr}^{ST}} R_iX + R_j^T$	$3.0 \cdot 10^6$	0	$3.0 \cdot 10^6$	11-13
	$R_i^T + R_j^TX \xrightarrow{k_{tr}^{TT}} R_i^TX + R_j^T$	$3.0 \cdot 10^6$	0	$3.0 \cdot 10^6$	11-13
	$R_i + R_j \xrightarrow{k_{tc,app}^{SS}} P_{i+j}$	$1.34 \cdot 10^9$	5.6		5,14,15
	$R_i + R_j^T \xrightarrow{k_{tc,app}^{ST}} P_{i+j}$	$2.73 \cdot 10^8$	5.6		5,14,15
termination by recombination	$R_i^T + R_j^T \xrightarrow{k_{tc,app}^{TT}} P_{i+j}$	$1.74 \cdot 10^7$	5.6	composite k_t model	5,14,15
	$R_i + R_0 \xrightarrow{k_{tc,0,app}^S} P_i$	$1.34 \cdot 10^9$	5.6		5,14,15
	$R_i^T + R_0 \xrightarrow{k_{tc,0,app}^T} P_i$	$2.73 \cdot 10^8$	5.6		5,14,15



Scheme I.1: Chemical pathways of the formation and disappearance reactions of the mid-chain radicals (MCRs) that are included in the kinetic model. For simplicity, no RAFT exchange involving tertiary radicals is assumed for the construction of this reaction scheme, although this is considered in the present work in a later stage. Termination is only depicted with a secondary radical species, whereas in the kinetic model termination reactions with any radical species present in the polymerization mixture is included (cf. Table I.1).

I.1 References

- (1) McKenna, T. F.; Villanueva, A.; Santos, A. M. *Journal of Polymer Science Part a-Polymer Chemistry* **1999**, *37*, 571-588
- (2) Buback, M.; Degener, B. *Makromolekulare Chemie-Macromolecular Chemistry and Physics* **1993**, *194*, 2875-2883
- (3) Asua, J. M.; Beuermann, S.; Buback, M.; Castignolles, P.; Charleux, B.; Gilbert, R. G.; Hutchinson, R. A.; Leiza, J. R.; Nikitin, A. N.; Vairon, J. P.; van Herk, A. M. *Macromolecular Chemistry and Physics* **2004**, *205*, 2151-2160
- (4) Arzamendi, G.; Plessis, C.; Leiza, J. R.; Asua, J. M. *Macromolecular Theory and Simulations* **2003**, *12*, 315-324
- (5) Nikitin, A. N.; Hutchinson, R. A.; Buback, M.; Hesse, P. *Macromolecules* **2007**, *40*, 8631-8641

- (6) Nikitin, A. N.; Hutchinson, R. A.; Kalfas, G. A.; Richards, J. R.; Bruni, C. *Macromolecular Theory and Simulations* **2009**, *18*, 247-258
- (7) Maeder, S.; Gilbert, R. G. *Macromolecules* **1998**, *31*, 4410-4418
- (8) Wang, W.; Nikitin, A. N.; Hutchinson, R. A. *Macromolecular Rapid Communications* **2009**, *30*, 2022-2027
- (9) Zorn, A. M.; Junkers, T.; Barner-Kowollik, C. *Macromolecules* **2011**, *44*, 6691-6700
- (10) Hirano, T.; Yamada, B. *Polymer* **2003**, *44*, 347-354
- (11) Coote, M. L.; Izgorodina, E. I.; Krenske, E. H.; Busch, M.; Barner-Kowollik, C. *Macromolecular Rapid Communications* **2006**, *27*, 1015-1022
- (12) Coote, M. L.; Krenske, E. H.; Izgorodina, E. I. *Macromolecular Rapid Communications* **2006**, *27*, 473-497
- (13) Meiser, W.; Buback, M.; Sidoruk, A. *Macromolecular Chemistry and Physics* **2013**, *214*, 2108-2114
- (14) Barth, J.; Buback, M.; Russell, G. T.; Smolne, S. *Macromolecular Chemistry and Physics* **2011**, *212*, 1366-1378
- (15) Junkers, T.; Theis, A.; Buback, M.; Davis, T. P.; Stenzel, M. H.; Vana, P.; Barner-Kowollik, C. *Macromolecules* **2005**, *38*, 9497-9508

Appendix J: Influence of the targeted chain length on the poly(butyl acrylate) microstructure in a microreactor at 343 K

The influence of the ratio of the initial monomer to RAFT CTA concentration (targeted chain length, TCL) on the cumulative branching fraction f_{branch} and the RAFT CTA functionality F_x is illustrated in Figure J.1 for four different TCLs at 343 K. A clear reduction of the branching level and concomitant increase of the degree of functionality is observed for lower TCLs. This is explained below based on reaction probabilities.

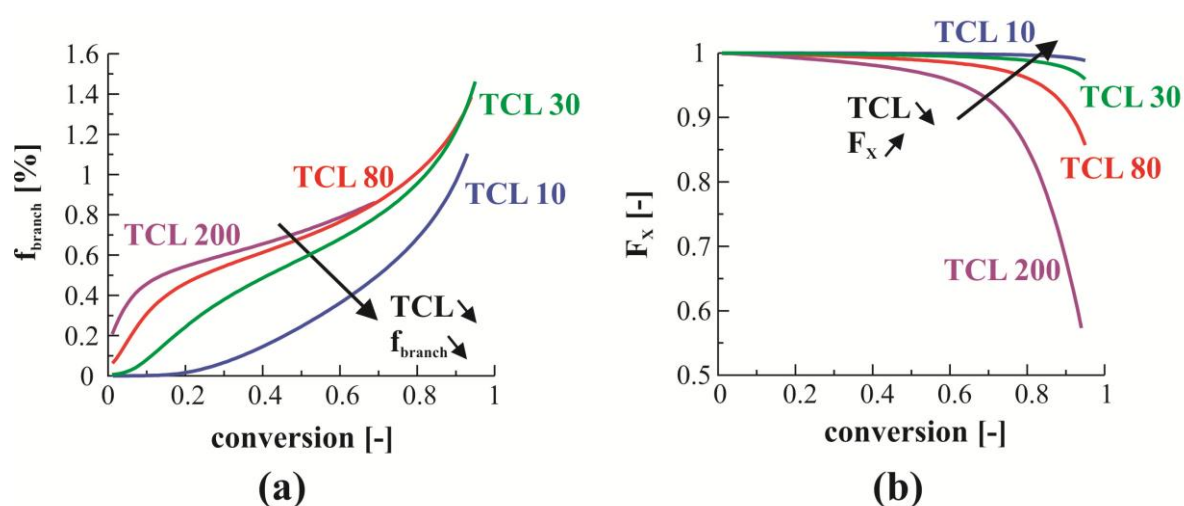


Figure J.1: (a) Simulated cumulative branching fractions at 343 K with 50 wt% solvent and four TCLs ($[AIBN]_0 = 2 \cdot 10^{-3} \text{ mol L}^{-1}$; TCL 10 (full blue line), TCL 30 (full green line), TCL 80 (full red line), TCL 200 (full purple line)). (b) Same as (a) but now for the RAFT CTA functionality F_x . Kinetic parameters in Table I.1 in Appendix I.

Similarly to the effect of a lower temperature, a decrease of the TCL and thus increase of the initial RAFT CTA concentration at a fixed temperature of 343 K leads to a higher probability for RAFT exchange (dashed line in Figure J.2a-d; *exch*) of the secondary macroradicals. Systematically smaller contributions of backbiting (full line in Figure J.2e-h; *backb*) and other side reactions (dashed line, termination; *term*) are obtained when moving from TCL 200 (purple, Figure J.2h) towards TCL 10 (blue, Figure J.2e). Concomitantly, the rate of the β -scission reactions of the formed tertiary radicals is decreased, which leads thus to higher F_x values for lower TCLs (cf. Figure J.1b). Importantly, Figure J.2e-f show a more pronounced

decrease of the probability for backbiting (full line) at low conversion. This is due to the corresponding lower number average chain lengths and thus higher contribution of oligomeric radicals incapable of backbiting ($i < 4$).

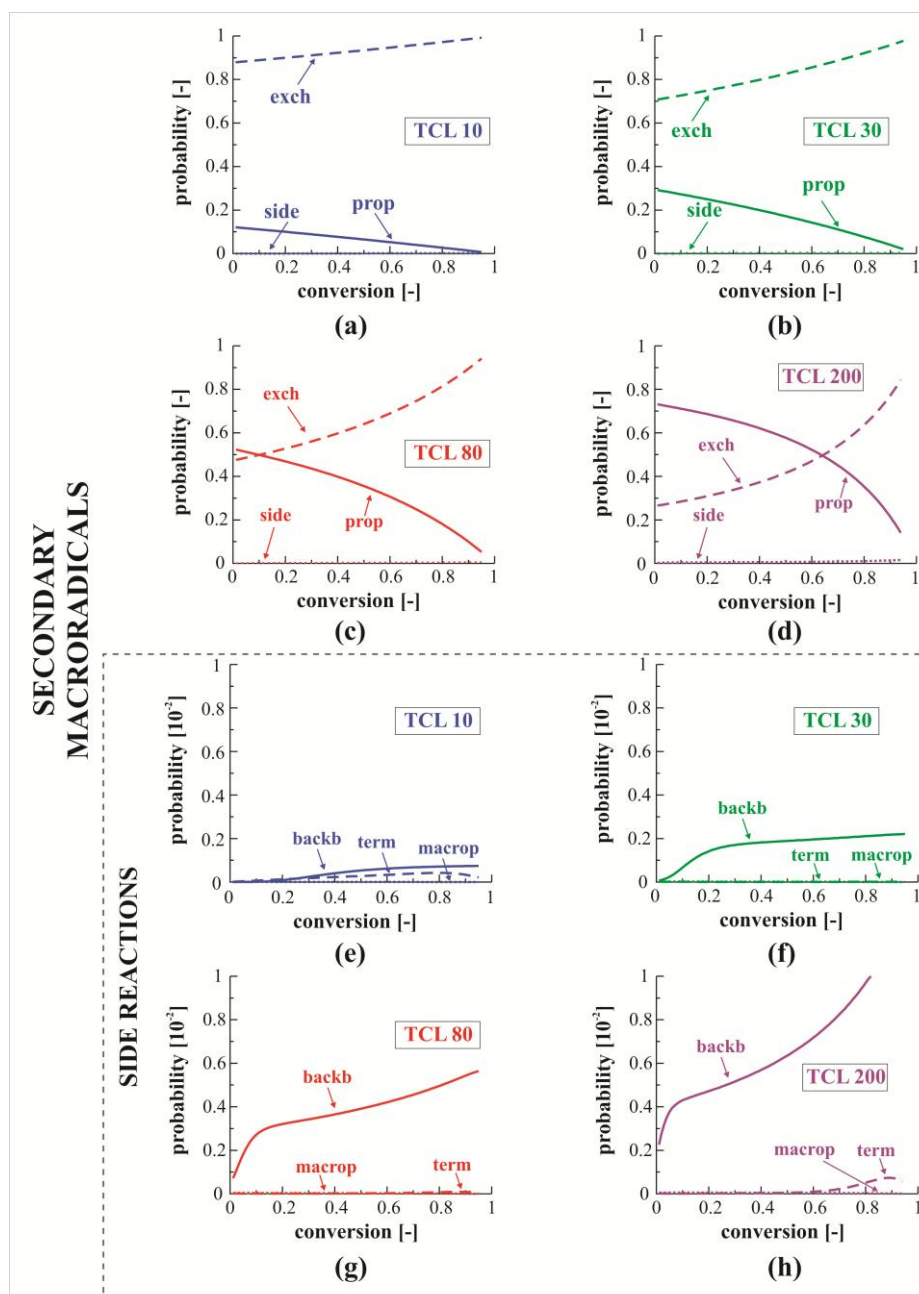


Figure J.2: (a)-(d) Simulated reaction probabilities for propagation (full line; prop), RAFT exchange (dashed line; exch) and all side reactions (dotted line; side) of the secondary radicals in an isothermal microreactor at 343 K for a targeted chain length of 10 (a), 30 (b), 80 (c) and 200 (d). (e)-(h) Simulated reaction probabilities for backbiting (full line; backb), termination (dashed line; term) and macropropagation (dotted line; macrop) of the secondary radicals at 343 K for a targeted chain length of 10 (e), 30 (f), 80 (g) and 200 (h). All simulations are performed under the reference conditions: $([n\text{BuA}]_0:[\text{DoPAT}]_0:[\text{AIBN}]_0 = 80:1:0.05; 50 \text{ wt}\% \text{ solvent}; \text{TCL } 80)$. Kinetic parameters in Table I.1 in Appendix I.

Appendix K: Alternative representation of the branching content

In this section, supplementary figures are presented to Figure 5.8 in Chapter 5 and Figure J.1 in Appendix J concerning the influence of the microreactor conditions and the RAFT exchange reactivity on the branching content. In Figure K.1-2 the evolution of the number of branches per chain is depicted instead of the cumulative branching fraction f_{branch} . This allows a classification of process conditions toward a targeted microstructure in a different manner.

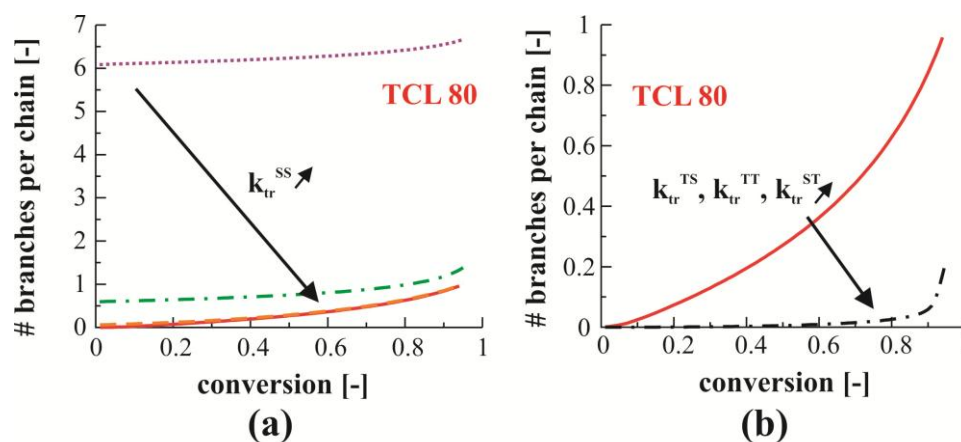


Figure K.1: (a) Similar to Figure 5.8a in Chapter 5, but now for the number (#) of branches per chain instead of the cumulative branching fraction (f_{branch}) as a function of conversion. The plotted lines represent the same conditions as the corresponding lines in Figure 5.8a. It is clear that the same factors that reduce f_{branch} also reduce the number of branches per chain. (b) Similar to Figure 5.8c in Chapter 5, but now the number of branches per chain instead of f_{branch} . Same color code and conditions for the plotted lines are used. Similarly, a higher RAFT exchange rate of the tertiary radicals induces a markedly lower number of branches per chain. Kinetic parameters in Table I.1 in Appendix I.

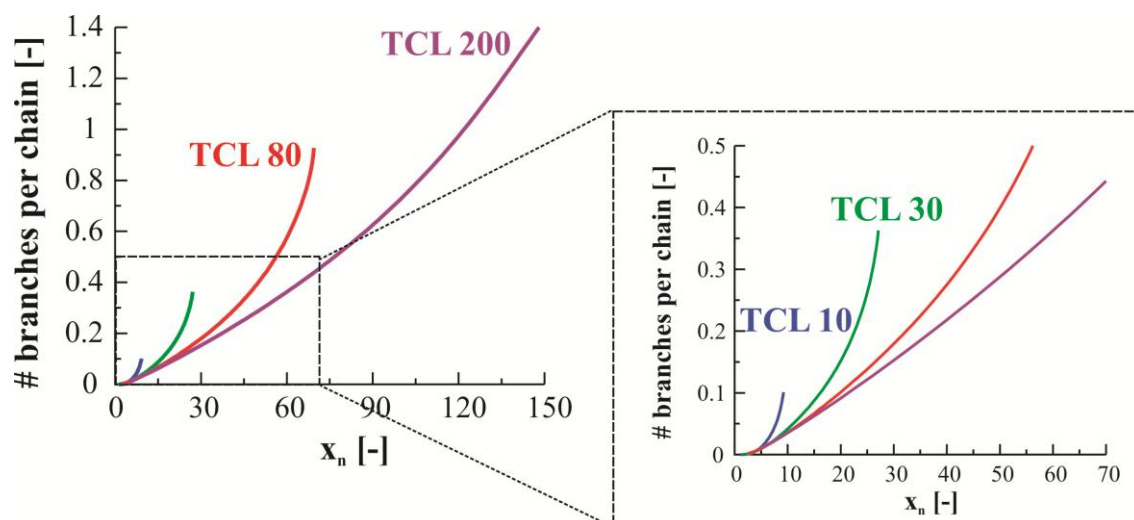


Figure K.2: Equivalent to Figure J.1a, the number of branches per chain is plotted for four TCLs at 343 K, but, on the x-axis now the number average chain length (x_n) is plotted instead of the conversion. Same conditions and color code as Figure J.1a. An inset for the lower number average chain lengths is shown on the right. This figure shows that increasing the TCL allows to obtain lower numbers of branches per chain for a given average chain length x_n . However, the amounts of the respective polymer obtained are much smaller as lower conversions are reached. Kinetic parameters in Table I.1 in Appendix I.

Appendix L: Glossary

Arrhenius activation energy of a reaction step:

E_a in $k = A \exp\left(\frac{-E_a}{RT}\right)$ with k the rate coefficient of the reaction step, R the universal gas constant, T the temperature and A the pre-exponential factor; measure for temperature dependence of the rate coefficient.

Apparent rate coefficient:

rate coefficient related to the observed kinetics, *i.e.* the rate coefficient determined by the intrinsic chemical rate coefficient and transport phenomena.

Center-of-mass diffusion of a component:

movement of the center-of-mass of the component, *i.e.* the movement of gravity.

Chain length of a polymer molecule:

the number of repeating units (coming from the monomer(s)) in a polymer molecule.

Chain transfer:

reaction leading to the transfer of the radical center between two species.

C_{tr} :

chain transfer coefficient, *i.e.* the ratio of the transfer rate coefficient k_{tr} to the propagation rate coefficient k_p .

Dead polymer molecule:

polymer molecule without end-group functionality

Degenerative reversible addition-fragmentation chain transfer (RAFT) polymerization:

RAFT polymerization for which the addition-fragmentation reactions are fast and cross-termination of the intermediate radical species with other radicals in the polymerization system is negligible so that the pseudo-steady state approximation holds for the former.

Dormant polymer molecule:

polymer molecule having end-group functionality

Elementary reaction step:

the irreducible act of reaction in which reactants are transformed in products directly, *i.e.* without passing through an intermediate that is susceptible of isolation.

End-group functionality:

functional group allowing further chemical modification. In RAFT polymerization, this group always contains a thiocarbonyl moiety.

Free volume theory:

theory that describes (translational) diffusion of a molecule as a jumping process of (part of) the molecule into the hole free volume of all molecules together.

Gel effect:

also known as the Trommsdorff effect. Autoacceleration of the polymerization reaction due to a strong decrease of the termination rate by diffusional limitations induced by the increase in viscosity.

Homotermination:

termination between macroradicals of equal chain length.

Livingness of the polymer:

is high if a large fraction of the polymer molecules contains end-group functionality.

Matrix effect:

effect of the composition of the polymer matrix on the termination rate.

Microreactor:

reactor with volume in μL range. Usually tubular reactor with lateral dimensions on the submillimeter scale.

Microstructured reactor:

network of microchannels in a specific geometry (usually U-shape) embedded in a tiny slab which is most commonly made of glass, polymer or silicon.

Monomer conversion:

monomer consumed with respect to initial amount.

Polymer dispersity of the chain length distribution of the polymer:

ratio of the mass to number average chain length; measure for the broadness of the molar mass distribution of the polymer.

Propagation of a radical:

reaction leading to chain growth, *i.e.* addition to monomer.

Rate coefficient:

the coefficient of proportionality for the calculation of a reaction rate.

Reaction diffusion:

movement of the center-of-mass of a molecule as a consequence of propagation.

Reversible addition-fragmentation chain transfer (RAFT) polymerization:

radical polymerization technique allowing ‘controlled’ polymer properties, *i.e.* a narrow chain length distribution and high livingness. RAFT polymerization is based on an exchange of the end-group functionality via an addition-fragmentation mechanism with (macro-) RAFT chain transfer agent.

RAFT exchange:

reversible chain transfer between a macroradical and (macro-) RAFT CTA by a consecutive addition and fragmentation reaction.

Reversible deactivation radical polymerization (RDRP):

radical polymerization technique in which control over the chain length distribution and livingness of the polymer is established by reversible deactivation of the macroradicals with a RDRP agent.

Short chain branching:

short branches consisting of three monomer units formed upon propagation of a tertiary radical that was generated by backbiting of a secondary macroradical.

Short-long termination:

termination between macroradicals of different chain length so that always a “short” and a “long” chain can be identified.

Population averaged rate coefficient:

average for a chain length dependent rate coefficient weighted based on the concentration contribution of each chain length.

sth order moment equation:

equation allowing the calculation of the product of the chain length to the sth power and the corresponding concentration as a function of polymerization time.

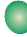


Termination of radicals:

reaction leading to the formation of (a) dead polymer molecule(s) with the disappearance of two radical reactive centers.

List of figures

- Figure 1.1:** Schematic representation of the RAFT polymerization mechanism as a RAFT exchange process superimposed on a conventional FRP scheme. For simplicity, both the conventional initiator-derived radicals (I^*) and the RAFT CTA derived radicals (R_0) are depicted in blue. R stands for macroradical, P for dead polymer, INT for intermediate radical species, M for monomer and X denotes the RAFT CTA functionality (yellow). Radical center indicated by black dot.....5
- Figure 1.2:** Principle of the pulsed laser polymerization – size exclusion chromatography (PLP-SEC) method. Left: Radical concentration for a pulse frequency of 500 Hz. Right: Characteristic chain length distribution. From the position of the inflection points (Equation (17)) the intrinsic propagation rate coefficient can be determined. Figure taken from D’hooge et al.¹⁵19
- Figure 1.3:** Homotermination rate coefficient as function of the chain length at low monomer conversion. Different diffusion mechanisms control the rate of diffusion depending on the chain length of the involved macroradicals. Figure taken from Johnston-Hall and Monteiro.⁴⁰23
- Figure 1.4:** Conceptual representation of the CLD method of Moad and coworkers.^{81,82} Full blue line is number CLD of dead polymer (y_n , Equation (1) if disproportionation is only termination mechanism); dotted red line is natural logarithm of the number CLD. Top 80% (highest signal to noise ratio) of CLD is marked by a shading as in that region the most accurate C_{tr} values are obtained.....34

- Figure 1.5:** Evolution of the number averaged chain length (x_n) with conversion for monomer $-R_0X$ combinations that exhibit hybrid behavior. An initial increase of the chain length (x_n^0) is obtained at the start of the polymerization.....39
- Figure 2.1:** The need to quantify short-long-termination reactivities in radical polymerization: a generic and flexible experimental platform is presented to measure such reactivities allowing to exploit the full potential of existing and next-generation polymerization processes and to fill the knowledge gap in current macromolecular diffusion theories.....54
- Figure 2.2:** Composition of the polymerization mixture at the start (top left) and at a certain time (top right) of a RAFT-CLD-T short-long-termination experiment; ● = monomer molecule M, ● = RAFT CTA molecule, ● = conventional radical initiator fragment I originating from conventional radical initiator I_2 and S/L^* = number average chain length of short/long chain length distribution; also given are SEC traces of dormant species with w the mass fraction and the full grey line in right subfigure the total SEC trace, with in turn the dashed yellow and dashed blue lines the individual peaks after deconvolution.....63

Figure 2.3: Importance of the use of the improved RAFT-CLD-T formula for homo-termination experiments ($b=1$ instead of 2 in Equation (6)): Schematic representation of (a) ideal and theoretical conditions in which all macrospecies possess a chain length i^* (dispersity $\mathfrak{D} = 1$; only case in which Equation (9) ($b=2$) is valid); (b) “well-Controlled” RAFT polymerization conditions with macrospecies possessing a chain length close or equal to i^* (\mathfrak{D} slightly different from one; Equation (9) ($b=1$) is valid);  = monomer molecule,  = RAFT CTA molecule and  = conventional radical initiator fragment originating from conventional radical initiator I_2 . (c) Correctness of the improved Equation (9) ($b=1$; dotted green line; logarithmic scale) to measure $k_t^{i^*i^*}$ during a RAFT-CLD-T experiment, as good agreement with the implemented $k_t^{i^*i^*}$ (dashed blue line); i^* = number average chain length (dashed-dotted orange line). The original RAFT-CLD-T equation (full red line; Equation (9) ($b=2$)) leads however to a mismatch. (d) Illustration of necessity of correct absolute values for $k_t^{i^*i^*}$ for optimization of radical polymerization processes (factor 2 difference between green and red lines for a representative RDRP case); Intrinsic kinetic parameters for (c): Table 2.2 and for (d): reference ⁽⁴⁵⁾.....69

- Figure 2.4:** Generic framework for the improved homo-termination (k_t^{i*i*}) surface for MMA polymerization at 353 K: (a) Improved RAFT-CLD-T k_t^{i*i*} surface (Equation (6); $b = 1$) for regression analysis (a) prior and (c) after a correction for the uncertainty on its input parameters (Table 2.3). This correction is obtained by adding the relative maximal error data in (b) as obtained via a propagation of uncertainty analysis as scatter; blue points are located above the surface function, whereas the red points are located below the surface; only conversions between 0.05 and 0.7 are included (cf. Appendix B.2). Drop lines indicate minor deviation from the surface; experimental conditions: entry 1-14 in Table 2.1; surface equations and regression characteristics are provided in Appendix B.4.....71
- Figure 2.5:** Comparison of conversion measurements via on-line DSC (full blue line) and off-line $^1\text{H-NMR}$ analysis (red squares); red error bars indicate 5% relative error; dashed blue lines represent error on the conversion via DSC (4.5%); the grey zone marks the 5% to 70% conversion region outside of which no data are considered to allow for a sufficient equilibration time of the DSC instrument and a sufficiently narrow macroradical chain length distribution and to prevent any significant interference of diffusional limitations on the conventional radical initiation process and propagation; Conditions: entry 4 in Table 2.1.....72
- Figure 2.6:** Very good agreement between conversion (a) and chain length (b) profiles for two duplicate experiments to check the reproducibility of the applied experimental procedure. Duplicate experiments were performed on different days. Conditions: entry 5(blue dots) and 11 (red dots) in Table 2.1.....73

- Figure 2.7:** Schematic representation of the beamlike error on the $\log[k_t(w_p, i^*)]$ values. In this work only the vertical error bar is considered as the deviations on $\log(i^*)$ and the polymer mass fraction are small.....74
- Figure 2.8:** Good reproducibility of the calculated termination rate coefficient in the RAFT-CLD-T homo-termination experiments on different days. Conditions: entry 5 (full blue line) and entry 11 (dotted red line) in Table 2.1.....75
- Figure 2.9:** A good agreement between the homo-termination rate coefficient obtained via the RAFT-CLD-T technique when started from a polymerization mixture containing macro-RAFT CTA instead of conventional RAFT agent (full green line) and the homo-termination rate coefficient derived from the homo-termination surface function in Figure 2.4c at the corresponding average chain lengths and polymer mass fractions (dashed red line).....76
- Figure 2.10:** Number average chain length (left), dispersity (middle) and polymer mass fraction data (right) for the modified RAFT-CLD-T homo-termination experiment starting from macro-RAFT CTA instead of conventional (small) RAFT CTA. For the conversion results, both the on-line DSC (full blue line) and the off-line $^1\text{H-NMR}$ data (red squares) are shown together with their respective error, similar to Figure 2.5.....76

- Figure 2.11:** Conceptual representation of a possible matrix effect with **(a)** non-uniform matrix with 100 monomer molecules, 10 chains of chain length CL 20 and 2 chains of CL 100 and with **(b)** the corresponding uniform matrix (CL=20) **(c)** Quantification of a possible matrix effect for k_t^{ii} by the ratio of the homo-termination coefficient obtained via the RAFT-CLD-T technique (Equation **(9)**; $b=1$; blue lines) in the presence of dead PMMA standard (non-uniform matrix; $k_{t,NU}^{ii}$), to the homo-termination rate coefficient assuming a uniform matrix as determined from the surface function in Figure 2.4c ($k_{t,U}^{ii}$); J_m^* : the mass average chain length of the polymer matrix; fuchsia lines: RAFT-CLD-T short-long-termination experiments (entry 20-23 in Table 2.1). **(d)** $k_{t,NU}^{ii}$ for increasing amounts of dead PMMA standard based on entry 16-19 in Table 2.1 but with a fixed (total) polymer mass fraction w_p and chain length i of the terminating radicals. Points for $w_{p,ST} = 0$ are derived from Figure 2.4c; the error bars are calculated via the propagation of error analysis; negligible matrix effect for the considered conditions as almost flat lines result; points of similar i and w_p are indicated in Figure 2.12.....79
- Figure 2.12:** Chain length of the terminating macroradicals versus the total polymer mass fraction for entry 15-19 in Table 2.1. Points of similar i and equal w_p are marked by a colored circle and yield two corresponding points with different mass fraction of PMMA standard ($w_{p,ST}$) in Figure 2.11d (same number).....80

Figure 2.13: Generic framework for the reliable quantification of short-long-termination reactivities and the validation of diffusion theories, applied to MMA polymerization at 353 K: **(a)** $\langle k_t \rangle$ (Equation (9), $b=1$) derived from DSC measurements (dashed grey line) **(b)** Illustration that $k_t^{L^*L^*}$ and $k_t^{S^*S^*}$ can be directly and reliably determined from the non-extrapolated region of the homo-termination surface (Figure 2.4c), taking into account that no correction for a matrix effect is needed (fuchsia lines in Figure 2.11c) **(c)** $k_t^{S^*L^*}$ for entry 20 in Table 2.1 assuming a constant f_1 given by the initial molar fraction of macro-RAFT CTA (dotted fuchsia line); $k_t^{L^*L^*}$ (full yellow line), $k_t^{S^*S^*}$ (full blue line) and $\langle k_t \rangle$ (dashed black line).....82

Figure 2.14: Short-long-termination rate coefficient as function of the polymer mass fraction for entry 20-23 in Table 2.1. The onset of the diffusional limitations on initiation shifts to lower polymer mass fractions for higher chain lengths. Entry 20, TCL 135, CL macroCTA 140: red; entry 21, TCL 166 CL macroCTA 140: green; entry 22, TCL 126 CL macroCTA 100: blue; entry 23 TCL 292 CL macroCTA: fuchsia.....83

Figure 2.15: Variation of f_1 as a function of time. In the case of equal transfer coefficients for the macro-addition/fragmentation and the one involving small molecules, f_1 is constant and can be approximated by the initial molar fraction of macro-RAFT CTA (dotted blue line). On the other hand, unequal values of the transfer coefficients induce a time dependency of f_1 which then reaches its final value according to (dashed green line) the conventional RAFT CTA conversion (full red line). Rate coefficients used in the simulation: Table 2.2; conditions: $[MMA]_0/[CTA_{tot}]_0 = 150$; $[CTA_{tot}]_0/[AIBN]_0 = 15$; $[macro-RAFT CTA]_0/[CTA_{tot}]_0 = 0.2$; initial CL macro- RAFT CTA = 100.....84

Figure 2.16: Only RAFT-CLD-T short-long-termination experiments with a sufficiently high initial molar fraction of macro-RAFT CTA (f_1) compared to conventional small RAFT CTA yield reliable short-long-termination data. Here the fuchsia line is the short-long-termination rate coefficient for the conditions: $[MMA]_0/[CTA_{tot}]_0 = 97$; $[CTA_{tot}]_0/[AIBN]_0 = 21.8$; $[macro-RAFT\ CTA]_0/[CTA_{tot}]_0 = 0.127$; initial CL macro-RAFT CTA = 260 (too low f_1). $\langle k_t \rangle$ (dashed grey line), $k_t^{L^*L^*}$ (full blue line) and $k_t^{S^*S^*}$ (full yellow line) are also shown.....85

Figure 2.17: (a) $k_t^{S^*L^*}$ for entry 20 in Table 2.1 assuming a constant f_1 given by the initial molar fraction of macro-RAFT CTA (dotted fuchsia line); $k_t^{L^*L^*}$ (full yellow line), $k_t^{S^*S^*}$ (full blue line) and $\langle k_t \rangle$ (dashed black line) (b) inset of (a) including a comparison with currently used simplified mean models (DMM, GMM, HMM; Equation (1)-(3)) (c) Comparison between surface function (green surface) fitted to experimental $k_t^{S^*L^*}$ data for specific chain length combinations and polymer mass fractions (full fuchsia lines; entry 20-23 in Table 2.1; constant f_1) and the surface (red) as obtained considering a simplified mean model. Clearly, a significant mismatch is obtained.....86

Figure 3.1: Schematic representation of the in silico procedure for the evaluation of the analytical literature methods to determine $C_{tr,0}$ or C_{tr} . $C_{tr,(0),IN}$ is the implemented $C_{tr,(0)}$ while $C_{tr,(0),OUT}$ is the value obtained after application of the considered method to the perfect simulated responses.....111

- Figure 3.2:** Natural logarithm of the concentration ratio of R_0X versus the natural logarithm of the concentration ratio of monomer (Equation (8)) for TCL 100 (full red line) and TCL 500 (dashed blue line) in case the transfer reactivity of the R_0 species with macro-RAFT CTA is high: $C_{-tr,0} = 150$ (situation 2); $C_{tr,0} = 15 = C_{tr}$. $[M]_0 = 9 \text{ mol L}^{-1}$; $[I_2]_0 = 9 \cdot 10^{-3} \text{ mol L}^{-1}$. $[R_0X]_0$ for TCL 100 and 500 respectively: 0.09 and 0.018 mol L^{-1} . Other kinetic parameters in Table 3.3.....116
- Figure 3.3:** (a) Left axis: comparison between the simulated polymer dispersity for a perfect experiment (full green line) and the polymer dispersity obtained by application of the analytical expression of Goto and Fukuda²⁰ (dashed blue line; Equation (10)) and Gao and Zhu⁴ (dotted red line; Equation (11)) with $C_{tr} = 15$; right axis: R_0X conversion. (b) Comparison between the implemented C_{tr} value (full green line) and the values for C_{tr} obtained from the application of Equations (10) (dashed blue line) and (11) (dotted red line) to the simulated polymer dispersity profile of the dormant chains. TCL=100; $C_{tr} = C_{tr,0} = C_{-tr,0} = 15$; $[M]_0 = 9 \text{ mol L}^{-1}$; $[I_2]_0 = 9 \cdot 10^{-3} \text{ mol L}^{-1}$. Other kinetic parameters in Table 3.3.....119
- Figure 3.4:** Left axis: comparison between the implemented C_{tr} values ($C_{tr,0,IN}$, black circle; $C_{tr,IN}$, black square) and the values for C_{tr} obtained from the application of Equations (10) (dashed blue line) and (11) (dotted red line) to the simulated polymer dispersity profile of the dormant chains. Right axis: R_0X conversion (full green line). TCL=100; $C_{tr,0} = C_{-tr,0} = 15$, $C_{tr} = 30$; $[M]_0 = 9 \text{ mol L}^{-1}$; $[I_2]_0 = 9 \cdot 10^{-3} \text{ mol L}^{-1}$. Other kinetic parameters in Table 3.3.....120

- Figure 4.1:** Summary of the methodology developed in the present work to determine $\langle C_{tr} \rangle$ as function of conversion via a flow chart, including input parameters (left figure) and schematic representation of the stepwise integration procedure (right figure). In red and green two consecutive integration intervals for the conversion are indicated. Q_1 and Q_2 calculated at the conversion separating both intervals are used as initial conditions in the next integration interval (Equation (9)-(11)).....138
- Figure 4.2:** $\langle C_{tr} \rangle$ as function of the monomer conversion obtained by solution of Equation (5)-(6) using the original Newton-Raphson convergence criterion (full blue line, convergence criterion A, Equation (12)) and the additional modified convergence criterion B (dashed green line, 1% deviation, Equation (13)) and C (dotted red line, 5% deviation, Equation (14)) which are only used for sensitivity purpose, for TCL 100; $C_{tr,0} = C_{-tr,0} = C_{tr} = 15 = C_{tr,0,IN}$ (black circle) **(a)** Data points every 1% monomer conversion. **(b)** Data points every 5% monomer conversion; conditions: entry 1 in Table 4.2; other kinetic parameters from Chapter 3.....141
- Figure 4.3:** Comparison between the dispersity profile calculated by the analytical expression for $\mathcal{D}(x)$ in Equation (5) using the $\langle C_{tr} \rangle$ values from convergence criterion A (full blue line, Equation (12)), the simulated total polymer dispersity (dotted black line) and the simulated dispersity of the dormant chains (dashed orange line coinciding with full blue line) as a function of (monomer) conversion for TCL 100; $C_{tr,0} = C_{-tr,0} = C_{tr} = 15$; conditions: entry 1 in Table 4.2; other kinetic parameters from Chapter 3.....143

Figure 4.4: $\langle C_{tr} \rangle$ as function of the monomer conversion obtained by solution of Equation (5)-(6) using the original Newton-Raphson convergence criterion (full blue line, convergence criterion A, Equation (12)) and the additional modified convergence criterion B (dashed green line, 1% deviation, Equation (13)) and C (dotted red line, 5% deviation, Equation (14)) which are only used for sensitivity purpose, for **(a)** TCL 100; entry 2 in Table 4.2 **(b)** TCL 200; entry 3 in Table 4.2 and **(c)** TCL 300; entry 4 in Table 4.2. $C_{tr,0} = C_{-tr,0} = 15 = C_{tr,0,IN}$ (black circle), $C_{tr} = 30 = C_{tr,IN}$ (black square). Vertical grey line indicates full conversion of R_0X , black cross is intersection point with full blue line. Simulated data points every 1% monomer conversion. Other kinetic parameters from Chapter 3.....144

Figure 4.5: $\langle C_{tr} \rangle$ as function of the monomer conversion obtained by solution of Equation (5)-(6) using the original Newton-Raphson convergence criterion (full blue line, convergence criterion A, Equation (12)) and the additional modified convergence criterion B (dashed green line, 1% deviation, Equation (13)) and C (dotted red line, 5% deviation, Equation (14)) which are only used for sensitivity purpose, for TCL 100. **(a)** $C_{tr,0} = C_{-tr,0} = 20 = C_{tr,0,IN}$ (black circle), $C_{tr} = 120$ (black square); entry 6 in Table 4.2. **(b)** $C_{tr,0} = C_{-tr,0} = 1 = C_{tr,0,IN}$ (black circle), $C_{tr} = 10 = C_{tr,IN}$; entry 5 in Table 4.2. Vertical grey line indicates full conversion of R_0X (only in a). Other kinetic parameters from Chapter 3.....145

- Figure 4.6:** $\langle C_{tr} \rangle$ as function of the monomer conversion obtained by solution of Equation (5)-(6) using the original Newton-Raphson convergence criterion (full blue line, convergence criterion A, Equation (12)) and the additional modified convergence criterion B (dashed green line, 1% deviation, Equation (13)) and C (dotted red line, 5% deviation, Equation (14)) which are only used for sensitivity purpose, for **(a)** TCL 100; entry 7 in Table 4.2 and **(b)** TCL 500; entry 8 in Table 4.2. $C_{tr,0} = 15 = C_{tr,0,IN}$ (black circle), $C_{-tr,0} = 150$, $C_{tr} = 30 = C_{tr,IN}$ (black square). Vertical grey line indicates full conversion of R_0X (black cross is intersection point with full blue line). Other kinetic parameters from Chapter 3.....146
- Figure 4.7:** In silico procedure applied to assess the sensitivity of the developed methodology (Figure 4.1) for possible chain length dependent RAFT transfer kinetics.....150

Figure 4.8: $\langle C_{tr} \rangle$ as function of the monomer conversion obtained by solution of Equation (5)-(6) using the original Newton-Raphson convergence criterion (full blue line, convergence criterion A, Equation (12)) and the additional modified convergence criterion B (dashed green line, 1% deviation, Equation (13)) and C (dotted red line, 5% deviation, Equation (14)) which are only used for sensitivity purpose, for TCL 100 and a chain length dependent RAFT transfer reactivity in case (a) all transfer coefficients are equal and chain length dependent (example 1), (b) $C_{tr,0} = C_{-tr,0} = 20 = C_{tr,0,IN}$ (black circle) are chain length independent, only chain length dependent C_{tr} (example 2). Chain length dependency of k_{tr} based on the composite k_t model determined by Johnston-Hall et al. for MMA^{23,33} and implemented explicitly with initial value of $C_{tr} = 120$ at $x = 0$ and chain length 1. Dashed-dotted black line is theoretical ‘observed’ variation of the RAFT transfer reactivity based on the number average chain length x_n . $[M]_0 = 9 \text{ mol L}^{-1}$; $[R_0X]_0 = 9 \cdot 10^{-2} \text{ mol L}^{-1}$; $[I_2]_0 = 9 \cdot 10^{-3} \text{ mol L}^{-1}$. Other kinetic parameters from Chapter 3.....152

Figure 4.9: Comparison between the simulated polymer dispersity profile for the case of chain length dependent (full blue line) and chain length independent (dashed green line) RAFT transfer kinetics for TCL 100 (a) all transfer coefficients are equal and chain length dependent (example 1), (b) $C_{tr,0} = C_{-tr,0} = 20 = C_{tr,0,IN}$ (black circle) are chain length independent, only chain length dependent C_{tr} (example 2). Chain length dependency of k_{tr} based on the composite k_t model determined by Johnston-Hall et al. for MMA^{23,33} and implemented explicitly with initial value of $C_{tr} = 120$ at $x = 0$ and chain length 1. $[M]_0 = 9 \text{ mol L}^{-1}$; $[R_0X]_0 = 9 \cdot 10^{-2} \text{ mol L}^{-1}$; $[I_2]_0 = 9 \cdot 10^{-3} \text{ mol L}^{-1}$. Other kinetic parameters from Chapter 3.....153

- Figure 4.10:** Comparison between the simulated RAFT CTA conversion (full blue line; full kinetic model) and the one calculated via Equation (16) (dashed red line) as a function of (monomer) conversion for TCL 100; $C_{tr} = C_{tr,0} = C_{-tr,0} = 15$; Entry 1 in Table 4.2; other kinetic parameters from Chapter 3.....155
- Figure 4.11:** $\ln([M]/[M]_0)$ vs. $\ln([R_0X]/[R_0X]_0)$ based on experimental data for the RAFT polymerization of MMA with CPDB as RAFT CTA and AIBN as conventional radical initiator (dashed black line is a trend-line for eye-guidance only). $[R_0X]/[R_0X]_0$ calculated via Equation (16). 353 K; $[MMA]_0:[CPDB]_0:[AIBN]_0 = 60:1:0.033$156
- Figure 4.12:** Experimental polymer dispersity as a function of (monomer) conversion **(a)** and corresponding $\langle C_{tr} \rangle$ as function of the monomer conversion obtained by solution of Equation (5)-(6) using the original Newton-Raphson convergence criterion (blue squares, convergence criterion A, Equation (12)) and the additional modified convergence criterion B (green triangles, 1% deviation, Equation (13)) and C (red circles, 5% deviation, Equation (14)) which are only used for sensitivity purpose, **(b)** for the RAFT polymerization of MMA with CPDB as RAFT CTA and AIBN as conventional radical initiator. 353 K; $[MMA]_0:[CPDB]_0:[AIBN]_0 = 60:1:0.033$; a higher TCL should be considered (Figure 4.13) for the accurate determination of $C_{tr,0}$ and C_{tr}156

Figure 4.13: Experimental polymer dispersity as a function of (monomer) conversion **(a)** and corresponding $\langle C_{tr} \rangle$ as function of the monomer conversion obtained by solution of Equation (5)-(6) using the original Newton-Raphson convergence criterion (blue squares, convergence criterion A, Equation (12)) and the additional modified convergence criterion B (green triangles, 1% deviation, Equation (13)) and C (red circles, 5% deviation, Equation (14)) which are only used for sensitivity purpose, **(b)** and $\ln([M]/[M]_0)$ vs. $\ln([R_0X]/[R_0X]_0)$ data **(c)** for the RAFT polymerization of MMA with CPDB as RAFT CTA and AIBN as conventional radical initiator. 353 K; $[MMA]_0:[CPDB]_0:[AIBN]_0 = 713:1:0.12$. $[R_0X]/[R_0X]_0$ calculated via Equation (16), full black line is obtained via linear regression: $y(x) = 15.00 x$157

Figure 4.14: Experimental polymer dispersity as a function of (monomer) conversion **(a)** and corresponding $\langle C_{tr} \rangle$ as function of the monomer conversion obtained by solution of Equation (5)-(6) using the original Newton-Raphson convergence criterion (blue squares, convergence criterion A, Equation (12)) and the additional modified convergence criterion B (green triangles, 1% deviation, Equation (13)) and C (red circles, 5% deviation, Equation (14)) which are only used for sensitivity purpose, **(b)** and $\ln([M]/[M]_0)$ vs. $\ln([R_0X]/[R_0X]_0)$ data **(c)** for the RAFT polymerization of MMA with CPDB as RAFT CTA and AIBN as initiator. 353 K; $[MMA]_0:[CPDB]_0:[AIBN]_0 = 741:1:0.1$. $[R_0X]/[R_0X]_0$ calculated via Equation (16), full black line is obtained via linear regression: $y(x) = 13.57 x$158

Figure 4.15: Experimental polymer dispersity as a function of (monomer) conversion **(a)** and corresponding $\langle C_{tr} \rangle$ as function of the monomer conversion obtained by solution of Equation (5)-(6) using the original Newton-Raphson convergence criterion (blue squares, convergence criterion A, Equation (12)) and the additional modified convergence criterion B (green triangles, 1% deviation, Equation (13)) and C (red circles, 5% deviation, Equation (14)) which are only used for sensitivity purpose, **(b)** and $\ln([M]/[M]_0)$ vs. $\ln([R_0X]/[R_0X]_0)$ data **(c)** for the RAFT polymerization of MMA with CPDB as RAFT CTA and AIBN as initiator. 353 K; $[MMA]_0:[CPDB]_0:[AIBN]_0 = 997:1:0.125$. $[R_0X]/[R_0X]_0$ calculated via Equation (16), full black line is obtained via linear regression: $y(x) = 11.32 x$158

Figure 5.1: (a) Experimental batch temperature (black diamonds) and conversion (red dots) evolution and simulated conversion profile (dotted red line) under reference conditions ($[nBuA]_0:[DoPAT]_0:[AIBN]_0=80:1:0.05$; 50 m% solvent; TCL 80; set temperature: 373 K) (b)-(c) Comparison between simulated and experimental number average molar mass M_n (b) and dispersity (c) profile for the reference conditions in batch (dotted red line vs. full red circle) and under microflow (full red line vs. open red triangles), and an additional condition under microflow (TCL 10; dashed blue line vs. open blue squares) (d)-(e) Simulated cumulative branching fraction (f_{branch}), number average macroradical chain length ($x_{n,R}$), RAFT CTA functionality (F_X) (also experimental data) and macromonomer fraction (F_{MM}) as a function of conversion for a TCL of 80 in batch (dotted red lines) and under microflow (full red lines), and for a TCL of 10 under microflow (dashed blue lines) (f) Comparison between simulated chain length distribution (CLD) under reference conditions in batch (dotted red line) and microflow (full red line) at a conversion of 0.8. Kinetic parameters in Table I.1 in Appendix I. Kinetic model: Equation (1)-(2) and Table 5.1. TCL defined as $[nBua]_0/[DoPAT]_0$177

Figure 5.2: (a)-(b) Simulated reaction probabilities for propagation (full line; prop), RAFT exchange (dashed line; exch) and all side reactions (dotted line; side) of the secondary radicals in an isothermal microreactor (a) and a non-isothermal batch reactor (b) with a set-temperature T_{set} of 373 K. (c)-(d) Simulated reaction probabilities for backbiting (full line; backb), termination (dashed line; term) and macropropagation (dotted line; macrop) of the secondary radicals in the microreactor (c) and the batch reactor (d). (e)-(f) Simulated reaction probabilities for termination (full line; termT), β -scission (dotted line; β -sc) or other side reactions (dashed line; other) of the tertiary radicals in microflow (e) and in batch (f); All simulations are performed under the reference conditions: $([\text{nBuA}]_0:[\text{DoPAT}]_0:[\text{AIBN}]_0 = 80:1:0.05; 50 \text{ wt\% solvent; TCL } 80)$. Kinetic parameters in Table I.1 in Appendix I. Kinetic model: Equation (1)-(2) and Table 5.1. TCL defined as $[\text{nBua}]_0/[\text{DoPAT}]_0$179

Figure 5.3: (a)-(b) Simulated reaction probabilities for propagation (full line; prop), RAFT exchange (dashed line; exch) and all side reactions (dotted line; side) of the secondary radicals in an isothermal microreactor at 373 K for TCL 10 (a; blue lines) and TCL 80 (b; red lines). (c)-(d) Simulated reaction probabilities for backbiting (full line; backb), termination (dashed line; term) and macropropagation (dotted line; macrop) of the secondary radicals at 373 K for TCL 10 (c; blue lines) and TCL 80 (d; red lines). Note that the scale of the ordinate is different for (c) and (d). All simulations are performed under the conditions: $([\text{DoPAT}]_0:[\text{AIBN}]_0 = 1:0.05; 50 \text{ wt\% solvent})$. Kinetic parameters in Table I.1 in Appendix I. Kinetic model: Equation (1)-(2) and Table 5.1. TCL defined as $[\text{nBua}]_0/[\text{DoPAT}]_0$181

Figure 5.4: Summary of the positive impact of the microreactor conditions on the control over **(a)** branching level f_{branch} and **(b)** RAFT CTA functionality F_X . Top to bottom in **(a)** and vice versa in **(b)**: a decrease of the polymerization temperature (373 to 343 K, TCL 80, $[M]_0$: 3.5 (50 wt% solvent); full to dashed red line), an additional lowering of the dilution degree ($[M]_0$: 3.5 to 5.25 M (25 wt% solvent)), dashed to dashed-dotted red line) and an additional lowering of TCL (TCL 80, to 10, dotted blue line). Kinetic parameters in Table I.1 in Appendix I. Kinetic model: Equation **(1)-(2)** and Table 5.1. TCL defined as $[n\text{Bua}]_0/[DoPAT]_0$182

Figure 5.5: **(a)-(b)** Simulated reaction probabilities for propagation (full line; prop), RAFT exchange (dashed line; exch) and all side reactions (dotted line; side) of the secondary radicals in an isothermal microreactor at 343 K (a) and 373 K (b). **(c)-(d)** Simulated reaction probabilities for backbiting (full line; backb), termination (dashed line; term) and macropropagation (dotted line; macrop) of the secondary radicals at 343 K (c) and 373 K (d). Note that the scale of the ordinate is different for (c) and (d). All simulations are performed under the reference conditions: $([n\text{BuA}]_0:[DoPAT]_0:[AIBN]_0 = 80:1:0.05; 50 \text{ wt\% solvent; TCL } 80)$. Kinetic parameters in Table I.1 in Appendix I. Kinetic model: Equation **(1)-(2)** and Table 5.1. TCL defined as $[n\text{Bua}]_0/[DoPAT]_0$183

Figure 5.6: (a)-(b) Simulated reaction probabilities for propagation (full line; prop), RAFT exchange (dashed line; exh) and total side reactions (dotted line; side) of the secondary radicals in an isothermal microreactor at 343 K in solution (a, $[M]_0 = 3.5$ M and b, $[M]_0 = 5.25$ M). (c)-(d) Simulated reaction probabilities for backbiting (full line; backb), termination (dashed line; term) and macropropagation (dotted line; macrop) of the secondary radicals in solution (c, $[M]_0 = 3.5$ M and d, $[M]_0 = 5.25$ M). All simulations are performed under the reference conditions: $([nBuA]_0:[DoPAT]_0:[AIBN]_0 = 80:1:0.05; TCL 80)$. Kinetic parameters in Table I.1 in Appendix I. Kinetic model: Equation (1)-(2) and Table 5.1. TCL defined as $[nBua]_0/[DoPAT]_0$184

Figure 5.7: Similar to Figure 5.4a but now for the number (#) of branches per chain instead of the cumulative branching fraction (f_{branch}). Top to bottom: a decrease of the polymerization temperature (373 to 343 K, TCL 80, $[M]_0$: 3.5 (50 wt% solvent); full to dashed red line), an additional lowering of the dilution degree ($[M]_0$: 3.5 to 5.25 M (25 wt% solvent)), dashed to dashed-dotted red line) and an additional lowering of TCL (TCL 80, to 10, dotted blue line). Kinetic parameters in Table I.1 in Appendix I. Kinetic model: Equation (1)-(2) and Table 5.1. TCL defined as $[nBua]_0/[DoPAT]_0$185

Figure 5.8: Simulated cumulative branching fractions (**a,c**) and RAFT CTA functionalities (**b, d**) at 343 K under reference conditions ($[\text{nBuA}]_0:[\text{RAFT CTA}]_0:[\text{AIBN}]_0=80:1:0.05$; 50 wt% solvent; TCL 80) (**a**)-(b) Influence of $k_{\text{tr}}^{\text{SS}}$: $k_{\text{tr}}^{\text{SS}} = 3 \cdot 10^6 \text{ L mol}^{-1} \text{ s}^{-1}$ (full red line, reference case), $k_{\text{tr}}^{\text{SS}} = 3 \cdot 10^5 \text{ L mol}^{-1} \text{ s}^{-1}$ (dashed orange line); $k_{\text{tr}}^{\text{SS}} = 3 \cdot 10^4 \text{ L mol}^{-1} \text{ s}^{-1}$ (dashed-dotted green line); $k_{\text{tr}}^{\text{SS}} = 3 \cdot 10^3 \text{ L mol}^{-1} \text{ s}^{-1}$ (dotted purple line) (**c**)-(d) Theoretical evaluation of the effect of RAFT exchange of tertiary radicals for TCL 80: $k_{\text{tr}}^{\text{TS}} = 3 \cdot 10^6 \text{ L mol}^{-1} \text{ s}^{-1}$ (dashed-dotted black line and $k_{\text{tr}}^{\text{TS}} = 3 \cdot 10^2 \text{ L mol}^{-1} \text{ s}^{-1}$ (dashed grey line) versus $k_{\text{tr}}^{\text{TS}} = 0 \text{ L mol}^{-1} \text{ s}^{-1}$ (full red line; reference case). Kinetic parameters in Table I.1 in Appendix I. Kinetic model: Equation (1)-(2) and Table 5.1. TCL defined as $[\text{nBua}]_0/[\text{RAFT CTA}]_0$186

Figure 5.9: (**a**)-(b) Simulated reaction probabilities for propagation (full line; prop), RAFT exchange (dashed line; exch) and all side reactions (dotted line; side) of the secondary radicals in an isothermal microreactor at 343 K for $k_{\text{tr}}^{\text{SS}} = 10^6 \text{ L mol}^{-1} \text{ s}^{-1}$ and $k_{\text{tr}}^{\text{SS}} = 10^5 \text{ L mol}^{-1} \text{ s}^{-1}$. (**c**)-(d) Simulated reaction probabilities for backbiting (full line; backb), termination (dashed line; term) and macropropagation (dotted line; macrop) of the secondary radicals for $k_{\text{tr}}^{\text{SS}} = 10^6 \text{ L mol}^{-1} \text{ s}^{-1}$ and $k_{\text{tr}}^{\text{SS}} = 10^5 \text{ L mol}^{-1} \text{ s}^{-1}$. Note that the scale of the ordinate is different for (c) and (d). All simulations are performed under the reference conditions: ($[\text{nBuA}]_0:[\text{RAFT CTA}]_0:[\text{AIBN}]_0= 80:1:0.05$; 50 wt% solvent; TCL 80). Kinetic parameters in Table I.1 in Appendix I. Kinetic model: Equation (1)-(2) and Table 5.1. TCL defined as $[\text{nBua}]_0/[\text{RAFT CTA}]_0$187

Figure 5.10: (a)-(b) Simulated reaction probabilities for propagation (full line; prop), RAFT exchange (dashed line; exch) and total side reactions (dotted line; side) of the secondary radicals in an isothermal microreactor at 343 K for $k_{tr}^{TS} = k_{tr}^{ST} = k_{tr}^{TT} = 0 \text{ L mol}^{-1} \text{ s}^{-1}$ (a) and $k_{tr}^{TS} = k_{tr}^{ST} = k_{tr}^{TT} = 10^2 \text{ L mol}^{-1} \text{ s}^{-1}$ (b). (c)-(d) Simulated reaction probabilities for backbiting (full line; backb), termination (dashed line; term) and macropropagation (dotted line; macrop) of the secondary radicals for $k_{tr}^{TS} = k_{tr}^{ST} = k_{tr}^{TT} = 0 \text{ L mol}^{-1} \text{ s}^{-1}$ (c) and $k_{tr}^{TS} = k_{tr}^{ST} = k_{tr}^{TT} = 10^2 \text{ L mol}^{-1} \text{ s}^{-1}$ (d). (e)-(f) Simulated reaction probabilities for termination (full line; termT), β -scission (dotted line; β -sc) or other side reactions (dashed line; other) of the tertiary radicals for $k_{tr}^{TS} = k_{tr}^{ST} = k_{tr}^{TT} = 0 \text{ L mol}^{-1} \text{ s}^{-1}$ (e) and $k_{tr}^{TS} = k_{tr}^{ST} = k_{tr}^{TT} = 10^2 \text{ L mol}^{-1} \text{ s}^{-1}$ (f); All simulations are performed under the reference conditions: $([nBuA]_0:[RAFT\ CTA]_0:[AIBN]_0=80:1:0.05; 50 \text{ wt\% solvent; TCL } 80)$. Kinetic parameters in Table I.1 in Appendix I. Kinetic model: Equation (1)-(2) and Table 5.1. TCL defined as $[nBua]_0/[RAFT\ CTA]_0$189

Figure 5.11: Comparison between the backbiting rate and the rate of tertiary propagation for reference conditions $([nBuA]_0:[RAFT\ CTA]_0:[AIBN]_0=80:1:0.05; 50 \text{ wt\% solvent; TCL } 80; 343 \text{ K})$ without ($k_{tr}^T = 0 \text{ L mol}^{-1} \text{ s}^{-1}$) (a) and with ($k_{tr}^T = 10^6 \text{ L mol}^{-1} \text{ s}^{-1}$) (b) RAFT exchange reactions of the tertiary radicals. Kinetic parameters in Table I.1 in Appendix I. Kinetic model: Equation (1)-(2) and Table 5.1.....190

Figure 5.12: Effect of the inclusion of RAFT exchange reactions for the tertiary radicals on number average chain length (a, M_n) and the polymer dispersity (b) at 343 K under reference conditions ($[nBuA]_0:[RAFT\ CTA]_0:[AIBN]_0=80:1:0.05$; 50 wt% solvent; TCL 80). In the simulations, all the transfer rate coefficients for RAFT exchange of the tertiary radicals are assumed to be equal ($k_{tr}^{TS} = k_{tr}^{ST} = k_{tr}^{TT} = k_{tr}^T$) with the corresponding rate coefficient for the secondary radicals as the upper limiting value (k_{tr}^{SS} ; dashed red line in a-b). The lower limit ($k_{tr}^T = 0$) corresponds to the full red line in a-b. The dashed grey line represents $k_{tr}^T = 10^2\ L\ mol^{-1}s^{-1}$ and the dashed-dotted black line corresponds to $k_{tr}^T = 10^6\ L\ mol^{-1}s^{-1}$. Kinetic parameters in Table I.1 in Appendix I. Kinetic model: Equation (1)-(2) and Table 5.1.....190

Figure 5.13: (a) Effect of the inclusion of RAFT exchange reactions for the tertiary radicals on the conversion profile at 343 K under reference conditions ($[nBuA]_0:[RAFT\ CTA]_0:[AIBN]_0=80:1:0.05$; 50 wt% solvent; TCL 80). In the simulations, all the transfer rate coefficients for RAFT exchange of the tertiary radicals are assumed to be equal ($k_{tr}^{TS} = k_{tr}^{ST} = k_{tr}^{TT} = k_{tr}^T$) with the corresponding rate coefficient for the secondary radicals as the upper limiting value. The lower limit ($k_{tr}^T = 0$) corresponds to the full red line. The dashed grey line represents $k_{tr}^T = 10^2\ L\ mol^{-1}s^{-1}$ and the dashed-dotted black line corresponds to $k_{tr}^T = 10^6\ L\ mol^{-1}s^{-1}$. (b) Comparison of the corresponding secondary and tertiary radical concentrations for the limiting situations: $k_{tr}^T = 0$ (full red line, λ_0 ; dotted red line, λ_0^T) and $k_{tr}^T = 10^6\ L\ mol^{-1}s^{-1}$ (dashed black line, λ_0 ; dashed-dotted black line, λ_0^T). The smaller figure on the right is an inset added for clarity. Other kinetic parameters in Table I.1 in Appendix I. TCL defined as $[nBuA]_0/[RAFT\ CTA]_0$192

- Figure 5.14:** Effect of the inclusion of RAFT exchange reactions for the tertiary radicals on the conversion profile **(a)** and the polymer properties **(b)-(d)** at 373 K under reference conditions ($[\text{nBuA}]_0:[\text{RAFT CTA}]_0:[\text{AIBN}]_0=80:1:0.05$; 50 wt% solvent; TCL 80). In the simulations, all the transfer rate coefficients for RAFT exchange of the tertiary radicals are assumed to be equal ($k_{\text{tr}}^{\text{TS}} = k_{\text{tr}}^{\text{ST}} = k_{\text{tr}}^{\text{TT}} = k_{\text{tr}}^{\text{T}}$). The lower limit ($k_{\text{tr}}^{\text{T}} = 0$) corresponds to the full red line in a-d and the dashed grey line represents $k_{\text{tr}}^{\text{T}} = 10^2 \text{ L mol}^{-1}\text{s}^{-1}$. Other kinetic parameters in Table I.1 in Appendix I. TCL defined as $[\text{nBuA}]_0/[\text{RAFT CTA}]_0$193
- Figure B.1:** Influence of volume contraction on the homo-termination rate coefficient. Ratio of value obtained via the RAFT-CLD-T technique through Equation (9) in the main text, i.e. without any volume effect taken into account, to the value obtained with Equation (B5), i.e. with inclusion of the volume contraction; conditions: entry 7 in Table 2.1 (blue line) and entry 17 in Table 2.1 (red line).....214
- Figure B.2:** Number average chain length (left), dispersity (middle) and conversion data (right) for all performed RAFT-CLD-T homo-termination experiments: entry 1-14 in Table 2.1 in Chapter 2. For the conversion results, both the on-line DSC (full blue line) and the off-line $^1\text{H-NMR}$ data (red squares) are shown together with their respective error.....218

- Figure C.1:** Number average chain length of the terminating radicals (left), dispersity (middle) and total polymer mass fraction data (right) for all the modified RAFT-CLD-T homo-termination experiments (entry 15-19 in Table 2.1 in Chapter 2) to quantify the matrix effects, i.e. in the presence of a certain amount of dead PMMA standard. For the conversion results, both the on-line DSC (full blue line) and the off-line $^1\text{H-NMR}$ data (red squares) are shown together with their respective error, similar to Figure B.2.....224
- Figure C.2:** Quantification of a possible effect of the polymer matrix on k_t^{ii} by the ratio of the homo-termination rate coefficient obtained via the RAFT-CLD-T technique in the presence of dead PMMA standard (non-uniform polymer matrix; $k_{t,\text{NU}}^{\text{ii}}$), to the homo-termination rate coefficient assuming a uniform polymer matrix as determined from the surface function in Figure 2.4c in Chapter 2 ($k_{t,\text{U}}^{\text{ii}}$); j_m^* : the mass average chain length of the polymer matrix.....226
- Figure D.1:** Evolution of the molar mass distribution of both the short chain (yellow) and long chain (blue) dormant population during a short-long-termination experiment. The depicted individual peaks are obtained after deconvolution of the SEC-trace at three different times for entry 21 in Table 2.1 in Chapter 2. Also, the calculation of the conventional RAFT CTA conversion (red squares) and concomitant f_1 value (green triangles; in case assumed time dependent) is illustrated.....230

- Figure D.2:** Short-long-termination rate coefficient (full fuchsia line) plotted together with an estimate of its actual error (dashed fuchsia line) and the maximum error (dotted top fuchsia line; overestimation of error) calculated via a propagation of error analysis. The corresponding homo-termination rate coefficients $k_t^{L*L^*}$ (full blue line) and $k_t^{S*S^*}$ (full yellow line) are also shown.....231
- Figure D.3:** Good agreement between polymer mass fraction data obtained via DSC (full blue lines) and $^1\text{H-NMR}$ sampling data (red points). 5% error for $^1\text{H-NMR}$ data (red error bars) and on-line DSC data are also indicated (dashed blue lines); conditions: entry 20-23 (a-d) in Table 2.1 in Chapter 2.....232
- Figure D.4:** Reproducibility of the RAFT-CLD-T short-long-termination experiments. Sampling data: **(a)** polymer mass fraction vs time; **(b)** number average chain length vs polymer mass fraction; **(c)** dispersity vs polymer mass fraction; Excellent agreement is obtained. Conditions: $[\text{MMA}]_0/[\text{CTA}_{\text{tot}}]_0 = 90$; $[\text{CTA}_{\text{tot}}]_0/[\text{AIBN}]_0 = 17$; $[\text{macro-RAFT CTA}]_0/[\text{CTA}_{\text{tot}}]_0 = 0.15$; initial CL macro-RAFT CTA = 140.....233
- Figure D.5:** Observed (overall) termination rate coefficient $\langle k_t \rangle$ measured via DSC (full green line) and its duplicate analysis (dashed red line), which almost coincide for the polymer mass fraction range of the short-long-termination experiments; conditions: entry 20-23 (a-d) in Table 2.1 in Chapter 2.....233
- Figure D.6:** Visual verification that the homo-termination rate coefficients $k_t^{S*S^*}$ (full yellow line) and $k_t^{L*L^*}$ (full blue line) are derived from the non-extrapolated region of the homo-termination surface (Equation **(B10)**) for all considered short-long-termination conditions (a-d): entry 20-23 in Table 2.1 in Chapter 2.....234

- Figure D.7:** Chain length and dispersity data for the performed short-long-termination experiments; entry 20-23 in Table 2.1 in Chapter 2. Yellow represents the short chain and blue the long chain distribution.....235
- Figure D.8:** (a)-(d) k_t^{S*L*} based on a constant (dotted fuchsia line) and a variable (full green line) f_1 versus the polymer mass fraction for entry 20-23 in Table 2.1 in Chapter 2. $\langle kt \rangle$ (dashed grey line), k_t^{S*S*} (full yellow line) and k_t^{L*L*} (full blue line) are also plotted. (a) is similar to Figure 2.13c and 17a in Chapter 2.....236
- Figure D.9:** Comparison between k_t^{S*L*} and the simplified mean models for entry 20-23 in Table 2.1 in Chapter 2 (a-d): diffusion mean model (DMM; dashed orange line), geometric mean model (GMM; dashed red line) and harmonic mean model (HMM; dashed pink line). A mismatch is observed for both the slope and the absolute values at low polymer mass fractions. A time dependent f_1 induces an even bigger deviation. At a certain polymer mass fraction indicated by the dashed grey line, the slope of k_t^{S*L*} becomes equal to the one of the simplified mean models and the termination behavior is no longer dominated by the diffusion of the short chain radicals, instead a mean behavior results.....237
- Figure D.10:** Comparison between surface function (green surface) fitted to experimental k_t^{S*L*} data for specific chain length combinations and polymer mass fractions (full fuchsia lines; entry 20-23 in Table 2.1 in Chapter 2; constant f_1) and the surface (red) as obtained considering a diffusion mean model (DMM; (a)), a geometric mean model (GMM; (b)) or a harmonic mean model (HMM; (c)). Clearly, a significant mismatch is obtained in case the simplified mean models are applied.....238

- Figure F.1:** Principle of the Newton-Raphson method to find the root x_0 of a non-linear function (full blue line). Based on the tangent line to the function in x_1 (dotted red line), a new estimate for the root is obtained, x_2 , until x_0 is reached.....253
- Figure F.2:** Newton-Raphson procedure applied in the methodology developed in Chapter 4 to determine the RAFT chain transfer reactivity $\langle C_{tr} \rangle$ based on a comparison between experimental dispersity data (\mathcal{D}_{exp}) and calculated dispersity data via analytical expressions ($\mathcal{D}(\langle C_{tr} \rangle)$; blue lines in figures in Chapter 4).....256
- Figure F.3:** Shape of the non-linear equation $f(\langle C_{tr} \rangle)$ obtained in the methodology developed in Chapter 4 to determine the RAFT chain transfer reactivity based on a comparison between experimental dispersity data (\mathcal{D}_{exp}) and calculated dispersity data via analytical expressions ($\mathcal{D}(\langle C_{tr} \rangle)$). The convergence criterion of the original Newton-Raphson method (convergence criterion A) is indicated in grey. The additional modified convergence criteria B and C are highlighted in respectively green and red (Equation (F2)).....257
- Figure F.4:** Modification of the convergence criterion of the Newton-Raphson procedure applied in the methodology developed in Chapter 4 to assess the sensitivity of the calculated $\langle C_{tr} \rangle$ for small fluctuations in the polymer dispersity values. Modified convergence criteria B and C are given by Equation (F2). Only procedure for 1% deviation is shown.....259

- Figure H.1:** ESI-MS spectra for [nBuA]₀:[DoPAT]₀:[AIBN]₀=10:1: 0.05; 50 wt% solvent; TCL 10 for monomer conversions $x=0.77$ and $x=0.88$. **(b)** and **(d)** are an inset of respectively **(a)** and **(c)**. Via a color code the observed polymer products are indicated. Only polymer species containing a RAFT end-group are discerned.....270
- Figure H.2:** ESI-MS spectra for [nBuA]₀:[DoPAT]₀:[AIBN]₀=80:1: 0.05; 50 wt% solvent; TCL 10; for monomer conversions $x=0.18$ and $x=0.27$. **(b)** and **(d)** are an inset of respectively **(a)** and **(c)**. Via a color code the observed polymer products are indicated. Only polymer species containing a RAFT end-group are discerned.....271
- Figure J.1:** **(a)** Simulated cumulative branching fractions at 343 K with 50 wt% solvent and four TCLs ($[AIBN]_0 = 2 \cdot 10^{-3} \text{ mol L}^{-1}$; TCL 10 (full blue line), TCL 30 (full green line), TCL 80 (full red line), TCL 200 (full purple line). **(b)** Same as (a) but now for the RAFT CTA functionality F_x . Kinetic parameters in Table I.1 in Appendix I.....277

Figure J.2: (a)-(d) Simulated reaction probabilities for propagation (full line; prop), RAFT exchange (dashed line; exch) and all side reactions (dotted line; side) of the secondary radicals in an isothermal microreactor at 343 K for a targeted chain length of 10 (a), 30 (b), 80 (c) and 200 (d). (e)-(h) Simulated reaction probabilities for backbiting (full line; backb), termination (dashed line; term) and macropropagation (dotted line; macrop) of the secondary radicals at 343 K for a targeted chain length of 10 (e), 30 (f), 80 (g) and 200 (h). All simulations are performed under the reference conditions: ($[n\text{BuA}]_0:[\text{DoPAT}]_0:[\text{AIBN}]_0 = 80:1:0.05$; 50 wt% solvent; TCL 80). Kinetic parameters in Table I.1 in Appendix I.....278

Figure K.1: (a) Similar to Figure 5.8a in Chapter 5, but now for the number (#) of branches per chain instead of the cumulative branching fraction (f_{branch}) as a function of conversion. The plotted lines represent the same conditions as the corresponding lines in Figure 5.8a. It is clear that the same factors that reduce f_{branch} also reduce the number of branches per chain. (b) Similar to Figure 5.8c in Chapter 5, but now the number of branches per chain instead of f_{branch} . Same color code and conditions for the plotted lines are used. Similarly, a higher RAFT exchange rate of the tertiary radicals induces a markedly lower number of branches per chain. Kinetic parameters in Table I.1 in Appendix I.....279

Figure K.2: Equivalent to Figure J.1a, the number of branches per chain is plotted for four TCLs at 343 K, but, on the x-axis now the number average chain length (x_n) is plotted instead of the conversion. Same conditions and color code as Figure J.1a. An inset for the lower number average chain lengths is shown on the right. This figure shows that increasing the TCL allows to obtain lower numbers of branches per chain for a given average chain length x_n . However, the amounts of the respective polymer obtained are much smaller as lower conversions are reached. Kinetic parameters in Table I.1 in Appendix I.....280

List of schemes

- Scheme 1.1:** RAFT polymerization scheme with as RAFT CTA R_0X . R_n : macroradical of chain length n ; P_n : dead polymer chain of chain length n ; R_n-X : dormant species with chain length n ; INT-(m,n): intermediate radical species with chain lengths m and n for the two arms; I^* : conventional initiator radical fragment; M : monomer; for I^* different from R_0 : no exchange considered with I^* and IX.....6
- Scheme 1.2:** Fundamental basis of the parallel encounter pair model for the description of apparent kinetics (k_{app}). Reactants can diffuse towards (k_{+diff}) or away from each other (k_{-diff}) and need to be at reaction distance (forming the encounter pair AB) for chemical reaction (k_{chem^*}) to occur.....9
- Scheme 1.3:** Decomposition scheme of AIBN in which nitrogen is released and subsequent main reaction possibilities of the cyano-isopropyl radicals. Undesired side reactions which are covered by the initiator efficiency f are marked in red. R_n : macroradical of chain length n ; P_n dead polymer species of chain length n14
- Scheme 1.4:** Simplified RAFT degenerative transfer mechanism based on the psuedo-steady state assumption for the calculation of the concentration of the intermediate radical species in Scheme 1.3 (INT). Only RAFT exchange reactions are shown.....36

- Scheme 3.1:** RAFT polymerization scheme with a dithioester as RAFT CTA (R_0X). R_n : macroradical of chain length n ; P_n : dead polymer chain of chain length n ; R_n-X : dormant species with chain length n ; INT-(m,n): intermediate radical species with chain lengths m and n for the two arms; I^* : conventional initiator radical fragment; M : monomer; for I^* different from R_0 no RAFT exchange involving I/IX species included; f : efficiency factor.....98
- Scheme 3.2:** Simplified RAFT degenerative transfer mechanism based on the pseudo-steady state assumption for the calculation of the concentration of the intermediate radical species in Scheme 1 (INT) (cf. Appendix E). Only RAFT exchange reactions are shown for simplicity.....99
- Scheme 4.1:** Simplified RAFT degenerative transfer mechanism based on the pseudo-steady state assumption for the calculation of the concentration of the intermediate radical species (cf. Appendix E). Only RAFT exchange reactions are shown for simplicity.....127
- Scheme E.1:** Full RAFT polymerization reaction mechanism focusing on addition-fragmentation reactions. Termination (red arrows) and propagation reactions (green arrows) are only shown in a conceptual way; efficiency f only defined for FRP reactions.....244
- Scheme E.2:** Degenerative transfer mechanism for RAFT polymerization, focusing on the RAFT exchange reactions. Termination (red arrows) and propagation reactions (green arrows) are only shown in a conceptual way. $n, m \geq 1$246

- Scheme E.3:** Further simplified degenerative transfer mechanism for RAFT polymerization, focusing on the RAFT exchange reactions. Termination (red arrows) and propagation reactions (green arrows) are only shown in a conceptual way. $n, m \geq 0$; used in Chapter 3 and most RAFT polymerization kinetic studies; influence of conventional radical initiator molecules is neglected.....247
- Scheme I.1:** Chemical pathways of the formation and disappearance reactions of the mid-chain radicals (MCRs) that are included in the kinetic model. For simplicity, no RAFT exchange involving tertiary radicals is assumed for the construction of this reaction scheme, although this is considered in the present work in a later stage. Termination is only depicted with a secondary radical species, whereas in the kinetic model termination reactions with any radical species present in the polymerization mixture is included (cf. Table I.1).....275

List of tables

- Table 2.1:** Overview of the experimental conditions applied for the RAFT-CLD-T homo-termination experiments (entry 1-14), modified homo-termination experiments to quantify matrix effects (entry 15-19) and short-long-termination experiments (entry 20-23) of methyl methacrylate (MMA) at 353 K in bulk. CPDB: 2-cyano-2-propyl dithiobenzoate; AIBN: azobis(isobutyronitrile); Subscript zero: initial concentration; CL: chain length. For entry 1-19, $[CTA_{tot}]_0 = [CPDB]_0$. For entry 15-19, $[macro-RAFT\ CTA]_0$ refers to initial concentration of dead PMMA standard ($M_n = 9800\text{ g mol}^{-1}$; $\bar{D} = 1.05$).....58
- Table 2.2:** Parameters used in the simulations performed in order to support the modification of the RAFT-CLD-T formula with a factor 2 (Equation (9) with $b=1$ in the main text). Parameters are taken from the work of Monteiro and coworkers.¹ C_{tr} is the transfer coefficient corresponding with the macro-addition-fragmentation. $C_{tr,0}$ corresponds with the addition-fragmentation reactions involving initiator species or conventional CTA.....68
- Table 2.3:** Input parameters of the RAFT-CLD-T equation (Equation (9)) and their standard deviation (STDEV). Specified values are based on literature data.....70
- Table 3.1:** Summary of the degenerative RAFT transfer coefficients used throughout this chapter (cf. Scheme 3.2 and Appendix E for a more detailed description of the reaction scheme and the assumptions made).....101
- Table 3.2:** Overview of the main methods to determine the transfer reactivity in RAFT polymerization.^{4,6,8,10,18-24,32}107

- Table 3.3:** Rate coefficients at 353 K used in the simulations and benchmark for the in silico experiments for RAFT polymerization of MMA initiated by AIBN (R_0 equal to I^*). Assumptions in Appendix E.....110
- Table 3.4:** Evaluation of the Mayo method⁶ (Equation (2)) and the chain length distribution (CLD) method⁸⁻¹⁰ (Equation (3)) for higher values of $C_{tr,0}$. The value of $C_{tr,0}$ implemented in the simulations of the perfect experiments ($C_{tr,0,IN}$) is compared with the value obtained by application of the respective method to the simulated chain length data at $x=0.01$ ($C_{tr,0,OUT}$) and the % deviation compared to the 'real' implemented value is shown. In all simulations $C_{-tr,0} = C_{tr} = C_{tr,0,IN}$; $[M]_0 = 9 \text{ mol L}^{-1}$; $[I_2]_0 = 9 \cdot 10^{-3} \text{ mol L}^{-1}$. $C_{tr,out}$ from four different TCLs ($= [M]_0/[R_0X]_0$): 100, 200,300 and 400; corresponding $[R_0X]_0$: 0.09, 0.045, 0.03 and $0.0225 \text{ mol L}^{-1}$ respectively. In case no CLD k_t : $k_t = 5 \cdot 10^8 \text{ L mol}^{-1} \text{ s}^{-1}$. Other kinetic parameters in Table 3.3.....112
- Table 3.5:** Evaluation of the method of Moad and coworkers²¹⁻²³ (Equation (8)) and the method of Theis et al.²⁴ (Equation (9)) to determine $C_{tr,0}$ ($C_{tr,0,OUT}$) in case the reaction of R_0 species with macro-RAFT CTA can be neglected, based on the simulation of perfect experiments. Different targeted chain lengths (TCLs $= [M]_0/[R_0X]_0$) and values for the implemented value for $C_{tr,0}$ ($C_{tr,0,IN}$) are covered. In all simulations $C_{-tr,0} = C_{tr} = C_{tr,0,IN}$ (situation 1); $[M]_0 = 9 \text{ mol L}^{-1}$; $[I_2]_0 = 9 \cdot 10^{-3} \text{ mol L}^{-1}$. For TCL 100, 200 and 300, $[R_0X]_0$ is respectively: 0.09, 0.04 and 0.03 mol L^{-1} . Other kinetic parameters in Table 3.3.....114

Table 3.6:	Summary of the conditions corresponding to the highest accuracy of the discussed literature methods to determine $C_{tr,0}$. ^{8-10,21,22,24} Summary of model assumptions for each method in Table 3.2 and detailed discussion in Chapter 1.....	117
Table 4.1:	Degenerative transfer RAFT polymerization scheme used for the model development of in the present work. M: monomer; R_nX : dormant species with chain length n, for n=0 small RAFT CTA; I_2 : conventional radical initiator with I^* identical to R_0 ; R_n : macroradical with chain length n; P: dead polymer species; all rate coefficients can be apparent, i.e. can vary as a function of conversion and chain length of the participating reactants. Assumptions in Appendix E.....	130
Table 4.2:	Conditions of the performed in silico experiments. Different targeted chain lengths (TCLs) and values for the implemented value for $C_{tr,0}$ ($C_{tr,0,IN}$), $C_{-tr,0}$ ($C_{tr,0,IN}$) and C_{tr} ($C_{tr,IN}$) (theoretical RAFT CTAs) are covered. Case 1: entry 1; Case 2: entry 2-6; Case 3: entry 7-8. $[M]_0 = 9 \text{ mol L}^{-1}$; $[I_2]_0 = 9 \cdot 10^{-3} \text{ mol L}^{-1}$; $[R_0X]_0$ for TCL 100, 200, 300 and 500: respectively 0.09, 0.045, 0.03 and 0.018 mol L^{-1}	140

Table 4.3:	In silico comparison of the accuracy of the different literature methods to determine $C_{tr,0}$ with the corresponding accuracy of the developed method in the present work. % deviation of the resulting value for $C_{tr,0}$ from the implemented value $C_{tr,0,IN}$ for the method of Moad ^{12,13} (% deviation 1), the method of Theis et al. ¹⁶ (% deviation 2) and the method presented in the current work (% deviation 3). Different targeted chain lengths (TCLs) and values for $C_{tr,0,IN}$ are covered. $[M]_0 = 9 \text{ mol L}^{-1}$; $[I_2]_0 = 9 \cdot 10^{-3} \text{ mol L}^{-1}$. $[R_0X]_0$ for TCL 100, 200 and 300: respectively 0.09, 0.045 and 0.03 mol L^{-1} . Other kinetic parameters from Chapter 3.....	148
Table 4.4:	Comparison of the values for $C_{tr,0}$ obtained via the method of Moad ^{12,13} ($C_{tr,0}$ 1; Equation (8) in Chapter 3), the method of Barner-Kowollik ¹⁶ ($C_{tr,0}$ 2; Equation (9) in Chapter 3), and the method developed in the present work ($C_{tr,0}$ 3) based on experimental data for the RAFT polymerization of MMA at 353 K with CPDB as RAFT CTA and AIBN as initiator. ²⁸ Entry 1-4 correspond to Figures 4.12-15. Different targeted chain lengths (TCLs) are considered. Mean value and maximum deviation for $C_{tr,0}$ determined by each method are also shown.....	159
Table 5.1:	Reactions for simulation of solution RAFT polymerization of nBuA. Secondary/tertiary nature: superscript S/T; M: monomer, R_0X : initial RAFT CTA, I: conventional initiator fragment, $R_i/R_iX/P_i$: radical/dormant/dead macrospecies with chain length i ; MM: macromonomer; f: efficiency; Arrhenius parameters: Table I.1 in Appendix I.....	172
Table B1:	Parameters of the surface function (Equation (B10)) and their respective t -values and 95% confidence intervals.....	221

Table C.1:	Parameters of the surface function (Equation (C1)) and their respective t-values and 95% confidence intervals.....	227
Table D.1:	Parameters of the surface function (Equation (D1)) and their respective t-values and 95% confidence intervals.....	239
Table D.2:	Parameters of the surface function (Equation (D2)) and their respective t-values and 95% confidence intervals.....	240
Table D.3:	Parameters of the surface function (Equation (D3)) and their respective t-values and 95% confidence intervals.....	241
Table E.1:	Overview of the assumptions made for the RAFT transfer rate coefficients in case the transition is made from Scheme E.2 to Scheme E.3: no distinction made between I^* and R_0	249
Table H.1:	Comparison between the final polymer properties obtained in a batch reactor with a reaction volume of 20 mL and 40 mL at 373.15 K.....	269
Table I.1:	Reactions for simulation of reversible addition-fragmentation chain transfer (RAFT) polymerization of n-butyl acrylate (nBuA). Secondary/tertiary nature of macrospecies denoted by superscript S/T; M: monomer, R_0X : initial RAFT chain transfer agent (CTA), I: conventional initiator fragment, $R_i/R_iX/P_i$ macroradical/dormant/dead species with chain length i; MM: macromonomer; f: efficiency; Arrhenius parameters are listed in the third (A, pre-exponential factor) and fourth (E_a , activation energy) column; the fifth column contains the value of the corresponding rate coefficient at 373 K; the sixth column is the literature reference. RAFT specific reactions are highlighted in grey.....	273

